MULTICOMPONENT DISTILLATION – MATHEMATICAL MODELING, GLOBAL OPTIMIZATION, AND PROCESS INTENSIFICATION

A Dissertation

Submitted to the Faculty

of

Purdue University

by

Zheyu Jiang

In Partial Fulfillment of the

Requirements for the Degree

of

Doctor of Philosophy

December 2018

Purdue University

West Lafayette, Indiana

THE PURDUE UNIVERSITY GRADUATE SCHOOL
STATEMENT OF DISSERTATION APPROVAL

Dr. Rakesh Agrawal, Chair

Davidson School of Chemical Engineering

Dr. Mohit Tawarmalani

Krannert School of Management

Dr. Gintaras V. Reklaitis

Davidson School of Chemical Engineering

Dr. Zoltan Nagy

Davidson School of Chemical Engineering

Approved by:

Dr. John A. Morgan

Head of the School Graduate Program

To my family and my *alma maters*.

ACKNOWLEDGMENTS

This is the most fun part of the thesis.

As my PhD journey is about to come to a stop, it is worthwhile to pause for a bit and reflect back on my past four years as a researcher, past twenty years as a student, and past twenty seven years as a member to my family and to this world. I would like to take this opportunity to thank all the people who raised me, educated me, and helped me in one aspect or another throughout the years. What they did have had tremendous impact on me. They shaped me into who I am today and have brought me all the way to this stage.

First and foremost, I would like to express my sincere thank to my advisor and my academic father, Professor Rakesh Agrawal. I can write an entire book to describe all the great lessons I have learnt from Prof. Agrawal and how wonderful he is as my research advisor and my role model in life. And I always believe without a doubt that having such an advisor to guide me during my PhD journey has been my biggest luck. Apart from his academic excellence, I am always inspired and moved by Prof. Agrawal's great passion and love on what he does. His enthusiasm towards research has always pushed me to dream big, work hard, and never give up. Without him, I cannot accomplish even a fraction of what I have accomplished. His philosophy of research has completely shaped my way of evaluating, approaching, and analyzing a research problem. His influence on me has reached far beyond research. It extends all the way to my outlook on the world, life and values. If there is one thing that I would really miss about leaving Purdue, then it would be the fact that I wouldn't be able to frequently meet with him and listen to him talking about research and life. If possible, I really want to be his student forever.

Second, I would like to thank my co-advisor, Professor Mohit Tawarmalani, who redefines what "excellence" means in my dictionary. When I look at his talent and intellectual power, I am looking at the sky. All I have is my pure admiration. Working with Prof. Tawarmalani is really some of the most precious things I can possibly have in my life. However, what is more valuable is his constant push for perfection and rigor in analyzing a given problem, which has significantly changed my way of thinking. Prof. Tawarmalani is never satisfied with an answer to a problem. Instead, he always wants the best answer. Meeting with him individually or in group has always been an intense but enjoyable experience. It is one of my biggest regrets that I did not have enough chance to learn more optimization from him. But the insights and suggestions that Prof, Tawarmalani has given have been so useful that they go far beyond the scope of research and I will never forget the essence of them.

I want to thank Professor Gintaras Reklaitis and Professor Zoltan Nagy for for taking their time to be in my defense committee and for their invaluable and constructive feedback during my defense. I also want to thank Prof. Joseph Pekny for his great questions and inputs to my research during my qualifying and preliminary exams.

I really want to thank the entire team of Prof. Agrawal's modeling group. I always believe that working in my group has been a fantastic experience. Everyone in the modeling group is extremely smart, productive, cooperative, and very nice to each other. I cannot find this kind of unique atmosphere anywhere else. I would like to thank my past and current members in the separations group, Dr. Gautham Madenoor Ramapriya, Dr. Parham Mobed, Radhakrishna Tumbalam Gooty, Tony Joseph Mathew, Jose Adrian Chavez Velasco. They are truly at the "top of the curve". Their passion and dedication to research as well as the sharp and brilliant questions and discussions have benefited my research a lot. Their enthusiasm and diligence towards research have been pushing me to overcome my intrinsic laziness and to keep working. I would like to thank members of the energy systems group, Dr. Emre Gencer, Dr. Taufik Ridha, Yiru Li, Zewei Chen, Wasiu (Peter) Oladipupo,

and Edwin Rodriquez, for their great discussions and support whenever I needed. I wish them all the best in their future endeavor. I especially want to thank Taufik for all the "short" food exploration trips we had. Taufik is a really nice person and I wish we have more opportunities to hang out together after we graduate. I wish him the best of luck!

I want to thank Melissa LaGuire for being so nice and helpful. She has done most of the hard administrative work for us so that we can simply focus on our research. I cannot imagine how my PhD life would look like without her.

I would like thank my *alma maters*, including Guangzhou Shihua Primary School, Guangzhou No. 86 Middle School, Guangdong Experimental High School, University of Minnesota, and Purdue University. I firmly believe that it must be a matter of luck for me to receive the best education one can possibly think of for the past twenty years. They taught me everything about being a good student, a good researcher, and a good person. I am especially grateful to my middle school and high school years, during which I met with some of the brightest people in this world, each with a strong character, and learnt how to work smart and think critically. I am very thankful to my choice of studying liberal arts and social sciences in high school, which has broadened my scope significantly.

I would like to thank Professor Michael Tsapatsis and Professor Kumar Varoon Agrawal for being my undergraduate research advisors and for teaching all the qualities a top-notch researcher should possess. I would like to thank Professor Edward Cussler for showing me what "teaching" really stands for. His lectures in Transport Phenomena and Process Control were unforgettable. It is hard to express in words, but I don't think anyone can ever give a lecture as compelling and informative as he did.

Last but not least, I would like to thank my beloved parents and family, for everything they have done. This thesis is dedicated to them.

TABLE OF CONTENTS

LIST OF TABLES

LIST OF FIGURES

Figure Page

Figure Page

Figure Page

SYMBOLS

V_i Vapor flow rate in general column section i

L_i Liquid flow rate in general column section i

V_{F_i} Vapor inflow rate in feed stream i

V_{W_i} Vapor outflow rate in sidedraw product stream i

$d_{j,i}$ Net material upward flow rate for component j in general column section i

$f_{j,i}$ Net material inflow rate for component j in feed stream i

$w_{j,i}$ Net material outflow rate for component j in sidedraw product stream i

c Total number of components in the multicomponent system of interest

$\gamma_{j,i}$ The jth root (counted in ascending order based on their values) to Equation (5.13) for column section i

α_k Relative volatility of component k with respect to the heaviest component in the multicomponent system of interest

$\theta_{j,i}$ The jth root (counted in ascending order based on their values) to equation $\sum_{k=1}^{c} \frac{\alpha_k f_{k,i}}{\alpha_k - \theta_{j,i}} = V_{F_i}$ or $\sum_{k=1}^{c} \frac{\alpha_k w_{k,i}}{\alpha_k - \theta_{j,i}} = V_{W_i}$

$\mu_{j,i}$ Binary variable which indicates if there exists two roots to $\sum_{k=1}^{c} \frac{\alpha_k d_{k,i}}{\alpha_k - x} = V_j$ in the interval (α_j, α_{j+1}) for any $j = 1, \cdots, c-1$ in column section i

$K_{j,i}$ Binary variable defined in Equation (6.3) for column section i

F_i Total material inflow rate for feed stream i, i.e. $F_i = \sum_{j=1}^{c} f_{j,i}$

W_i Total material outflow rate for sidedraw product stream i, i.e. $W_i = \sum_{j=1}^{c} w_{j,i}$

γ^*	The root to Equation (5.13) satisfying Equation (6.1)
N_F	Total number of feed streams in the MFMP column
N_W	Total number of sidedraw product streams in the MFMP column

ABBREVIATIONS

SA	Shah and Agrawal
CTC	Completely thermally coupled
PTC	Partially thermally coupled
TC	Thermally coupled
PI	Process intensification
FTC	Fully thermally coupled
LOT	Liquid-only transfer
HMI	Heat and mass integration
HMA	Heat and mass integration with additional section
HMP	HMA between final product ends for CTC configurations
DWC	Dividing wall column
GMA	Global minimization algorithm for total reboiler vapor duty requirement of distillation configurations
GMAC	Global minimization algorithm for total cost of distillation configurations
CEPCI	Chemical Engineering Plant Cost Index
TAC	Total annualized cost
FCI	Fixed capital investment
YOC	Yearly operating cost
COM	Cost of manufacturing
TM	Total module
LMTD	Log-mean temperature difference
BARON	The Branch-And-Reduce Optimization Navigator
TMA	Two-step minimization algorithm

GMAE	Global minimization algorithm for total exergy loss of distillation configurations
HPW	Heat pump work
NGL	Natural gas liquid
NLP	Nonlinear programming
MINLP	Mixed-integer nonlinear programming
MFMP	Multi-feed, multi product
CMO	Constant molar overflow assumption
CRV	Constant relative volatility assumption
VLE	Vapor-liquid equilibrium
CR	Constant reflux
VR	Variable reflux
IR	Intermediate reboiler
IC	Intermediate condenser
FUG	Fenske-Underwood-Gilliland correlation
RHS	Right hand side

ABSTRACT

Jiang, Zheyu Ph.D., Purdue University, December 2018. Multicomponent Distillation – Mathematical Modeling, Global Optimization, and Process Intensification. Major Professor: Rakesh Agrawal.

Distillation is the most important separation process that accounts for 90–95% of all separations in the chemical industries. Even slight improvements can tremendously impact the landscape of the chemical economy world. The goal of this thesis is to develop mathematical modeling and global optimization approaches as well as systematic process intensification strategies to design and synthesize compact, easy-to-operate, energy-efficient, and cost-effective multicomponent distillation systems.

Towards this goal, we discuss the following aspects in this thesis:

1. We solve a longstanding challenge in chemical engineering of developing a short-cut method to determine the minimum reflux condition for any multi-feed, multi-product distillation column separating ideal multicomponent mixtures. The classic Underwood's method turns out to be a special case of our approach.

2. We develop the first enumeration based global optimization algorithm to identify optimal distillation configurations that can potentially save up to 50% of total cost or total exergy loss compared to conventional schemes from the immense configuration search space. For the first time in the literature, global optimality is guaranteed.

3. We propose a systematic and comprehensive multi-layer approach for process intensification in multicomponent distillation. For the first time, industrial practitioners have an easy-to-follow recipe to generate an array of completely new and attractive highly intensified configuration designs that further enhance operability, improve efficiency, and reduce total costs.

1. INTRODUCTION

1.1 Motivation

Distillation is among the oldest unit operations and has been around since the dawn of human civilization. The earliest application of distillation as a batch process to extract essential oils from herbs dates back to ∼3500 BC [1]. Since then, it remained primarily as a batch unit operation until Jean-Baptiste Cellier-Blumenthal invented the first continuously working distillation column in France and patented it in 1813 [2]. Facilitated by this hallmark of distillation, the entire world of chemical and process engineering came into a new era. Nowadays, distillation has become the single most important separation process that accounts for 90-95% of all separations and consumes more than 40% of energy in the chemical and refining industries [3]. It deals with some of world's largest and most profitable separations, such as crude oil fractionation, hydrocarbon separations from steam cracking, and natural gas liquids (NGL) separations. For instance, the United States processed over 13.1 million barrel of petroleum crude per day in the year of 2017 [4], and petroleum fractionation consumes energy at the equivalent of roughly 2% of the crude processed [5]. This works out to 0.26 million barrel per day, or equivalently 0.55 quadrillion (i.e. 10^{15}) Btu per year. In comparison, the total energy production in the United States is about 87.5 quadrillion Btu in 2017 [6]. In other words, 0.6% of energy produced in the U.S. is used for petroleum crude fractionation alone, making it one of the most energy-intensive industrial processes. Distillation is also a capital-intensive process. According to one estimate [3], there are more than 40,000 distillation columns currently in operation in the United States. Each distillation column used in refineries or commodity chemical plants can cost tens of millions of dollars to build and install. As a result, even modest improvements to the existing design and operation of distillation process have

significant impact on the overall landscape of chemical and processing industries, and ultimately, on U.S.'s energy security as well as the world's sustainability and environment.

1.2 A Single Distillation Column

A distillation column is a device that accepts heat at a higher temperature and then rejects it at a lower temperature while providing the work of separation. Essentially, distillation column offers the energy required to partially vaporize a liquid mixture as well as the locations for the resulting liquid and vapor phases to contact each other and reach thermodynamic equilibrium. Since different constituent components in the mixture have different "tendencies" to leave the liquid phase and enter the vapor phase, as thermodynamic equilibrium is established, the vapor phase is enriched in more volatile components while the liquid phase is enriched in less volatile components. In a staged distillation column, such process takes place in a number of stages or trays. Eventually, the desired separation of constituent components can be achieved, provided the distillation column has enough energy supply and sufficient number of stages. The stream enriched in more volatile components is withdrawn at the top of the distillation column as the *distillate* product, whereas the stream enriched in less volatile components is withdrawn at the bottom of the distillation column as the *bottoms* product.

A typical continuous staged distillation column is shown in Figure 1.1. In the column, the vapor and liquid phases are in continuous contact with each other on the stages. The liquid flows downward to the bottom of the column where part of it passes through a *reboiler* and gets vaporized before it is sent back to the bottom of the column. The rest of the liquid is withdrawn as bottoms product. The vapor flows upward to the top of the column where some or all of it is condensed into liquid in the *condenser*. The condensed liquid that is sent back to the distillation column is also known as *reflux*. The rest of the condensed liquid is withdrawn as distillate product. As we can see, distillation is a typical countercurrent separation process. The feed

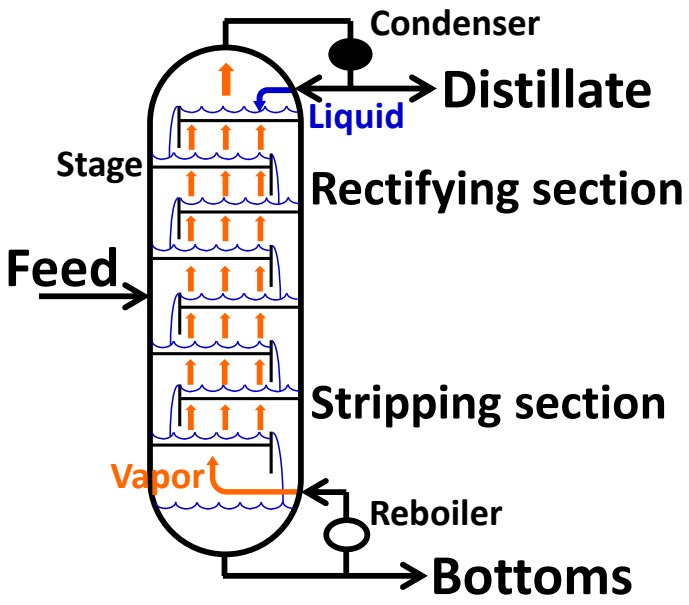

Figure 1.1. A continuous distillation column.

stream enters the distillation column somewhere in the middle, separating the column into two *column sections*. The section above the feed is known as the *rectifying section* in which the more volatile (or lighter) components are "rectified" and become more and more enriched in the material stream travelling upward compared to the feed stream composition. And the section below the feed location is known as the *stripping section* in which the lighter components are "stripped off" from the material stream flowing downward compared to the feed stream composition.

1.3 Multicomponent Distillation Configurations

A large fraction of industrial separations are performed for multicomponent mixtures containing more than two components. To separate a multicomponent mixture that contains n components into n pure products through distillation, a sequence of distillation columns known as a *distillation configuration* is generally required. As one would expect, there exists multiple distinct configurations that ultimately perform the same separation task for a multicomponent mixture. Figure 1.2 lists some of

the possible distillation configurations to separate a three-component non-azeotropic mixture ABC into three pure component streams, namely A, B, and C. In Figure 1.2 and througout the remainder of this thesis, capital letters A, B, C, and so on represent pure components with their volatilities decreasing in alphabetical order. Here, ABC could be any industrially relevant mixture such as benzene/toluene/xylene, hexane/heptane/octane, nitrogen/agron/oxygen, etc. Also, we refer to streams that are transferred between distillation columns as *submixtures* to differentiate them from the main feed and the final product streams. For instance, in Figure 1.2a, stream AB is a submixture stream.

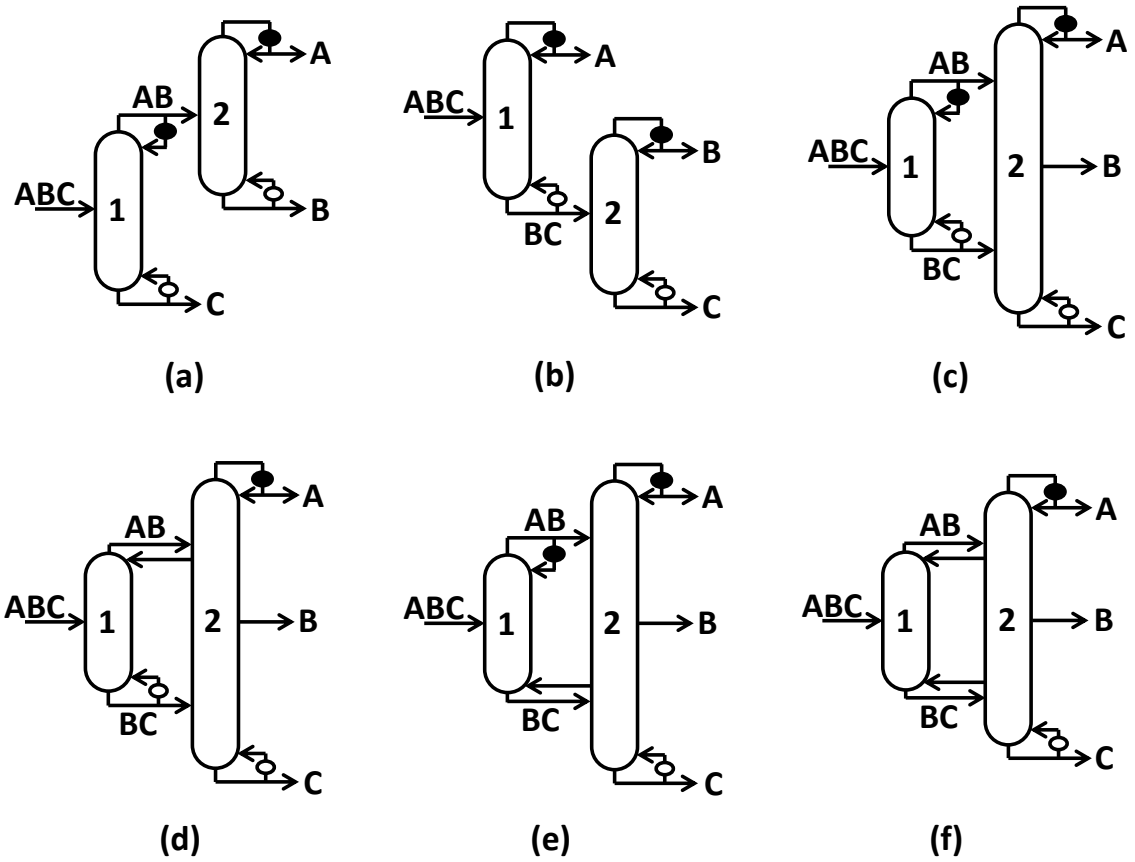

Figure 1.2. Some of the possible three-component distillation configurations. (a) to (c) draws three distinct basic configurations, whereas (d) to (f) draws all three possible thermally coupled configurations that can be derived from the basic configuration of (c).

Distillation configurations can be categorized in many ways. One way is to classify configurations based on the number of columns used, namely *regular-column* (using exactly $n-1$ columns), *sub-column* (using $< n-1$ columns), and *plus-column* (using $> n-1$ columns) *configurations* [7]. All configurations drawn in Figure 1.2 are regular-column configurations. Systematic analyses on these classes of configurations reveal that sub-column configurations can be systematically enumerated from regular-column configurations [8]. Meanwhile, the best plus-column configuration, though having more columns, could never outperform the best regular-column configuration for any given separation in terms of heat duty [9]. Therefore, the complete set of regular-column configurations is considered as the proper and reasonable choice of search space of configurations [9].

Distillation configurations can also be categorized based on the nature of split involved. A *split* is the smallest unit in a distillation configuration. It represents the separation of a mixture into two product streams. For instance, there are two splits in column 2 of the configuration of Figure 1.2c, $AB \rightarrow A/B$ and $BC \rightarrow B/C$. Sharp split produce top and bottom product streams with no overlapping components, whereas non-sharp splits produce product streams with a non-negligible amount of overlapping components. Accordingly, distillation configurations can be classified as either sharp split configurations if all their splits are sharp or non-sharp split configurations if at least one split is non-sharp [9]. In the case of Figure 1.2, the configurations of 1.2a and b are sharp split configurations, and those of 1.2c thru f are all non-sharp split configurations.

Finally, a distillation configuration can be further categorized as either *basic* or *thermally coupled* (TC). A configuration is called basic if each column has one reboiler and one condenser [10]. TC configurations can be derived from each basic configuration by replacing one or more of its intermediate heat exchangers with two-way vapor-liquid transfers known as *thermal couplings*. For example, the configurations of Figure 1.2d thru f are TC configurations derived from the basic configuration of 1.2c. Introducing thermal couplings to basic configurations rapidly expands the

search space of regular-column configurations. Among all TC configurations, one can further identify one *completely thermally coupled* (CTC) configuration in which all submixtures are placed with thermal couplings from the rest of *partially thermally coupled* (PTC) configurations. Figure 1.2f represents a CTC configuration, whereas 1.2d and e are PTC configurations.

1.4 Synthesis of Regular-Column Configurations

Identification of attractive distillation configurations for a given separation task requires complete enumeration of all possible configurations in the defined regular-column configuration search space. The first attempt to identify an optimal distillation sequence from among known sequences probably dates back to Lockhart [11]. Since then, it has become a classic process synthesis problem in chemical engineering [12] and has attracted a number of researchers over the past decades. In particular, Thompson and King [13] provided a method to generate all sharp split configurations. Sargent and Gaminibandara [14] proposed a superstructure framework to include both sharp and non-sharp split configurations, but this framework was incomplete. Agrawal [15] extended the superstructure to include the missing satellite configurations. Later, Agrawal [10] generalized the observations of a feasible basic distillation configuration into a set of rules and proposed a stepwise enumeration procedure to synthesize all basic and thermally coupled regular-column configurations. This laid the foundation for subsequent formulations proposed by Caballero and Grossmann [16], Ivakpour and Kasiri [17], and Shah and Agrawal [7]. Nevertheless, it was found by Giridhar and Agrawal [18] that this method still omits certain configurations for $\geq$ 5-component separations. To address this, they proposed a network formulation based on a set of general logical constraints that successfully enumerated all basic regular-column configurations. Finally, Shah and Agrawal [7] developed a simple and elegant six-step method to systematically generate the complete search space of all sharp and non-sharp split basic and thermally coupled regular-column configurations, which we refer to as the SA method from hereon.

Here, we briefly layout the key steps involved in the SA method, as it lays the foundation for many of the algorithms and approaches discussed in this thesis. For illustration, we focus on synthesizing distillation configurations for ternary mixture separations.

STEP 1: Based on the problem definition, identify the value of n, the number of components in the feed to be separated as pure product streams. In this case, $n = 3$.

STEP 2: Generate an $n \times n$ upper triangular matrix. Each element in the upper triangular portion uniquely corresponds to a stream that can be present in a configuration. For example, for ternary separation, all possible streams that may possibly be present in a conguration are ABC, AB, BC, A, B, and C. This is illustrated in Figure 1.3.

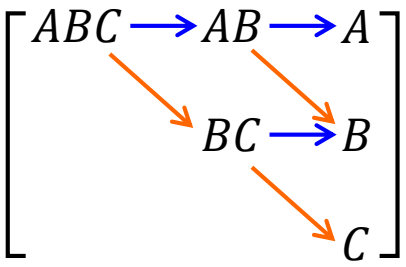

Figure 1.3. Upper triangular matrix synthesized in STEP 2 for $n = 3$. Blue arrows indicate the search directions for possible distillate products that a stream can produce, and orange arrows indicate the search directions for possible bottoms products.

As seen from Figure 1.3, if we pick any stream in the matrix, possible distillate products that this stream can produce must always lie on the horizontal path to the right of the stream. Similarly, possible bottoms products that the stream can produce must always lie on the diagonal path to the right of the stream. For example, for the main feed stream ABC, either AB or A can be produced as distillate product, and either BC or C can be produced as bottoms product.

STEP 3: Identify matrix elements corresponding to submixture streams. In any distillation configuration, the main feed stream and all final product streams are

always present. However, not all possible submixture streams have to be present in a configuration. Therefore, we need to identify the locations of submixture streams in the matrix. The main feed stream always corresponds to the $(1,1)$th element of the matrix, whereas all final product streams occupy the last column of the matrix. Therefore, the rest of the $n(n+1)/2-1-n = (n-2)(n+1)/2$ elements of the matrix correspond to submixture streams. In this case, the $(1,2)$th and $(2,2)$th elements of the matrix respectively correspond to submixtures AB and BC.

STEP 4: Generate numerical matrices that represent all permutations accounting for the presence or absence of submixture streams. If a stream is present in a distillation configuration, the corresponding numerical matrix element is assigned a value of 1. Otherwise, it is assigned a value of 0. As a result, the $(1,1)$th element as well as the n elements in the last column of the numerical matrix always take 1. On the other hand, the rest of the matrix elements symbolizing submixtures take binary values of either 0 or 1. Hence, a total of $2^{(n-2)(n+1)/2}$ distinct numerical matrices can be generated. Each numerical matrix is a candidate distillation configuration.

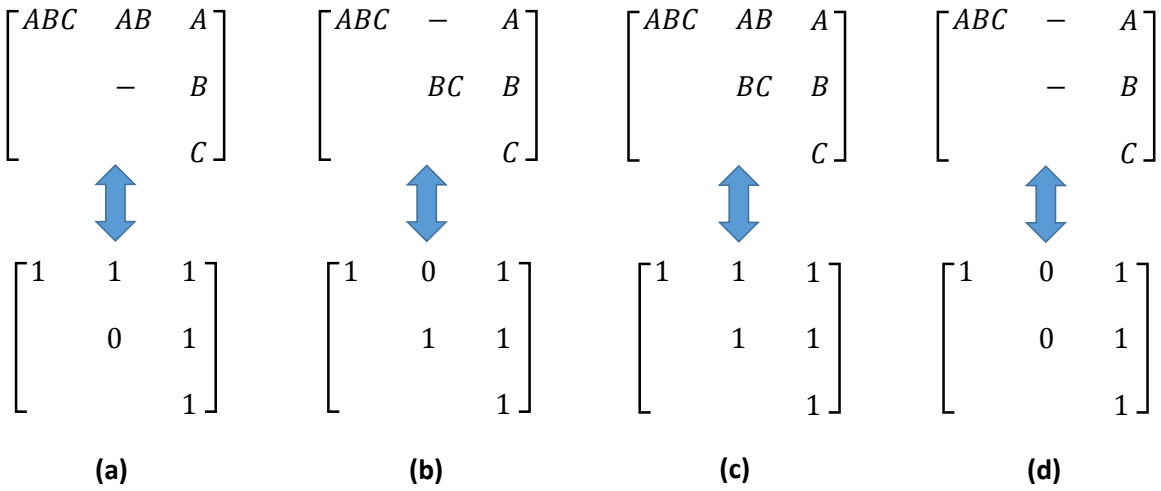

Figure 1.4. Numerical matrices synthesized in STEP 4 for $n = 3$. Each matrix corresponds to a candidate distillation configuration.

STEP 5: Eliminate infeasible configurations. Shah and Agrawal [7] provide mathematical constraints in terms of linear inequalities to ensure that only matrices corresponding to feasible basic congurations are included in the search space. These constraints essentially perform the following two checks: (1) Except the main feed stream, any stream that exists in a distillation configuration must be produced by another stream; and (2) all components that enter a distillation column must also leave the distillation column. For our example, the matrix of Figure 1.4d violates the first check as final product B is not produced by any stream. Thus, it is discarded from feasible configuration search space.

STEP 6: Finally, draw the configuration from a feasible matrix. Notice that any two splits producing a common submixture or final product stream are grouped into the same distillation column, in which the common stream is withdrawn as *sidedraw* (e.g. final product B in column 2 in the configuration of Figure 1.2c). The basic regular-column configurations drawn from the matrices of Figure 1.4a to c are shown in Figure 1.2a to c, respectively.

Once we obtain all feasible basic configurations, we can replace some of all of submixture reboilers and condensers with thermal couplings. In this example, we can synthesize a total of 5 thermally coupled configurations out of the 3 possible basic configurations. And we expect that the number of basic and thermally coupled configurations grows combinatorially with respect to the n.

1.5 Research Objective and Overview

The complete enumeration of basic and thermally coupled configurations is just the beginning towards the overall objective of designing compact, easy-to-operate, energy-efficient, and cost-effective distillation systems for separation of non-azeotropic multicomponent mixtures. This thesis is devoted to moving towards this overarching goal by analyzing this problem from a conceptual design perspective at three different levels (See Figure 1.5).

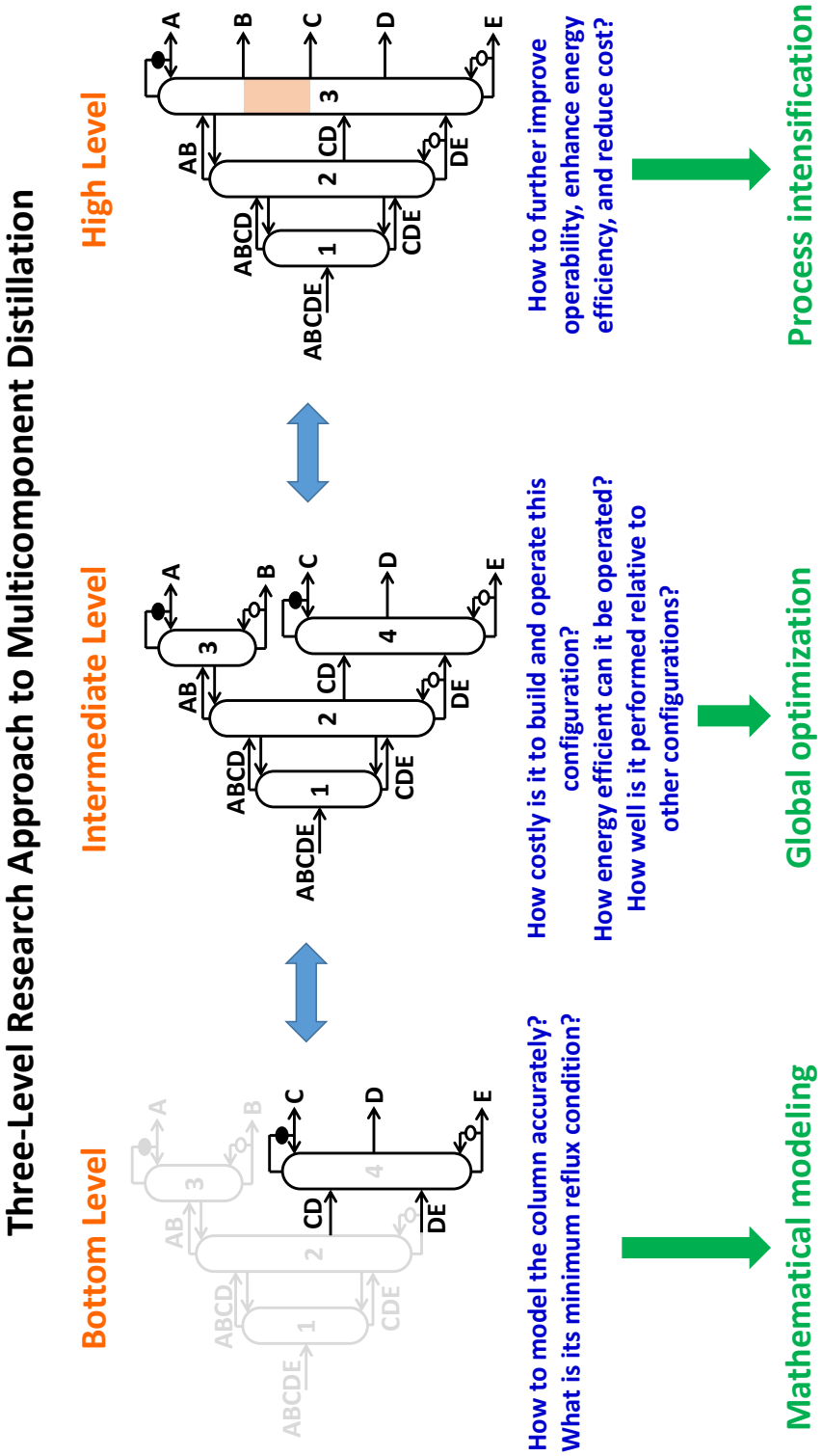

Figure 1.5. Three-level research approach.

At the bottom level, we would like to understand the mathematical principles governing the mass transfer between liquid and vapor phases that are in contact inside any single distillation column, even those containing multiple feed streams and/or one or more sidedraw streams. In particular, we want to study the underlying physical and mathematical properties of the model when a general multiple distillation column is operated at minimum reflux. Gaining such fundamental understanding about how the composition profile within a distillation column behaves is an absolute necessity and serves as the foundation to the construction of an accurate mathematical model for an entire multicomponent distillation configuration.

At the intermediate level, we will use novel mathematical programming techniques to develop the first enumeration based global optimization algorithm that can quickly and accurately identifies the optimal or a set of optimal distillation configurations from the enormous search space of possible distillation configurations for a given multicomponent separation task, based on industrially concerned objectives such as minimizing capital and operating costs as well as maximizing the thermodynamic efficiency. For the first time, industrial practitioners have a ranklist of all configurations in terms of these objectives. Using this ranklist, one can conduct further analyses, including performing rigorous process simulations on selected attractive configurations using commercially available software packages such as Aspen Plus to evaluate their actual total cost and/or thermodynamic efficiency attractiveness.

Once a subset of attractive configurations have been identified in the intermediate level, at the highest level, we can further enhance operability, improve energy efficiency, and reduce equipment size and cost of these selected configurations using novel process intensification strategies based on the newest advancements in the field of multicomponent distillation. Often, several of these strategies are used simultaneously to produce a synergistic effect.

Having introduced all three levels of tackling this research objective, we adopt a top-down research approach to organize this thesis:

Chapter 2: Process intensification in multicomponent distillation. For the first time, we propose a systematic and comprehensive multi-layer approach for process intensification in multicomponent distillation. We discuss the key elements comprised in this process intensification approach in detail, including thermally coupled distillation, multi-effect distillation, simultaneous heat and mass integration, and dividing wall columns. Equipped with this powerful methodology, industrial practitioners now have an easy-to-follow recipe to synthesize an array of completely new and highly attractive intensified multicomponent distillation system designs.

Chapters 3 and 4: Global minimization algorithm of total cost and total exergy loss of distillation configurations. We develop the first robust and efficient enumeration based global optimization algorithm to identify the optimal configuration or generate the complete ranklist of distillation configurations based on the least minimum total costs or minimum total exergy loss from the immense search space of regular-column configurations synthesized by the SA method [7]. Based on the results obtained from selected case studies, we also come up with several heuristics and insights that can help design engineers select attractive configurations that are more attractive to build and retrofit. Furthermore, we apply several novel process intensification strategies discussed in Chapter 2 in conjunction with this global optimization algorithm to generate new configurations with improved total cost and energy efficiency performances.

Chapters 5 and 6: Minimum reflux condition for multi-feed, multi-product distillation columns. We solve a 80-year challenge in chemical engineering of developing a shortcut, algebraic based method to model a general multi-feed, multi-product distillation column separating ideal or near-ideal multicomponent mixtures and to determine its minimum reflux ratio. It turns out that the classic Underwood's method [19] is just a special case of our proposed method. By providing several counterexamples, we revisited and revised several well accepted heuristics and design assumptions that industrial practitioners commonly use. Furthermore, we show that our method can be applied to understand various other industrially important applications.

Chapter 7: Reversible distillation model. We use the method developed in Chapters 5 and 6 to understand the physics and mathematics behind a distillation column in which some part of its column sections is operated at a reversible manner.

Chapter 8: Multicomponent batch distillation. To conclude this thesis, we extend the research outcomes discussed so far in continuous distillation to the area of batch distillation. In particular, we attempt to construct an accurate shortcut based model for batch distillation process using the results obtained in Chapters 5 and 6. We discuss the potential applications in which batch distillation might be a more attractive option than continuous distillation.

2. PROCESS INTENSIFICATION IN MULTICOMPONENT DISTILLATION

Process Intensification (PI) is an emerging concept in chemical engineering that describes the design innovations that lead to significant shrinkage in size and boost in efficiency of a process plant. Distillation, which is the most commonly used separation technique in the chemical industries, is a crucial component of PI. Here, we present the following systematic, multi-layer approach for peroforming PI in multicomponent distillation, including 1) Introducing thermal couplings to strategically eliminate reboilers and condensers at submixture levels to save energy and capital cost; 2) Improving operability of thermally coupled columns by converting thermal couplings to liquid-only transfer streams or by column section rearrangement; 3) Performing simultaneous heat and mass integration among thermally coupled columns to eliminate distillation columns and further reduce heat duty; and 4) Conducting any thermally coupled distillation in 1 to $n-2$ column shells using dividing wall columns that are operable. We demonstrate these aspects of PI through examples and illustrate how synergistic use of them can lead to the design of compact, easy-to-operate, energy efficient and cost effective multicomponent distillation systems.

2.1 Introduction

Different distillation configurations, while performing the same separation task, generally have very distinct capital and operating costs. Moreover, due to their structural differences, some configurations are easier to operate and control than others. These design and operational considerations naturally raise the following question: "*Given a multicomponent separation problem, which distillation configuration(s) is/are more attractive to build, operate, and/or retrofit?*" To address this central issue from a conceptual design perspective, a series of design strategies and approaches

have been developed over the past two decades. These strategies and methodologies all follow under the umbrella of "**Process Intensification** (PI)", a concept that has been in use for quite some time but has truly emerged as an important design philosophy in chemical engineering only in the past decade [20]. The idea of PI was first introduced to the chemical industry in the 1970s and has led to some of the brilliant equipment and process designs that are still being used to this day, such as the static mixer and reactive distillation process [21]. Over the past decades, PI has attracted increasingly more academic and industrial interest as a guideline for process improvements in designing new facilities as well as retrofitting existing ones to meet the increasing demands for sustainable production. However, the question remains: What really is process intensification? In the 1st International Conference on Process Intensification for the Chemical Industry in 1995, Ramshaw [22] offered one of the first definitions of PI as a strategy to reduce the size of a chemical plant by reducing the number of unit operations and equipment pieces involved. However, as pointed out by Stankiewicz and Moulijn [23], Ramshaws definition is somewhat limited in scope as it exclusively concerns with reduction of plant and/or equipment size [22]. In turn, they broadened the span of PI by redefining it as the development of new equipment and processes that significantly decrease equipment and plant size, reduce waste production, and finally result in cheaper and more sustainable production [23]. Ponce-Ortega et al. [24] and Reay [21] further expended the definition of PI to include principles such as process safety, increase in energy efficiency and production throughput, as well as reduction of inventory and the use of raw materials. All these definitions provide valuable insights to researchers and engineers in understanding what PI means for different industrial applications and scales. But in the context of multicomponent distillation, we believe that PI stands for *innovative process synthesis strategies that minimize the number of equipment pieces, reduce total cost, while boosting energy efficiency of multicomponent distillation systems.* Under this definition, the overall goal for PI is to synthesize *compact, easy-to-operate, energy efficient and cost effective distillation configurations* based on a given separation task.

In this chapter, we introduce a comprehensive, multi-layer analysis approach for PI in multicomponent distillation which is summarized in Figure 2.1. Starting from any basic regular-column configuration, we will first discuss the attractiveness of replacing some or all of submixture reboilers and/or condensers with thermal couplings in terms of energy and cost savings. This idea is carried over throughout different layers of PI and is the heart and soul of PI in multicomponent distillation. Next, we will discuss strategies to reduce or even eliminate the operational difficulties associated with conventional TC configurations, while still retaining their energy and cost benefits. These strategies are highly useful in arriving at the subsequent layers of PI. By applying these strategies, we can synthesize operable multi-effect distillation systems for multicomponent separation to significantly reduce the heat duty requirement. Meanwhile, we can also perform novel simultaneous heat and mass integration in a strategic manner for a selected subset of regular-column configurations. This leads to the discovery of a special class of intensified sub-column configurations that, for many applications, could have the lowest possible total vapor duty requirement among all configurations in the entire search space. Finally, for the first time, we are able to synthesize and build an array of hitherto unknown dividing wall columns, many of which are operable, for any basic and TC configuration. Through illustrative examples, we provide readers with a comprehensive review of the important layers of PI in multicomponent distillation. We hope that the readers could have a better understanding as well as appreciation of the great opportunities for PI in multicomponent distillation.

2.2 Energy Efficient Configurations Synthesized by Introducing Thermal Couplings

Thermal couplings are two-way liquid-vapor transfer stream between distillation columns within a configuration. Some historical examples of TC configurations include the use of a side-rectifier to recover argon in air distillation [25], and side-strippers to produce different fractions in petroleum crude distillation [5]. A sequence of TC configurations can be derived from one basic configuration by replacing some

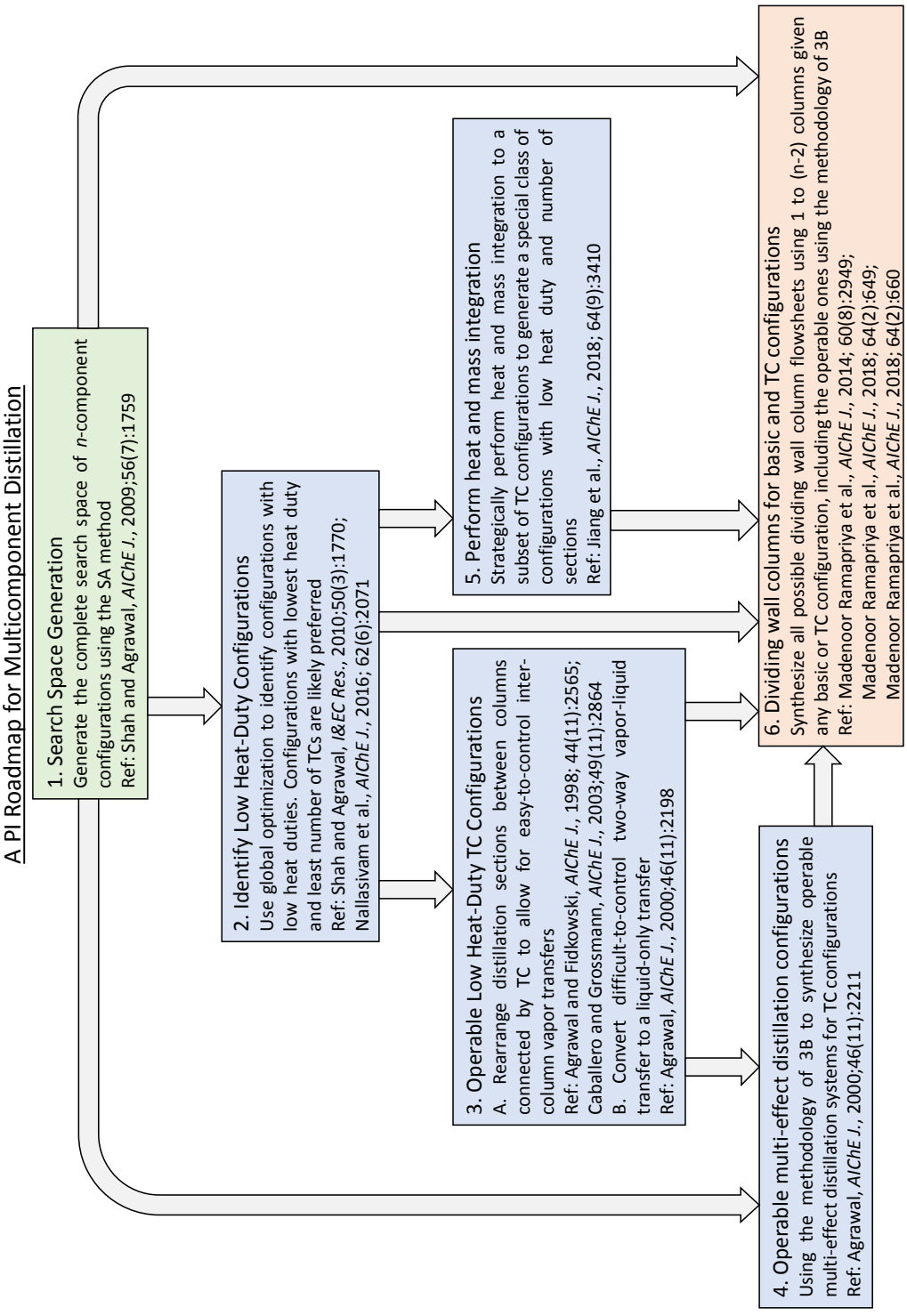

Figure 2.1. A roadmap of PI for multicomponent distillation. In this roadmap, we have listed the key references that highlight each PI strategy.

or all reboilers and/or condensers associated with intermediate transfer streams, also known as submixtures, with thermal couplings [26, 27]. While some examples of TC configurations have been known for a while, it is not until the 1980s when TC configurations started to receive more attention due to their potentials for large heat duty savings [28–32]. At the same time, the lower heat demand for a TC configuration also leads to smaller diameters for a number of column sections and overall heat exchanger sizes. Together with the elimination of reboilers and/or condensers, introducing thermal couplings generally results in lower capital investment and more compact plant being built.

Figure 2.2 shows the systematic introduction of thermal couplings to one of the 203 basic configurations synthesized by the SA method [7] for a 5-component $ABCDE$ mixture to produce five product streams, each enriched in one of the components. The configuration of Figure 2.2a is a basic configuration with no thermal coupling. Instead, it involves one-way liquid transfers of submixtures BCD, CD, and DE as well as one-way vapor transfers of submixtures $ABCD$. Starting from the basic configuration of Figure 2.2a, submixtures associated with heat exchangers can be systemically replaced by thermal couplings between distillation columns as shown in Figure 2.2b to o. Configurations of Figure 2.2b to e has one thermal coupling; configurations of Figure 2.2f to 1k has two thermal couplings; configurations of Figure 2.2l to 1o have three thermal couplings; and finally, the configuration of Figure 2.2p is completely thermally coupled (CTC), i.e. all submixture heat exchangers are replaced by thermal couplings. Overall, for this particular basic configuration of Figure 2.2a, we can derive a total of $2^4 - 1 = 15$ TC configurations, including one CTC configuration and 14 partially TC ones. These configurations have the same column and split arrangement as the basic configuration. The only difference among these configurations is the placement of thermal couplings and heat exchangers at all submixtures. Thus, they can be considered as configurations within the same family. Each family has a family tree. In this case, we can draw the family tree for a family of configurations by considering each individual configuration as the parent or child of other configurations. A child

configuration contains all the thermal couplings that the parent configuration has, plus one additional thermal coupling. As expected, each family must always have exactly one basic configuration and one CTC configuration. Also, it is worth noting that the configuration of Figure 2.2l, even though has three thermal couplings, is not the child of configuration of Figure 2.2f that has two thermal couplings.

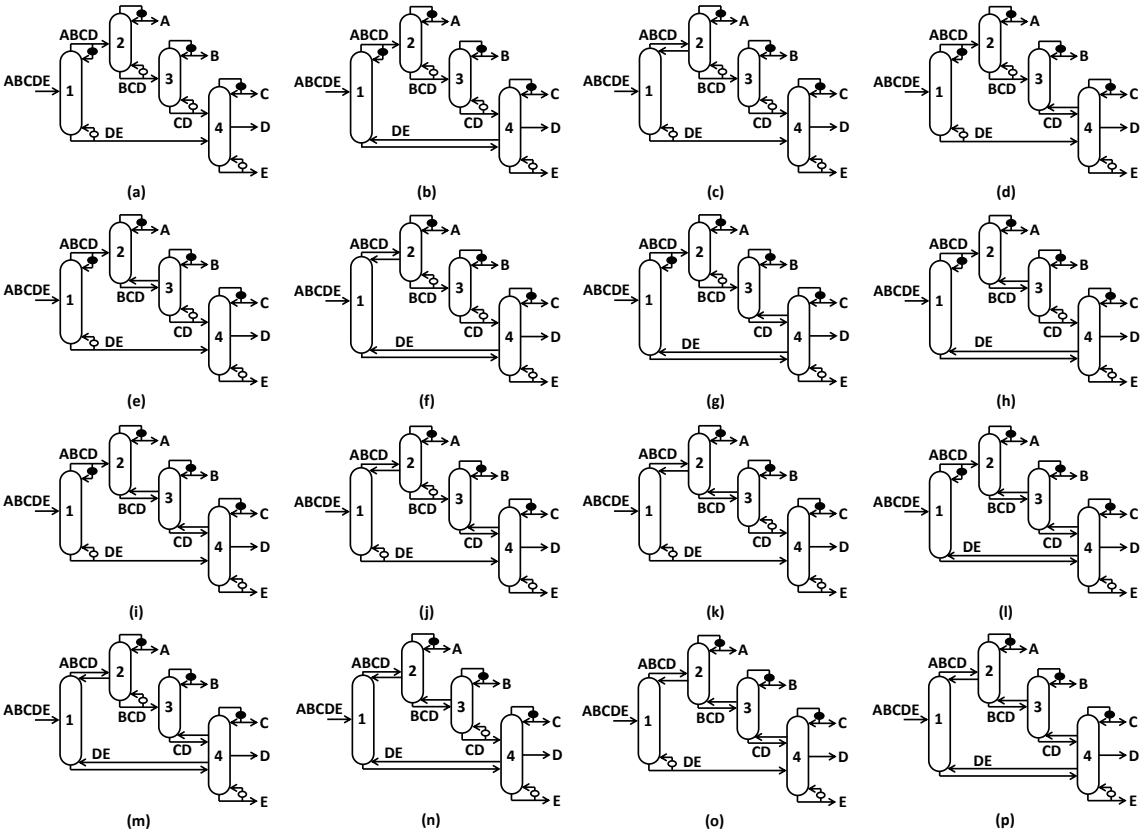

Figure 2.2. A family of regular-column configurations: (a) basic configuration with no thermal coupling; (b) to (e) configurations with one thermal coupling; (f) to (k) configurations with two thermal couplings; (l) to (o) configurations with three thermal couplings; and (p) CTC configuration with all four thermal couplings.

As the number of components in the feed increases, the number of regular-column configurations increases combinatorially, much faster than the number of basic configurations [7]. This greatly expands the of regular-column configurations search

space. Table 2.1 summarizes the enumeration results of basic and TC regular-column configurations for up to eight-component mixture separations. For instance, for a five-component feed, there exists 203 structurally distinct basic configurations and 5925 TC ones. When it comes to six-component feed, the total number of basic configurations is 4373, but the number of TC configurations explodes to 502539. The large search space of regular-column configurations certainly poses a challenge to industrial practitioners in identifying the attractive configurations for a given separation problem. As a result, there is definitely an urge for a quick and reliable screening tool that can accurately evaluate each and every configuration in the search space within reasonable amount of time [33].

Table 2.1.
Complete search space of regular-column configurations synthesized by the SA method [7]. The total number of sharp split configurations can be obtained using the closed form formula presented by Thompson and King [13].

n	**Total number of basic configurations**	**Number of sharp split basic configurations**	**Total number of TC configurations**	**Number of sharp split TC configurations**
3	3	2	5	2
4	18	5	134	15
5	203	14	5925	98
6	4373	42	502539	630
7	185421	132	85030771	4092
8	15767207	429	29006926681	27027

To evaluate these configurations, we first need an objective function that characterizes the performance of each configuration quantitatively. The operating cost of a distillation configuration relative to others is often characterized by its total vapor duty requirement, which is the sum of vapor flow generated at all reboilers per unit time at its operating condition. The minimum total reboiler vapor duty requirement, $V_{tot}^{\min}$, is thus a direct representation of a configurations first-law energy consumption, i.e. heat duty without considering the temperature level at which the heat is pro-

duced or rejected [32]. Therefore, $V_{tot}^{\min}$ is commonly used as the objective function for comparing the heat duty requirement of distillation configurations [33, 34].

Due to the combinatorial explosion in the size of regular-column configuration search space with the number of components in the feed [18], evaluating each and every configuration in the search space rigorously using process simulators such as Aspen Plus is never an easy and efficient option. Needless to mention the amount of effort required to guarantee convergence and global optimality for each and every simulation flowsheet. One almost always needs to formulate an optimization problem to consider and solve all configurations in the search space in a timely and accurate manner. Caballero and Grossmann [35] presented a superstructure based on state task network representation to synthesize all TC configurations, including the completely thermally coupled (CTC) ones. The superstructure was modelled as a generalized disjunctive program. Afterwards, Caballero and Grossmann [16] extended the superstructure to capture all basic and TC regular-column configurations. The resulting generalized disjunctive program was formulated and solved as a mixed integer nonlinear program (MINLP) to identify the configuration that minimizes the total cost. However, the MINLP could not be solved to global optimality as the local nonlinear programming (NLP) solver fails to give a feasible solution due to convergence difficulties such as singularity issues associated with disappearing column sections [35]. To account for these issues, they proposed an algorithm based on a modified version of logic-based outer-approximation algorithm. Nevertheless, they were still unable to guarantee global optimality with this approach [35].

Caballero and Grossmann [16] then introduced a two-step iterative optimization procedure to solve the MINLP by first identifying the best CTC configuration, followed by determining the best submixture heat exchanger placement for the configuration identified in the first step. These authors have also extended this solution procedure to consider heat integration [36], column section rearrangements [37], and dividing wall columns [38] in their designs. Despite the attempts to solve individual

MINLP in each step to global optimality, overall this two-step optimization procedure still does not always yield the true optimal solution.

Besides the MINLP based approach summarized above, a fundamentally different approach to identify optimal distillation configuration is to first synthesize the complete search space, followed by formulating individual optimization problem for each configuration in the search space. Inspired by this, Nallasivam et al. [34] proposed a nonlinear programming (NLP) based approach to determine $V_{tot}^{\min}$ for any configuration using Underwoods method for minimum vapor duty calculations in each column section [19]. It is shown that NLP optimization solvers such as BARON [39] guarantee global optimality for each configuration [33, 34]. Though this shortcut based algorithm uses underlying assumptions of ideal liquid-vapor equilibrium, constant relative volatility, and constant molar overflow [34], it is found that the rank-list of configurations obtained by these NLP calculations is consistent with that obtained by running rigorous Aspen Plus simulations using real thermodynamic models for zeotropic multicomponent separations [40].

We evaluate the minimum total vapor duty requirement for the family of configurations considered in Figure 2.2. For five-component separations, $2^5 - 1 = 31$ different representative feed compositions can be formulated4, depending on whether each component is rich or lean in the feed. For example, $ABcDe$ denotes that the feed is rich in components A, B, D and lean in components C and E. Lean components, if theres any, are assigned a mole fraction of 0.05 in the feed, whereas the rich components share the leftover mole fraction equally. Here, we consider the example feed condition of saturated liquid feed with feed composition of $abcDE$ (i.e. mole fractions of $A = B = C = 0.05$, $D = E = 0.425$) and flow rate of 1 kmol/s. The relative volatility set considered between each consecutive component is $\{\alpha_{AB}, \alpha_{BC}, \alpha_{CD}, \alpha_{DE}\} = \{1.1, 2.5, 1.1, 1.1\}$, in which an α value of 1.1 is a representative of difficult split and an α value of 2.5 an easy split. The results are summarized in Figure 2.3, in which the vertical axis is the normalized $V_{tot}^{\min}$ relative to the lowest vapor duty requirement among all configurations within the family. Data points a

thru p in Figure 2.3 correspond to the configurations of Figure 2.2a thru p, respectively. Combining the vapor duty results of Figure 2.3 with the configurations shown in Figure 2.2, we can easily make the following observations that can be generalized to any family of configurations.

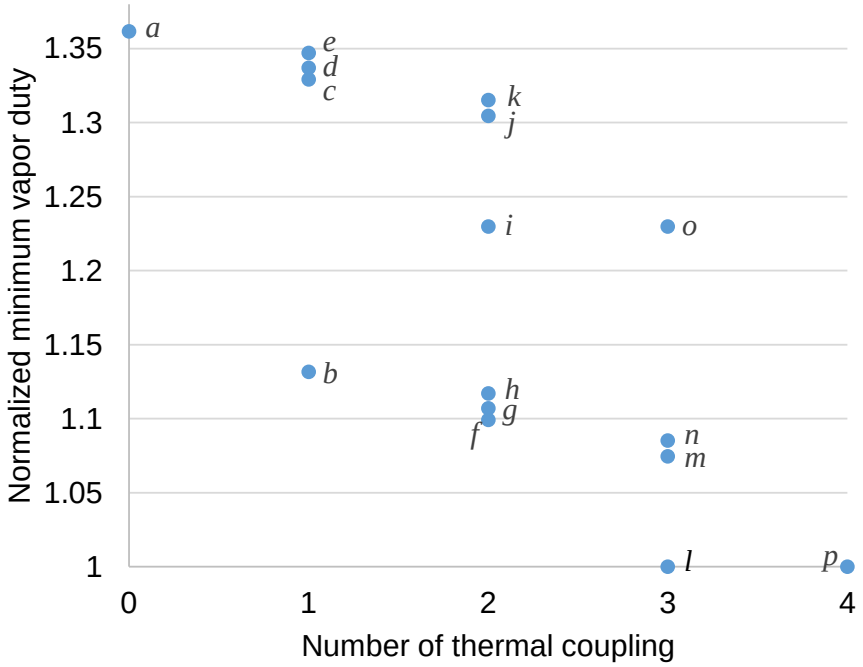

Figure 2.3. Normalized minimum vapor duty requirement of the family of configurations in Figure 2.2 with respect to the number of thermal couplings involved. This example deals with feed composition of $abcDE$ and relative volatility of $\{\alpha_{AB}, \alpha_{BC}, \alpha_{CD}, \alpha_{DE} = 1.1, 2.5, 1.1, 1.1\}$

.

First, any child configuration must always have a lower or at least the same $V_{tot}^{\min}$ compared to any of its parent configuration. In other words, $V_{tot}^{\min}$ of any child configuration is always upper bounded by the lowest $V_{tot}^{\min}$ among all its parent configurations. For example, as illustrated in Figure 2.3, the child configuration of Figure 2.2j, which consists of two thermal couplings at submixtures $ABCD$ and CD, has a lower $V_{tot}^{\min}$ than its parent configuration of either Figure 2.2c or d. The basic configuration (e.g. point a of Figure 2.3) and the CTC configuration (e.g. point p of Figure 2.3) must al-

ways respectively have the highest and lowest $V_{tot}^{\min}$ among all configurations within a family. In this example, the basic configuration requires 36.2% more minimum vapor duty than the CTC configuration.

While it is true that introducing thermal couplings to a configuration will never worsen its minimum total vapor duty, it is generally not needed to replace all submixture heat exchangers with thermal couplings to achieve the maximum vapor duty savings [41]. This guideline is concerned with a more fundamental question related to thermal coupling: "*Is it always more energy efficient to introduce more thermal couplings to a distillation configuration?*" To answer this question, it is no longer sufficient to focus merely on the absolute value of the total vapor duty requirement (first-law heat-duty savings) of the configuration. Instead, one also needs to consider the temperature levels at which the vapor duties are produced and condensed which directly affect the costs of utilities that drive the distillations. This aspect of temperature-level penalty is especially important for sub-ambient temperature distillations, heat pump assisted distillations, as well as applications in which the boiling points of the components involved are very different. In this example, the configuration of Figure 2.2l has the same $V_{tot}^{\min}$ as the CTC configuration but uses only three thermal couplings. On a similar note, the parent configuration of Figure 2.2i, which has two thermal couplings, consumes exactly the same $V_{tot}^{\min}$ as one of its child configurations of Figure 2.2o. In either case, it is not useful to include the additional thermal coupling at submixture BCD, since the total vapor duty will not improve any further and yet the utility cost is likely to increase when all the required heat duty would be generated at the reboiler of E which operates at the highest temperature level. In other words, additional thermal couplings no longer provide any additional vapor duty benefits. These extra thermal couplings should be avoided as they could incur unnecessary penalties in utility costs and thus lower the thermodynamic efficiency of the configuration [32].

On the other hand, in some cases, introducing thermal couplings to certain submixture locations of the configuration would potentially provide significant first-

law heat duty savings without bringing any penalties in utility costs. Shah and Agrawal [41] presented some heuristics to enable quick identification of such useful thermal couplings. For example, we find out that when thermal coupling is introduced to the basic configuration at submixture DE, the resulting TC configuration of Figure 2.2b requires significantly less minimum vapor duty than configurations of Figure 2.2i, j, and k that use two thermal couplings, as well as the configuration of Figure 2.2o which uses three thermal couplings. In fact, when closely examining configurations of Figure 2.2b, f, and m, which respectively correspond to the best TC configurations with exactly one, two, and three thermal couplings from Figure 2.3, we recognize that all of them have a thermal coupling at submixture DE. To understand this, notice that in column 4, the lower $DE \rightarrow D/E$ split requires significantly more vapor flow than the upper $CD \rightarrow C/D$ split, as the mass flow of component C into the column is small compared to that of component D or E. Therefore, by replacing the reboiler at sumixture DE with a thermal coupling, the excess vapor duty generated by the reboiler at E can now transfer to column 1 to facilitate the $ABCDE \rightarrow ABCD/DE$ split there. As a result, the total vapor duty requirement of the TC configuration of Figure 2.2b is greatly reduced compared to that of the basic configuration. At the same time, no additional utility cost is created. When building energy efficient distillation systems, it is always important to keep in mind the synergistic effect of strategically introducing thermal couplings to the right submixtures in order to achieve the best trade-off between maximum vapor duty savings and low utility costs.

So far, we have been analyzing configurations within one family. Now, let us back up from scrutinizing each individual configuration and compare configurations of different families. To do so, we need a common benchmark configuration for comparison. The well-known fully thermally coupled (FTC) configuration is a special CTC configuration that uses the maximum possible number of $n(n-1)$ distillation column sections and only one reboiler and one condenser [26]. As an example, the FTC configuration for five-component separation is shown in Figure 2.4. It uses a

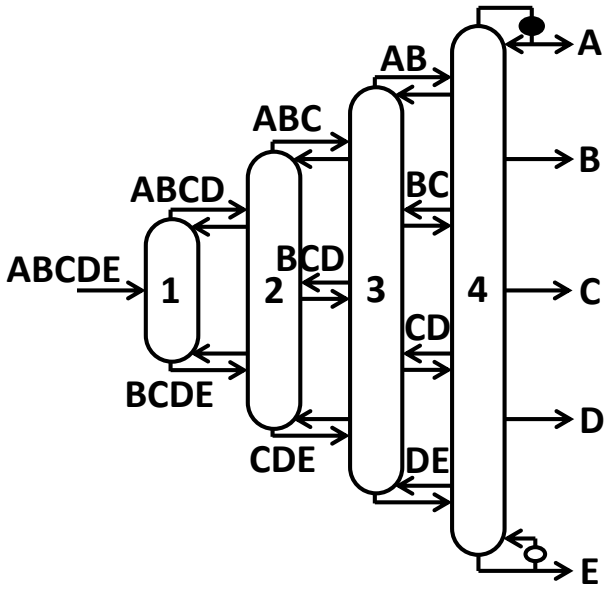

Figure 2.4. Fully thermally coupled (FTC) configuration for five-component mixture separation. Intermediate sidedraws BCD, BC, and CD are two-phase streams that allow both liquid and vapor transfers between distillation column.

total of 20 column sections, 9 submixture transfer streams, and 6 thermal couplings. For ternary and quaternary separations, it is found that the FTC configuration always preserves the lowest possible $V_{tot}^{\min}$ among all basic and TC configurations in the regular-column configuration search space [29, 31, 42]. For example, for ternary mixture separations, several studies have shown that the FTC configuration can potentially reduce the total vapor duty by 10% to 50% compared to conventional direct and indirect split configurations [43–45]. For separations involving a higher number of components, it is conjectured [31, 46] and later demonstrated [34] that the FTC configuration indeed has the maximum vapor duty benefits compared to any other configuration in the search space. Because of this, for a long time, people have believed that the FTC configuration is also more thermodynamically efficient than other configurations for most separations [44]. However, this contradicts the reality that the FTC configuration has not found a wide industrial use [47], especially for quaternary separations and above. There are many reasons why the FTC configuration

is never implemented in large scale, despite that it has been known for nearly 70 years [27]. One important reason is that the FTC configuration has the maximum possible number of column sections and submixture transfer streams, which makes it particularly expansive to build and difficult to operate [48, 49]. Nevertheless, another important reason that hinders the FTC configuration from being widely built is that, even though it requires the lowest possible heat duty, this heat is generated at the highest temperature reboiler (e.g. reboiler at E of Figure 2.4) and rejected at the lowest temperature condenser (e.g. condenser at A of Figure 2.4). Because of this, the actual thermodynamic efficiency of the FTC configuration often turns out to be significantly lower than other configurations in the search space. For ternary separation, Agrawal and Fidkowski [47] conducted thermodynamic efficiency analysis and showed that the range of feed specifications (composition and relative volatilities) in which the FTC configuration has a higher thermodynamic efficiency than other configurations is quite limited. Flores et al. [50] also reached similar conclusions when considering a set of cases involving ternary and quaternary separations.

Because of this, one may naturally start questioning him/herself: *Is the FTC configuration ever needed to be built?* To answer this question, we need to compare the FTC benchmark configuration with other configuration families. Recall the five-component separation case that we previously considered. In this case, it turns out that the partially TC configuration of Figure 2.2l, which requires the same minimum total vapor duty as the CTC configuration of Figure 2.2p, also achieves identical minimum total vapor duty as the FTC configuration of Figure 2.4. Since it uses additional reboilers and condensers that operate at intermediate temperature levels, the configuration of Figure 2.2l preserves the same vapor duty benefits of the FTC configuration while having higher thermodynamic efficiency. Furthermore, this configuration also uses only 3 thermal couplings and 10 column sections, half of what is needed for the FTC configuration. Therefore, there is for sure no need to build the FTC configuration for this specific separation task. To determine if this claim is true in general, we generate a total of 496 distinct representative feed specifications following Girid-

har and Agrawal [9] by enumerating all possible combinations of representative feed composition and relative volatility sets (31 representative compositions $\times$ 16 representative relative volatilities). We perform exhaustive NLP calculations [34] for all 496 feed cases on all 6128 configurations in the search space. From the optimization results summarized in Figure 2.5, we find out that it is almost always possible to find at least one non-FTC configuration which requires the same $V_{tot}^{\min}$ as the FTC configuration while requiring less number of column section. The FTC configuration has the lowest $V_{tot}^{\min}$ among all configurations in the search space under only 6 out of 496 feed cases (1.2%). And in 137 out of 496 cases (27.6%), the same lowest $V_{tot}^{\min}$ can be obtained from configurations with just 10 column sections, as opposed to the FTC configuration which requires 20 sections. These non-FTC configurations identified in Figure 2.5 have at least one reboiler or condenser that uses milder temperature-level utility, making them more thermodynamically efficient than the FTC configuration. Hence, for most industrial applications, we believe that, unless absolutely needed, building the FTC configuration is never the first choice; that is, it is always possible to find non-FTC substituents that require the same minimum vapor duty as the FTC configuration, yet perform superior in terms of capital investment, compactness, as well as thermodynamic efficiency. Finally, we realize that none of the sharp split configurations has the same minimum total vapor duty as the FTC configuration in any of the 496 feed cases. This result is consistent with our previous observations for four-component mixture separations that non-sharp split configurations generally have much lower heat duty than sharp split ones [9].

2.3 Strategies that Improve Operability of Thermally Coupled Columns

As we have mentioned, the operational difficulty associated with thermal couplings is one of the major reasons that impede the construction of FTC configuration for industrial uses. This is perceived to be due to the opposite directions of vapor transfer streams in two thermal couplings between two distillation columns [51]. Consider, for example, the first two columns of the five-component FTC configuration shown in

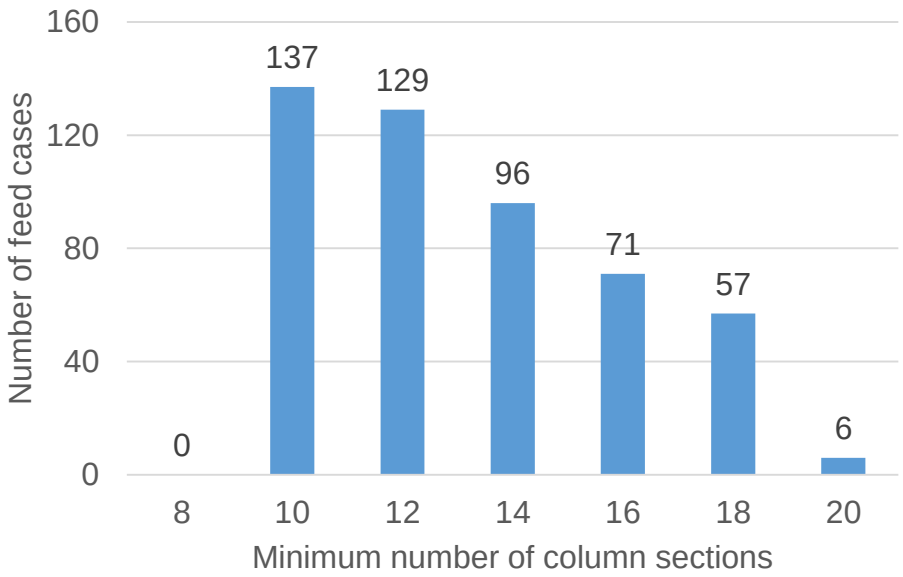

Figure 2.5. The horizontal axis shows the minimum number of column sections required for the configurations to achieve the same $V_{tot}^{\min}$ as the FTC configuration. The vertical axis shows the corresponding number of feed cases. Note that for five-component separation, sharp split configurations use $2(n-1) = 8$ column sections, whereas the FTC configuration uses $n(n-1) = 20$ sections.

Figure 2.4. The vapor stream associated with the thermal coupling at $BCDE$ has to be transferred back from column 2 to column 1, whereas the vapor stream associated with the thermal coupling at $ABCD$ is transferred from column 1 to column 2. This means neither column 1 nor 2 could have a uniformly lower or higher pressure than the other column. Careful control of the pressure profiles within both columns needs to be conducted to ensure that the pressure in the bottom of column 1 is always lower than the pressure in the bottom of column 2; whereas the pressure at the top of column 1 is always greater than the pressure at the feed point of $ABCD$ near the top of column 2. Similar controllability issues are present for subsequent columns as well. As the number of components to be separated increases, the resulting conventional FTC configuration will suffer from increasingly more difficult control and stringent

operational requirements, making it less attractive or even impossible for industrial implementations.

The operability issue associated with thermal couplings is not just limited to the FTC configuration. For any TC configuration that has two distillation columns simultaneously connected by two thermal couplings, the vapor flow direction of the top thermal coupling will always be in the opposite direction to that of the bottom thermal coupling. Unless we can figure out a way to solve the operational challenge, industrial practitioners will be concerned and reluctant to build any TC configuration. Here, we present two strategies to overcome this operational difficulty from a conceptual design perspective. The first strategy deals with rearranging column sections connected by thermal couplings to synthesize a sequence of new TC configurations, many of which are operable [37, 51–54]. Some well-known examples include the side-rectifier and side-stripper arrangement derived from the direct and indirect split configuration, respectively [55, 56]. Agrawal and Fidkowski [51] introduced the ceoncept of thermodynamically equivalent TC configurations, whereby for any thermal coupling originating from the top/bottom of one distillation column, one can first disjoint the upper/lower column section of the next column from its original location, followed by restacking it right above/below the column from which the thermal coupling is originated [52]. Through column section rearrangements, the newly generated configurations are completely thermodynamically equivalent to the original TC configuration, since all we do is to simply reconnect some of the column sections without changing the temperature profile, composition profile, and the L/V ratio for every column section.

Caballero and Grossmann [37] applied the concept of thermodynamically eqivalent TC configuration to generate the complete set of thermodynamically equivalent configurations for any given TC configuration. Consider the TC configuration shown in Figure 2.6a. This configuration has four thermal couplings at submixtures $ABCD$, CDE, AB, and DE. As a result, a total of $2^4 - 1 = 15$ thermodynamically equivalent versions can be systematically derived. In Figure 2.6b to e, we show 4 out of

these 15 thermodynamically equivalent versions that involve only one column section rearrangement. It can be easily verified that, in the original configuration of Figure 2.6a, the vapor transfer streams of thermal couplings at submixtures $ABCD$ and CDE flow in opposite directions, making it hard to control. Among the four thermodynamically equivalent versions shown in Figure 2.6, the ones of Figure 2.6c and e overcome the operational difficulty both vapor streams associated with thermal couplings $ABCD$ and CDE are now transferred unidirectionally from one column to the other. By simply maintaining the column from which the vapor streams are supplied at a slightly higher pressure than the other column, the flow of both vapor transferred can be easily regulated through a valve. At the same time, the liquid streams can be transferred through static head or liquid pumps [30].

Besides resolving the operational difficulty from a conceptual design perspective, there are two additional apparent advantages of performing column section rearrangement to TC configurations. The first advantage, as we have discussed, is due to the thermodynamic equivalence nature of these newly derived arrangements compared to the original TC configuration. Therefore, as long as we start from a TC configuration that has been identified to be energy efficient, the new equivalent versions are guaranteed to be energy efficient as well. To some extent, this strategy allows us to gain operational ease "for free" without sacrificing any heat duty benefits. The second advantage is that, through column section rearrangement, some equivalent versions may have lower capital costs compared to the original configuration if sections with similar vapor duty (i.e. similar diameter) are now stacked together. Hence, column section rearrangement might be a useful technique to any TC configurations, even the ones with no operational difficulties associated with the opposite direction of vapor flows. Again, consider the configuration of Figure 2.2f and the same case study discussed in the previous section. In this configuration, since the two thermal couplings of column 1 connect to two different columns (column 2 and column 4), column 4 can then be operated at slightly higher pressure than column 1, which is itself maintained at slightly higher pressure than column 2. No operational difficulty related to vapor

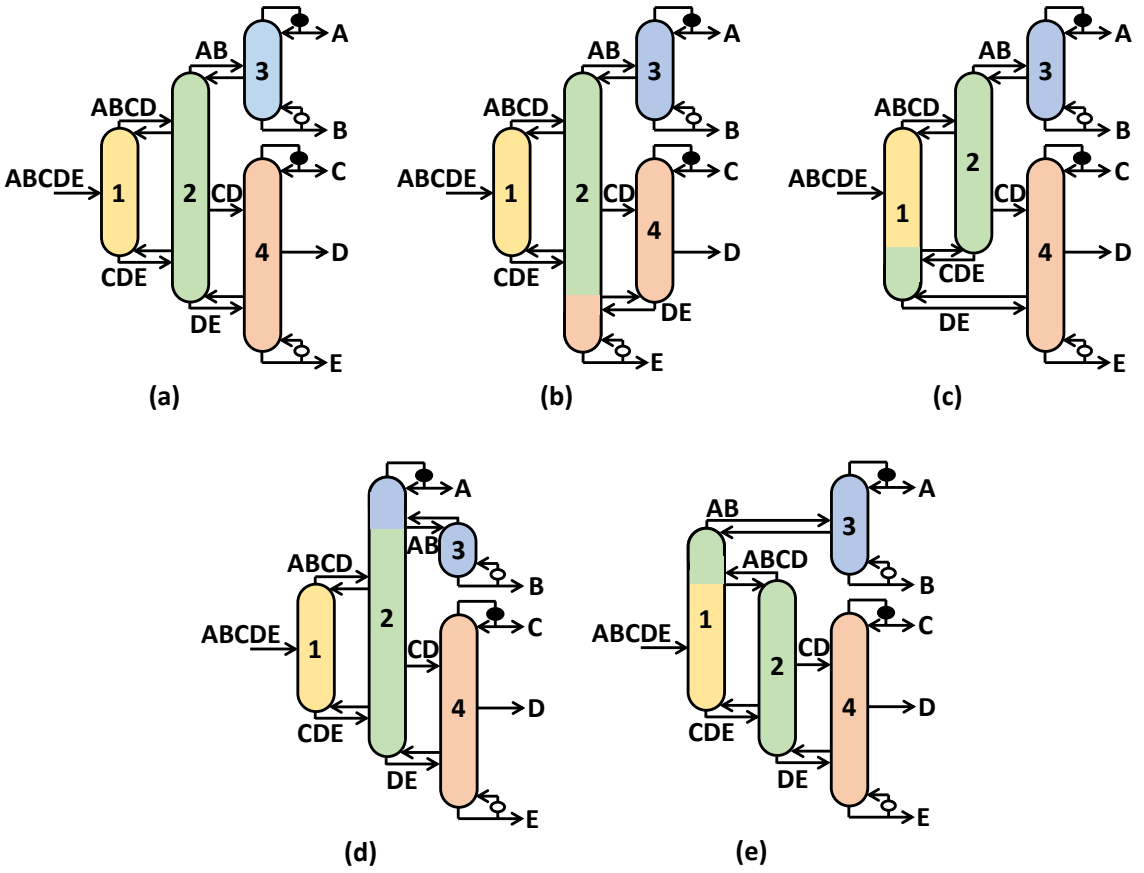

Figure 2.6. (a) A five-component CTC configuration; (b) to (e) thermodynamically equivalent versions of (a) by rearranging one column section. There are 11 more thermodynamically equivalent versions that can be further derived by rearranging more than one section simultaneously. Note that the sidedraw stream CD is withdrawn from the column 2 as saturated liquid.

transfers will be experienced. However, since most of the vapor duty generated at column 4 reboiler is transferred through thermal coupling at DE to column 1, the diameter of the original column 4 is likely to shrink above the location where DE stream is introduced, resulting in higher capital cost. By restacking the bottom section of column 4 below column 1, the resulting new arrangement is expected to be cheaper to build as the column sections are better rearranged so that the newly stacked columns have more uniform diameters.

As one might have concluded, based on the discussion so far, that the root cause of the operational challenge associated with thermal coupling comes from the vapor transfer, which is inherently more difficult to control than a liquid transfer stream. A bold but reasonable question one can then ask is: "*Is there a way to keep the energy benefit of a thermal coupling while getting rid of vapor transfer completely?*" Agrawal [57] provided a solution by introducing a strategy for converting any thermal coupling, originally as a two-way liquid-vapor transfer, into liquid-only transfer (LOT) stream. Figure 2.7 illustrates Agrawal's LOT conversion for a thermal coupling which originates at the top of a column. The procedure is quite simple and yet powerful. First, duplicate the upper part of the column (including any associated product or stream) associated with net material inflow and stack the duplicated part onto the column associated with net material outflow. After that, change the two-way liquid-vapor thermal coupling link to a LOT stream. For example, in the configuration of Figure 2.7b, a new section S4, which is a duplication of section S2 along with its associated condenser and final product X, is placed on top of section S1. The thermal coupling that connects the two columns is then converted into a LOT stream with liquid flowrate of M. Based on physical reasoning, Agrawal [57] concluded that the new configuration of Figure 2.7b would have the same overall vapor duty requirement as the original TC configuration of Figure 2.7a, and hence, is thermodynamically equivalent to the original configuration.

Madenoor Ramapriya et al. [58] presented a mathematical proof by showing that a physically feasible flowrate M in Figure 2.7b for the LOT stream must always exist such that the L/V ratio of section S4 ($\frac{L+M}{V}$) and section S2 ($\frac{L'-M}{V'}$) in the new configuration is identical. And it is also equal to the L/V ratio of section S2 ($\frac{L+L'}{V+V'}$) in the original configuration of Figure 2.7a. A similar proof can be constructed when a thermal coupling that originates from the bottom of a column is converted to a LOT stream. We can easily visualize the thermodynamic equivalence between the two arrangements of Figure 2.7 by tracing their liquid and vapor flow paths. By having a two-way liquid-vapor transfer in the TC configuration of Figure 2.7a, the vapor

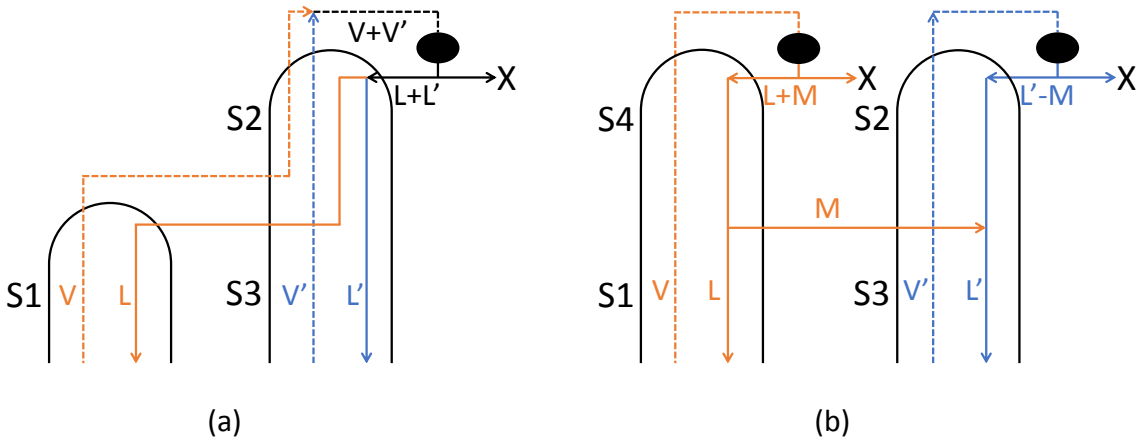

Figure 2.7. (a) A conventional TC arrangement that produces product or submixture stream X; (a) TC arrangement of (a) replaced with liquid-only transfer stream and a new section S4 on top of S1. Note that the orange curves indicate liquid and vapor flows that belong to the first column, whereas the blue curves indicate liquid and vapor flows that belong to the second column. Dashed curve represents vapor flow paths and solid line represents liquid flow path.

and liquid traffic inside section S1, combined with those in section S3, are transferred respectively to and from section 2 where the single condenser is located. In other words, when thermal coupling is in place, both the separation tasks that take place in sections S1 and in S3 are assigned to the condenser on top of section S2. However, by adding an additional section S4 on top of S1 and placing a new condenser on top of S4, we simply redirect the vapor and liquid traffic inside section S1 so that, instead of diverting them respectively to and from the next column, they now stay inside the same column. By doing so, the new section S4 and the condenser on top of it are used exclusively for the separation inside section S1. This also enables section S2 as well as the condenser on top it to focus entirely on its own separation task inside S3. The configuration of Figure 2.7b requires the same total vapor duty as the original TC configuration by manipulating flowrate M for the LOT, which can be easily accomplished using a valve. At the same time, the additional condenser on top

of S4 also gives extra controllability to the configuration of Figure 2.7b. Therefore, this approach successfully solves the operational difficulty associated with thermal coupling and allows us to come up with a sequence of operable designs that are thermodynamically equivalent to the TC configuration that we start with.

In Figure 2.8, we draw some of the equivalent configurations derived from the configuration of Figure 2.6a. Note from Figure 2.8 that the operational benefit associated with each conversion of a thermal coupling to one-way LOT comes with a price of an additional column section and a heat exchanger. However, the number of heat exchangers can be reduced by collecting the overhead vapor/bottom liquid streams that produce the same product and sending them to a common condenser/reboiler containing separate passages. Each passage is designed with a tailored active heat transfer area to match the approach temperature required for condensing/vaporizing the associated vapor/liquid stream [59]. The overall active heat transfer area of the common heat exchanger will be similar to the sum of active heat transfer areas for all individual exchangers, as the overall total vapor duty requirement remains the same.

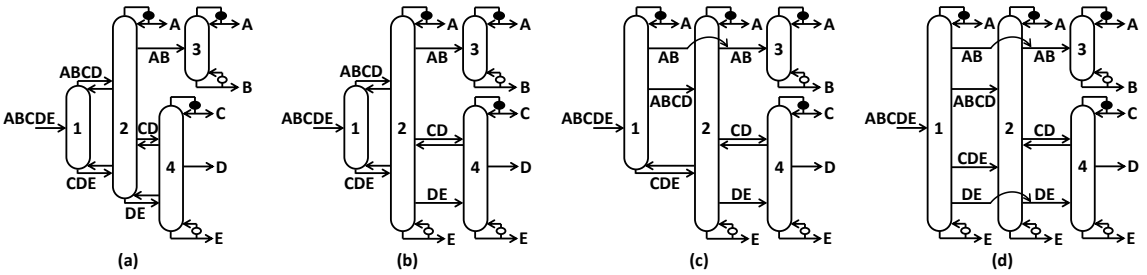

Figure 2.8. (a) Equivalent configuration of Figure 2.6a by replacing thermal coupling at submixture AB with LOT stream; (b) equivalent configuration with LOT streams at submixtures AB and DE; (c) equivalent configuration with LOT streams at submixtures $ABCD$, AB and DE; (d) equivalent configuration with LOT streams at submixtures $ABCD$, CDE, AB and DE.

The Agrawal's LOT method [57], apart from offering operability convenience, provides additional benefits: (i) reduction in heat duty due to thermal coupling be-

comes clear; (ii) double-effect and multi-effect distillations for TC columns, in order to further reduce heat duty, become feasible; and (iii) new dividing wall column configurations including those which are more operable can be drawn. To understand (i), first consider the conventional arrangement of Figure 2.8a where the submixture stream produced as the top product of column 1 is associated with a condenser. This submixture is fed to column 2 as saturated vapor stream. And the liquid reflux of column 1 is generated by condensing part of its overhead vapor. In column 2, final pure product X is produced by condensing all the vapor coming from the vapor feed as well as the vapor flow below the feed point in the column. In contrast, as we can see from the LOT arrangement of Figure 2.9b that is thermodynamically equivalent to having a thermal coupling at the submixture, the condenser C1 of column 1 now participates in distilling a portion of the pure product stream X, i.e. sharing part of this separation task originally belonging to C2 as shown in Figure 2.9a. Meanwhile, condenser C1 in the LOT arrangement also provides the liquid reflux required for column 1. This suggests that, if the split associated with the top of column 2 is critical and controls the overall vapor duty requirement in the column, then the condensing duty of C2 of Figure 2.9b is less than that of Figure 2.9a. This leads to an overall reduction in heat duty of the entire LOT arrangement of Figure 2.9b (i.e. the TC configuration) compared to the basic configuration of Figure 2.9a. In this case, placing the condenser C1 at submixture location lowers the separation efficiency by unnecessarily condensing part of the overhead vapor in column 1. Such inefficiency in the basic configuration of Figure 2.9a is generally manifested in the literature through the discussion of so-called "remixing losses" caused by thermodynamic irreversibility when a single-phase submixture stream enters column 2 [60, 61].

Up till this stage, we have been discussing the advantages of building TC configurations over conventional basic configurations as well as addressing the operational issues associated with traditional thermal couplings through innovative PI strategies. These approaches and insights related to thermal couplings, when combined with other existing PI strategies such as multi-effect distillation, simultaneous heat and

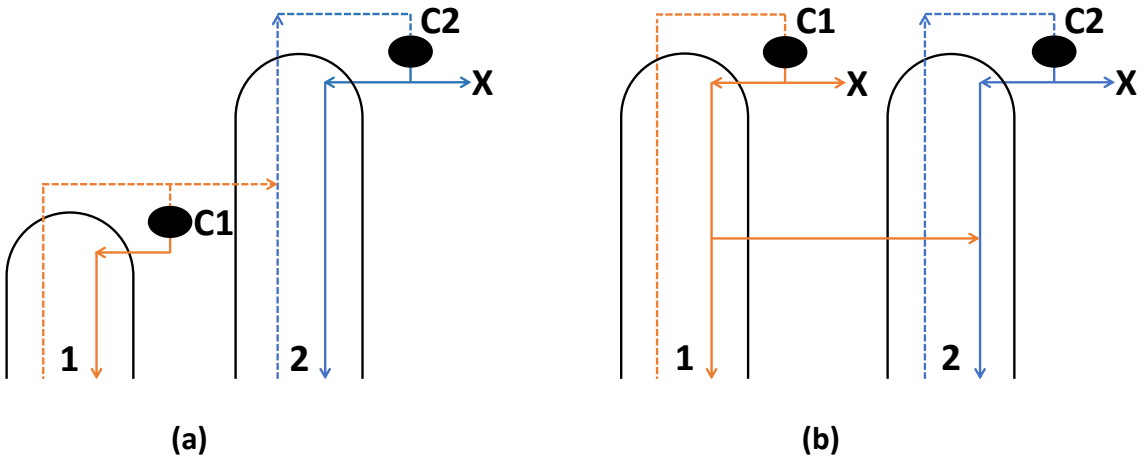

Figure 2.9. (a) The distillate stream of column 1 is associated with condenser C1 and transferred as saturated vapor to column 2 where the final pure product X is produced by condenser C2; (b) the LOT arrangement of TC column of Figure 2.7a. Both condensers produce final pure product X.

mass integration, and dividing wall columns, can create an amazing array of synergistic possibilities that produces numerous attractive distillation configurations that were hitherto unknown to us before. The remaining discussions of this chapter will be devoted to describing these combinations.

2.4 Energy Efficient, Operable Multi-Effect Distillation for Thermally Coupled Configurations

One of the first and direct applications of all PI strategies discussed earlier is the synthesis of energy efficient and operable multi-effect distillation systems for TC configurations. Multi-effect distillation, which involves distillation columns operating at different pressures, performs various heat integrations between the condenser associated with a higher-pressure column and reboiler at a lower-pressure column. Through heat integration, the overall heat usage of the distillation system can be significantly reduced. Wankat [62] performed detailed calculations for a series of double- and

multi-effect distillation configurations for binary mixtures and concluded that these configurations could lead to significant heat duty savings with only a modest increase in capital cost. For ternary separations, Cheng and Luyben [63] found that double-effect configurations derived from conventional basic direct-split, indirect-split, and prefractionator schemes could result in 20-45% decrease of heat duty requirement. Although the overall savings of heat duty depend on the feed composition and relative volatilities as well as the operating conditions for both columns, double-effect distillation has the potential to reduce heat duty up to 50% over basic configurations [64, 65]. Several control studies also showed that these double-effect versions of basic configurations could be quite operable [66, 67].

Moreover, a number of parametric analyses [45, 68, 69] demonstrate that double-effect systems for basic configurations outperform the best TC configuration in almost all feed conditions. These results are striking given the fact that TC configurations already consume significant less heat duty than the basic configurations. It makes people naturally wonder if it is possible to introduce multi-effect distillation to TC configurations to achieve even greater heat duty savings. Following the conventional procedure to draw the double-effect version from a basic configuration, an initial attempt [64] to draw double-effect configuration is shown in Figure 2.10b for the ternary FTC configuration of Figure 2.10a, which is an operable thermodynamically equivalent version of the Petlyuk column [26] and can be easily synthesized by using Agrawal's method of column section rearrangement described earlier [30]. In this double-effect configuration, the vapor streams of thermal couplings AB and BC are first compressed and then sent to the high-pressure column 2, whereas the liquid streams of both thermal couplings are transferred from the high-pressure column 2 to low-pressure column 1. There is no reboiler or condenser in this configuration to generate vapor or liquid externally, which introduces a difficult challenge for column startup. Specifically, since the high-pressure column 2 has no external source for vapor generation, all the vapor duty required for column 2 must be supplied by the vapor streams from the low-pressure column 1 via thermally couplings. But

at the same time, the vapor duty for column 1 is in turn generated by the heat obtained from condensing the vapor from the top of the column 2. This endless-loop type scenario makes the startup and operation of such a double-effect configuration especially challenging. To build multi-effect configurations for TC separations that are operable, it will be desirable to include external heating and cooling utilities for distillation instead of relying solely on the vapor and liquid flows transferred via thermal couplings.

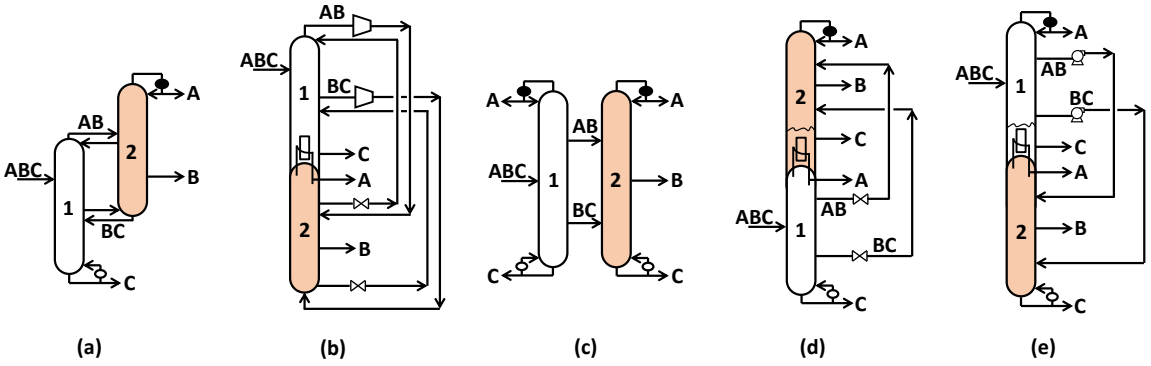

Figure 2.10. (a) Ternary FTC configuration; (b) initial attempt to draw a double-effect configuration from (a); (c) equivalent configuration of (a) by converting all thermal couplings to LOT streams; (d) operable double-effect configuration using forward heat integration [64]; (e) operable double-effect configuration using reverse heat integration.

Agrawal [64] introduced the conversion of thermal coupling to LOT stream by adding a heat exchanger as the right tool to solve this operability issue and his method will now be illustrated through Figure 2.10. Figure 2.10c with LOTs is one of the equivalent configurations of the FTC configuration of Figure 2.10a. It has a reboiler and a condenser in each column, making it similar to a basic configuration from process control perspective. From this equivalent configuration, we can then draw the corresponding double-effect system in which the overhead vapor of one column is heat integrated with bottoms liquid of the other column. This double-effect configuration

will be fully operable. Two possible operable double-effect configurations, one with forward heat integration (feed enters the high-pressure column) and the other with reverse heat integration (feed enters the low-pressure column), are shown in Figure 2.10d and e. In comparison with the initial drawing of the double-effect configuration in Figure 2.10b, these new configurations produce pure products A and C from both columns. Each column has either a condenser or a reboiler, making the startup and operation of the double-effect configuration much easier.

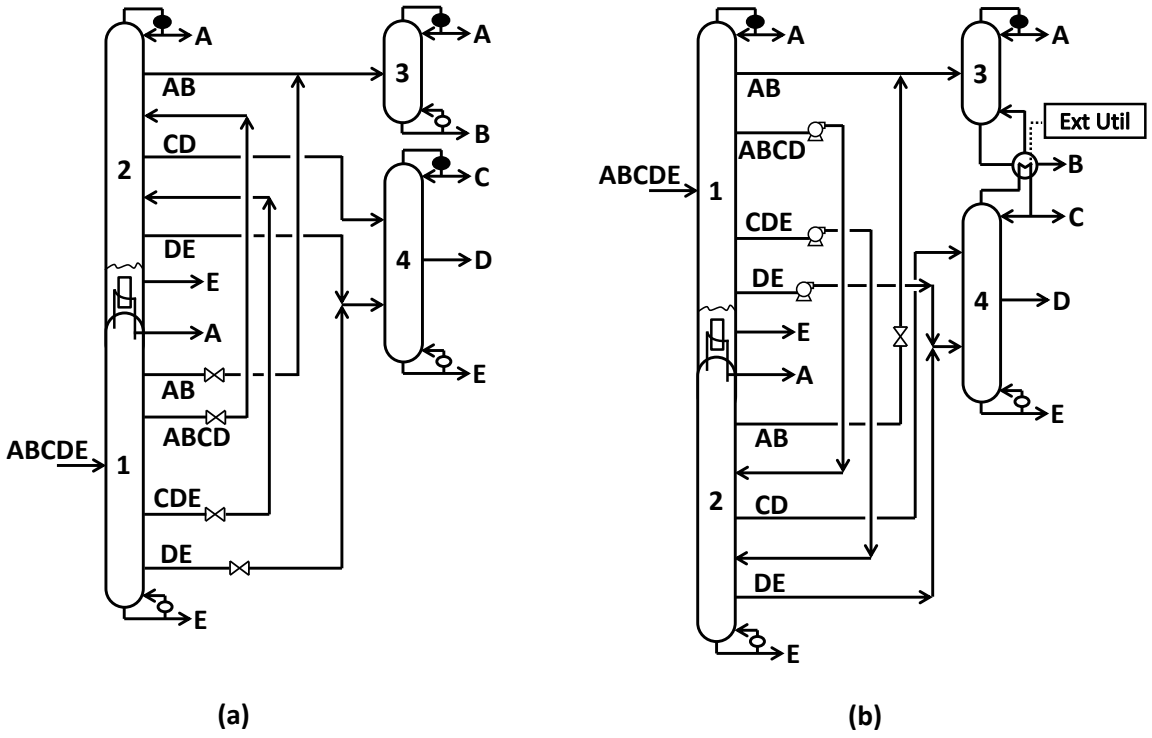

Figure 2.11. (a) Operable double-effect configuration with forward heat integration between column 1 and column 2 for the configuration of Figure 2.10d; (b) operable double-effect configuration with reverse heat integration between column 1 and column 2, with column 3 and column 4 being heat integrated (external heating or cooling utilities may be needed).

As another example, we examine some of the possible double- and multi-effect arrangements for the configuration of Figure 2.8d, which we recall is an equivalent

configuration of Figure 2.5a. With a total of four columns, many operable double-effect arrangements are possible. For instance, any two of these four distillation columns can be heat integrated through double-effect. The other two columns can be either be or themselves double-effect heat integrated. For each combination of these columns, there are again two possible schemes: forward heat integration or reverse heat integration. Alternatively, any three of the four columns or all the four columns can be multi-effect heat integrated by creating operating the distillation columns at three or four different pressures, respectively. All these arrangements are operable. Figure 2.11 shows two possible double-effect configuration designs. In the first configuration of Figure 2.11a, double-effect forward heat integration takes place between the top of the column 1 and bottom of column 2. Columns 3 and 4 can be operated at any suitable pressure. In the second configuration of Figure 2.11b, we present a double-effect configuration with reverse heat integration between the top of column 2 and the feed column. Note that in this configuration, columns 3 and 4 is heat integrated without creating any pressure difference, since the pure product B produced at the bottom of column 3 is lighter than the pure product C produced at the top of column 4. As a result, there is sufficient temperature gradient allowing for heat integration between column 3 and column 4, which reduces the overall heat duty and increases energy efficiency even further. We will discuss this specific type of distillation configurations in detail in the context of simultaneous heat and mass integration in the next section.

It is worth noting per our earlier discussion that one generally will not need all four thermal couplings shown in Figure 2.6a in order to achieve the maximum heat duty benefit. For a given feed to be separated, it is very likely that most, if not all, of the heat duty benefit can be achieved with one or two thermal couplings. This means that the number of LOTs between columns 1 and 2, in an optimaized version of the configuration of Figure 2.11a or b, will be substantially lower than the ones currently shown in Figure 2.11 and will contribute towards attractiveness of the configuration. In conclusion, the PI strategy of converting thermal coupling to liquid-only transfer

stream opens up a window of new operable multi-effect distillation opportunities for TC configurations.

A word of caution towards finding the lowest heat-duty multi-effect configuration with low heat duty, once a lowest heat duty subset of regular-column configurations with or without thermal couplings, have been identified through global optimization, it is not guaranteed that their multi-effect versions will yield the lowest heat-duty multi-effect options. Reduction in heat duty, when two columns are integrated through a double effect, depends on how close the heat duties are for each of the columns prior to and after the integration. When the two columns have nearly equal heat duty requirements, a potential reduction of 50% could be realized. Thus, one can envision a scenario where a configuration has an overall higher heat duty but due to better matching between the heat duties of the columns, leads to lowest heat duty subsequent to multi-effect integration. This calls for an independent optimization of the multi-effect configurations.

2.5 Attractive Thermally Coupled Configurations Synthesized by Novel Heat and Mass Integration Strategy

Heat and mass integration (HMI) to consolidate distillation columns in a configuration is mostly known as simultaneous elimination of a reboiler and a condenser producing the same final product streams or submixtures. HMI of this kind has been commonly used to synthesize regular-column configurations [8, 9, 14, 15, 17, 35, 70]. However, HMI is not just limited to removing reboilers and condensers associated with the same final products or intermediate streams. For example, in the 4-component basic sharp split configuration shown in Figure 2.12a, the bottom product B produced at column 2 is lighter than the top product C produced at column 3. Therefore, instead of using two independent columns, we can consolidate columns 2 and 3 to form a single column 2-3, as drawn in Figure 2.12b, in which the vapor generated at the reboiler of D and the liquid produced by the condenser at A now respectively provide the vapor and liquid flow needed for both $AB \rightarrow A/B$ and $CD \rightarrow C/D$

splits. The resulting configuration, first synthesized by Brugma [71], can reduce the overall heat duty significantly. Further, with the expense of an additional column section in column 2-3, the Brugma configuration simultaneously eliminates the use of one distillation column, a reboiler that originally produces product B, and a condenser that originally produces product C. Both final product streams B and C are now withdrawn from column 2-3 as liquid sidedraws. Such HMI achieved by means of an additional section is referred to as heat and mass integration with additional section, or simply HMA [72]. The additional section is called the HMA-section and is provided with enough stages to allow smooth heat and mass transfer between the ascending vapor from the lower part and descending liquid from the upper part of the column [8]. The resulting capital and operating costs reduction due to HMA makes it attractive for industrial applications.

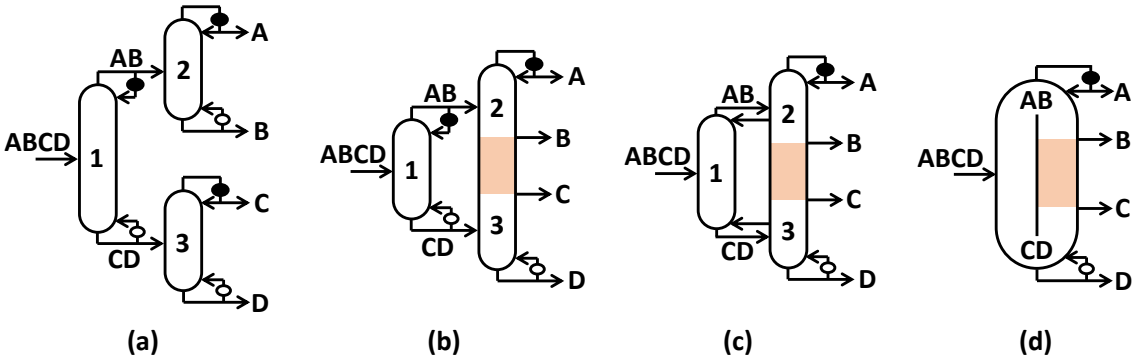

Figure 2.12. (a) A 4-component basic sharp split configuration; (b) the Brugma configuration [71]; (c) the Cahn and Di Miceli configuration [73]; (d) the Kaibel column [53].

According to generalization of Brugma's concept [71] by Madenoor Ramapriya et al. [72], HMA can be introduced between any two distillation columns as long as the bubble point of the liquid stream leaving the condenser to be eliminated is higher than the dew point of the vapor stream leaving the reboiler to be eliminated, since it guarantees the required approach temperature for heat transfer to happen. It suggests that, in theory, HMA can take place between any two distillation columns

if one column produces a less volatile top final product/submixture stream whereas the other column produces a more volatile bottom final product/submixture stream. Thus, systematic enumeration of all HMA opportunities can generate numerous new HMA configurations [72]. For example, for the basic configuration of Figure 2.13a, the reboilers associated with submixture BC and/or final product C can be heat and mass integrated with condensers associated with submixture DE and/or final product D. This leads to a total of six possible combinations of HMA arrangements. In addition, for each of the six HMA configurations synthesized, one can further draw its TC derivatives. Two of the thermally coupled HMA configurations are illustrated in Figure 2.13b and c. Additional thermodynamically equivalent HMA configurations can also be generated by Agrawal's method to convert some of the thermal couplings to LOT streams [57]. For instance, consider a new HMA configuration [74] drawn in Figure 2.13e, which is thermodynamically equivalent to the HMA configurations of Figure 2.13b and c. This HMA configuration is obtained from the CTC version of Figure 2.13a by first converting thermal couplings at BC and DE with LOTs, as shown in Figure 2.13d, followed by performing two HMAs between columns 2 and 3 as well as between columns 4 and 5. Notice that final product streams C and D are now withdrawn from the resulting configuration of Figure 2.13e as liquid sidedraws from two different consolidated columns. This technique, also known as "strategic side-stream withdrawal", is first discovered by Shenvi et al. [8] as a new way to further reduce the heat duty of a slightly modified version of Figure 2.13c by making streams BC and DE as liquid sidedraws instead of two-way liquid-vapor transfers. It is now clear that this heat duty reduction is really attributed to the combined effect of thermal coupling and heat integration. This also verifies the observation made by Shenvi et al. [8] that pure C and D can be produced as sidedraws in the consolidated column 2-3.

Although HMA can potentially reduce the overall heat duty, it may lead to higher utility costs since the reboiler and condenser operated at intermediate temperature levels are simultaneous eliminated due to HMA. To minimize the utility costs, one

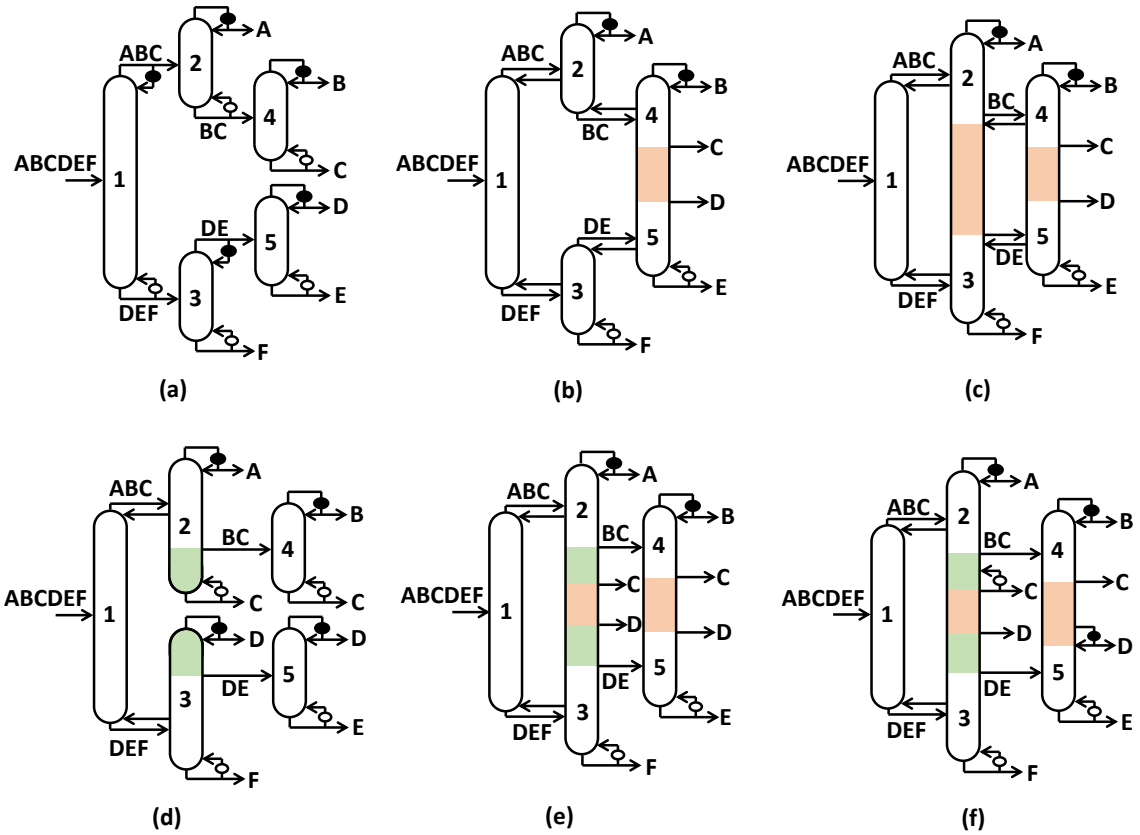

Figure 2.13. (a) A 6-component basic configuration; (b) the HMP configuration derived from (a) by coupling reboiler at C with condenser at D; (c) another thermally coupled HMA configuration derived by coupling reboilers BC and C with condensers DE and D, respectively; (d) thermodynamically equivalent configuration of the CTC version of (a) with LOTs; (e) a HMA configuration derived from (d) containing two HMAs. This configuration is thermodynamically equivalent to the HMP configuration of (b), but has more column sections and sidedraws; (f) same configuration of (e) with an intermediate reboiler at C in column 2-3 and an intermediate condenser at D in column 4-5 to reduce the temperature-level penalty when $ABC \rightarrow A/BC$ split requires more heat duty than $DEF \rightarrow DE/F$ split in column 2-3, and $DE \rightarrow D/E$ split requires more heat duty than $BC \rightarrow B/C$ split in column 4-5.

can introduce intermediate reboiler/condenser at appropriate locations of the consolidated column [8,72]. Suppose, for the HMA configuration of Figure 2.13e, the upper

$ABC \rightarrow A/BC$ split is more energy intensive than the lower $DEF \rightarrow DE/F$ split in column 2-3, while the lower $DE \rightarrow D/E$ split is more energy intensive than the upper $BC \rightarrow B/C$ split in column 4-5. Then, for column 2-3, instead of generating all the required heat for both splits at the reboiler of F which operates at the highest possible temperature level, an intermediate reboiler can be placed at sidedraw product C to generate the extra heat duty needed for the upper $ABC \rightarrow A/BC$ split. Similarly, for column 4-5, instead of rejecting all the heat at the condenser of B, an intermediate condenser can be placed at sidedraw product D to condense the excess vapor from the lower $DE \rightarrow D/E$ split. *The key message is that, starting from a basic configuration, the concept of HMA, especially when combined with other PI strategies, can lead to numerous new and potentially attractive HMA configurations.*

Among all the new HMA configurations synthesized from the basic configuration of Figure 2.13a, it can be seen that the one which always has the lowest overall heat duty requirement and meanwhile has the highest degree of structural simplicity is shown in Figure 2.13b. For example, this configuration, which is thermodynamically equivalent to the HMA configurations of Figure 2.13c and e that respectively require 12 and 14 column sections to build, only uses 11 column sections. Such HMA configurations of Figure 2.13b share the unique feature of the existence of a thermal coupling at every submixture and HMA only between pure component products. By virtue of this feature, Jiang et al. [74] have shown that such a configuration minimizes the remixing losses caused by thermodynamic irreversibility among all possible HMA configurations synthesized from a basic configuration. Thus, for each basic configuration synthesized by the SA method [7], we can quickly check if there simultaneously exists any reboiler that produces a pure component product which is more volatile than any final pure component product produced from a condenser. If so, HMA at submixture level is not required for this configuration to achieve the maximum heat duty savings. Instead, delaying HMA until the final product ends followed by introducing complete thermal coupling to replace all submixture heat exchangers can lead to a new, energy efficient HMA configuration which we refer to as the **HMP configuration** whose

name highlights the aspect that HMA is only introduced between two final product streams [74].

Table 2.2.
The number of basic configurations that are candidates for HMP and the number of HMP configurations for up to 6-component separation (Source: Jiang et al. [74])

n	**Total number of basic configurations**	**Total number of basic configuration candidates for HMP**	**Number of sharp split basic configuration candidates for HMP**	**Total number of possible HMP configurations**
4	18	1	1	1
5	203	15	6	17
6	4373	282	26	347

Table 2.2 summarizes the enumeration results of HMP configurations for up to six-component mixture separations [74]. The second and third column of Table 2.2 list the total number of basic configurations and the subset of basic configuration identified as HMP candidates, respectively. For four-component system, there exists one and only one candidate basic configuration shown in Figure 2.12a that can undergo HMP. The resulting HMP configuration of Figure 2.12c is readily derived from the Brugma configuration by introducing complete thermal coupling to submixture AB and CD, and is also known as the Cahn and Di Miceli configuration [73]. For five-component system, all 15 basic configurations that are candidates for HMP have been explicitly drawn by Jiang et al. [74]. It is worth noting that some basic configuration candidate can lead to more than one HMP configurations. This multiplicity has been accounted for as listed in the last column of Table 2.2. The fourth column of Table 2.2 specifies the number of sharp split basic configuration candidates for HMP. These values are consistent with the results derived by Rong et al. [70] who only investigate sharp split HMP configurations. As we can see, the subset of sharp split HMP configurations constitutes a continually shrinking fraction of the set formed by all HMP configurations.

Among all possible HMA arrangements for a basic configuration, the HMP configuration features the principles of PI the most since it exhibits the maximum heat duty savings due to both thermal coupling and HMA and also has the simplest structure to build. Through several case studies of five-component separations, Jiang et al. [74] quantify the magnitude of potential heat duty savings for the first time by introducing HMP to basic configuration candidates. They show that many HMP configurations can often even have the same $V_{tot}^{\min}$ as the FTC configuration of Figure 2.4, which as mentioned before always yields the lowest minimum total vapor duty requirement among all configurations in the search space [29,31,34,42]. For example, consider the CTC configuration of Figure 2.6a from which one of the 17 HMP configurations for five-component separations, as shown in Figure 2.14a, can be directly synthesized by consolidating column 3 and column 4. This HMP configuration uses 3 columns, 13 column sections, 5 submixtures, and 4 thermal couplings, as opposed to having 4 columns, 20 sections, 9 submixture, and 6 thermal couplings for the FTC configuration of Figure 2.4.

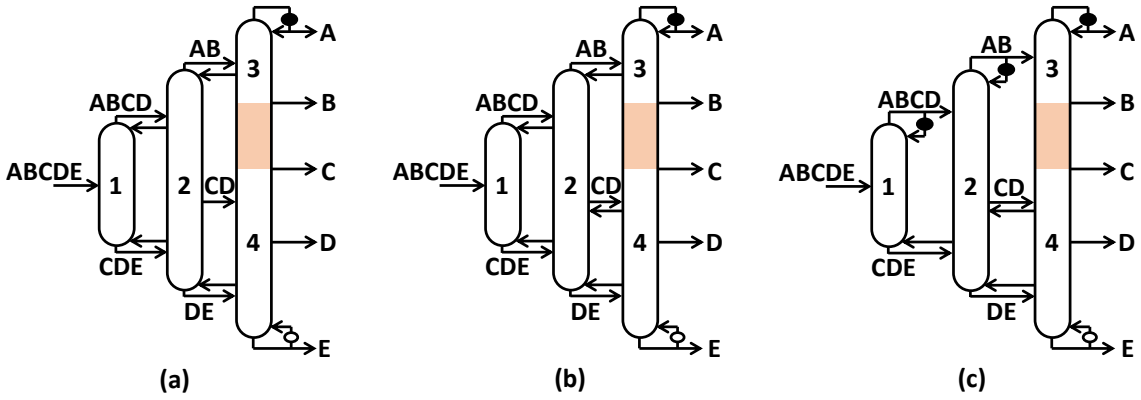

Figure 2.14. (a) HMP configuration derived from the configuration of Figure 2.6a. In this configuration, the sidedraw stream CD is taken out from column 2 as saturated liquid, as shown in Figure 2.6; (b) the same HMP configuration of (a) allowing two-phase flow for sidedraw stream CD; (c) a partially TC configuration derived from the configuration of (b) by introducing condensers back to submixtures $ABCD$ and AB.

As an illustration, we consider the case in which the relative volatility set between each consecutive component is $\{\alpha_{AB}, \alpha_{BC}, \alpha_{CD}, \alpha_{DE}\} = \{2.5, 2.5, 1.1, 1.1\}$. The feed is taken as saturated liquid. NLP calculations for all 31 (i.e. $2^5 - 1$) representative feed compositions report that this HMP configuration gives exactly the same $V_{tot}^{\min}$ as the FTC configuration under 12 cases. Note that in this HMP configuration, sidedraw stream CD is withdrawn from column 2 as a liquid-only stream which is expected to be easier to control than a two-phase stream. However, if we relax this restriction by allowing the sidedraw CD to be a two-phase stream, then the number of cases under which the corresponding HMP configuration of Figure 2.14b achieves the same $V_{tot}^{\min}$ as the FTC configuration increases from 12 to 19. For the remaining 12 cases, the HMP configuration has a slightly higher $V_{tot}^{\min}$ than the FTC configuration, but no more than 3.5%. More interestingly, extensive NLP calculations for all HMP as well as regular-column configurations disclose that, among all the configurations that give the same $V_{tot}^{\min}$ as the FTC configuration, the one that requires the least number of column sections corresponds to one of the HMP configurations under a number of feed conditions. From a practitioners perspective, this suggests that the HMP configurations are capable of providing the most heat duty savings and capital cost reductions to a wide window of feed conditions. Last but not least, in some cases, the heat duty saving benefits are preserved even when some thermal couplings in the original HMP configuration are replaced back with heat exchangers [74]. For instance, for the same relative volatility set considered above, when the thermal couplings at submixtures $ABCD$ and AB are replaced with condensers for the HMP configuration of Figure 2.14b, the resulting partially TC configuration, shown in Figure 2.14c, still has the same $V_{tot}^{\min}$ as the FTC configuration under 16 out of 31 cases. Note that now every column has at least one reboiler and/or condenser, which makes the configuration of Figure 2.14c much more effective to operate than the FTC configuration. This also supports our earlier argument that, for a given separation task, it is always possible to synthesize some non-FTC configurations through various PI strategies that would

require the same heat duty savings as the FTC configuration, but are more thermodynamically efficient, much cheaper to build, and easier to operate and control.

2.6 Systematic Synthesis of All Dividing Wall Columns for Any Conventional Distillation Configurations

Lastly, we now present how one can combine all the PI strategies together to synthesize all useful dividing wall columns (DWCs) using a single column shell or multiple shells ranging from 2 to $n-2$ for any basic or TC configuration, including any HMP configuration. A DWC is a distillation column containing one or more vertical partitions inside to distill a multicomponent mixture into pure components. The concept of DWC was first proposed for the Petlyuk column [26] by Wright [27] as early as 1940s. As illustrated in Figure 2.15a and b, the idea is to perform both the separation tasks originally associated with the prefractionator and with the main column in a single column shell. To achieve this goal, a vertical partition is placed inside the distillation column to create two separate zones that allow different separation tasks to take place within the same column without disturbing each other's heat and mass transfer. These two zones essentially mimic the prefractionator and the main column of the original Petlyuk column. The thermal couplings at AB and BC in the Petlyuk column are in turn transformed into the free space that allows for two-way liquid-vapor communication above and below the partition, respectively. As a result, the DWC of Figure 2.15b is completely thermodynamically equivalent to the original Petlyuk column of Figure 2.15a. Likewise, the well-known Kaibel column [53] of Figure 2.12d, which is the first industrial implementation of DWC [58], is thermodynamically equivalent to the original configuration of Figure 2.12c, also known as the Cahn and Di Miceli configuration [73]. In fact, for any multicomponent system, each and every conventional distillation configuration has at least one thermodynamically equivalent DWC version that performs all separations in a single column shell.

To synthesize single- and multi-shell DWC for any distillation configuration for the first time, Madenoor Ramapriya et al. [76] introduce an easy-to-use, step-wise

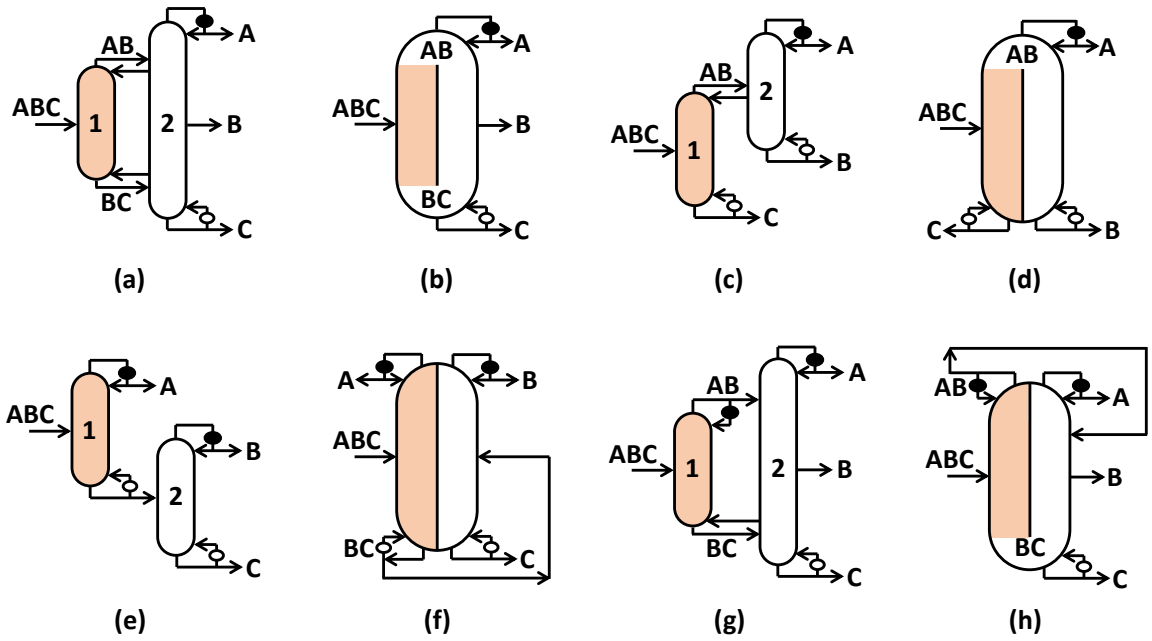

Figure 2.15. Selected ternary distillation configurations and their corresponding DWC versions: (a) the FTC configuration (i.e. Petlyuk column); (b) DWC version of (a) proposed by Wright [27]; (c) the indirect split TC configuration which is equivalent to the side-stripper arrangement [57]; (d) DWC version of (c) proposed by Agrawal [75]; (e) the basic direct split configuration; (f) DWC version of (e); (g) a partially TC version of (a); (h) DWC version of (g) [30].

procedure. Besides single-column DWCs, more configurations containing DWCs and use from 2 to $n-2$ column shells can be systematically derived by following the same consolidation procedure but for any suitable subset of distillation columns. Their work thus greatly expands the search space of useful configurations for separating a multicomponent mixture. Several conventional configurations for ternary separations, such as the direct split configuration and side-stripper arrangement, as well as their respective DWC versions, are explicitly drawn in Figure 2.15 for illustration. This one-to-one correspondence between any basic or TC configuration and a DWC enables us to directly transform the problem of determining the heat duty requirement of a DWC into an equivalent but much simpler problem of calculating

the heat duty of its corresponding conventional configuration. This also allows one to ranklist different DWCs in terms of heat duty by simply performing the same task for the conventional configurations through, for example, NLP calculations [34]. More importantly, there has long been a myth among people that distillations using DWCs save energy compared to using conventional systems. We point out that the attractiveness of DWCs in terms of heat duty is not due to the use of DWCs, but is attributed to the heat duty benefits associated with the original configurations from which the DWCs are derived. For example, the DWC of Figure 2.15b introduced by Wright [27] requires less heat duty than conventional sequences simply because the ternary FTC Petlyuk column of Figure 2.15a has the requires the least heat duty among all configurations in the search space [29, 31, 34, 42]. On the other hand, if we start with a conventional sequence thats itself energy intensive, e.g. the basic direct split configuration of Figure 2.15e, we would never expect the resulting DWC, shown in Figure 2.15f, to have a lower heat duty requirement compared to conventional configurations. Therefore, it is important for practitioners to first consider the entire search space of configurations and perform the screening process through optimization to identify a few attractive flowsheets before generating their DWC versions by following the procedure of Madenoor Ramapriya et al. [76, 77].

Although a DWC does not intrinsically result in operating costs reduction by itself, it does save considerable amount of capital cost as well as land requirement as it reduces the number of column and other equipment pieces used for distillation [38,75]. As much as 30% of capital cost reduction for ternary separations has been reported as DWCs are used in place of conventional sharp split configurations [78–81]. Thus, the compactness and cost effectiveness of DWC makes it an exciting path for PI in multicomponent distillation.

Because of these potential benefits, we have seen a rapid increase in the use of DWCs for industrial applications. According to Dejanovi et al. [81], the number of DWCs installed has passed over 100 in 2009. However, compared to the number of conventional distillation columns currently in operation in the chemical industry,

this number is still quite minuscule. Also, almost all industrial implementations of DWC have been for ternary separations [82]. So far, the only reported quaternary DWC for industrial use is a Kaibel column built by BASF which still uses only one partition [83]. This DWC incorporates complex internal design together with various proprietary reflux splitters and liquid distributors for controllable operation. And we have not yet seen any industrial implementation of DWC with multiple unextended partitions for $\geq$ 5-component separations.

We believe that the primary reason why DWCs have not been implemented in large scale is due to the following. For a long time, industrial practitioners were only aware of the existence of DWCs synthesized from a few selected conventional configurations, such as the FTC configuration [26] of Figure 2.15a and the Cahn and Di Miceli configuration [73] of Figure 2.12c. One of the distinct characteristics these configurations share is that they all involve several thermal couplings. While these thermal couplings lower the heat duty of the resulting DWCs compared to the DWCs synthesized from basic configurations, they also make the resulting DWCs harder to control and operate. Optimal operation of DWCs derived from conventional configurations with several thermal couplings is particularly strenuous because it is generally difficult to achieve the desired vapor split below the vertical partition as discussed in Madenoor Ramapriya et al. [58]. For example, consider the DWC of Figure 2.15b which is derived from the Petlyuk column [26]. Clearly, the vapor flow generated at the reboiler of C cannot be regulated as it travels upwards and gets split by the partition. In other words, the control of vapor flows in the two parallel zones created by the vertical partition is missing in this DWC. And it is difficult to operate and maintain the DWC at the optimal L/V ratio in either parallel zone. In the end, the promising heat duty benefits from the DWC due to thermal couplings cannot be seen as a result of its inferior performance. In fact, a much higher heat duty is generally required in practice to achieve the desired product purities. This challenge gets compounded when higher-component DWCs are built, as the number of unregulated vapor splits increases as number of vertical partitions of this sort in the

corresponding DWC increases. Because of this, so far we have not seen any industrial implementation of DWC with two or more vertical partitions.

Recently, Madenoor Ramapriya et al. [58] finally solved this longstanding challenge by utilizing Agrawal's method [57] to convert any thermal coupling to a thermodynamically equivalent LOT stream. Starting from the original FTC configuration of Figure 2.15a containing two thermal couplings, 3 (i.e. $2^2 - 1$) additional equivalent configurations can be synthesized by converting thermal coupling at AB, or thermal coupling at BC, or thermal couplings at both AB and BC, to LOTs. These equivalent configurations and their resulting DWCs are drawn in Figure 2.16. Any of the three equivalent DWCs is now equipped with at least one reboiler and/or condenser for each of the two zones created by the partition, which allows independent precise control of L/V ratio in each zone. Thus, the DWCs shown in Figure 2.16 no longer suffer from the controllability issue that is associated with the conventional DWC of Figure 2.15b.

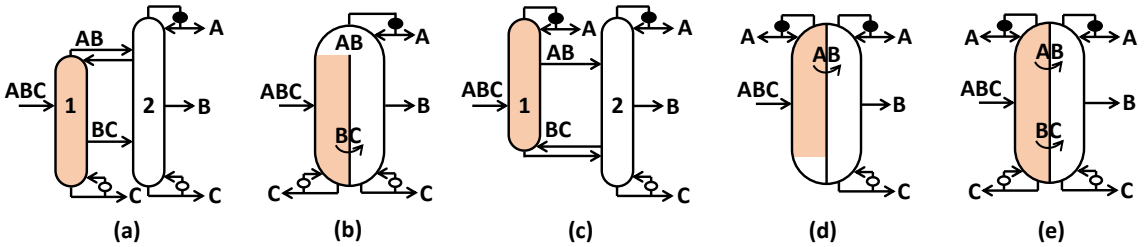

Figure 2.16. (a) Equivalent configuration of ternary FTC configuration of Figure 2.15a by converting thermal coupling at BC to a LOT; (b) the resulting DWC of (a); (c) equivalent configuration of ternary FTC configuration by converting thermal coupling at AB to a LOT; (d) the resulting DWC of (c); (e) the DWC derived from the configuration of Figure 2.10c.

Similarly, any conventional TC configuration including the HMP configurations that were lately discovered, a slew of thermodynamically equivalent DWC versions that are hitherto unknown can be drawn systematically [77]. These equivalent DWCs are systematically generated by successively applying Agrawal's LOT strategy [57]

to the DWCs synthesized from the stepwise procedure of Madenoor Ramapriya et al. [76]. A large portion of these newly generated DWCs are fully operable and controllable. For instance, Figure 2.17 shows some of the DWC examples synthesized from the HMP configuration of Figure 2.14b. Starting from Figure 2.17a thru d, the associated DWCs demonstrate increasing operability, as more thermal couplings are converted to LOT streams. In particular, the last two DWCs of Figure 2.17c and d are fully operable, since each of the three parallel zones is associated with at least one reboiler and/or condenser. Among all of the fully operable DWCs, the ones with the least number of heat exchangers and LOTs are drawn in Figure 2.17e and f. These two operable DWCs are more compact and cost-effective, making them more attractive among practitioners. For DWCs synthesized by the methodology of Madenoor Ramapriya et al. [77], the LOT streams transfer materials from one zone to another externally via connecting pipes and liquid pumps. The specifications for these liquid-only streams, such as flow rate and temperature, can be precisely monitored and controlled as needed. Plausible industrial implementations for such operable DWCs have also been discussed [59].

Meanwhile, notice from Figure 2.17h that the simplest operable DWC version for the five-component FTC configuration of Figure 2.4 has a total of 3 partitions and 9 submixtures. On the other hand, the single-shell operable DWCs of Figure 2.17e and f, which have the same $V_{tot}^{\min}$ as the FTC configuration under various feed conditions as discussed earlier, require only 2 vertical partitions and 5 submixtures. The structural simplicity associated with these DWC versions is inherited from the original HMP configuration of Figure 2.14b. Finally, it is worth pointing out that combining the methodologies of Madenoor Ramapriya et al. [76, 77] allows us to enumerate all possible equivalent configurations containing DWCs using 2 to $n-2$ column shells. Figure 2.17g shows one possible equivalent arrangement of the HMP configuration of Figure 2.14b by consolidating the first two columns in the HMP configuration in the form of a DWC, while leaving the last column as a standalone column. As a result, the DWC in Figure 2.17g uses only one vertical partition and is fully operable

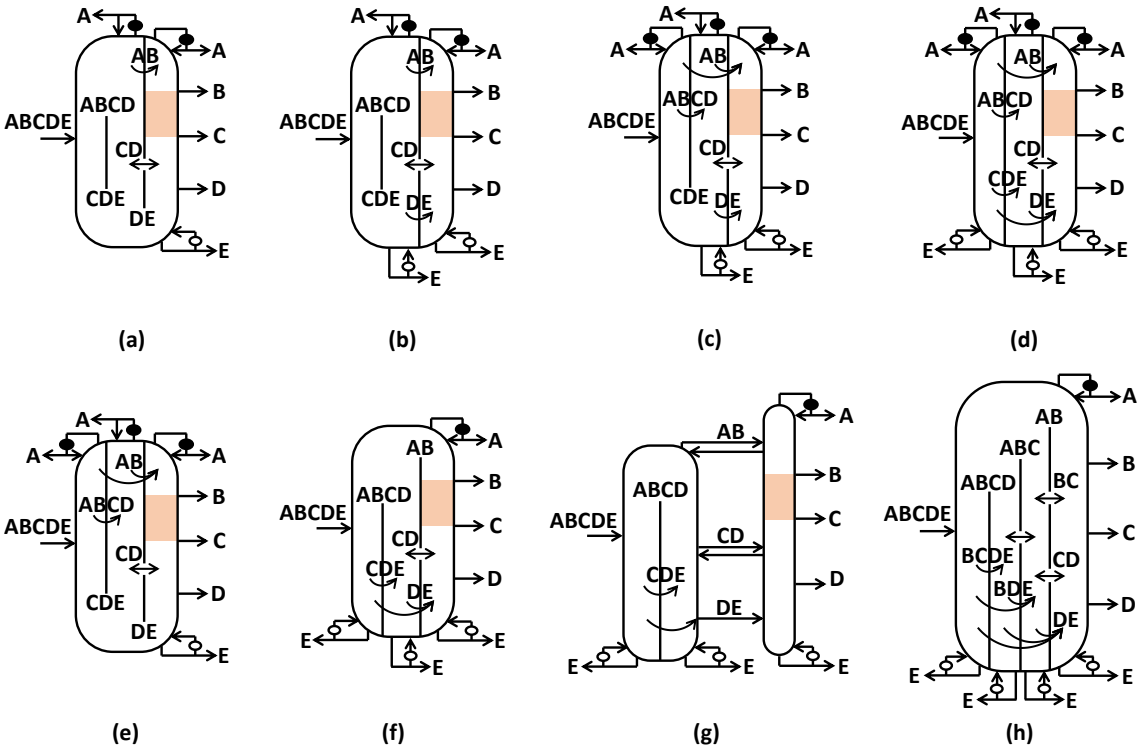

Figure 2.17. (a) to (d) Some possible DWCs for the HMP configuration of Figure 2.14b with increasing operability. These DWCs are derived from the equivalent conventional configurations of Figure 2.8. The DWCs in (c) and (d) are fully operable since each parallel zone has at least one reboiler and/or condenser; (e) to (f) fully operable DWC versions that require the least total number of heat exchangers as well as LOT streams; (g) an operable version of the HMP configuration that uses 2 column shells; (h) an operable DWC for five-component FTC configuration of Figure 2.4 synthesized based on the methodology of Madenoor Ramapriya et al. [58].

by converting thermal couplings at CDE and DE to LOT streams. Similarly, one could draw another equivalent arrangement by consolidating the last two columns the original HMP configuration of Figure 2.14b into a DWC, and leave the first column as it is. The point is, for the first time, instead of knowing only a few DWCs which are inoperable, industrial practitioners can apply different PI strategies to simultaneously synthesize an array of new attractive intensified configurations using operable

DWCs. To a great extent, the discovery of equivalent configurations containing fully operable DWCs can be considered as the ultimate form of PI.

2.7 Summary

Process Intensification has gained tremendous attention in the chemical industry. In spite of this increasing interest of PI among researchers and industrial practitioners, the full landscape of PI remains unexploited in the area of multicomponent distillation. Over the past decades, several new methodologies have been developed that allow us to synthesize compact, easy-to-operate, energy efficient and cost-effective multicomponent distillation configurations. All these strategies fall under the category of PI. In this chapter, we piece these PI strategies together in an organized manner and, for the first time, propose a systematic, multi-layer approach for PI in multicomponent distillation.

This approach starts from the complete enumeration of all possible basic regular-column configurations using the SA method [7]. Once a basic configuration is identified, systematic introduction of thermal couplings can be applied to synthesize TC derivatives. Strategic replacement of submixture reboilers and/or condensers with thermal couplings establishes the foundation to all subsequent PI strategies. With the help of state-of-art global optimization algorithms [34], the best performing TC derivative in terms of heat duty and utility (temperature-level) cost can be identified. Next, two independent PI strategies, namely column section rearrangement [52] and conversion of thermal coupling to liquid-only transfer [57], can be implemented to reduce the operation difficulty of a TC configuration without affecting its heat duty benefit. This leads to a series of new thermodynamically equivalent configurations, many of which are easy-to-operate and cost-effective. For a given TC configuration, systematic utilization of these PI strategies leads to a series of new thermodynamically These two strategies also play an essential role in constructing subsequent layers of PI.

By converting thermal coupling links with LOT streams, operable multi-effect distillation becomes a feasible and attractive option for TC columns for the first time [64]. Independently, we also discover a simple but powerful rule recently about simultaneous HMI [74] for a special set of CTC configurations. We show that for these CTC configurations, HMI only between final pure product ends is sufficient to offer the maximum heat duty savings. This forms a new class of simple, easy-to-build HMP configurations which require the least number of column sections among all configurations in the search space to achieve the same heat duty benefits as the FTC configuration under many feed conditions.

Finally, we integrate the PI strategies discussed above to successfully synthesize all possible DWCs associated with any basic or TC configuration [76] and solve the longstanding operational challenge that hinders DWCs from being implemented in large scale in industry [58, 77]. The discovery of compact, energy efficient, cost-effective multicomponent distillation systems containing fully operable DWCs and using 1 to $n-2$ column shells is a classic example of PI at its best.

Overall, the systematic, multi-layer PI approach opens the door to the great opportunities for PI in multicomponent distillation. We hope that the analyses and examples discussed in this chapter serve the purpose of inspiring and guiding industrial practitioners towards designing and building novel and attractive intensified multicomponent distillation systems.

3. GLOBAL MINIMIZATION OF TOTAL COST FOR MULTICOMPONENT DISTILLATION CONFIGURATIONS

We introduce a general economic based global optimization framework for determining the minimum cost required to distill any ideal or near-ideal multicomponent mixture into its individual constituents using a sequence of columns. This new framework extends the Global Minimization Algorithm (GMA) introduced in Nallasivam et al. [34]; and we refer to the new framework as the Global Minimization Algorithm for Cost (GMAC). The GMAC guarantees global optimality by formulating a nonlinear program (NLP) for each and every distillation configuration in the search space and solving it using global solvers. The case study presented in this work not only demonstrates the need for developing such an algorithm, but also shows the flexibility and effectiveness of the GMAC, which enables process engineers to design and retrofit energy efficient and cost-effective distillation configurations.

3.1 Introduction

The overall goal of synthesizing new and attractive distillation configurations for a given separation task requires that process engineers to have the capability to efficiently and accurately identify a configuration or a set of configurations which yield the minimum total cost, especially when considering the magnitude of differences in capital and operating costs different configurations can have even if they all perform the same separation task. Due to the combinatorial increase in the size of the regular-column configuration search space with the number of components in the feed [7, 18], performing rigorous simulations for each and every configuration in the search space using process simulators such as Aspen Plus in order to identify attractive configurations is certainly too inefficient and expansive to be even possible. One almost always

needs to formulate an optimization problem to consider and solve all configurations in the search space in a timely and accurate manner. Caballero and Grossmann [35] presented a superstructure based on state task network representation to synthesize all thermally coupled configurations, including completely thermally coupled (CTC) ones in which all intermediate heat exchangers in a configuration are replaced with thermal couplings. The superstructure was modelled as a generalized disjunctive program. Afterwards, Caballero and Grossmann [16] extended the superstructure to capture all basic and thermally coupled regular-column configurations. The resulting generalized disjunctive program was formulated and solved as a mixed integer nonlinear program (MINLP) to identify the configuration that minimizes the total cost. However, the MINLP could not be solved to global optimality as the local nonlinear programming (NLP) solver fails to give a feasible solution due to singularity issues associated with disappearing column sections [35]. Also, the iterations are very time-consuming. And even if a solution is found, it often corresponds to a poor local optimum. To account for these issues, they proposed an algorithm based on a modified version of logic-based outer-approximation algorithm. Nevertheless, they were still unable to guarantee global optimality with this approach [35].

Caballero and Grossmann [16] then introduced a two-step iterative optimization procedure to solve the MINLP by first identifying the best CTC configuration, followed by determining the best submixture heat exchanger placement for the configuration identified in the first step. These authors have also extended this solution procedure to consider heat integration [36], column section rearrangements [37], and dividing wall columns [38] in their designs. Essentially, this two-step iterative procedure decomposes the original problem of simultaneously finding the optimal topological structure and the optimal submixture heat exchangers placement into two subproblems. Thus, the optimal solution obtained from this process may not correspond to the true optimal solution of the original optimization problem. For a general case, such a decomposition may lead to local optimal solution.

Also, the cost model developed under this two-step procedure is somewhat oversimplified. For example, a fixed capital cost of $150,000 is assumed for all reboilers and condensers [84], whereas in practice, heat exchangers costs should be dependent on various factors such as the type of heat exchanger used, actual heating or cooling duty requirement, etc. Also, the actual number of stages in a distillation column in the model of Caballero and Grossmann [35] does not account for the dependence of the actual reflux ratio of the column. Instead, the model is forced to use twice the minimum number of stages calculated by the Fenske equation [85] as the actual number of stages. Moreover, in the model of Caballero and Grossmann [16], all condensers, including the ones at submixtures, are total condensers, i.e. all submixtures fed into the next distillation column are saturated liquid streams. However, using total condensers at submixture levels may result in unnecessary penalty in energy requirement and total cost. These oversimplifications and modeling assumptions may lead to mis-identification of attractive configurations with low total cost because they tend to unfairly favor either capital cost contribution over operating cost contribution to total cost or vice versa.

Besides these oversimplifications, the accuracy and thus the usefulness of this model is also questionable due to the way the distillation column diameter is calculated. It is known that non-sharp split configurations constitute a large portion of distillation configurations in the search space [7]. For non-sharp split configurations, at least one distillation column contains more than one split. For such a distillation column consisting of multiple splits, the model of Caballero and Grossmann [16] calculates individual column diameter for each split in their two-step procedure instead of using an uniform diameter for all the splits involved in the same distillation column. This split-based method of calculating column diameter may result in multiple contractions and/or expansions in a single column shell, causing significant increase in capital expenditure since special design and materials are required for construction.

Furthermore, we found out that the constraints implemented in Caballero and Grossmann [16] to calculate the minimum vapor duty requirement of a distillation

column using the Underwood's method [19] are incomplete, in the sense that too much flexibility has been granted to the system, which results in solutions that turn out to be physically infeasible to be achieved. Clearly, there is a need to correct the erroneous constraints and improve the cost model.

Besides the MINLP based approach discussed above, a fundamentally different approach to identify the optimal distillation configuration is to first synthesize the complete search space, followed by formulating individual optimization problem for each configuration in the search space. Nallasivam et al. [34] recently adopted this enumeration based approach by proposing an algorithm to formulate a NLP problem to minimize the total reboiler vapor duty requirement for each and every basic and thermally coupled regular-column configuration in the search space generated by the SA method [7]. Each NLP problem is solved to global optimality using global solver BARON [39]. This algorithm is then given the name of Global Minimization Algorithm (GMA); and it is the first-of-its-kind that guarantees global optimality for such a problem. Although the GMA does require the computation effort of solving each and every individual configuration in the search space before the single best configuration can be identified, it is amenable to parallelization and a number of optimization strategies such as bounding tightening [34], all of which can reduce the computational time substantially. Therefore, in this chapter we focus on developing a general NLP based formulation based on the GMA approach that minimizes the total cost of any regular-column distillation configuration. This general formulation is referred to as the Global Minimization Algorithm for Cost, or simply GMAC for short.

The total cost of a distillation configuration comprises of two parts: the capital cost and the operating cost. The capital cost of a configuration depends on the number and sizes of distillation columns and trays, reboilers, condensers, and so forth. Assuming that all reboilers use similar heating utility and all condensers use similar cooling utility, the operating costs associated with reboilers and condensers are directly proportional to the sum of vapor duties generated at all reboilers and condensed

at all condensers, respectively. Moreover, considering the operating life of the facility, the annual interest rate as well as inflation must be incorporated into the overall cost. All these factors will be captured in the GMAC formulation. In this formulation, the majority of the GMA framework is retained with few modifications; additional cost related relations and constraints are added. We will present these equations in the next section. The strategies and techniques used to improve convergence and reduce computational time of the NLP problem are elucidated in Nallasivam et al. [34].

After presenting the NLP formulation, we will study a five-component alcohol mixture separation example to demonstrate the usefulness and robustness of the GMAC approach. We will then compare our results with the solution obtained from the TMA process to suggest the need for a global optimization algorithm. Different objective function scenarios are also considered and discussed to show how the final optimal solutions change accordingly. These analyses effectively illustrate the flexibility that our GMAC approach can achieve, which will allow process engineers to not only design new attractive distillation systems, but also retrofit existing ones in a chemical plant.

3.2 NLP Formulation

Any optimization problem is described by the decision variables, the objective function, and the constraints. In the GMAC formulation, all the decision variables and most of the constraints from the GMA framework described in Nallasivam et al. [34] have been retained. On the other hand, the objective in the GMAC framework is to minimize the total annualized cost TAC which is defined as a linear combination of the fixed capital investment FCI and yearly operating cost YOC:

$$\min \quad TAC = k_{FCI} FCI + k_{YOC} YOC \tag{3.1}$$

in which the coefficients k_{FCI} and k_{YOC} are nonnegative constants provided by the users based on their specific needs. For example, if a user is interested in finding

out the configurations that are cheap to build, then k_{FCI} is set to be 1 and k_{YOC} is set as 0 to optimize only the capital cost. Conversely, if operating cost is the primary concern, the user can specify $k_{FCI} = 0$ and $k_{YOC} = 1$. When both capital and operating costs need to be considered, it is common to use the total annualized cost as the objective function [86], in which $k_{YOC} = 1$ and FCI is annualized by assuming certain depreciation period L (typically 8 to 10 years) and estimating an annual interest rate r as well as an annual inflation rate f. The effective interest rate r', after accounting for inflation, is thus given by $\frac{r-f}{1+f}$ [86]. With this, the coefficient k_{FCI} for total annualized cost estimation is determined as:

$$k_{FCI} = \frac{r'(1+r')^L}{(1+r')^L - 1} \tag{3.2}$$

A feasible distillation column operation must satisfy vapor-liquid equilibrium and appropriate mass balance relations. In addition, the vapor flow requirement for carrying out a given separation in a distillation column section satisfies Underwood's equations [19]. The full set of constraints implied by these relationships has been throughly discussed in Nallasivam et al. [34] and is retained in this chapter with one exception. In practice, the optimal operation of a distillation column is usually achieved between 1.1 to 1.5 times its minimum reflux ratio [87]. Using the heuristic that the actual reflux ratio is 20% higher than the minimum reflux ratio, we have, for each split s:

$$V_s^{\text{top}} \geq 1.2V_s^{\min} - 0.2\sum_{k=1}^{n} \overline{X}_{s,k} \qquad \forall s = 1, \cdots, n_s \tag{3.3}$$

where as described in Nallasivam et al. [34], V_s^{top} is the actual vapor flow in the upper column section of split s, $V_s^{\min}$ is the minimum upper section vapor flow determined by Underwood's distillate constraint [19], $\overline{X}_{s,k}$ stands for the net material upward flow in the upper section of split s. The quantity $DISTS_s$ gives the stream number associated with the split's top product as discussed in Nallasivam et al. [34]. Mean-

while, $ROW(m)$ corresponds to the lightest component number in material stream m, and $COL(m)$ is equal to the number of components present in stream m [7, 34]. For instance, when $m = BCD$, $ROW(m) = 2$ which stands for the second most volatile component (i.e. component B), and $COL(m) = 3$. Finally, n_s is the number of splits present in the configuration.

We need to point out that the minimum vapor duty constraints presented in Caballero and Grossmann [16] and also in Nallasivam et al. [34] used to calculate $V_s^{\min}$ for each split s have not been formulated correctly. Instead of allowing them to be inequality constraints, these Underwood's distillate constraint [19] must be introduced as an equality constraint with respect to the active Underwood roots associated with split s, which are related to the key components of the split [88]:

$$V_s^{\min} = \sum_{k=i}^{n-j+i} \frac{\alpha_k \overline{X}_{s,k}}{\alpha_k - \theta_{s,r}} \quad \forall r = i+1, \cdots, n-j+i-1;$$
$$i = ROW(DISTS_s);\ j = COL(DIST_s);\ \forall s = 1, \cdots, n_s \quad (3.4)$$

From Equation (3.4), it is clear that only the active Underwood roots $\theta_{s,r}$ whose magnitudes are in between the relative volatilities of heavy key and light key components associated with split s are selected. If these Underwood's distillate constraints are introduced as inequalities instead, then the system would have too much flexibility than it should have. This makes the model of Caballero and Grossmann [16] incomplete. As pointed out by Tumbalam Gooty et al. [89], the solution of $\overline{X}_{s,k}$ identified by the optimization program may in fact turn out to be physically infeasible. Fortunately, even though Nallasivam et al. [34] did not present the Underwood's distillate constraint formulation correctly, the actual model did implement the correct formulation in the GMA framework, and thus the results obtained from the examples considered in the work of Nallasivam et al. [34] are still accurate. Nevertheless, here we explicitly remind the readers about the right way of formulating the Underwood's distillate constraint.

We will now introduce the detailed cost model to estimate the FCI and YOC. The FCI is estimated by the total module cost C_{TM} which can be approximated by the product of the total purchased costs of major pieces of process equipment in the facility and the appropriate Lang factor F_{lang} [86, 90]:

$$FCI \approx C_{TM} = F_{lang} k_{CEPCI} \left(\sum_{c \in REB} C_{reb,c} + \sum_{c \in COND} C_{cond,c} + \sum_{s=1}^{n_s} C_{col,s} + \sum_{s=1}^{n_s} C_{tray,s} \right) \tag{3.5}$$

in which $C_{col,s}$, $C_{tray,s}$, $C_{reb,c}$, and $C_{cond,c}$ are purchased equipment costs associated with column shell associated with split s, tray stages in the column associated with split s, reboiler at column c, and condenser at column c, respectively. Here, sets REB and $COND$ keep track of the distillation column indices in a configuration that are associated with reboilers and condensers, respectively. Fluid processing plants typically have a Lang factor of 4.74 [86]. The multiplier k_{CEPCI} is the ratio of Chemical Engineering Plant Cost Index (CEPCI) between the present time and the time when the capital cost correlations are tabulated. It accounts for the increase of purchased equipment costs due to inflation.

Next, we will examine the purchased equipment cost correlations present in Equation (3.5). The tray cost $C_{tray,c}$ is a function of tray type, the diameter of distillation column c (A_c), as well as the total number of tray stages in the column (N_c). Such correlations for various tray types have been tabulated in several references including Turton et al. [86]. These correlations are expressed or can be fitted as second-order polynomials with respect to A_c:

$$C_{tray,c} = N_c(k_{tray,0} + k_{tray,1} A_c + k_{tray,2} A_c^2) \tag{3.6}$$

where $k_{tray,0}$, $k_{tray,1}$, $k_{tray,2}$ are constants specified by the users based on the actual implementation. The total number of trays N_c in distillation column c can be estimated by a number of ways. One way is to use the Fenske-Underwood-Gilliland method to first estimate the number of trays associated with each split s in column

c followed by adding them together. Eduljee [91] presented an alternative equation form for the Gilliland's correlation [92] as follows:

$$\frac{N_s - N_{s,\min}}{N_s + 1} = 0.75\left[1 - \left(\frac{R_s - R_{s,\min}}{R_s + 1}\right)^{0.5688}\right] \tag{3.7}$$

in which N_s is related to the minimum number of stages $N_{s,\min}$ which is determined from the Fenske equation [85], the minimum reflux ratio $R_{s,\min}$ for split s, and finally the actual reflux ratio in operation R_s which is $1.2R_{s,\min}$ as already mentioned. As we can readily see, Equation (3.7) is highly nonlinear and nonconvex. To avoid potential computational issues when solving the optimization model, Caballero and Grossmann [38] simply replaced the right hand side (RHS) of Equation (3.7) by a constant, after evaluating the RHS at a range of $R_{s,\min}$ where most distillation columns are operated and realizing that it is relatively insensitive to the change in $R_{s,\min}$. Or, one could also use a simple power law fit in terms of $R_{s,\min}$ to approximate the RHS of Equation (3.7). In our GMAC formulation, users have the flexibility to choose the equation form for the RHS as they desire, based on their expected range of operating reflux ratios of the distillation columns. Note that one can easily show, according to Equation (3.7), that N_s is lower and upper bounded by $1.917N_{s,\min} + 0.917$ and $4N_{s,\min} + 3$, respectively. Knowing these bounds on decision variables can tighten the GMAC formulation and foster convergence.

For split s, the minimum number of stages $N_{s,\min}$ is calculated a priori using the Fenske equation [85] by pre-specifying the fractional recovery β of the light key in the distillate and the fractional recovery δ of the heavy key in the bottoms product:

$$N_{s,\min} = \frac{\ln\left(\frac{\beta\delta}{(1-\beta)(1-\delta)}\right)}{\ln \alpha} \qquad \forall s = 1, \cdots, n_s \tag{3.8}$$

in which α is the relative volatility ratio of the light key and heavy key components for split s. For example, for $ABCD \rightarrow AB/BCD$ split, the light key is component A and heavy key is component C, so in this case $\alpha = \alpha_A/\alpha_C$.

The cross sectional area $A_{col,s}$ of a column section is calculated for each split s from Doherty and Malone [93]:

$$A_{col,s} = \frac{M_{av}}{\sqrt{\rho_v \rho_l}} \frac{k}{\phi_{flood} c_0} \max\{V_s^{\text{top}}, V_s^{\text{bot}}\} \qquad \forall s = 1, \cdots, n_s \tag{3.9}$$

where M_{av} is the average molecular weight of the components in the system; ρ_v and ρ_l are respectively the mass density of liquid and vapor present on the tray; ϕ_{flood} is the fraction of flooding velocity desired in the design, typically between 0.6 and 0.75; And c_0 is a constant in Fair's correlation [94] that is related to the tray spacing. For a tray spacing of 24 inches (61 cm), c_0 is estimated to be 439 m/hr [93]. Coefficient k here stands for the inverse of the fraction of total cross sectional area available for flow. A typical value for k is given by $1/0.8 = 1.25$. Finally, V_s^{top} and V_s^{bot} are the vapor flows in the upper and lower column sections associated with split s, respectively. These constants and coefficients are all made user-defined in the NLP formulation.

As we have previously mentioned, for a non-sharp split configuration, at least one distillation column contains more than one split. To accurately estimate the column shell cost and tray cost for such a distillation column, we need to appropriately modify Equation (3.9) such that each distillation column is associated with a uniform diameter and it is given by the maximum diameter determined for all splits involved in the column:

$$A_{col,c} \geq \frac{M_{av}}{\sqrt{\rho_v \rho_l}} \frac{k}{\phi_{flood} c_0} \max\{V_s^{\text{top}}, V_s^{\text{bot}}\} \qquad \forall c = 1, \cdots, n-1,\ s \in COLS_c \tag{3.10}$$

where the set $COLS_c$ gives the split indices associated with distillation column c. The height of the column shell H_s associated with split s is related to N_s by $H_s = k_H N_s\ \forall s = 1, \cdots, n_s$, where k_H is the desired tray spacing specified by the users, typically between 0.3 m to 0.6 m. Thus, the total height of a column shell is simply given by the sum of column heights associated with all the splits in the distillation column, plus an extra spacing denoted as h for liquid sump at the bottom of the

column as well as for the surge capacity and vapor disengaging space that may be required at the top [93]:

$$H_c = \sum_{s \in COLS_c} H_s + h \tag{3.11}$$

Once $A_{col,c}$ and N_c have been defined, we can write down the purchased cost for column shell associated with column c, $C_{col,s}$, as:

$$C_{col,c} = k_{col,0} + k_{col,1} A_{col,c} H_c \qquad \forall c = 1, \cdots, n-1 \tag{3.12}$$

The reboiler and condenser costs in distillation column c, $C_{reb,c}$ and $C_{cond,c}$, are functions of heat exchanger type, construction material type, and the heat transfer area. The heat transfer area is related to the overall heat transfer coefficient of the heat exchanger and its approach temperature. Again, these parameters are user-defined in the GMAC model. Assuming that the distillation system operates at or near ambient pressure so that no special material is required, we can formulate the heat exchanger cost as a linear function of heat transfer area:

$$\begin{aligned} C_{reb,c} &= k_{reb,0} + k_{reb,1} A_{reb,c} \qquad \forall c \in REB \\ C_{cond,c} &= k_{cond,0} + k_{cond,1} A_{cond,c} \qquad \forall c \in COND \end{aligned} \tag{3.13}$$

As we have pointed out, when using a fixed capital cost for heat exchangers in a distillation configuration, the total annualized cost TAC in Equation (3.1) may favor more towards FCI than YOC. This will inaccurately penalize thermally coupled configurations which have lower energy requirements. To avoid this, it is not recommended to use fixed capital costs for heat exchangers in an economic based optimization formulation. The heat transfer area for reboiler ($A_{reb,c}$) and condenser ($A_{reb,c}$) associated with distillation column c can be estimated from the heat transfer rate Q once the values of overall heat transfer coefficient U and log mean temperature difference ($LMTD$) are specified by the user. To simplify our model without losing

key information, we assume that $LMTD$ are the same for all reboilers and condensers, all reboilers have an identical U_{reb}, and all condensers have an identical U_{cond}:

$$\begin{aligned} A_{reb,c} &= \frac{Q_{reb,c}}{U_{reb}LMTD} = \frac{V_s^{\text{bot}}}{U_{reb}LMTD}\frac{\sum_{k=i}^{n-j-i} X_{m,k}\Delta H_k}{\sum_{k=i}^{n-j-i} X_{m,k}} \\ &\quad \forall c \in REB,\ s = SBOT_c,\ m = BOTTS_s,\ i \in ROW(m),\ j \in COL(m) \\ A_{cond,c} &= \frac{Q_{cond,c}}{U_{cond}LMTD} = \frac{V_s^{\text{top}} - V_m}{U_{cond}LMTD}\frac{\sum_{k=i}^{n-j-i} X_{m,k}\Delta H_k}{\sum_{k=i}^{n-j-i} X_{m,k}} \\ &\quad \forall c \in COND,\ s = STOP_c,\ m = DISTS_s,\ i \in ROW(m),\ j \in COL(m) \end{aligned} \tag{3.14}$$

where ΔH_k is the molar latent heat of vaporization for component k. The elements in the sets $SBOT_c$ and $STOP_c$ correspond to the splits respectively located at the bottom and top of distillation column c. Looking back at Equation (3.14), it is clear that the term $\sum_{k=i}^{n-j-i} X_{m,k}\Delta H_k / \sum_{k=i}^{n-j-i} X_{m,k}$ gives the average molar latent heat of vaporization for the mixture or pure component of stream m, assuming that the binary interaction between any two components in the mixture is negligible.

This completes the discussion of related equations and correlations for estimating the FCI. There are several ways to estimate the YOC of a distillation configuration, one of which is to use the concept of cost of manufacturing (COM) which can be expressed as a function of the utility costs (C_{ut}) as well as the fixed capital investment (FCI) that accounts for maintenance and supplies, depreciation, administration costs, local taxes and insurances, etc. [86, 95, 96]:

$$\begin{aligned} YOC \approx COM &= k_{COM,0}FCI + k_{COM,1}C_{ut} \\ &= k_{COM,0}FCI + k_{COM,1}\left(\sum_{c\in REB} C_{ut,reb,c} + \sum_{c\in COND} C_{ut,cond,c}\right) \end{aligned} \tag{3.15}$$

in which $k_{COM,0}$ is generally estimated to be 0.28 when considering an annual depreciation of 10% of FCI, whereas a typical value for $k_{COM,1}$ is 1.23 [86]. The utility cost associated with reboiler or condenser i is simply given by:

$$\begin{aligned} C_{ut,reb,c} &= Q_{reb,c} \times OpHr \times C_{heat} \qquad \forall c \in REB \\ C_{ut,cond,c} &= Q_{cond,c} \times OpHr \times C_{cool} \qquad \forall c \in COND \end{aligned} \tag{3.16}$$

where $OpHr$ is the operating hours per year (typically around 8000 hours), and C_{heat} as well as C_{cool} represent unit heating and cooling utility cost, respectively. Again, as a first estimate, we assume that the heating/cooling utilities used in all reboilers/condensers have similar costs. With this, the optimization model formulation for the GMAC is now finalized. In summary, the cost model developed in the GMAC framework improves that developed by Caballero and Grossmann [16] in the following major aspects:

1. The Underwood's distillate constraint to determine the minimum vapor duty required for a split has been correctly implemented.

2. Reboiler and condenser capital costs are no longer fixed. Instead, heat exchanger cost is now a function of the total heat transfer area required, which is proportional to the vapor duty generated or condensed in the heat exchanger.

3. Rather than fixing the total number of trays in a distillate column to be exactly twice of the minimum number of trays, users have the flexibility to specify the correlation as they desire, e.g. the Fenske-Underwood-Gilliland correlation.

4. For a distillation column consisting of multiple splits, a uniform column diameter is used for the entire column.

The NLP problem for each and every configuration synthesized using the SA method [7] is solved in GAMS using global solver BARON [39]. In the next section, we will consider a specific case study in detail to illustrate the reliability and robustness of the GMAC approach.

3.3 Case Study – Alcohols Separation

We consider a five-component atmospheric pressure distillation example studied in Caballero and Grossmann [16, 36] involving the separation of alcohols mixture: ethanol (component A), isopropanol (B), 1-propanol (C), isobutanol (D), and 1-butanol (E). The relative volatilities of these components are determined from Poling et al. [97] as $\{\alpha_A, \alpha_B, \alpha_C, \alpha_D, \alpha_E\} = \{4.1, 3.6, 2.1, 1.42, 1.0\}$, indicating that these separations are relatively difficult to perform. The feed is a saturated liquid stream whose component flow rates are given by $\{f_A, f_B, f_C, f_D, f_E\} = \{20, 20, 80, 60, 20\}$ kmol/hr. The latent heats of vaporization for all components are estimated to be $\{\Delta H_A, \Delta H_B, \Delta H_C, \Delta H_D, \Delta H_E\} = \{38.80, 39.41, 41.62, 46.37, 45.41\}$ MJ/kmol.

3.3.1 Scenario 1 – Minimizing Minimizing Total Annualized Cost

Scenario 1 concerns the minimization of combined annualized capital cost and operating cost, i.e. the total annualized cost of a distillation configuration. Under this scenario, we use the cost parameters listed in Table 3.1. We formulate the general NLP problem for each of the 6128 distillation configurations in MATLAB and solve each NLP problem in GAMS using BARON solver [39] by connecting MATLAB and GAMS via the GAMS/MATLAB interface [98]. All 6128 configurations are solved to global optimality ($\leq 1\%$ duality gap) within 4.91 hours of CPU time using a Dell OptiPlex 5040 desktop that simultaneously utilizes all four of its Intel Quad-Core i7-6700 processors with the help of the Parallel Computing Toolbox in MATLAB.

Among all 6128 flowsheets, the best configuration with the lowest total annualized cost of 1.691 million USD (in 2017's value) is shown in Figure 3.1a. Table 2.2 shows the main results and optimal operating conditions for this configuration. The GAMC approach not only gives the single best performing configuration of Figure 3.1a, but also generates the ranklist of distillation configurations based on their minimum total annualized cost. This ranklist is useful because it allows industrial practitioners to quickly identify attractive candidates that have similar minimum total annualized

Table 3.1.
Cost related parameters for GMAC in the Scenario 1.

Cost Parameters	**Unit**	**Value**
Annual interest rate r	%	9
Annual inflation rate f	%	2.5
Operating life L	year	10
k_{CEPCI} between the year 2017 and 2001	–	535.3/397=1.348
$k_{tray,0}$, $k_{tray,1}$, $k_{tray,2}$ for sieve tray	\$, $\$/m^2$, $\$/m^4$	555.9, 411.12, 22.138
Fractional recovery of light key/heavy key component	–	0.98/0.99
Average liquid and vapor density ρ_l, ρ_v	kg/m^3	723.9, 2.63
ϕ_{flood} of Equation (3.10)	–	0.7
c_0 of Equation (3.10)	m/hr	439
Inverse of free area fraction k of Equation (3.10)	–	1.25
Tray spacing k_H, additional spacing for each column h	m	0.6, 4
$k_{col,0}$, $k_{col,1}$	\$, $\$/m^3$	4373.5, 672.28
$k_{reb,0}(k_{cond,0})$, $k_{reb,1}(k_{cond,1})$	\$, $\$/m^2$	18538, 60.173
U_{reb} and U_{cond} for fixed-tube exchangers	W/Km^2	800
$LMTD$ across heat exchangers	K	10
$k_{COM,0}$, $k_{COM,1}$ in Equation (3.15)	–	0.28, 1.23
Yearly operating hours YOC	hr	8000
Cost of low pressure steam C_{heat}	\$/GJ	2
Cost of cooling water C_{cool}	\$/GJ	0.12

cost compared to the globally best configuration but are easier to build and/or to operate. Industrial practitioners can then perform more detailed analysis only on these attractive candidates to evaluate their actual potential savings. For example, the configuration of Figure 3.1b, which is among the top 1% of all 6128 configurations in terms of minimum TAC (1.745 million USD), has the same topological structure as the optimal configuration of Figure 3.1a but uses two more reboilers at submixtures $BCDE$ and CD. These additional reboilers offer more potential opportunities for heat integration with other process units in the plant, resulting in further reduction in total cost. Furthermore, the presence of submixture reboilers increases the thermodynamic efficiency of the distillation process, as part of the heat duty originally completely supplied by reboilers at DE and E as shown in Figure 3.1a can now be generated by these submixture reboilers which operate at less extreme temperature levels.

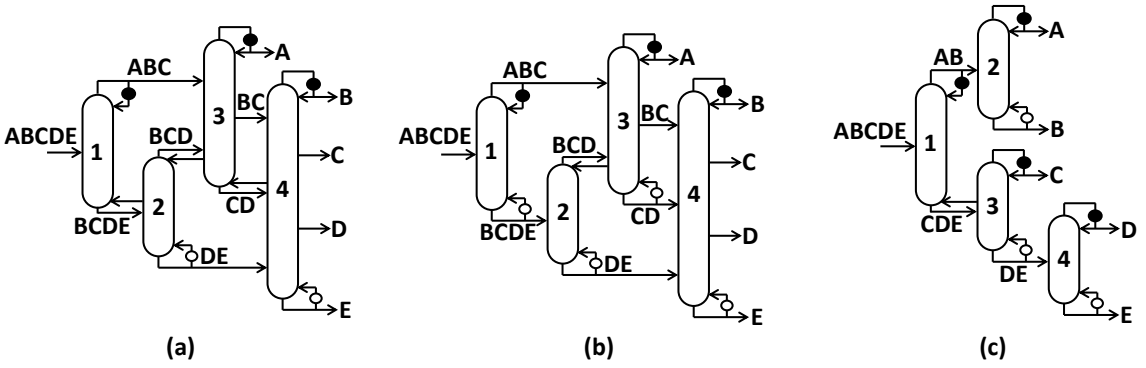

Figure 3.1. (a) The optimal configuration with the lowest TAC among all 6128 configurations under Scenario 1; (b) a second configuration that has the same topological structure as the configuration of (a) but with only one thermal coupling. It is among the top 1% in terms of TAC of all 6128 configurations; (c) the best sharp split configuration in terms of minimum TAC that has a ranking of 4685 out of 6128 configurations.

For a long time, design engineers have been used to designing and building sharp split configurations for most industrial separations. Despite their structural simplicity,

Table 3.2.
Main results for the configuration of Figure 3.1a under Scenario 1

Split	**Section**	**Vapor flow (kmol/hr)**	**Liquid flow (kmol/hr)**
$ABCDE \rightarrow ABC/BCDE$	Rec	177.05	119.88
	Strip	177.05	319.88
$BCDE \rightarrow BCD/DE$	Rec	221.91	140.60
	Strip	398.97	460.48
$ABC \rightarrow A/BC$	Rec	382.18	362.18
	Strip	325.01	362.18
$BCD \rightarrow BC/CD$	Rec	325.01	295.37
	Strip	103.09	154.77
$BC \rightarrow B/C$	Rec	132.24	112.24
	Strip	132.24	179.05
$CD \rightarrow C/D$	Rec	132.24	99.05
	Strip	235.34	253.82
$DE \rightarrow D/E$	Rec	235.34	193.82
	Strip	235.34	255.34
Distillation column	**Number of Trays**	**Cross sectional area (m^2)**	**Q_{reb}/Q_{cond} (kW)**
1	5	1.06	-/1332
2	12	2.39	5104/-
3	77	2.29	-/4119
4	60	1.43	2969/1448

sharp split configurations are known to suffer from high energy requirement compared to non-sharp split ones [18]. In this example, the best sharp split configuration in terms of minimum total annualized cost among all basic or thermally coupled sharp split configurations is explicitly drawn in Figure 3.1c. This configuration, which has a minimum TAC of 2.405 million USD, is 42.2% more "expansive" to build and operate than the global optimal configuration and is ranked 4685th out of all 6128 configurations. Albeit sharp split configurations use the least number of column sections (i.e. $2(n-1)$ for n-component separation), they generally consume significantly more heat duty than non-sharp split configurations, thereby significantly increasing distillation column and heat exchanger sizes.

3.3.2 Scenario 2 – Minimizing Capital Cost

In industrial practices, there are many circumstances where engineers are more interested in identifying distillation flowsheets requiring the least capital investment to build. For example, in a highly integrated chemical complex where the multicomponent distillation system is just a part of the plant, the operating costs of distillation columns are not too much of concern to process engineers since excess heating and cooling utilities are generally available from other parts of the plant so the distillation system can essentially operate "for free". Needless to mention the recent shale gas boom which has caused the energy price in the US to drop significantly over the past decade. To minimize only the annualized capital cost of a distillation configuration using the GMAC approach, one may simply set k_{YOC} in the objective function of Equation (3.1) to 0. In the same alcohols separation case with the same cost parameters as listed in Table 2.1, we identify that the optimal configuration with the lowest minimum annualized capital cost (1.078 million USD, in 2017's value) is the one in Figure 3.2. Surprisingly, it turns out that the second best configuration based on capital cost actually corresponds to the same optimal configuration as shown in Figure 3.1a with the lowest TAC under Scenario 1. This configuration has a minimum annualized capital cost of 1.088 million USD, which is only 1% higher than

the global optimal solution of Figure 3.2. In fact, these two configurations are even structurally similar. The major difference is that column 2 in the configuration of Figure 3.2 performs $BCDE \rightarrow BCD/CDE$ split, whereas column 2 in Figure 3.1a undergoes $BCDE \rightarrow BCD/DE$ split. This difference causes column 3 in Figure 3.2 to have two additional column sections compared to the configuration of Figure 3.1a and subsequently leads the presence of an additional split of $CDE \rightarrow CD/DE$.

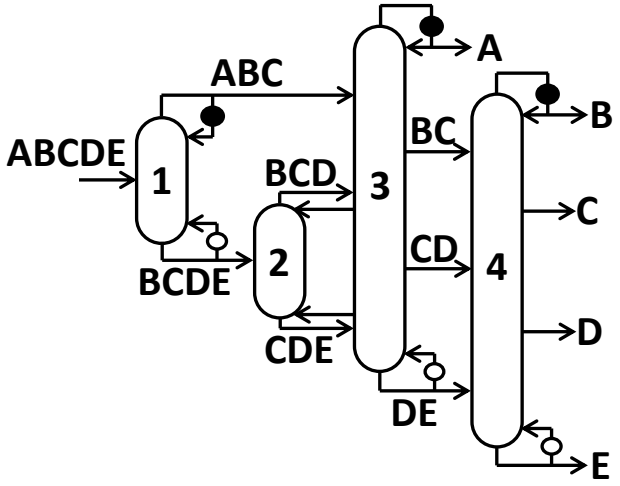

Figure 3.2. The optimal configuration with lowest annualized capital cost among all 6128 configurations.

Just by visually inspecting these two configurations, one might tend to think that the structurally more complex configuration of Figure 3.2 should have a higher capital cost than the configuration of Figure 3.1a. So what makes this configuration actually cheaper to build? To answer this question, we need to examine the internal vapor and liquid flows inside these distillation columns in both configurations to see how the column sizes and costs are affected accordingly. From Tables 3.3 and 3.4, we realize that columns 2 and 4 of Figure 3.2 have much smaller column diameters compared to columns 2 and 4 of Figure 3.1a, respectively. As a consequence, the increase in column shell cost associated with column 3 in the configuration of Figure 3.2 due to the additional column sections is small in comparison to the decrease in column shell costs of columns 2 and 4. The reason why columns 2 and 4 in the

configuration of Figure 3.1a have larger diameters is primarily because of the presence of thermal couplings at submixtures $BCDE$ and CD. In this case, the vapor duty required for $ABCDE \rightarrow ABC/BCDE$ split in column 1 is completely generated by the reboiler of column 2 before it is transferred to column 1 by thermal coupling at $BCDE$. Therefore, the internal vapor flow in the stripping section of column 2 (409.35 kmol/hr) is significantly more than what is needed for the separation of $BCDE \rightarrow BCD/DE$. This increases the diameter of column 2 considerably. On the other hand, in the configuration of Figure 3.2, the internal vapor traffic inside column 2 at optimal operation is 230.72 kmol/hr, resulting in a much smaller diameter of the column. Similarly, in the configuration of Figure 3.1a, part of the vapor duty required for column 3 is supplied by the reboiler of column 4 via thermal coupling at submixture CD. This greatly increases the vapor traffic in the lower part of column 4 (233.13 kmol/hr) compared to its upper part (131.40 kmol/hr), again causing a larger diameter of the column. For the same reason, even though the configuration of Figure 3.2 requires 12 more trays, the overall tray cost $\sum_{c=1}^{4} C_{tray,c}$ of this configuration (\$ 499.9k) is still lower than than that of Figure 3.1a (\$ 513.3k).

Figure 3.3 plots the optimal minimum capital costs for all 6128 configurations in the search space along with their corresponding overall reboiler vapor duty requirements. The overall reboiler vapor duty requirement of a distillation configuration, which is the sum of vapor duties generated at all reboilers, has been commonly used as an indicator of its operating cost [34]. As a result, industrial practitioners may find such plot useful in designing energy efficient and cost-effective multicomponent distillation systems. For example, the green box in Figure 3.3 contains a total of 113 configurations that are potentially useful since they require $< 10\%$ more capital investment compared to the best performing configuration in the search space. These 113 configurations belong to 34 distinct configuration "families". A configuration "family" is defined as a group of distillation configurations with the same topological structure but have different heat exchanger/thermal coupling placements. Process engineers thus have a variety of flowsheet design options to choose from based on

Table 3.3.
Main results for the best performing configuration of Figure 3.2 under Scenario 2.

Split	**Section**	**Vapor flow (kmol/hr)**	**Liquid flow (kmol/hr)**
$ABCDE \rightarrow ABC/BCDE$	Rec	209.77	167.37
	Strip	209.77	367.37
$BCDE \rightarrow BCD/CDE$	Rec	230.72	144.26
	Strip	230.72	301.86
$ABC \rightarrow A/BC$	Rec	355.59	335.59
	Strip	313.19	335.59
$BCD \rightarrow BC/CD$	Rec	313.19	257.67
	Strip	82.47	113.42
$CDE \rightarrow CD/DE$	Rec	82.47	57.39
	Strip	313.19	359.26
$BC \rightarrow B/C$	Rec	150.89	130.89
	Strip	150.89	208.80
$CD \rightarrow C/D$	Rec	150.89	128.80
	Strip	150.89	184.83
$DE \rightarrow D/E$	Rec	150.89	124.83
	Strip	150.89	170.89
Distillation column	**Number of Trays**	**Cross sectional area (m^2)**	**Column shell cost ($\times$1000\$)**
1	7	1.26	17.03
2	7	1.38	17.75
3	92	2.13	209.26
4	62	0.92	66.74

Table 3.4.
Main results for the second best configuration of Figure 3.1a under Scenario 2.

Split	**Section**	**Vapor flow (kmol/hr)**	**Liquid flow (kmol/hr)**
$ABCDE \rightarrow ABC/BCDE$	Rec	191.65	141.07
	Strip	191.65	341.07
$BCDE \rightarrow BCD/DE$	Rec	217.70	131.82
	Strip	409.35	472.89
$ABC \rightarrow A/BC$	Rec	370.00	350.00
	Strip	319.42	350.00
$BCD \rightarrow BC/CD$	Rec	319.42	283.69
	Strip	101.73	151.87
$BC \rightarrow B/C$	Rec	131.40	111.40
	Strip	131.40	177.71
$CD \rightarrow C/D$	Rec	131.40	97.71
	Strip	233.13	249.58
$DE \rightarrow D/E$	Rec	233.13	189.58
	Strip	233.13	253.13
Distillation column	**Number of Trays**	**Cross sectional area (m^2)**	**Column shell cost ($\times$1000\$)**
1	6	1.15	14.46
2	13	2.45	41.33
3	76	2.22	178.62
4	61	1.42	100.34

factors such as maximum number of thermal couplings, layout of the facility, requirement on the presence and/or absence of certain splits/submixture streams (which is important for retrofitting), etc. Also, note that these 113 configurations cover a wide range of overall reboiler vapor duty requirements. Depending on the actual plant design, some of these configurations with higher reboiler duties might be more attractive than others to provide heat integration opportunities for these reboilers with other process units.

Figure 3.3. A plot showing the optimal objective function values (minimum capital cost) and their corresponding total reboiler vapor duty requirements for all 6128 configurations in the search space under Scenario 2. Each dot represents a configuration. The red and yellow dots in the plot corresponds to the configurations of Figure 3.4a and b, respectively.

Two example configurations are highlighted as the red and yellow dots in Figure 3.3 and are explicitly drawn in Figure 3.4a and b, respectively. The configuration of Figure 3.4a turns out to be the fully thermally coupled (FTC) configuration with sid-

edraw streams BCD, BC, and CD are withdrawn as liquid-only streams. Although it yields the lowest total reboiler vapor duty requirement among all configurations in the search space, the FTC configuration requires the maximum possible number of column sections (i.e. $n(n-1)$ for n-component separation) and submixture streams (i.e. $(n-2)(n+1)/2$), making it complex and expansive to build and difficult to operate [74, 99]. From Figure 3.3, we see that the configuration of Figure 3.3 has a minimum capital cost of 1.828 million USD, which is 69.7% higher than that of the global optimal solution. Fortunately, one can almost always find at least one non-FTC configuration which consumes almost the same lowest reboiler vapor duty but is much cheaper to build. In this case, we identify 60 additional configurations that would require $< 5\%$ more total reboiler heat duty than the configuration of Figure 3.4a but with lower capital costs, among which the best performing configuration has a minimum annualized capital cost of 1.186 million USD. Hence, for most industrial applications, we believe that building the FTC configuration should never be considered as the first choice.

Next, we would like to analyze the example configuration of Figure 3.4b which has the highest minimum capital cost compared to all other configurations and a relatively high reboiler vapor duty requirement. This configuration resembles a indirect split configuration except that column 3 performs a non-sharp split of $ABC \rightarrow AB/BC$, making column 4 a two-feed distillation column. Since the main feed enters column 1 as a saturated liquid stream, a large quantity of vapor duty is required to boil all components but E to vapor state so that stream $ABCD$ can be produced at the top of column 1. This not only increases the capital and operating costs of reboiler at E, but also significantly increases the diameters of column 1 as well as all subsequent distillation columns due to the presence of thermal couplings at submixtures $ABCD$, ABC, and AB. In addition, these sharp splits in the configuration increase the number of trays to achieve the desired separations substantially. The consequence is that giant column shells and many large-sized trays are unavoidable. In fact, the annualized capital costs attributed to trays and column shells are respectively 1.522

and 1.046 million USD, more than twice of the corresponding average costs of 0.727 and 0.508 million USD when considering all 6128 configurations. This example clearly emphasizes the importance of feed conditions, including its thermal quality, on the identification of cost-effective configurations from a different perspective.

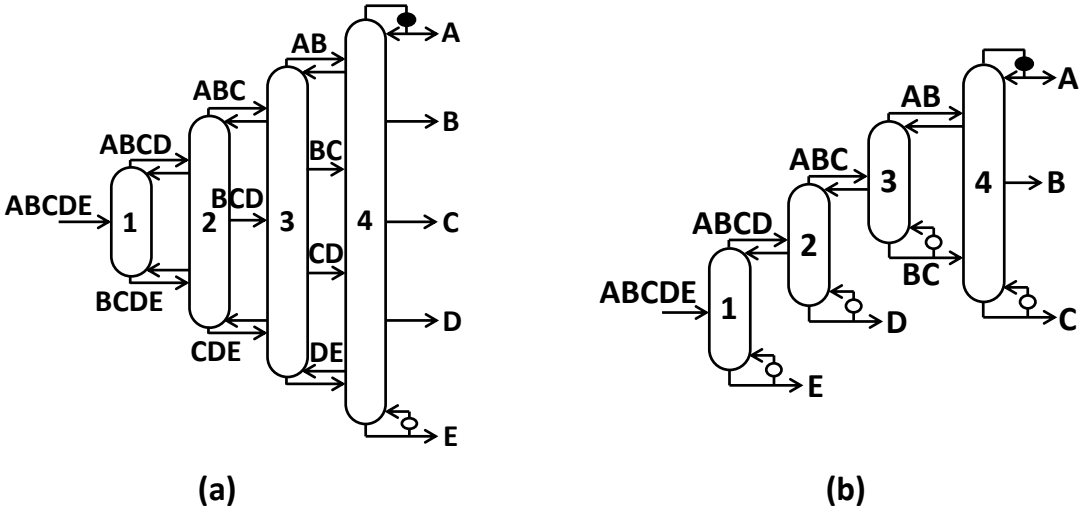

Figure 3.4. (a) Example configuration highlighted as red dot in Figure 3.3; (b) example configuration highlighted as yellow in Figure 3.3.

One interesting observation regarding the ranklist of configurations based on minimum annualized capital cost is that sharp split configurations could achieve much higher rankings compared to Scenario 1. For example, the best performing sharp split configuration, which turns out to be the basic configuration version of Figure 3.1c (i.e. thermal coupling at submixture CDE is replaced with a reboiler), has a minimum annualized capital cost of 1.217 million USD. It is ranked 252nd out of 6128 configurations in the search space (top 4.1 %). Notice that under Scenario 1, this sharp split configurations is placed at the 3967th out of all 6128 configurations in terms of minimum total annualized cost. Therefore, it is important for industrial practitioners to have a clear idea of what they need in practice based on the actual status of the plant such as plant-wise energy balances in order to choose the most suitable objective function to use.

3.4 Ensuring Global Optimality

As we have discussed, the NLP based GMAC framework guarantees global optimality for each and every configuration using global solver BARON [39]. As a comparison with the two-step iterative optimization procedure introduced by Caballero and Grossmann [16], we construct the following equivalent two-step iterative process using the GMAC framework. This is referred to as the two-step minimization algorithm (TMA). In the first step of the iterative procedure of Caballero and Grossmann [16], all binary variables associated with submixture reboilers and condensers are set to zero, indicating the absence of submixture heat exchangers. Equivalently, in the TMA, only CTC configurations are considered during the first stage. All CTC configurations are optimized in the GMAC framework to obtain a ranklist of them with respect to their optimal objective function values. In the second step of the iterative procedure of Caballero and Grossmann [16], the binary variables associated with the same topological structure (i.e. intercolumn connectivity) as the top CTC configuration in the ranklist are fixed, whereas the binary variables associated with submixture heat exchangers now become decision variables. This subproblem essentially solves for the optimal arrangement of submixture reboilers and condensers, and the optimal solution from this second step is recorded. In the equivalent TMA approach, all basic and partially thermally coupled configurations belonging to the same family of the top CTC configuration are identified using the SA method and solved to global optimality in the GMAC framework, and the best optimal objective function value among the family of configurations is recorded. Next, the second-best CTC configuration based on the ranklist of the first step is optimized for the optimal submixture heat exchanger placement in the second step the same way as the best CTC configuration is optimized. If the newly identified configuration has a lower total cost than the one identified earlier, we examine the third-best CTC configuration on the ranklist of the first step. This process is repeated iteratively until the optimal solution obtained from the second step starts worsening. It is then claimed that the

configuration identified by the time the solution starts worsening corresponds to the best configuration with the lowest total cost across all configurations in the search space. A process flow chart illustrating the TMA method is shown in Figure 3.5.

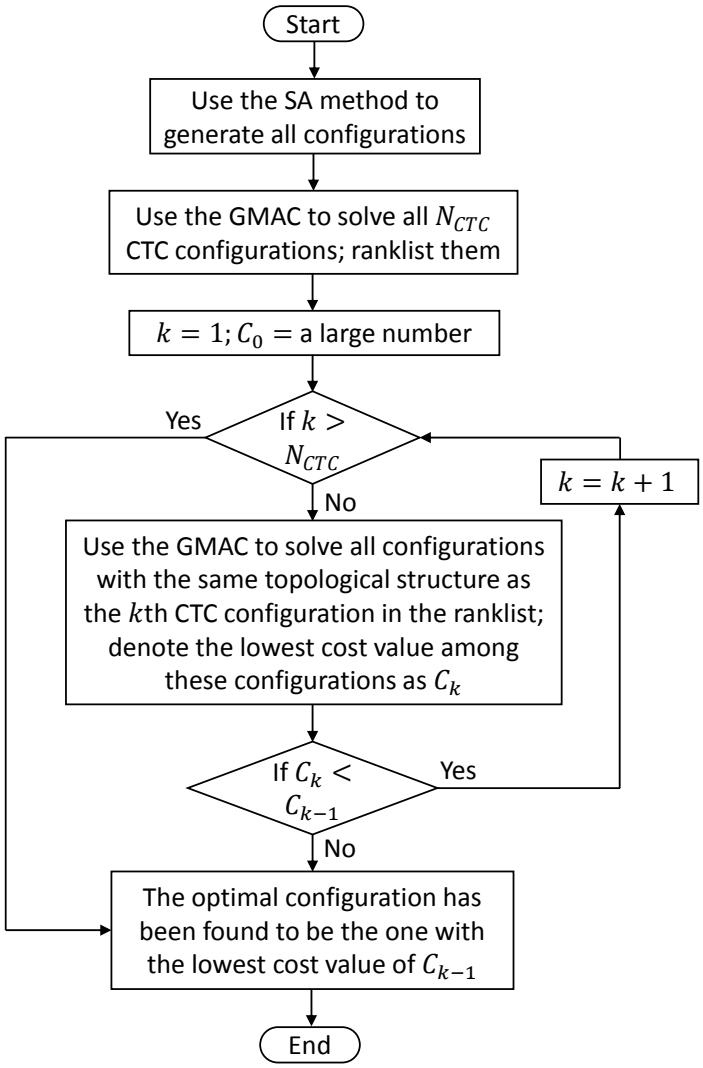

Figure 3.5. Process flow chart that simulates the TMA process using the GMAC approach.

In Scenario 1 of the alcohols separation example, our objective is identify the optimal configuration which has the lowest minimum total annualized cost. Recall from previous discussion that the optimal configuration among all 6128 configurations synthesized by the SA method corresponds to the one drawn in Figure 3.1a. We

find out that the best configuration concluded using the TMA method also turns out to be same one identified by the GMAC framework. In fact, based on various case studies that we have examined, when the objective is to minimize the total annualized cost and the payback period is relatively long (8 to 10 years or more), the optimal configuration identified by the TMA method is always among the few best configurations, if not the best configuration itself, identified by optimizing the entire search space of configurations using the GMAC approach. This is primarily because, as the payback period gets longer, the contribution of the annualized fixed capital investment FCI to the objective function of Equation (3.1), which is represented by the value of coefficient k_{FCI}, because smaller as a result of Equation (3.2) compared to the operating cost contribution. Therefore, configurations with lower YOC (in other words, total vapor duty requirement) are more likely to have lower minimum TAC compared to other configurations with higher YOC. As a result, the CTC configuration ranklist obtained in the first step of the TMA in terms of minimum TAC is expected to match well with the actual ranklist of configurations obtained in the second step. This means that the global optimal configuration is more likely to come from the configuration family where the best CTC configuration comes from. In this case, the two-step iterative procedure of Caballero and Grossmann [16] actually works pretty well.

On the other hand, in scenario 2 of the example in which the objective is to minimize the capital cost, or in the case when the payback period is short, the two-step iterative procedure no longer gives the correct global optimal configuration. This is because the YOC contribution to the objective function now becomes small compared to the FCI contribution. Thus, the CTC configuration ranklist obtained in the first step of the TMA in terms of minimum TAC no longer matches well with the actual ranklist of configurations obtained in the second step. To see this, we use the TMA approach to ranklist the configurations following the steps in Figure 3.5. The green dots in Figure 3.6 represent the minimum annualized capital costs corresponding to the top 23 CTC configurations identified in Step 1 in the ranklist. And the blue

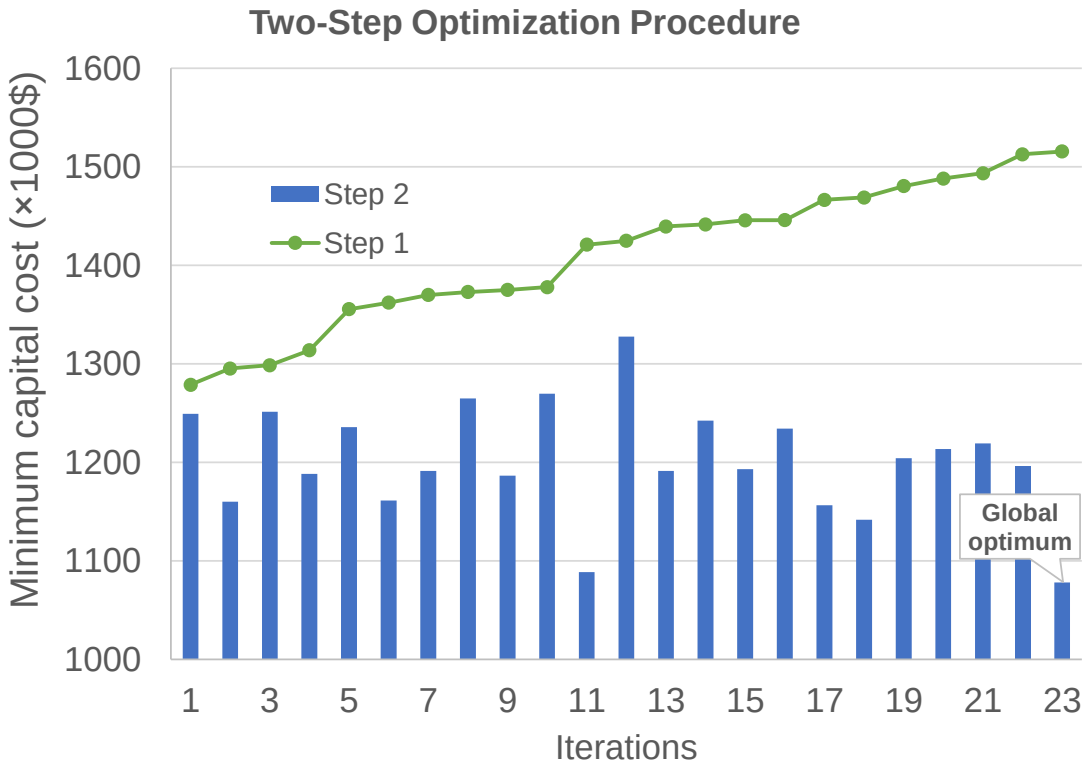

Figure 3.6. Results obtained from the two-step optimization procedure (TMA) for Scenario 2. Following the steps shown in Figure 3.5, the TMA process would have terminated at the third iteration, even though the true global optimal solution actually corresponds to the 23rd iteration.

bars represents the lowest minimum capital costs obtained in Step 2 corresponding to the best heat exchanger arrangements. Each iteration stands for a configuration family. It turns out that the true global optimum, confirmed to be so by the GMAC after solving all 6128 configurations to global optimality, corresponds to the 23rd best configuration family identified in Step 1. However, based on the stopping criterion of Caballero and Grossmann [16], the TMA process would terminate after the first three iterations is finished and conclude that the configuration identified in Step 2 of the 2nd iteration, which has a minimum capital cost of 1.160 million USD, is the "global optimal" solution. In total, one can find 49 configurations with a lower

minimum capital cost than that identified by the TMA method, many of which are attractive candidates from an industrial perspective. This counterexample shows that the two-step iterative procedure proposed by Caballero and Grossmann [16] does not always give the optimal or near-optimal solution for a general problem. Surprisingly, we find out that by simply changing Step 1 from ranklisting all CTC configurations to ranklisting all basic configurations, the global optimal configuration of Figure 3.2 is correctly identified in the modified TMA method. After examining several case studies, we conclude that this modified TMA approach can be used to identify the optimal or near-optimal configuration when the objective function comes to minimizing only the capital costs. It can also be used in cases where the objective is to minimize the total annualized cost but the payback period is short. Of course, this heuristic may still fail to give even the near-optimal solution when the capital cost contribution to the objective function is of similar magnitude compared to the operating cost contribution. In this case, one must rely on the GMAC approach to identify the best performing configuration or to generate an accurate ranklist of configurations in terms of total costs.

3.5 Further Exploration of Process Intensification Opportunities

For a given multicomponent separation task, our GMAC framework gives the ranklist of all basic and thermally coupled regular-column configurations synthesized by the SA method [7] based on their minimum capital and operating costs. One may naturally ask this question: "How to further reduce the capital and operating costs of a distillation configuration?"

Recent advances in process intensification (PI) in multicomponent distillation have offered us the right tools to address this question. In Chapter 2, we introduce the first systematic, multi-layer approach to conduct PI in multicomponent distillation starting from any basic regular-column configuration. Compared to the original configuration, newly synthesized highly intensified configurations, such as the heat and mass integrated configurations and dividing wall columns, are much more compact,

easy-to-operate, energy efficient, and cost-effective to build and operate. In this section, we will demonstrate some of the PI opportunities one may want to explore to further improve the compactness and cost-effectiveness of top configuration candidates identified by the GMAC approach in the alcohols separation example.

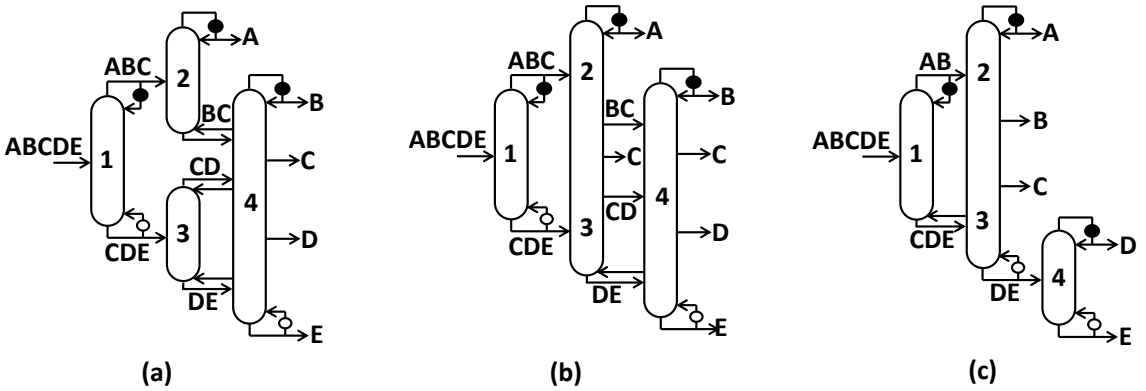

Figure 3.7. (a) the configuration within the top 1% of TAC that uses the lowest number of column sections (12 sections); (b) an intensified, more operable configuration derived from (a) following the strategy of Shenvi et al. [8]; (c) a heat and mass integrated configuration derived from Figure 3.1c.

In Scenario 1 of the alcohols separations example, we identify through GMAC that, among the top 1% of configurations with the lowest minimum TAC, the one requiring the least number of column sections is drawn in Figure 3.7a. This configuration, whose minimum total annualized cost is 1.777 million USD, has two non-sharp splits ($ABCDE \rightarrow ABC/CDE$ and $CDE \rightarrow CD/DE$) and uses only 12 column sections. In this configuration, submixture streams BC and CD are thermal couplings that respectively connect column 2 and column 3 with column 4 in which the common component C is withdrawn as final product. It turns out that one can further reduce the TAC of this configuration as well as enhancing its operability by first converting both thermal couplings of BC and CD into liquid-only transfer streams [100], followed by performing simultaneous heat and mass integration to consolidate columns 2 and 3 into a single column shell of column 2-3 while producing the common final product

C as a sidedraw stream [8]. The resulting intensified configuration is shown in Figure 3.7b. Compared with the original configuration of Figure 3.7a, this new configuration uses only three column shells and requires a smaller reboiler at final product E as the heat duty can be reduced by heat and mass integration [8, 99]. Thus, despite having to introduce an additional column section to the consolidated column 2-3, the configuration of Figure 3.7b is likely to have an even lower minimum TAC compared to the original configuration of Figure 3.7a. Apart from being more cost-effective, this new configuration is also more operable than the original configuration since submixtures BC and CD are now completely transferred from column 2-3 to column 4 as liquid-only streams whose flow rates can be controlled precisely. Moreover, the operability issue associated with thermally coupled columns 3 and 4 in Figure 3.7a, as a result of stringent pressure requirement [101], is now resolved in the new configuration of Figure 3.7b when column 2-3 in the new configuration is allowed to be operated at a uniformly lower pressure with respect to column 4 so that the vapor generated at reboiler of E can flow to column 2-3 naturally.

Likewise, one PI strategy to possibly reduce the total cost of the best performing sharp split configuration drawn in Figure 3.1c is to perform heat and mass integration between a lighter pure product reboiler and a heavier pure product condenser [102]. As shown in Figure 3.7c, the heat and mass integrated configuration is derived from the original sharp split configuration by first eliminating the reboiler associated with final product B and the condenser associated with final product C, followed by consolidating column 2 and 3 into one single column 2-3 while withdrawing pure products B and C as sidedraws. Of course, the strategy of heat and mass integration can also take place between reboiler at B and condenser at D. However, one can easily calculate these heat exchanger duties and verify that the integration between reboiler at B and condenser at C offers greater heat duty savings and thus more potential savings on heat exchanger costs. Overall, by simultaneously eliminating two heat exchangers and one column shell, we believe that the heat and mass integrated configuration of

Figure 3.7c has the potential to offer substantial reductions in capital and operating costs compared to the original sharp split configuration of Figure 3.1c.

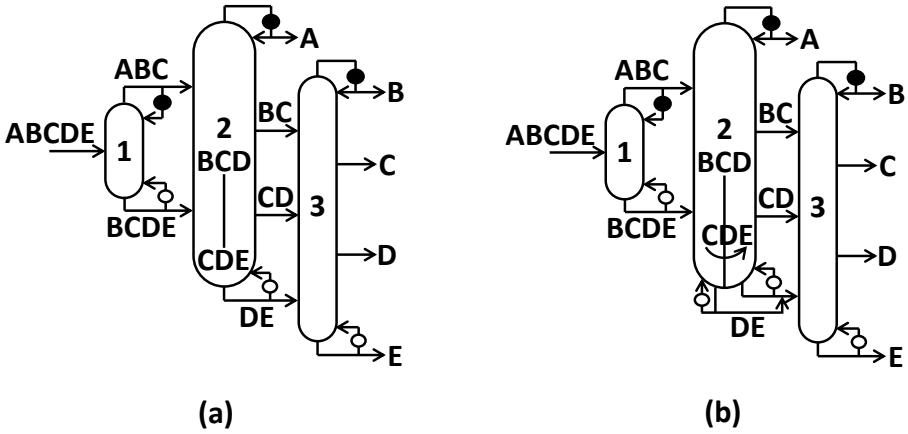

Figure 3.8. (a) A thermodynamically equivalent version of Figure 3.2 by consolidating columns 2 and 3 into one column shell with a vertical partition. This dividing wall column arrangement is expected to have a lower capital cost compared to that of Figure 3.2; (b) an equivalent, operable version of (a) derived by following the methodologies of Medenoor Ramapriya et al. [77]. Submixture CDE is now transferred from one zone in the dividing wall column to the other as a liquid-only stream.

In Scenario 2 of the alcohols separation example, we have concluded from the GMAC approach that the optimal configuration with the lowest annualized capital cost among 6128 configurations is the one shown in Figure 3.2. We realize that columns 2 and 3 in the optimal configuration of Figure 3.2 are especially suitable for PI using a dividing wall column (DWC). Compared to conventional distillation configurations, DWCs have been known to substantially reduce the capital cost as well as land requirement since they use less number of column shells and other equipment pieces [38, 75]. For example, as much as 30% of capital cost reduction for ternary separations has been reported when DWCs are used in place of conventional sharp split configurations [79]. For the configuration of Figure 3.2, vapor duty generated by the reboiler at DE is first split into two fractions, one continues to travel upward within column 3 while the other goes to column 2 through the thermal coupling at

CDE. These two fractions of vapor traffic will eventually merge back to column 3 above the thermal coupling at BCD. Based on this observation, it is expected that when consolidating columns 2 and 3 of Figure 3.2 into a single column shell with a vertical partition as shown in Figure 3.8a, the resulting DWC will have the the same or at least similar diameter and height as column 3 in the original configuration of Figure 3.2. This means that we have essentially eliminated column 2 of Figure 3.2 with no penalty but only savings in column shell costs! In addition, the new configuration of Figure 3.8a is thermodynamically equivalent to the original regular-column configuration [77]. In other words, the heat exchanger costs and duties are unlikely to change notably after process intensification. Of course, one also needs to consider the cost of the vertical partition, as well as any additional cost associated with specially designed column internals and trays for the DWC. However, this intensified configuration of Figure 3.8a is still expected to perform even better than its original regular-column configuration in terms of annualized capital investment.

Despite having the potential to offer further capital savings compared to the configuration of Figure 3.2, the DWC in the intensified configuration of Figure 3.8a might face challenges in achieving the desired vapor split at the bottom of the vertical partition. To solve this operability difficulty, Madenoor Ramapriya et al. [77] proposed a systematic approach from which one can arrive at a thermodynamically equivalent version shown in Figure 3.8b. In this version, submixture CDE is transferred from one zone in the DWC to the other externally as a liquid-only stream. The features of extended vertical partition and an additional reboiler producing the same mixture DE make this DWC easy to operate and control, as the desired L/V ratio in both zones of the DWC can be reached and maintained precisely. Note that the sum of heat duties generated at both reboilers that produce the same submixture DE of Figure 3.8b is equal to that generated at the single reboiler at DE of Figure 3.8a, meaning that the heat exchanger costs for these two configurations should be similar.

As we can see from these illustrations, synergistic use of the powerful global optimization tool such as the GMAC and conceptual design strategies based on PI can

lead to the discovery of completely new and highly intensified configuration flowsheets that are compact and inexpansive to build and easy to operate. It has opened up many great opportunities for industrial practitioners, many of which are hitherto unknown to them before. Of course, to truly identify the global optimal configuration design, it would be more desirable to include these new and intensified configurations into the search space of attractive and useful configurations and incorporate them into the GMAC framework. This would require us to first come up with a new superstructure formulation like the SA method [7] to systematically enumerate the search space that also includes these intensified configurations. And second, we need to update the cost model in the current GMAC framework to accurately estimate the capital and operating costs associated with these new intensified configurations. This will be one of our research directions in the future.

3.6 Conclusion

For the first time, we develop an enumeration based global optimization algorithm for the economic optimization (GMAC) of any regular-column distillation configuration synthesized by the SA method [7] that distills any ideal or near-ideal multicomponent mixture. This method greatly extends the GMA framework [34] developed recently to minimize the total reboiler vapor duty requirement of any regular-column configuration. Compared with existing models in the literature, more accurate cost models have been incorporated in the GMAC framework. Cost related parameters and correlations can be specified by users as they wish, making the GMAC a robust and flexible tool to use. Moreover, the GMAC approach guarantees global optimality for any configuration in the search space synthesized by the SA method [7], which enables us to obtain the complete ranklist of configurations based on any cost related objective.

The effectiveness and robustness of the GMAC model are demonstrated on various 4- to 6-component separation examples in the literature. It is found that the GMAC method can solve all distillation configurations to global optimality for all

cases within minutes to hours, depending on the problem size. In this article, we present a case study involving a five-component alcohols separation example in detail, from which many valuable insights are generated to help industrial practitioners to choose and design energy efficient and cost-effective configurations provided the specific separation task. The energy requirement, capital cost, as well as operability of the attractive configurations identified by the GMAC approach can be further improved by applying new process intensification strategies such as heat and mass integration and dividing wall column as discussed in Chapter 2. Combining the powerful global optimization algorithm such as the GMAC as a useful screening tool with novel conceptual design techniques will enable process engineers to quickly shortlist a few attractive configuration candidates and generate highly attractive designs which can undergo further, more detailed analysis.

We demonstrate that the two-step iterative optimization procedure which decomposes the original problem into two independent subproblems, cannot guarantee global optimality on the result it finds. The GMAC method is thus the only economic optimization framework available as of now that guarantees global optimality. In the next phase, we will devote ourselves to developing an effective and efficient MINLP based global optimization model for economics analysis and its solution strategies to identify the single best configuration or the top-K best configurations within seconds or minutes.

4. GLOBAL MINIMIZATION OF TOTAL EXERGY LOSS FOR MULTICOMPONENT DISTILLATION CONFIGURATIONS

The operating cost of a multicomponent distillation system comprises two major aspects: the overall heat duty requirement and the temperature levels at which the heat duties are generated and rejected. The second aspect, often measured by the thermodynamic efficiency of the distillation system, can be quantified by its total exergy loss. In this chapter, we introduce a global optimization framework for determining the minimum total exergy loss required to distill any ideal or near-ideal multicomponent mixture using a sequence of columns. Desired configurations identified by this new framework tend to use milder-temperature reboilers and condensers and are thus attractive for applications such as heat pump assisted distillation. Through a case study of shale gas separations, we demonstrate the effectiveness of this framework and present some useful physical insights for designing energy efficient distillation systems.

4.1 Introduction

The operating cost or energy consumption of a distillation configuration comprises two major aspects: the total reboiler heat duty requirement, which is proportional to the sum of vapor flows generated at all reboilers per unit time, as well as the temperature levels at which the heat duties are generated by the reboilers and rejected by the condensers [47]. The first aspect is associated with the first-law heat-duty demand of a distillation configuration, whereas the second aspect is closely related to the heating and cooling utility costs (second-law temperature-level costs) of the reboilers and condensers. Here, we clearly distinguish the difference between “energy” and “heat”. While most people have been primarily focusing on the absolute value of

overall heat duty needed in a configuration, less attention is paid on the temperature levels at which the generation and removal of heat duties occur, i.e. the qualities of the heat duties. Failure to recognize and consider both aspects may lead to the design of inefficient distillation systems [47, 103].

Thermodynamic efficiency analysis is an useful tool to evaluate the energy performance of a multicomponent distillation system [104]. One of the classic industrial examples that illustrates the importance and potency of thermodynamic efficiency analysis is the separation of air into high purity nitrogen, oxygen, and argon products. This separation, which is conducted at cryogenic conditions, is primarily driven by *work* instead of *heat*. Thus, the thermodynamic efficiency of this process is characterized using the following definition [105]:

$$\eta = \frac{\text{minimum work of separation}}{\text{total work of separation}} \tag{4.1}$$

Under this definition of Equation (4.1) based on total work input, Agrawal and Fidkowski [47] calculated the thermodynamic efficiency for each of the three ternary thermally coupled configurations shown in Figure 4.1. In this figure, and also in all subsequent figures, capital letters A, B, C, and so on represent pure components with their volatilities decreasing in alphabetical order. It is determined that the side-rectifier configuration of Figure 4.1b has the highest thermodynamic efficiency of 44.52%, which is consistent with the industrial practice for argon recovery that has been in use for over 85 years [106]. On the other hand, the three-component fully thermally coupled (FTC) Petlyuk configuration [26] of Figure 4.1c, which is known to always have the lowest total heat duty requirement among all configurations, has only 1/3 the thermodynamic efficiency as the side-rectifier configuration. This is because, even though the FTC configuration requires the lowest possible heat duty, all the heat is generated at the highest temperature reboiler (i.e. reboiler at C of Figure 4.1c) and removed at the lowest temperature condenser (i.e. condenser at A of Figure 4.1c). Thus, it is not surprising that, in spite of many attempts trying to improve

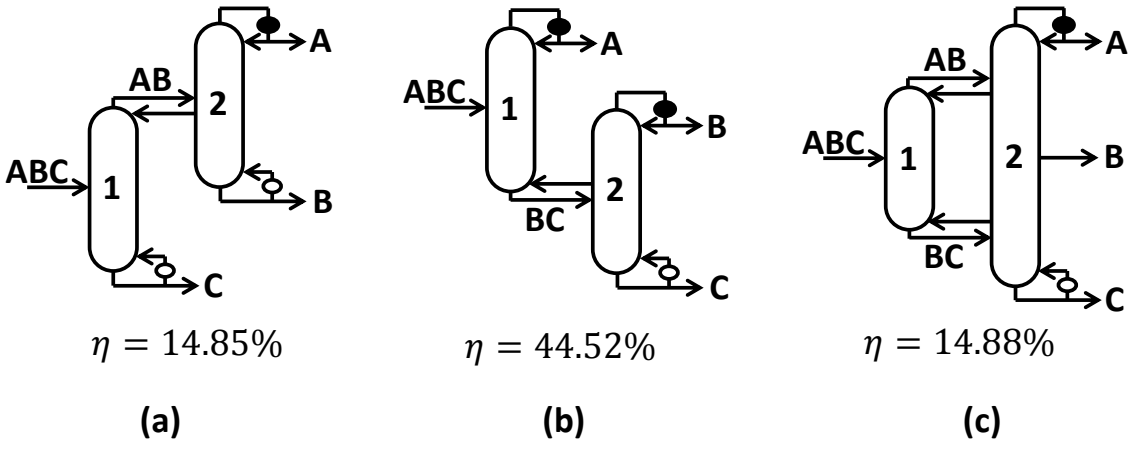

Figure 4.1. (a) Indirect split thermally coupled configuration, which is equivalent to the side-stripper scheme; (b) direct split thermally coupled configuration, which is equivalent to the side-rectifier scheme; (c) the fully thermally coupled (FTC) Petlyuk column [26]. The thermodynamic efficiencies for these configurations are determined by Agrawal and Fidkowski [47]. In this example, A = nitrogen, B = argon, and C = oxygen.

the energy efficiency of the FTC configuration [107], it has not found any successful application in cryogenic air separation. In fact, for ternary separations, the range of feed conditions under which the FTC configuration has a higher thermodynamic efficiency than other configurations turns out to be quite limited [47]. Flores et al. [50] also reached similar conclusions when considering a set of cases involving ternary and quaternary separations.

The usefulness of thermodynamic efficiency analysis is not only limited to cryogenic separations, but also in applications such as heat pump assisted distillation, multi-effect distillation, heat integrated distillation, vapor recompression distillation, etc. These applications may or may not have to be operated at subambient conditions. It is worth pointing out that the definition of thermodynamic efficiency of Equation (4.1) is more accurate and reasonable than various other definitions [3, 108] where minimum work of separation is directly compared to the total heat supplied to the reboiler, which implicitly assumes that this heat cannot be reused anywhere else as it

gets removed by the condenser. This underlying assumption is clearly inaccurate for the applications listed above and for highly integrated plants where the rejected heat is often used elsewhere. In fact, the thermodynamic efficiency of distillation process calculated based on such definitions is usually abnormally small and can never reach 100% even for a fully reversible process [109, 110], which often leads to the misconception that distillation is always inefficient to operate compared to other separation processes such as membranes. The definition of Equation (4.1), on the other hand, captures the true thermodynamic efficiency of the distillation process itself.

The total work of separation in the denominator of Equation (4.1) is often explicitly expressed as the sum of minimum work of separation and *exergy loss* of the process [104, 105, 111–113]:

$$\text{total work of separation} = \text{minimum work of separation} + \text{exergy loss} \tag{4.2}$$

The exergy of a stream is equal to the maximum work obtainable when it is brought to the reference conditions via a reversible path [114]. To understand this, consider the schematic diagram of Figure 4.2, in which two equal quantities of heat duty Q_H (Q_C) at two different temperatures above (below) the reference point are brought to the reference condition using reversible heat engines (reversible heat pumps). Combining the first and the second law of thermodynamics, one can easily show that the work outputs from the reversible heat engines (heat pumps) are given by:

$$\begin{aligned} W_H = Q_H\Big(1 - \frac{T_0}{T_H}\Big) > W'_H = Q_H\Big(1 - \frac{T_0}{T'_H}\Big) > 0 \\ W_C = Q_C\Big(1 - \frac{T_0}{T_C}\Big) < W'_C = Q_C\Big(1 - \frac{T_0}{T'_C}\Big) < 0 \end{aligned} \tag{4.3}$$

in which a negative work output (i.e. W_C or W'_C) simply means that work input is required to "pump" the heat Q_C from a lower temperature level T_C or T'_C to the reference temperature T_0. From Equation (4.3), one can readily see that for the same

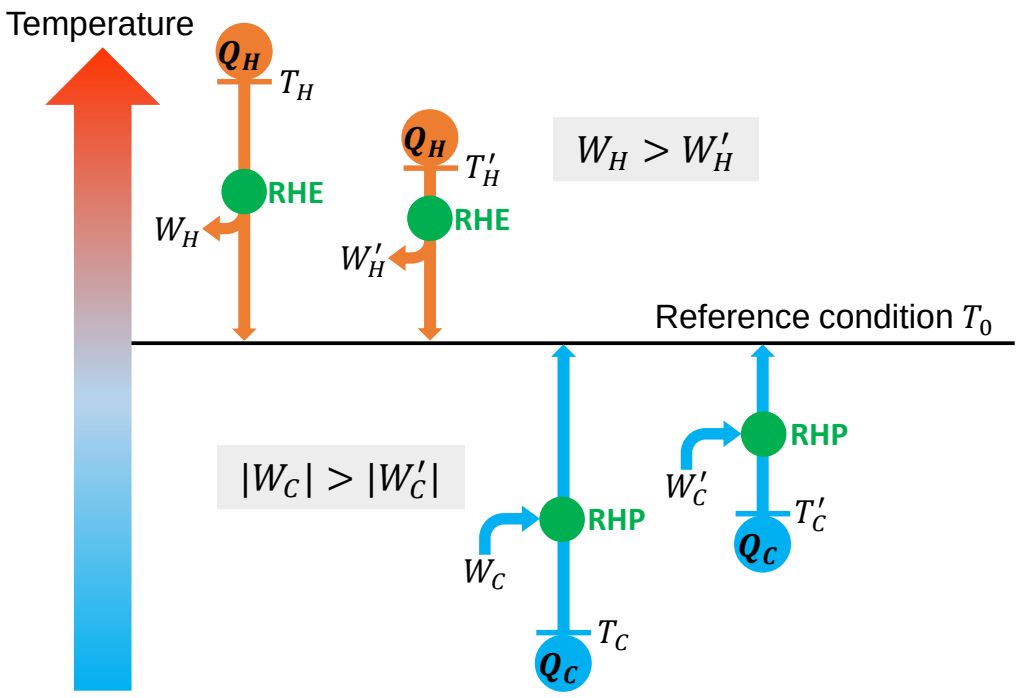

Figure 4.2. For the same amount of heat Q_H at two different temperature levels ($T_H > T'_H$) above the reference temperature T_0, the one at T_H generates more work W_H from the reversible heat engine (RHE) than the one at T'_H when both heats are brought to T_0 ($W_H > W'_H > 0$). Similarly, for the same amount of heat Q_C at T_C and T'_C ($T_C < T'_C$) which are lower than T_0, the one at the lower temperature T_C requires more work input from the reversible heat pump (RHP) than the one at T'_C when they are brought to T_0 ($W_C < W'_C < 0$).

amount of heat at different temperature levels, the one at more extreme temperature produces or requires more work (exergy) than the one at a milder temperature. Thus, we can determine the thermodynamic efficiency of the distillation process itself based on the exergy loss within the distillation column, which can be characterized by the temperature level at which the reboiler and condenser are operated [105, 115].

Agrawal and Herron [115] applied the concept of exergy analysis to determine the optimal thermodynamic efficiency of a distillation column separating ideal binary mixtures for several feed conditions and relative volatilities. Following the simplifying assumptions of ideal vapor-liquid equilibrium relations, constant relative volatilities,

and constant and equal latent heats of vaporization for both components over the operating temperature range of the column, the authors made a groundbreaking discovery that temperatures do not appear explicitly in the final efficiency expressions [115]. Based on this finding, Agrawal and Herron [116] analyzed the optimal placement of an intermediate reboiler and/or intermediate condenser in a binary distillation column and generated several heuristics [117]. While previous studies have been centered on binary mixture distillations, Agrawal and Fidkowski [109] also studied the thermodynamic efficiencies for conventional as well as "improved" direct and indirect split basic configurations for ternary mixture separations. As shown in Figure 4.3, the improved configurations modify the reboiler and condenser associated with interconnecting stream between the two distillation columns (also called submixture) to simultaneously produce two streams with the same composition, one as saturated liquid and the other as saturated vapor, that enter the next distillation column as feed. Using modified reboilers and condensers at submixtures locations reduces the total exergy loss of the distillation process [109, 118]. Agrawal and Fidkowski [103] later extended the idea of Agrawal and Herron [109] to analyze the thermodynamic efficiencies of ternary direct and indirect split thermally coupled configurations. However, since then, there has not been many attempts in the literature to further generalize this methodology to systematically account for distillation configurations that separate four or more components.

As the size of regular-column configuration search space quickly explodes as the number of components in the feed increases [7, 18], it quickly becomes too computationally expansive to possibly perform total exergy loss calculations for each and every configuration in the search space using process simulators such as Aspen Plus. One almost always needs to formulate an optimization problem that can be quickly solved to explore the entire search space within reasonable amount of time in order to identify one or a set of energy efficient configurations for a given separation task. The search for the global optimal configuration in the entire search space can be carried out using two distinct approaches. The first approach is to formulate the optimization

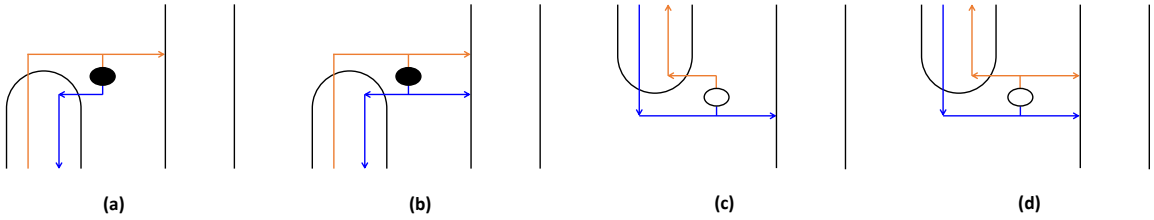

Figure 4.3. (a) A conventional submixture condenser; (b) modified condenser configuration generating two feed streams to the next column; (c) conventional submixture reboiler; (d) modified reboiler configuration producing two feed streams to the next column. Orange lines indicate vapor flows and blue lines indicate liquid flows.

problem as a single mixed-integer nonlinear programming (MINLP) problem [16,35]. If succeeded, this MINLP based approach can find the global optimal solution without enumerating all the configurations in the search space. However, for many cases, the resulting MINLP could not be solved to global optimality due to various convergence difficulties [35]. Despite various attempts that tried to tackle these issues, including proposing an alternative algorithm based on a modified version of logic-based outer-approximation algorithm [35] as well as decomposing the optimization problem into subproblems followed by introducing an iterative optimization procedure to solve them [16], the MINLP based approach still fails to guarantee global optimality [119].

Besides the MINLP based approach discussed above, a fundamentally different approach to search for the optimal distillation configuration is to first synthesize the complete search space, followed by formulating an optimization problem for each configuration in the search space. This is also known as the enumeration based approach [33]. Recently, Nallasivam et al. [34] developed an enumeration based global minimization algorithm (GMA) to minimize the total reboiler vapor duty requirement for each and every basic and thermally coupled regular-column configuration synthesized by the SA method [7]. In the GMA approach, the optimization for each configuration is formulated as a nonlinear programming problem (NLP) and can be solved to global optimality using global solver BARON [39] in GAMS in a matter

of seconds. A number of strategies, such as parallelization and bound tightening techniques [34], can further bring down the computational time significantly. The objective of this chapter is to develop a general NLP based global optimization algorithm that minimizes the total exergy loss (i.e. maximizes thermodynamic efficiency since the minimum work of separation in Equation (4.1) is a constant if feed and product specifications are known) for any regular-column distillation configuration. This algorithm is referred to as the Global Minimization Algorithm for Exergy, or simply GMAE.

In the GMAE formulation, the majority of the GMA framework [34] is retained; additional exergy related relations and constraints are added and will be explained in the next section. Once the complete GMAE framework is introduced, we will examine a five-component case study involving natural gas liquids (NGLs) recovery and fractionation to demonstrate the usefulness and robustness of the GMAE approach. By investigating several representative configurations in detail, We explore some of the physical insights behind them and show how these insights can generate useful heuristics and guidelines for process engineers to identify energy efficient configurations. Next, several process intensification strategies discussed in Chapter 2 will be considered to further improve the thermodynamic efficiency, eliminate equipment pieces, and save capital cost of a distillation configuration.

4.2 NLP Formulation

Any optimization problem is described by the decision variables, the objective function, and the constraints. In the GMAE formulation, all the decision variables and constraints from the GMA framework described by Nallasivam et al. [34] are retained. In particular, we use the Underwood's method for minimum vapor duty calculations in each column section [19]. This implies that the GMAE model is constructed based on the same underlying assumptions as the GMA model, i.e. ideal vapor-liquid equilibrium, constant relative volatility, as well as constant and equal latent heats for all components throughout the distillation columns [34]. Despite

having to make these assumptions to simplify the model, it is found that the GMA approach still gives very accurate total reboiler duty estimates compared to the results obtained by performing rigorous Aspen Plus simulations using real thermodynamic models for zeotropic multicomponent separations [40].

Instead of using the total reboiler vapor duty requirement as in the GMA framework, the objective function for the GMAE is to minimize the total exergy loss $\Delta\mathcal{E}_{loss}$ for all distillation columns in a configuration. To formulate the $\Delta\mathcal{E}_{loss}$ expression of any distillation configuration, consider an example configuration shown in Figure 4.4 involving four-component mixture separation. The configuration of Figure 4.4a uses conventional heat exchangers at submixtures ABC and BCD, each producing one single-phase stream which then enters the next distillation column. On the other hand, the configuration of Figure 4.4 adopts the modified heat exchanger configurations at ABC and BCD following Figure 4.3 to simultaneously produce two streams with the same composition but different phases to enter the next column. In the GMAE model, users have the flexibility to specify either submixture heat exchanger scheme.

For illustration, let us examine the improved configuration of Figure 4.4b whose control volume for exergy loss calculations is explicitly drawn in Figure 4.4c. To calculate the total exergy loss of the distillation process alone for this configuration, only the exergy losses associated with material streams entering and leaving the distillation columns are considered. Exergy losses within the reboilers and condensers are excluded from the calculations. This is reflected in Figure 4.4c in which the green boxes around all heat exchangers are subtracted from the region enclosed by the large green box around the configuration. Notice that the material streams entering and leaving the reboilers and condensers are still included in the control volume. The objective function is simply to minimize the difference between the exergies associated

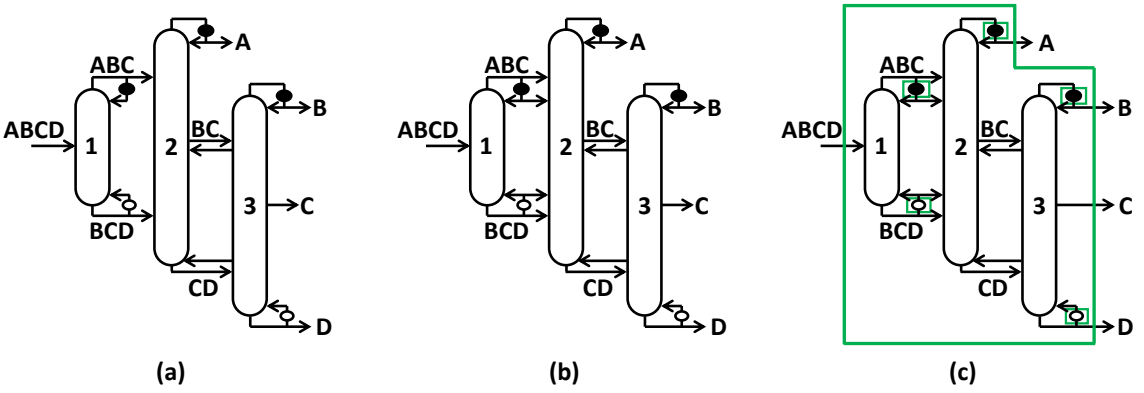

Figure 4.4. (a) An example configuration for four-component separation; (b) an improved configuration of (a) using modified reboiler at BCD and modified condenser at ABC following Figure 4.3; (c) the same configuration of (b) highlighting the control volume for exergy loss calculations. The control volume is defined as the large green box around the entire configuration followed by subtracting all the small regions enclosed by green boxes around all reboilers and condensers to indicate that exergy losses associated with heat exchangers are excluded from the control volume.

with all material inflows and the exergies associated with all material outflows of the control volume:

$$\min \quad \Delta\mathcal{E}_{loss} = \mathcal{E}_{ABCD} - \sum_{i=A}^{D} \mathcal{E}_i + \sum_{i \in REB} (\mathcal{E}_{i,in} - \mathcal{E}_{i,out}) + \sum_{i \in COND} (\mathcal{E}_{i,in} - \mathcal{E}_{i,out}) \quad (4.4)$$

in which the sets REB and $COND$ respectively store the indices of streams associated with reboilers and condensers, including the ones producing final pure products. In this example, $REB = \{BCD, D\}$ and $COND = \{ABC, A, B\}$.

Each exergy term in the objective function of Equation (4.4) is contributed by the exergy associated with mixing ($\mathcal{E}^M$), thermal ($\mathcal{E}^T$) and pressure ($\mathcal{E}^P$) exergy associated with temperature and pressure change from the reference state to the saturated liquid state, as well as thermal exergy as a result of phase change ($\mathcal{E}^\phi$). In other words, $\mathcal{E} = \mathcal{E}^M + \mathcal{E}^P + \mathcal{E}^T + \mathcal{E}^\phi$. Note that $\mathcal{E}^M = 0$ for pure components and

$\mathcal{E}^{\phi} = 0$ for any saturated liquid stream, including the final products which are taken as saturated liquid streams as shown in Figure 4.4. When a material stream of one phase undergoes phase change inside a reboiler or condenser, the only contributor to the exergy difference is the thermal exergy associated with phase change. And this exergy difference between a saturated liquid stream and a saturated vapor stream with the same composition, temperature, and pressure is given by [114]:

$$\begin{aligned} &\text{For pure component stream } i\text{: } \mathcal{E}_i^{vap} - \mathcal{E}_i^{liq} = F_i \Delta H \Big(1 - \frac{T_0}{T_i}\Big) \\ &\text{For mixture stream } i\text{: } \mathcal{E}_i^{vap} - \mathcal{E}_i^{liq} = F_i \Delta H \int_0^1 \Big(1 - \frac{T_0}{T_i}\Big) dq \end{aligned} \tag{4.5}$$

where ΔH is the molar latent heat of vaporization used to represent the multicomponent system (recall the constant and equal latent heat assumption for all components), F_i is the molar flow rate of material stream i, T_0 is the reference temperature, q stands for the thermal quality (liquid fraction) of the stream. Notice that the temperature T_i for mixture stream i varies during phase change and is a function of the thermal quality q of the stream. On the other hand, for pure component streams, the temperature remains constant during phase change.

Also, through extensive calculations for various mixtures, it is found numerically that the thermal or pressure exergy associated with a multicomponent mixture stream at its saturated liquid state is approximately equal to the sum of thermal or pressure exergies of the individual components at their saturated liquid states [47, 109]. Combining this valid simplification with Equation (4.5) gives the exergy difference between the main feed stream $ABCD$ with thermal quality of q_F and the sum of exergies of final product streams, i.e. pure A, B, C, and D as shown in Figure 4.4c:

$$\mathcal{E}_{ABCD} - \sum_{i=A}^{D} \mathcal{E}_i = F_{ABCD} \left[RT_0 \sum_{i=A}^{D} z_{i,F} \ln z_{i,F} + \Delta H \int_{q_F}^{1} \Big(1 - \frac{T_0}{T_{ABCD}}\Big) dq \right] \tag{4.6}$$

in which $F_{ABCD} = \sum_{i=A}^{D} F_i$ is the total molar flow rate of feed $ABCD$, R is the universal gas constant, and $z_{i,F} = F_i / F_{ABCD}$ is the net composition of component i

in the main feed. The quantity $-F_{ABCD}RT_0\sum_{i=A}^{D} z_{i,F}\ln z_{i,F}$ exactly corresponds to the minimum work of separation in Equation (4.2) per unit time, whose magnitude is equal to the Gibbs free energy change of mixing for an ideal solution. Substituting Equations (4.6) and (4.5) into (4.4) yields:

$$\begin{aligned}\Delta\mathcal{E}_{loss} = F_{ABCD}RT_0\sum_{i=A}^{D} z_{i,F}\ln z_{i,F} + F_{ABCD}\Delta H\int_{q_F}^{1}\Big(1-\frac{T_0}{T_{ABCD}}\Big)dq \\ + \sum_{i\in REB} B_i\Delta H\int_0^1\Big(1-\frac{T_0}{T_i}\Big)dq - \sum_{i\in COND} D_i\Delta H\int_0^1\Big(1-\frac{T_0}{T_i}\Big)dq\end{aligned} \tag{4.7}$$

where B_i and D_i stand for the material flow rates that enter the reboiler and condenser associated with stream i, respectively.

Before simplifying Equation (4.7), we would like to introduce an alternative approach to derive the total exergy loss expression based on simple physical intuitions. Based on the control volume drawn in Figure 4.4c and Equation (4.3), one can easily realize that the quantity $\sum_{i\in REB}(\mathcal{E}_{i,in}-\mathcal{E}_{i,out})+\sum_{i\in COND}(\mathcal{E}_{i,in}-\mathcal{E}_{i,out})$ in the objective function of Equation (4.4) is nothing but the total reversible heat pump work needed to utilize all the heat duties removed by the condensers to supply all heat duties required by the reboilers in the configuration. This analogy between exergy loss and reversible heat pump work makes the derivation of Equation (4.9) easier and more intuitive. First, we may bring all the condenser duties to the reference temperature T_0 using reversible heat pumps. Notice that without loss of generality, we have assumed here that T_0 is higher than the boiling point of the heaviest component, T_D; but this does not need to be the case. From Figure 4.2 and Equation (4.3), the total reversible heat pump work input associated with condenser duties, denoted as HPW_{COND}, is simply:

$$HPW_{COND} = \sum_{i\in COND} D_i\Delta H\int_0^1\Big(\frac{T_0}{T_i}-1\Big)dq$$

Of course, HPW_{COND} is more than what is needed to supply the reboiler duties at $T_i \quad i \in REB$ which are all lower than T_0. Thus, in the next step, we need to determine the excess reversible heat pump work that needs to be subtracted from HPW_{COND} to obtain the true work requirement. And this excess work is simply the work input required to pump all the reboiler duties to T_0 reversibly:

$$HPW_{REB} = \sum_{i \in REB} B_i \Delta H \int_0^1 \Big(\frac{T_0}{T_i} - 1\Big) dq$$

As a result, the true reversible heat pump work requirement, i.e. the quantity $\sum_{i \in REB}(\mathcal{E}_{i,in} - \mathcal{E}_{i,out}) + \sum_{i \in COND}(\mathcal{E}_{i,in} - \mathcal{E}_{i,out})$, is:

$$\begin{aligned} HPW_{COND} - HPW_{REB} = & \sum_{i \in COND} D_i \Delta H \int_0^1 \Big(\frac{T_0}{T_i} - 1\Big) dq \\ & - \sum_{i \in REB} B_i \Delta H \int_0^1 \Big(\frac{T_0}{T_i} - 1\Big) dq \end{aligned}$$

which matches with the related terms in Equation (4.7) exactly.

Next, to simplify Equation (4.7), we follow the procedure of Agrawal and Herron [115–117] to perform an overall enthalpy balance on the control volume, which suggests that the sum of condenser duties must equal to the sum of reboiler duties as well as the heat input required to vaporize a portion of the main feed to the specified thermal quality:

$$\sum_{i \in COND} D_i \Delta H = \sum_{i \in REB} B_i \Delta H + (1 - q_F) F_{ABCD} \Delta H$$

which can also be expressed as:

$$\sum_{i \in COND} D_i \Delta H \int_0^1 dq = \sum_{i \in REB} B_i \Delta H \int_0^1 dq + F_{ABCD} \Delta H \int_{q_F}^1 dq \tag{4.8}$$

Now, multiplying both sides of Equation (4.8) with a constant factor $1 - \frac{T_0}{T_D}$ and substituting the resulting expression into Equation (4.7) gives:

$$\begin{aligned}\Delta\mathcal{E}_{loss} = {} & F_{ABCD}RT_0\sum_{i=A}^{D} z_{i,F}\ln z_{i,F} - F_{ABCD}T_0\Delta H\int_{q_F}^{1}\Big(\frac{1}{T_{ABCD}} - \frac{1}{T_D}\Big)dq \\ & - T_0\sum_{i\in REB} B_i\Delta H\int_0^1\Big(\frac{1}{T_i} - \frac{1}{T_D}\Big)dq + T_0\sum_{i\in COND} D_i\Delta H\int_0^1\Big(\frac{1}{T_i} - \frac{1}{T_D}\Big)dq\end{aligned} \tag{4.9}$$

Although the total exergy loss expression of Equation (4.9) does involve temperature, in the context of the GMAE model assumptions, the Clausius-Clapeyron relation actually implies that the need for temperature calculations can be completely eliminated [115, 120, 121].

$$\begin{aligned}&\text{For pure component } i\text{: } \Delta H\Big(\frac{1}{T_i} - \frac{1}{T_D}\Big) = R\ln\alpha_i \\ &\text{For mixture stream } i\text{: } \Delta H\Big(\frac{1}{T_i} - \frac{1}{T_D}\Big) = R\ln\Big(\sum_{j=A}^{D}\alpha_j x_{j,i}\Big)\end{aligned} \tag{4.10}$$

in which α_j is the relative volatility of component j with respect to the heaviest component D, and $x_{j,i}$ is the liquid mole fraction of component j in stream i. This simple but powerful result allows us to reformulate the objective function of Equation (4.9) for every distillation configuration by using only the decision variables introduced in the GMA framework. Substituting Equation (4.10) into Equation (4.9), the total exergy loss of the entire configuration of Figure 4.4c can now be solely expressed in terms of relative volatilities and material stream composition variables:

$$\begin{aligned}\frac{\Delta\mathcal{E}_{loss}}{RT_0} = {} & F_{ABCD}\sum_{i=A}^{D} z_{i,F}\ln z_{i,F} - F_{ABCD}\int_{q_F}^{1}\ln\Big(\sum_{j=A}^{D}\alpha_j x_{j,ABCD}\Big)dq \\ & - B_{BCD}\int_0^1\ln\Big(\sum_{j=A}^{D}\alpha_j x_{j,BCD}\Big)dq + D_{ABC}\int_0^1\ln\Big(\sum_{j=A}^{D}\alpha_j x_{j,ABC}\Big)dq \\ & + D_A\ln\alpha_A + D_B\ln\alpha_B\end{aligned} \tag{4.11}$$

which does not require explicit knowledge about any reboiler or condenser temperature [115–117]!

Again, we remind that $x_{j,i}$ in Equation (4.11), the liquid phase composition of component j in submixture stream i with a net material composition of $z_{j,i}$, is a function of thermal quality q which is governed by the phase equilibrium as:

$$z_{j,i} = qx_{j,i} + (1-q)\frac{\alpha_j x_{j,i}}{\sum_{k=A}^{D} \alpha_k x_{k,i}} \qquad i \in \{ABC, BCD\} \tag{4.12}$$

To evaluate the integrals in Equation (4.11) numerically, we find that the two-point Gaussian quadrature method [122], which approximates a definite integral of a function as a weighted sum of function values at two specific points, is sufficiently accurate for all practical cases that we have encountnered. In other words, we replace each integral term in Equation (4.11) with the weighted sum of integrand evaluated at two representative thermal quality values by solving Equation (4.12). When Equation (4.12) is written out and solved at the two thermal quality values for every component, the resulting set of solutions of liquid compositions can be substituted to evaluate the integrand to approximate the corresponding exergy loss term.

For higher accuracy, three-point or even higher Gaussian quadrature formula can be used. Nevertheless, as the number of weights used increases, the number of decision variables and nonconvexities also increase rapidly, unnecessarily making the GMAE formulation harder to solve to global optimality. In this case, there definite exists a trade-off between numerical accuracy and the complexity of the problem, and users need to make the appropriate balance based on their needs. With this, the GMAE model formulation is now finalized. The NLP problem for each and every configuration synthesized by the SA method [7] is solved in GAMS using global solver BARON [39]. In the next section, we will examine an example involving shale gas separations in detail to illustrate the reliability and robustness of the GMAE framework as well as to generate some useful insights into the design and retrofit of energy efficient distillation configurations.

4.3 Case Study – NGL Recovery and Fractionation

The recent shale gas boom has transformed the energy landscape of the world, especially the United States. Apart from methane and nitrogen, shale resources contain a substantial amount of natural gas liquids (NGLs), including ethane, propane, n-butane, i-butane, and other heavier hydrocarbons [123]. After acid gas removal and dehydration, the shale gas stream undergoes a series of separation steps using distillation to recover natural gas (mostly methane and small amount of nitrogen) for storage or transport, as well as individual components of NGLs for downstream processing. In this study, we consider the NGLs recovery and fractionation process for a typical shale gas stream produced from the Eagle Ford basin in Texas Shale Plays at a flow rate of 5000 kmol/hr. Specifically, we consider the complete separation of five major components in the shale gas, namely natural gas (methane and nitrogen), ethane, propane, butane, and pentane (plus heavier hydrocarbons), which are respectively denoted as components A, B, C, D, and E. These pure components are finally produced as saturated liquid streams. After acid gas removal and dehydration, the shale gas is sent to the distillation trains as saturated vapor feed. The molar composition of these five components in a typical shale gas stream in Eagle Ford can be found in He and You [124], and the relative volatility information is obtained from Aspen Plus using Peng-Robinson equation of state model. These feed specifications are summarized in Table 4.3. The reference temperature T_0 taken as the ambient temperature of 298K.

Table 4.1.
Feed specifications for a typical shale gas stream in Eagle Ford basin (Reference: He and You [124]).

Component	**Mole fraction (%)**	**Relative volatility**
Natural gas (A)	78.46	27.11
Ethane (B)	13.19	3.713
Propane (C)	5.27	1.579
Butane (D)	2.24	1.218
Pentane (E)	0.84	1

We formulate the NLP problem automatically in MATLAB for each of the 6128 possible regular-column configurations in the search space generated by the SA method [7]. After it is sent to GAMS via the GAMS/MATLAB interface [98], each NLP problem is solved in GAMS using the BARON solver [39]. BARON has well-defined convex relaxations for standard bilinear and fractional nonlinear functions [125]. These convex relaxations are used in the solver to arrive at the global optimal solution. All 6128 configurations are solved to global optimality ($\leq$ 1% duality gap) within 4.54 hours of CPU time in a Dell OptiPlex 5040 desktop that simultaneously utilizes all four of its Intel Quad-Core i7-6700 processors with the help of the Parallel Computing Toolbox in MATLAB.

Current industrial practices for NGLs recovery and fractionation have been using the classic basic direct-split configuration drawn in Figure 4.6a. The GMAE determines that the minimum total exergy loss for this configuration is 5775.46 MJ/hr (1.604 MW), and the corresponding reboiler vapor duty is given by 4397.17 kmol/hr (1221.4 mol/s). To compare the other 6127 configurations in the search space with this "benchmark", we normalize the minimum total exergy losses of these configurations along with their corresponding total reboiler vapor duties respectively based on the values of the basic direct-split configuration. These results are illustrated in Figure 4.5. A number of interesting and important observations can be drawn from this plot. And we will present some of them by discussing a few selected configurations highlighted in Figure 4.5, which are explicitly drawn in Figures 4.6 and 4.7.

First, the conventional basic direct-split configuration, which is represented by the red dot located at the lower right corner in Figure 4.5, is ranked 30th out of all 6128 configurations in the search space in terms of minimum total exergy loss (top 0.49%). Despite requiring a relatively high total reboiler duty as it involves all sharp split separations [9], this conventional scheme is among the most thermodynamically efficient configurations. Meanwhile, another sharp-split configuration drawn in Figure 4.6e, which requires only about 0.4% more reboiler vapor duty than the conventional

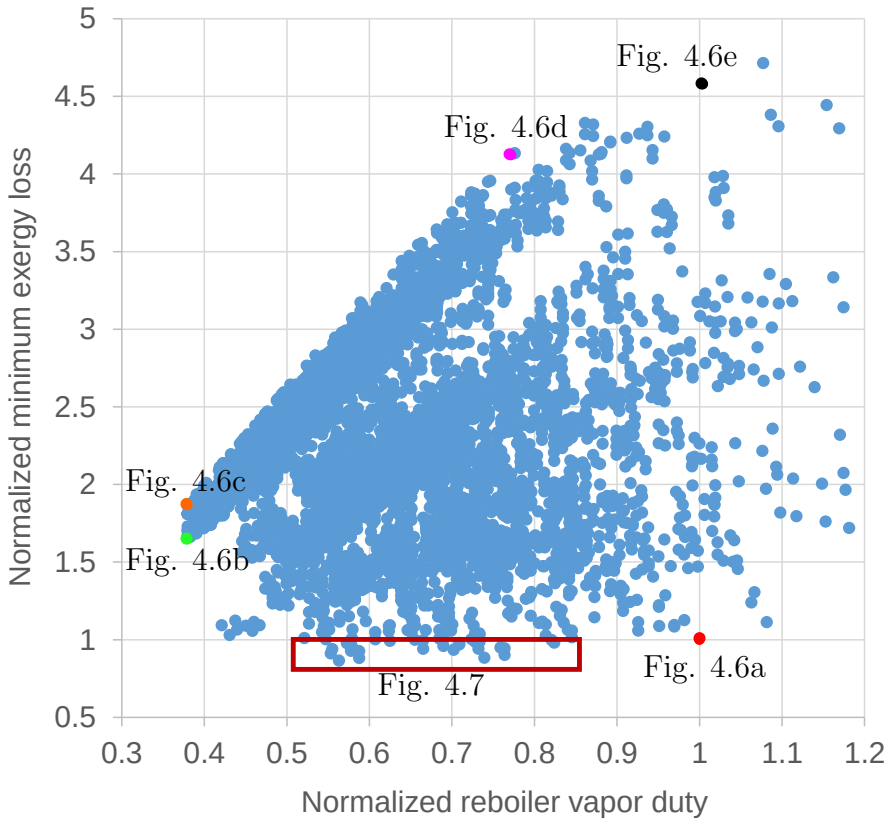

Figure 4.5. A plot showing the normalized minimum total exergy losses and the corresponding normalized total reboiler vapor duty requirements for all 6128 configurations. Each dot represents a configuration. The red, green, orange, pink, and black dots in the plot are chosen as representatives and are drawn in Figure 4.6a thru e, respectively. Potentially attractive configurations belonging to three major configuration families are also boxed. The representative configurations from each family are drawn in Figure 4.7.

scheme, has $> 357.8\%$ more minimum total exergy loss, making it the second worst configurations in the entire search space in terms of energy efficiency!

To understand why these two configurations have drastically different minimum total exergy losses, recall from Table 4.3 that the natural gas stream (component A) is significantly more volatile compared to any other component in the system. Any condenser that produces a submixture containing natural gas stream (i.e. associated with submixture $ABCD$, ABC or AB) or produces the final natural gas product

is operated at considerably cryogenic temperature level and thus requires expensive cooling utility. Therefore, a small increase of cooling duty in any of these condensers will result in a significant increase in total exergy loss (utility cost) of the overall configuration. To improve the thermodynamic efficiency of the NGLs recovery and fractionation process, it is critical to keep the condenser duties associated with streams containing component A small.

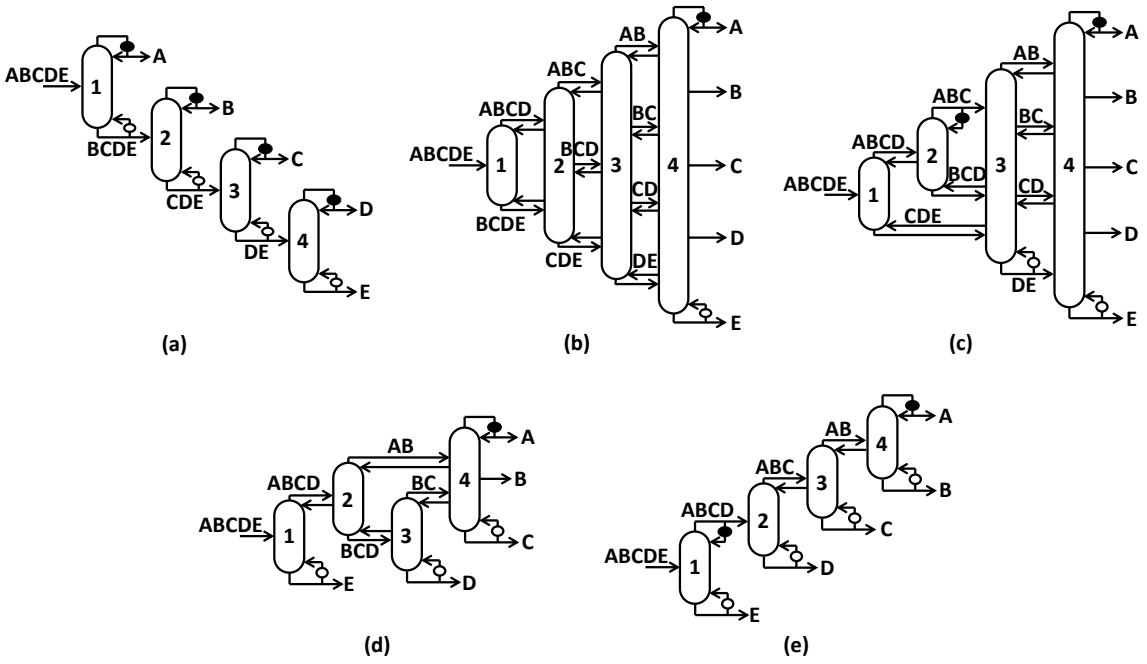

Figure 4.6. (a) Conventional basic direct-split configuration; (b) the fully thermally coupled (FTC) configuration; (c) the configuration with the lowest minimum total exergy loss among all configurations that require the same reboiler vapor duty as the FTC configuration; (e) a basic sharp-split configuration which consumes almost the same reboiler vapor duty as (a) but has significantly more minimum total exergy loss.

For the conventional configuration of Figure 4.6a, the natural gas stream is directly produced from column 1, whose condenser duty is given by 5630.9 kmol/hr. On the other hand, in the configuration of Figure 4.6e, the sum of cooling duties at condensers $ABCD$ (1508.3 kmol/hr) and A (7906.2 kmol/hr) increases to 9414.5 kmol/hr, which

leads to significant increase in total exergy loss. Clearly, a configuration with low reboiler vapor duty does not always correspond to a low total exergy loss. Likewise, a configuration that requires a high vapor duty may turn out to be quite efficient. Also, it is worth noting that the condenser duty associated with the final natural gas product A increases by 40.4% compared to that in the conventional configuration mainly because of the presence of thermal couplings at submixtures ABC and AB. Although introducing thermal couplings at these two submixtures might benefit the first-law heat duty, it really "hurts" the thermodynamic efficiency of the configuration. In this case, the basic configuration version for Figure 4.6e requires 7.3% more reboiler duty than the original thermally coupled configuration but has 13.5% less minimum total exergy loss. Thus, for applications in which the second-law temperature level penalty is more influential to the operating cost of a distillation configuration than the first-law heat duty benefit, thermal couplings of this sort should be avoided [41].

The same reasoning can be applied to analyze other representative configurations drawn in Figure 4.6 as well. For instance, the fully thermally coupled (FTC) configuration of Figure 4.6b is known to always have the lowest total reboiler vapor duty among all configurations in the search space [46]. Despite requiring 62.0% less vapor duty, the FTC configuration has 86.8% more minimum total exergy loss than the conventional configuration of Figure 4.6a, since all the vapor duty is generated at the highest temperature reboiler of E and condensed at the lowest temperature condenser at A. Fortunately, as we can see from Figure 4.5, there exists a total of 17 non-FTC configurations which have the same total vapor duty requirement as the FTC configuration but lower exergy loss. Among these 17 configurations, the one with the lowest minimum total exergy loss is drawn in Figure 4.6c. This configuration has two reboilers at DE and E as well as two condensers at ABC and A, thereby allowing the heat duty to be generated and removed by heat exchangers operated at milder temperature levels. Hence, for most industrial applications, we believe that building the FTC configuration should not be considered as the first choice [47, 99]. This is also consistent with the observations we made earlier in Chapter 2.

One interesting observation that one can make from Figure 4.5 is that for a given total reboiler vapor duty value, there seems to exist an upper bound on the minimum total exergy loss that a configuration can ever obtain. More interestingly, this upper bound seems to be linear with respect to the total reboiler vapor duty. Based on previous discussions, it should not be a surprise that such a linear upper bound exists. Among all configurations having the same reboiler vapor duty, the configuration with the highest minimum total exergy loss always corresponds to a completely thermally coupled (CTC) configuration in which all submixture heat exchangers are replaced by thermal couplings. The FTC configuration is a special CTC configuration. Eliminating submixture heat exchangers especially condensers forces the heat duty to be respectively generated and rejected by reboilers and condensers associated with final pure products, which in general incur greater exergy loss. In this case, it turns out that the configurations lying on the upper bound curve as shown in Figure 4.5 correspond to the CTC configurations with only one condenser at A. Final pure component products of intermediate relative volatilities (i.e. components B, C, and D) are either produced by reboilers or withdrawn from the distillation system as side-draw streams. It is easy to see why such CTC configurations always have the lowest thermodynamic efficiencies among all configurations requiring the same heat duty, as the only heat sink available in the entire configuration is at an absurdly cryogenic temperature level compared to other streams. And as a result of this, we also expect to see that the upper bound curve in Figure 4.5 to be a linear function of total vapor duty generated at all reboilers based on the total exergy loss expression.

We have just discussed the FTC configuration which is located at the lower left endpoint of the upper bound line. The configuration corresponding to the other endpoint is shown in Figure 4.6d. As we can see, all but one split involved in this configuration are sharp splits, suggesting a high vapor duty requirement for this configuration. Thus, this CTC configuration is expected to lead to very high total exergy loss. We believe that this result can be generalized for other multicomponent distillation problems as well. It is also an useful heuristic from an optimization

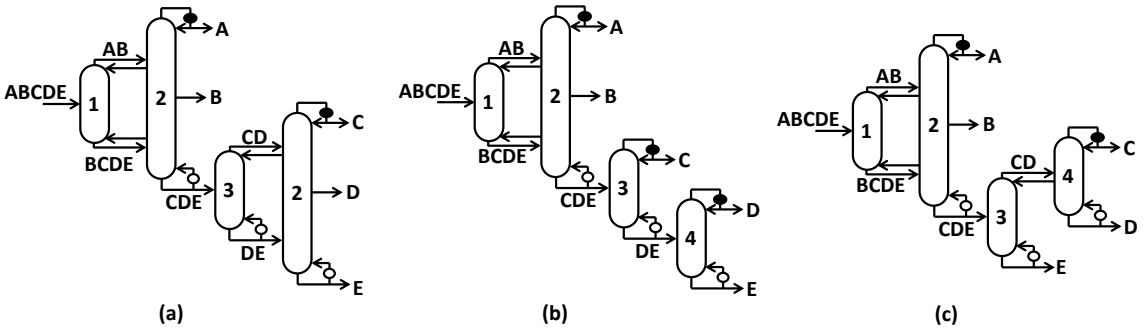

Figure 4.7. (a)-(c) The best performing configurations associated with each of the three configuration families highlighted in the box shown in Figure 4.5. The configurations of (a), (b), and (c) are respectively ranked the 1st, 3rd, and 20th among all 6128 configurations in the search space in terms of minimum total exergy loss.

perspective since it provides a valid upper bound on the objective function value which tightens the feasible region and helps convergence to the global optimal solution.

Finally, we would like to examine the best performing configurations identified by the GMAE with the highest thermodynamic efficiencies, which can be categorized into three distinct groups of configurations shown in Figure 4.5. Configurations belonging to the same group have the same splits and thus are topologically indifferent; the only difference lies in their thermal coupling placements. In Figure 4.7, we draw the best configuration in terms of minimum total exergy loss of each group. Compared with the conventional basic direct-split scheme, configurations of Figure 4.7a thru c have 13.4%, 11.6%, and 2.0% less minimum total exergy loss while requiring 43.7%, 26.1%, and 29.1% less total reboiler vapor duty, respectively. In fact, the configuration of Figure 4.7a is also the best performing configuration among all 6128 configurations in the entire search space. As we can see, the first two distillation columns in all three configurations of Figure 4.7 perform the same splits: one non-sharp split, $ABCDE \rightarrow AB/BCDE$, as well as two sharp splits, $AB \rightarrow A/B$ and $BCDE \rightarrow B/CDE$. The vapor duty needed for these three splits in columns 1 and 2 either comes from the saturated vapor feed stream or is generated by the reboiler CDE at 866.4 kmol/hr.

For the conventional configuration of Figure 4.6a, the sum of vapor duties generated by reboilers $BCDE$ and CDE for the first two distillation columns is given by 2012.9 kmol/hr. By performing an enthalpy balance around columns 1 and 2, we can see that the sum of condenser duties in these two columns in the configurations of Figure 4.7 is 16.3% less than that of the conventional scheme. Thus, the sum of exergy losses associated with the first two distillation columns is reduced in these best performing configurations.

We notice that the total reboiler duties of these top ranklisted configurations span a wide range as shown in Figure 4.5. This offers design engineers more options in choosing the appropriate configuration to build or retrofit based on the actual mass and heat balances of the plant, since some of these configurations with higher heat duties may turn out to be more attractive as they provide more heat integration opportunities with other process units. Also, configurations belonging to the group of Figure 4.7b are especially amenable for retrofit purposes, as two out of the four distillation columns in the conventional configuration, namely columns 3 and 4 of Figure 4.6a, are exactly the same as the ones in these attractive configurations and can thus remain unchanged. Last but not least, innovative process intensification strategies such as dividing wall columns (DWCs) [76, 77] can be implemented to further reduce the size and capital cost of these attractive configurations while maintaining the same thermodynamic efficiencies [79]. Figure 4.8 shows one possible DWC implementation for each of the representative configurations drawn in Figure 4.7 [76]. Note that three possible versions of DWC associated with the main feed stream are drawn in Figure 4.8. These DWC versions are completely thermodynamically equivalent [58], however the ones shown in Figure 4.8b and c are fully operable in the sense that each separate zone divided by the vertical partition is associated with one reboiler or condenser so that the desired L/V ratio inside each zone can be achieved and precisely regulated [77]. Of course, more possible DWC versions that use 1 to 3 column shells can be systematically synthesized for each of the regular-column configurations of Figure 4.7 [76].

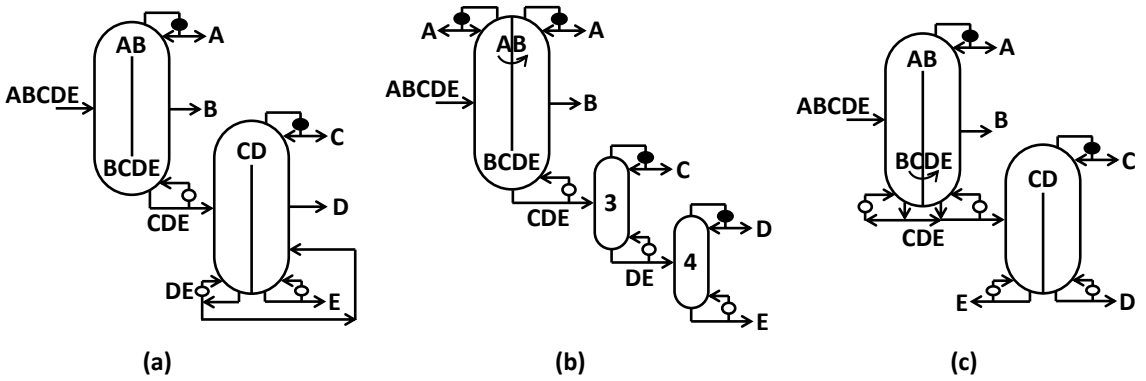

Figure 4.8. (a) One of the dividing wall column (DWC) versions of the configuration of Figure 4.7a; (c) a DWC version of the configuration of 4.7b; (c) a DWC version of the configuration of 4.7c.

4.4 Additional Improvement and Retrofit Strategies

In this section, we would like to explore options to further improve the heat duty and thermodynamic efficiency of an existing distillation system such as the conventional scheme of Figure 4.6a without having to change the topological structure of the configuration. In previous discussions, we have introduced the concept of using modified heat exchangers at submixture locations. These modified designs for submixture reboiler and condenser have been drawn in Figure 4.3b and d, respectively. These modified submixture heat exchanger configurations help improve the thermodynamic efficiency of a distillation configuration by granting it with more flexibility to allow two-phase submixtures [118]. From an optimization perspective, the improved configuration using the modified submixture heat exchangers is essentially a relaxation of the original configuration using only conventional heat exchangers. Thus, solving improved configuration for its minimum total exergy loss is equivalent to solving a relaxed problem of the original configuration. Consequently, the optimal objective function value of the new configuration must always improve, or at least stay the same, compared to that of the conventional configuration.

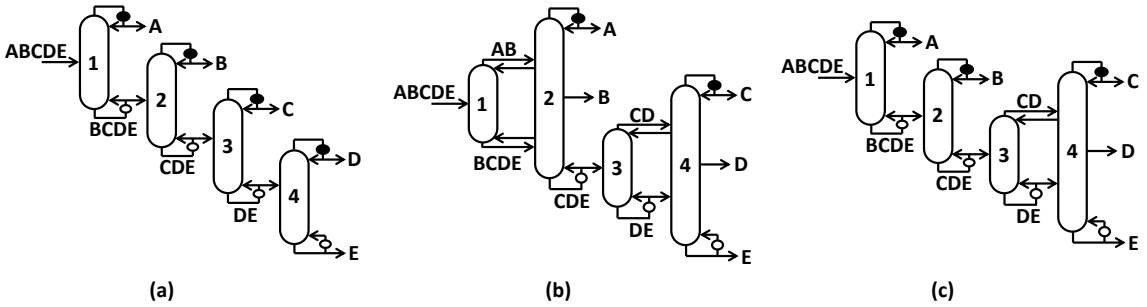

Figure 4.9. (a) Optimal retrofit design of the conventional scheme of Figure 4.6a using modified heat exchangers at submixtures. Notice that reboilers associated with submixtures $BCDE$, CDE and DE now vaporizes all the bottoms liquid and produce vapor-only feed streams that enter the subsequent columns; (b) optimal retrofit design of the configuration of Figure 4.6b using modified heat exchangers at submixtures CDE and DE. This configuration also corresponds to the best performing configuration when using conventional submixture heat exchangers; (c) a new, attractive configuration design that ranked 2nd among all 6128 configurations in the new ranklist.

Our proposed GMAE formulation is sufficiently generalized and flexible such that users can easily specify the type of submixture heat exchangers they want by simply relaxing the appropriate bounds on the liquid or vapor flow rate variables in the submixture streams. By enabling submixture heat exchangers to take such modified structures in the GMAE framework, we are able to obtain the new ranklist of distillation configurations in terms of their minimum total exergy losses. Compared to the original ranklist of configurations based on conventional submixture heat exchanger designs, the ranking associated with the conventional configuration scheme jumps from the 30th to the 5th. Figure 4.9a shows the optimal reboiler configuration at $BCDE$, CDE, and DE. This new reboiler arrangement reduces the minimum total exergy loss of the conventional scheme by 13.2% to 5015.9 MJ/hr compared to original arrangement of Figure 4.6a. Of course, to implement this new retrofit option in reality, apart from modifying the related pipelines, valves, and fittings of the original

configuration, the reboiler associated with submixture $BCDE$ needs to be replaced to accommodate the large increase in heat transfer area.

It turns out that, in the new ranklist obtained after implementing modified submixture heat exchangers, the configuration with the lowest minimum total exergy loss, which is drawn in Figure 4.9b, is also the optimal configuration (See Figure 4.7a) in the original ranklist obtained using conventional submixture heat exchangers. As reboilers of CDE and DE now vaporize all the bottoms liquid to produce vapor-only submixture streams, the minimum total exergy loss of this new design is 3.3% lower (4834.6 MW/hr) compared to that of the conventional heat exchanger arrangement of Figure 4.7a (4999.8 MW/hr).

It is also worth noting that the second best configuration in the new ranklist with a minimum total exergy loss of 4873.0 MJ/hr turns out to be the one shown in Figure 4.9c. In this configuration, the first two distillation columns perform the same direct splits as in the conventional scheme of Figure 4.9a, while columns 3 and 4 resemble a Petlyuk-type arrangement [26] except that submixture DE is associated with a reboiler instead of thermal coupling. As a result, columns 3 and 4 can be consolidated into single dividing wall column which can lead to significant capital cost savings. In addition, compared to the improved conventional scheme of Figure 4.9a, this new configuration of Figure 4.9c requires 17.3% less reboiler vapor duty, again suggesting lower capital and operating costs. Also, needless to mention the retrofit benefit associated with this new configuration when the first two columns in the conventional scheme could be kept as they are. Overall, this configuration is particularly attractive for retrofit purposes.

A natural extension of the idea of modifying the conventional submixture heat exchangers to produce two-phase feed streams is to vaporize or condense a portion of the main feed stream before it enters the distillation system to further improve the thermodynamic efficiency of the overall process. This also opens up more opportunities for heat integration with other process units and utilities in the plant. This can

be done in the GMAE formulation by allowing the thermal quality q_F in the final objective function of Equation (4.11) to be a decision variable.

Last but not least, in the current GMAE formulation, all pure component streams are produced as saturated liquid products. However, depending on the actual problem, producing some or all of the final pure component products as saturated vapor or even two-phase streams may further improve the thermodynamic efficiency of a configuration significantly. Similar to the strategy of feed preheating or precooling, this new retrofit strategy can also be easily incorporated in the GMAE framework. In subsequent publications, we will discuss the synergistic use of these strategies in the design of energy efficient multicomponent distillation systems in detail.

4.5 Conclusion and Future Work

The operating cost of a distillation configuration depends not only on the first-law heat duty requirement but also on the temperature level at which heat duty is generated and rejected. The later aspect, which is closely related to the thermodynamic efficiency of a distillation system, is often quantified by exergy analysis. For the first time, we develop an enumeration based global optimization algorithm based on the GMA framework developed by Nallasivam et al. [34] recently to minimize the total exergy loss (GMAE) of any regular-column distillation configuration synthesized by the SA method [7] distilling any ideal or near-ideal multicomponent mixture. Based on the reasonable simplifying assumptions embedded in the GMAE framework, we show that the final exergy loss expression does not explicitly involve the calculation of temperature. Instead, the only information required for exergy loss calculation is the composition and relative volatility of each component present in the material streams. The GMAE formulation is particularly useful for analyzing the operating cost of heat pump assisted distillation systems as well as separations that are mainly work-driven rather than heat-driven. In this article, we consider an example of the NGLs recovery and fractionation process to demonstrate the efficiency and usefulness of the GMAE framework. Through the discussion of this example, we construct

several physical insights and observations regarding heat duty, thermodynamic efficiency, and exergy loss. In particular, a configuration with low heat duty does not mean that it is always thermodynamically efficient (e.g. the FTC configuration). At the same time, a configuration that requires a high vapor duty may turn out to be quite thermodynamically efficient. The submixtures and final pure product streams present in a given configuration do not have equal importance in terms of exergy loss contribution. A small change in the reboiler or condenser duty associated with certain critical streams may result in a significant change in the total exergy loss of the entire configuration. Replacing submixture heat exchangers with thermal couplings can lead to similar effect. Introducing thermal couplings at certain submixture locations may incur significant penalty in thermodynamic efficiency without adding any first-law heat duty benefit. Meanwhile, it is also possible that some types of thermal couplings can offer considerable heat duty savings without exhibiting any efficiency penalty [41]. The GMAE thus provides industrial practitioners a quick and reliable screening tool to identify the best thermal coupling arrangement.

Once an attractive, energy efficient distillation configuration is identified by the GMAE, various process intensification strategies described in Chapter 2, such as consolidating multiple distillation columns into a single column shell in the form of dividing wall column, can be implemented by users to further enhance its operability, increase its energy efficiency, and reduce its size and capital cost. On the other hand, for an existing configuration, a simple retrofit option, namely using modified heat exchangers at submixtures, can be applied to further improve its thermodynamic efficiency and operational flexibility. It is shown that this simple approach has the potential to significantly reduce the total exergy loss of a configuration without increasing much capital expenditure.

Finally, we would like to point out that the GMAE framework can be further extended to consider more complex problems as well as more advanced applications, including multi-effect distillation, heat integrated distillation, etc. For instance, while the total exergy loss characterizes the operating cost and energy efficiency of a distil-

lation system that is work-driven, in practice few multicomponent distillation systems are solely operated by either heat or work. Instead, for most multicomponent systems, especially those in which the boiling points of components cover a wide range (e.g. hydrocarbon separations from steam cracking), some distillation columns are operated by heat, whereas others are operated by work. In this case, a new objective function regarding the true operating cost or energy efficiency of a distillation configuration needs to be established. This new objective function must account for the both the heat duty and work input requirement in a fair manner. To do this, we need to extend the current GMAE framework so that it is capable of identifying which form of energy is more suitable for driving a submixture or final product heat exchanger in order to minimize the new objective function.

In the current GMAE framework, all distillation columns are assumed to be operated at similar pressures. However, in more advanced applications such as multi-effect and heat integrated distillation systems, different columns can have different operating pressures such that heat integration can potentially take place between any two streams present in the configuration. Thus, allowing pressure variations across distillation columns generates a large number of new process intensification opportunities for synthesizing highly compact, energy efficient, and cost-effective integrated distillation systems [64]. To do this, one needs to relate the temperature of a multicomponent mixture with its pressure. This can be done by extending the simplified version of the Clausius-Clapeyron relation of Equation (4.10) as [121]:

$$\ln\left(\frac{P_1 \sum_{i=1}^{n} \alpha_i x_{i,2}}{P_2 \sum_{i=1}^{n} \alpha_i x_{i,1}}\right) = \frac{\Delta H}{R}\left(\frac{1}{T_2} - \frac{1}{T_1}\right) \tag{4.13}$$

where P_1 and P_2 stand for the pressure of two mixtures 1 and 2 respectively at two different temperatures T_1 and T_2. Again, we emphasize that the validity of Equation (4.13) is built upon the simplifying assumptions of ideal vapor-liquid equilibrium, constant relative volatility, and constant and equal latent heats for all components. The simplicity of Equation (4.13) makes it particular useful to the formulation of the

new GMAE framework that can handle more these advanced applications involving pressure variations. We will devote the advancements and findings in these future directions in subsequent works.

5. AN ACCURATE MINIMUM REFLUX CALCULATION METHOD FOR MULTI-FEED, MULTI-PRODUCT DISTILLATION COLUMNS DISTILLING IDEAL MULTICOMPONENT MIXTURES: 1. MATHEMATICAL MODEL

Multi-feed, multi-product distillation columns are ubiquitous in multicomponent distillation systems. The minimum reflux ratio of a distillation column is directly related to its energy consumption and capital cost. Thus, it is a key parameter for distillation systems design, operation, and comparison. In this work, we solve this longstanding challenge in chemical engineering by presenting a simple and easy-to-use shortcut based algorithmic method to determine the minimum reflux condition for any general multi-feed, multi-product distillation column separating any ideal multicomponent mixture. Compared with other existing approaches, this method does not involve any rigorous tray-by-tray calculation nor requires iterative guessing of key components.

5.1 Introduction

Most configurations contain distillation columns with multiple feed streams and/or one or more side-stream withdrawals. Compared to configurations that use only simple columns which all have exactly one feed stream and two product streams, configurations having one or more multi-feed, multi-product (MFMP) columns can lead to significant energy and capital cost savings [9]. These MFMP columns have been widely used in industrial applications such as crude oil fractionation, air separation, extractive distillation, multi-effect distillation.

The minimum energy requirement of a distillation column, often characterized by its minimum reflux ratio at pinched condition, is an important parameter that provides critical information on the column's optimal design and operation. With the

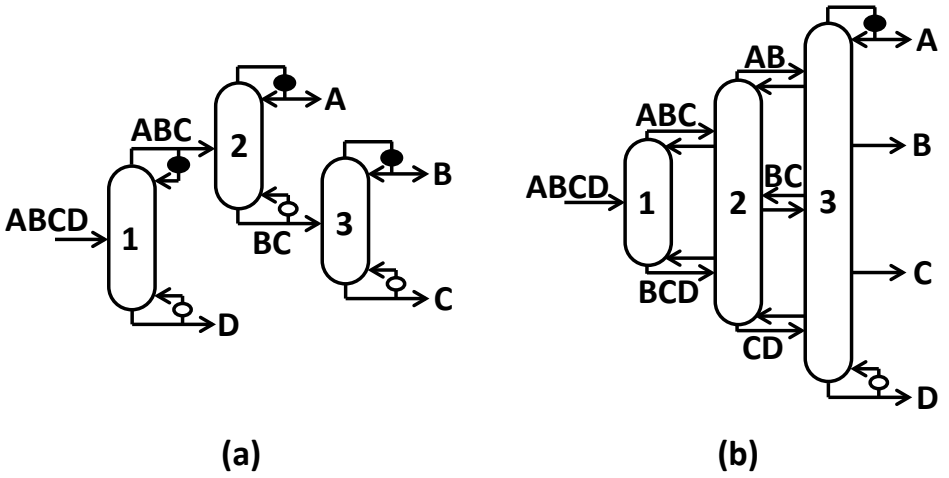

Figure 5.1. (a) A four-component configuration containing only simple columns; (b) the well-known fully thermally coupled configuration [126] in which column 2 and 3 are both MFMP columns. Here, letters A, B, C, and so on represent pure components with their volatilities decreasing in alphabetical order. Also, we indicate reboilers by open circles and condensers by filled circles.

knowledge of minimum reflux ratio, process engineers can estimate the actual reflux ratio of the distillation column that corresponds to the optimal balance of capital and operating costs [93, 127]. The minimum reflux ratio of a distillation system also serves as a direct indicator for its capital investment, as it is closely related to the number of stages, height and diameter of the column, as well as reboiler and condenser sizes. Because of these reasons, the minimum energy requirement has been extensively chosen as the objective function for comparing and ranklisting different multicomponent distillation systems/configurations [32, 34, 128, 129]. As a result, an accurate and quick calculation of the true minimum reflux condition for a general MFMP column is crucial for designing and identifying attractive multicomponent distillation systems, whereas failing to do so often leads to unnecessarily large and inefficient plants being built and operated.

Over the past decades, a number of attempts have been made to determine the true minimum reflux condition for MFMP columns that carry out ideal/near ideal,

non-ideal, or even azeotropic mixture separations. These methods fall under the categories of shortcut, geometric, or rigorous. Most rigorous methods involve detailed tray-by-tray calculations achieved by simultaneously solving the MESH equations that incorporate mass and energy balances as well as phase equilibrium relations [130–133]. These methods are now standard in most process simulation tools such as Aspen Plus. However, as the problem size increases, these tray-by-tray calculations quickly become too computationally expansive to be put into an global optimization framework under which one configuration containing multiple columns [34] or even the entire search space of distillation configurations needs to be solved to global optimality in reasonable amount of time.

In addition to rigorous methods, a number of geometric based approaches have been proposed to address the minimum reflux problem in an iterative manner. A literature survey of these geometric methods can be found in Lucia et al. [134]. For example, Levy and Doherty [135] developed first-order finite difference approximation for estimating the liquid composition profile within a column section under the assumption of constant molar overflow (CMO) for multi-feed columns. In this method, the minimum reflux condition can be determined using the boundary value method, in which the composition profile for each column section is obtained by numerical integration. The minimum reflux condition is achieved when all composition profiles are connected, meanwhile two of them that are associated with adjacent column sections just touch each other. Later, Koehler et al. [136] introduced a minimum angle criterion, whereby the angle between the top and bottom section pinch compositions and a feed composition is minimized to identify a candidate minimum reflux ratio. However, the minimum angle criterion does not have solid physical basis. Other methods (e.g. zero-volume method, separation driving force method, rectification body method) have also been proposed to determine the minimum reflux ratio of a simple column but for non-ideal and/or azeotropic mixture separations [137–142]. Although some of these geometric based algorithms can be extended to MFMP columns [143–145], they still suffer from computational inefficiency and convergence issues due to model

complexity and numerical instability. Moreover, while some of the methods work well for ternary or quaternary mixture separations under which they can be visualized, directly extending them to higher-component systems can be quite tricky or even dangerous to do. To avoid these complications, there is definitely a need to develop an accurate and robust shortcut based method that does not involve rigorous tray-by-tray calculations or tedious iterations.

Most shortcut based methods to determine the minimum reflux condition for MFMP columns in multicomponent distillation are derived by extending the well-known Underwood's method [19, 146] which was originally developed for describing a simple column. The Underwood's method liberates one from performing rigorous tray-by-tray calculations by making three major underlying assumptions of ideal liquid-vapor equilibrium (VLE), constant relative volatility (CRV), and constant molar overflow (CMO). Despite having to make these assumptions to simplify the mathematical model, it is found that the minimum reflux ratio can be estimated with reasonable accuracy even for many nonideal systems without azeotropes that cover a wide range of industrially important separations [147].

Barnes et al. [148] extended the Underwood's method to estimate the minimum reflux ratio for multi-feed columns. However, their solution procedure still requires iterative calculations and hence cannot be easily implemented in a global optimization framework. Wachter et al. [149] modified the Underwood's method to estimate minimum reflux ratio for MFMP columns, but their method depends on the ability to identify key components of a split. In general, identifying the key components is not a straightforward task for MFMP columns. Sugie and Lu [150] generalized the Underwood's method to one-feed, multi-product columns containing only saturated-liquid sidedraws. They claimed that in such columns, the pinch zone must occur at the feed location. Later, Glinos and Malone [151] presented approximated design equations for multi-product columns with saturated liquid feed, in which they also made the same claim about the pinch zone location. Nikolaides and Malone [152] extended the work of Glinos and Malone [151] to MFMP columns. They assume

that a MFMP column can be decomposed into a series of simple columns, each containing exactly one feed/sidedraw stream and two column sections sandwiching it. The classic Underwood's method can then be applied to determine the minimum reflux ratio for each decomposed simple column. They argue that the true minimum reflux ratio of the original MFMP column is given by the largest minimum reflux ratio determined for all decomposed simple columns, since it "controls" the entire separation. This assumption has been widely accepted and adopted by a number of publications, including some of the recent ones such as Ruiz-Marn et al. [153], Adiche and Vogelpohl [154], Gmez-Castro et al. [155], and Adiche and Aissa [156].

As we can see, to extend the applicability of Underwood's method to MFMP columns, existing approaches have to incorporate various additional constraints and assumptions which make the resulting methods quite restricted and sometimes even incorrect to use. Therefore, the ultimate goal of this work is to develop a simple and easy-to-use shortcut method to determine the minimum reflux ratio of a general MFMP column for multicomponent distillation without making any unnecessary constraints or assumptions. In particular, our method should not be constrained by the number of feed and sidedraw streams, the physical properties (e.g. thermal quality) for each feed and/or sidedraw, the number of components involved in the separation, etc. Furthermore, it should be simple enough to be incorporated in a global optimization framework such as the one recently developed by Nallasivam et al. [34].

Furthermore, by developing this first-of-its-kind shortcut based approach, we hope to address the following questions:

1. How to model a MFMP column accurately?

2. What is the minimum energy requirement of a general MFMP column?

3. What is the optimal arrangement of feed and/or sidedraw streams? Is it always better to sequence these streams based on their temperature levels?

4. Is it always true that a MFMP column can be decomposed into individual simple columns, and its true minimum reflux ratio is determined by the largest minimum reflux of all decomposed simple columns?

Although some of these questions may seem "silly" from the first glance, it is always worth a second thought before any definite conclusion is drawn. We shall see later that the answers to these questions can sometimes be quite surprising and counterintuitive.

5.2 Solution Approach

We propose a bottom-up approach to solve this long-standing problem in chemical engineering. Our approach starts with realizing the fact that the smallest unit of a general MFMP column is a column section which can be modeled as a general countercurrent mass exchange unit. Though the topmost and bottommost sections in a MFMP column are respectively equivalent to the rectifying and stripping section in a simple column (See Figure 5.2), the presence of intermediate column sections sets MFMP column apart from a simple column. As we will see later, these intermediate sections demand special mathematical treatment. Therefore, instead of decomposing a MFMP column into a series of simple columns, we will build a shortcut model for each general column section based on the assumptions of ideal VLE, CRV, and CMO. Each general column section, now modeled as a countercurrent mass exchanger, exhibits a set of physical and mathematical properties, some of which have can be easily visualized in cases involving ternary or quaternary systems. We will explore these properties and use them to derive important algebraic relations corresponding to the minimum reflux condition. These relations turn out to be the necessary and sufficient conditions for a MFMP column to be at minimum reflux. Finally, incorporating these constraints in a global optimization framework allows us to accurately and efficiently solve any distillation configuration or system of configurations to global optimality.

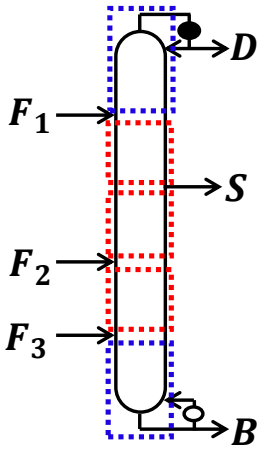

Figure 5.2. A general MFMP column. The topmost and bottommost column sections are universally present in both simple columns and MFMP columns. However, the intermediate sections, highlighted by red boxes, are unique to MFMP columns.

5.3 Modeling of General Column Section as Countercurrent Mass Exchange Unit

We consider a general column section shown in Figure 5.3. As a result of constant molar overflow, the total vapor or liquid flow rate, respectively denoted as V and L, does not change from stage to stage within this section. Thus, the total net material upward flow $D = V - L$ is constant as well. In terms of each individual component i, its net material upward flow rate d_i, which is determined by $d_i = v'_{i,n-1} - l'_{i,n} = v_{i,n} - l_{i,n-1} \quad n = 1, 2, \cdots$, also remains unchanged within the section. In any general column section within a MFMP column, the component vapor flow ($v'_{i,n}$ or $v_{i,n}$) and liquid flow ($l'_{i,n}$ or $l_{i,n}$) leaving any stage n for any component i always follow the direction depicted in Figure 5.3. However, the sign of d_i does not necessarily have to be the same for all the components. When $d_i < 0$ for some component i in a section, it simply means that the direction of its net material flow is downward. As a special case, $d_i \geq 0 \ \ (\leq 0)$ for all components in the rectifying (stripping) section of a simple column or the topmost (bottommost) section in a MFMP column. Once we understand this, we can start the formal analysis on the lower and upper part of a general column section separately. And then, we will examine the pinch condition

in the column section as the number of stages n in both the upper and lower part approaches to infinity.

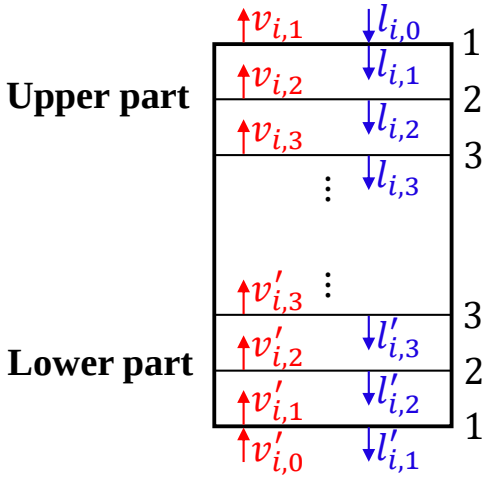

Figure 5.3. Schematic diagram of a countercurrent mass exchange unit. Notice the nomenclature: the vapor and liquid flow rate for component i leaving stage n for the lower (upper) part of mass exchange unit is given by $v'_{i,n}$ $(v_{i,n})$ and $l'_{i,n}$ $(l_{i,n})$, respectively.

5.3.1 Modeling of Lower Part of Column Section

We begin modeling the lower part of a column section by writing down the component mass balance equation:

$$l'_{i,n+1} = v'_{i,n} - d_i \quad \forall i = 1, \cdots, c;\ n = 0, 1, \cdots \tag{5.1}$$

where c denotes the total number of components in the system. The nonlinearity of the problem comes from the ideal VLE on stage n which says that:

$$v'_{i,n} = V \frac{\alpha_i l'_{i,n}}{\sum_{k=1}^{c} \alpha_k l'_{k,n}} \qquad \forall i = 1, \cdots, c;\ n = 0, 1, \cdots$$

in which α_i stands for the relative volatility of component i with respect to the heaviest component of component 1. The relative volatility for each component thus

follows the convention $\alpha_c > \alpha_{c-1} > \cdots > \alpha_1 = 1$. First, let us consider $n = 1$ and substitute the VLE relation above into Equation (5.1):

$$\begin{aligned}
\begin{pmatrix} l'_{1,2} \\ \vdots \\ l'_{c,2} \end{pmatrix} &= \frac{V}{\sum_{i=1}^{c} \alpha_i l'_{i,1}} \begin{pmatrix} \alpha_1 l'_{1,1} \\ \vdots \\ \alpha_c l'_{c,1} \end{pmatrix} - \begin{pmatrix} d_1 \\ \vdots \\ d_c \end{pmatrix} \\
&= \frac{1}{\sum_{i=1}^{c} \alpha_i l'_{i,1}} \left[\begin{pmatrix} V\alpha_1 & & \\ & \ddots & \\ & & V\alpha_c \end{pmatrix} \begin{pmatrix} l'_{1,1} \\ \vdots \\ l'_{c,1} \end{pmatrix} - \sum_{i=1}^{c} \alpha_i l'_{i,1} \begin{pmatrix} d_1 \\ \vdots \\ d_c \end{pmatrix} \right] \\
&= \frac{1}{\sum_{i=1}^{c} \alpha_i l'_{i,1}} \begin{pmatrix} \alpha_1(V - d_1) & \cdots & -\alpha_c d_1 \\ \vdots & \ddots & \vdots \\ -\alpha_1 d_c & \cdots & \alpha_c(V - d_c) \end{pmatrix} \begin{pmatrix} l'_{1,1} \\ \vdots \\ l'_{c,1} \end{pmatrix}
\end{aligned}$$

Therefore, one can define a $c \times c$ matrix $\mathbf{A}$ as:

$$\mathbf{A} = \begin{pmatrix} \alpha_1(V - d_1) & -\alpha_2 d_1 & \cdots & -\alpha_c d_1 \\ -\alpha_1 d_2 & \alpha_2(V - d_2) & \cdots & -\alpha_c d_2 \\ \vdots & \vdots & \ddots & \vdots \\ -\alpha_1 d_c & -\alpha_2 d_c & \cdots & \alpha_c(V - d_c) \end{pmatrix} \tag{5.2}$$

observe that all elements in $\mathbf{A}$ are independent of the stage number.

As a result, the mass balance equation can also be represented as:

$$l'_{i,2} \sum_{j=1}^{c} \alpha_j l'_{j,1} = \sum_{j=1}^{c} \mathbf{A}_{ij} l'_{j,1} \quad \forall i = 1, \cdots, c$$

in which the ijth element of $\mathbf{A}$ is denoted as $\mathbf{A}_{ij} = \alpha_i(V\delta_{ij} - d_j)$. The Kronecker delta $\delta_{ij} = 1$ when $i = j$ and equals 0 otherwise.

In fact, one can easily show by induction that in general:

$$l'_{i,n+1} \prod_{j=1}^{n} \sum_{k=1}^{c} \alpha_k l'_{k,j} = \sum_{m=1}^{c} \mathbf{A}_{im} l'_{m,n} \prod_{j=1}^{n-1} \sum_{k=1}^{c} \alpha_k l'_{k,j} \quad \forall i = 1, \cdots, c;\ n = 1, 2, \cdots$$

Thus, the nonlinearity associated with the VLE relation can be encapsulated by defining a new variable $\mathcal{L}'_{i,m}$ for the lower part of the column section as:

$$\mathcal{L}'_{i,n} = l'_{i,n} \prod_{j=1}^{n-1} \sum_{i=1}^{c} \alpha_i l'_{i,j} \qquad \forall i = 1, \cdots, c;\ n = 1, 2, \cdots \tag{5.3}$$

from which we obtain a linear system in terms of the new variable $\mathcal{L}'$:

$$\mathcal{L}'_{n+1} = \begin{pmatrix} \mathcal{L}'_{1,n+1} \\ \vdots \\ \mathcal{L}'_{c,n+1} \end{pmatrix} = \mathbf{A}\mathcal{L}'_{n} \qquad n = 1, 2, \cdots \tag{5.4}$$

The boundary case, $\mathcal{L}'_1$, is given by $(l'_{1,1}, \cdots, l'_{c,1})^T$. Another way to obtain the linear system of Equation (5.4) is to write down the mass balance equation of Equation (5.1) for each stage in the lower part of the column section:

$$\begin{aligned} l'_{i,n+1} &= \frac{V\alpha_i}{\sum_{i=1}^{c} \alpha_i l'_{i,n}} l'_{i,n} - d_i \\ l'_{i,n} &= \frac{V\alpha_i}{\sum_{i=1}^{c} \alpha_i l'_{i,n-1}} l'_{i,n-1} - d_i \\ &\vdots \\ l'_{i,2} &= \frac{V\alpha_i}{\sum_{i=1}^{c} \alpha_i l'_{i,1}} l'_{i,1} - d_i \end{aligned} \tag{5.5}$$

A standard technique to obtain the general expression for $l'_{i,n+1}$ is to multiply both sides of the second equality in Equation (5.5) by $\frac{V\alpha_i}{\sum_{i=1}^{c} \alpha_i l'_{i,n}}$, multiply both sides of the third equation by $\frac{V^2\alpha_i^2}{\left(\sum_{i=1}^{c} \alpha_i l'_{i,n}\right)\left(\sum_{i=1}^{c} \alpha_i l'_{i,n-1}\right)}$, and so on. Therefore, if we add these n equalities together, most terms will cancel out, leaving just the following equation:

$$\begin{aligned} l'_{i,n+1} = \frac{\alpha_i^n V^n}{\prod_{j=1}^{n} \sum_{i=1}^{c} \alpha_i l'_{i,j}} l'_{i,1} - d_i \Big(1 + \frac{\alpha_i V}{\sum_{i=1}^{c} \alpha_i l'_{i,n}} \\ + \frac{\alpha_i^2 V^2}{\sum_{i=1}^{c} \alpha_i l'_{i,n} \sum_{i=1}^{c} \alpha_i l'_{i,n-1}} + \cdots + \frac{\alpha_i^{n-1} V^{n-1}}{\prod_{j=2}^{n} \sum_{i=1}^{c} \alpha_i l'_{i,j}} \Big) \end{aligned} \tag{5.6}$$

We can further write Equation (5.6) as the following:

$$l'_{i,n+1}\prod_{j=1}^{n}\sum_{i=1}^{c}\alpha_i l'_{i,j} = \alpha_i^n V^n \prod_{j=1}^{n} l'_{i,1} - d_i\Big(\prod_{j=1}^{n}\sum_{i=1}^{c}\alpha_i l'_{i,j} + \alpha_i V\prod_{j=1}^{n-1}\sum_{i=1}^{c}\alpha_i l'_{i,j} + \cdots + \alpha_i^{n-1}V^{n-1}\prod_{j=2}^{n}\sum_{i=1}^{c}\alpha_i l'_{i,1}\Big) \quad (5.7)$$

Thus, by defining the new variable $\mathcal{L}'$ as in Equation (5.3), we can easily express Equation (5.7) as:

$$\mathcal{L}'_{i,n+1} = \alpha_i^n V^n \prod_{j=1}^{n} l'_{i,1} - d_i\Big(\sum_{i=1}^{c}\alpha_i \mathcal{L}'_{i,n} + \alpha_i V\sum_{i=1}^{c}\alpha_i \mathcal{L}'_{i,n-1} + \cdots + \alpha_i^{n-1}V^{n-1}\prod_{j=2}^{n}\sum_{i=1}^{c}\alpha_i \mathcal{L}'_{i,1}\Big) \quad (5.8)$$

by noting that $\prod_{j=1}^{m}\sum_{i=1}^{c}\alpha_i l'_{i,j} = \sum_{i=1}^{c}\alpha_i \mathcal{L}'_{i,m}$ by simply expanding $\prod_{j=1}^{m}\sum_{i=1}^{c}\alpha_i l'_{i,j}$ as $\sum_{k=1}^{c}\left(\alpha_k l'_{k,m}\prod_{j=1}^{m-1}\sum_{i=1}^{c}\alpha_i l'_{i,j}\right)$.

Similarly, we can express $\mathcal{L}'_{i,n}$ as:

$$\mathcal{L}'_{i,n} = \alpha_i^{n-1} V^{n-1} \prod_{j=1}^{n-1} l'_{i,1} - d_i\Big(\sum_{i=1}^{c}\alpha_i \mathcal{L}'_{i,n-1} + \alpha_i V\sum_{i=1}^{c}\alpha_i \mathcal{L}'_{i,n-2} + \cdots + \alpha_i^{n-2}V^{n-2}\prod_{j=2}^{n-1}\sum_{i=1}^{c}\alpha_i \mathcal{L}'_{i,1}\Big) \quad (5.9)$$

If we multiply both sides of Equation (5.9) with $\alpha_i V$ followed by subtracting it from Equation (5.8), we will finally linearize Equation (5.1) in terms of the new variable $\mathcal{L}'_{i,j}$:

$$\mathcal{L}'_{i,n+1} = V_n \alpha_i \mathcal{L}'_{i,n} - d_i \sum_{j=1}^{c}\alpha_j \mathcal{L}'_{j,n} \quad (5.10)$$

which, in matrix form, is exactly equivalent to Equation (5.4). One can easily show that the characteristic polynomial of $\mathbf{A}$ is given by:

$$\det(\lambda\mathbf{I}-\mathbf{A}) = \Big(1-\sum_{i=1}^{c}\frac{\alpha_i d_i}{V\alpha_i-\lambda}\Big)\prod_{i=1}^{c}\big(V\alpha_i-\lambda\big) = 0 \tag{5.11}$$

As a result, the eigenvalues of $\mathbf{A}$ are:

$$\begin{aligned} \lambda_i &= V\alpha_i \qquad \forall i \text{ such that } d_i = 0 \\ \lambda_i &= V\gamma_i \qquad \forall i \text{ such that } d_i \neq 0 \end{aligned} \tag{5.12}$$

where γ_i represents the ith root of the following equation:

$$\sum_{j=1}^{c}\frac{\alpha_j d_j}{\alpha_j-\gamma_i} = V \qquad i = 1,\cdots,c \tag{5.13}$$

and by convention, $\gamma_c > \cdots > \gamma_1$.

Equation (5.13) looks familiar. It is known as the Underwood's distillate equation the column section stands for the rectifying section of a simple column [146]. In this special case, we readily see that the Underwood roots γ_i are nothing but the eigenvalues of $\mathbf{A}$ divided by the total vapor flow V. Each Underwood root is uniquely bounded by: $\gamma_i \in (\alpha_{i-1}, \alpha_i)$ for $i = 1,\cdots,c$ (and $\alpha_0 = 0$). In the case of a general column section, suppose there exists $k \in \{1,\cdots,c\}$ such that $d_c,\cdots,d_{k+1} > 0$ and $d_k,\cdots,d_1 < 0$, the root behavior of Equation (5.13) is instead illustrated in Figure 5.4.

The eigenvector $\mathbf{z}_i$ corresponding to the eigenvalue γ_i can be determined:

$$\mathbf{z}_i = \Big(\frac{\gamma_i d_1}{\alpha_1-\gamma_i},\cdots,\frac{\gamma_i d_c}{\alpha_c-\gamma_i}\Big)^T \tag{5.14}$$

The eigenvector is closely related to the pinch composition. A pinch zone is a region in a general column section in which the liquid/vapor composition remains unchanged from stage to stage as the number of stages approaches infinity. At pinch,

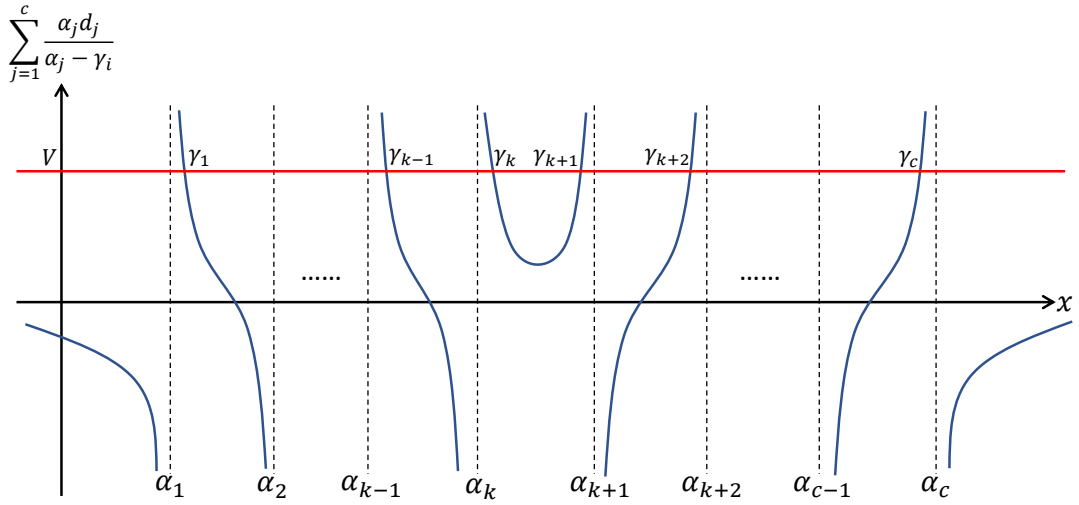

Figure 5.4. The root behavior of Equation (5.13) as the component net material upward flow $d_c, \cdots, d_{k+1} > 0$ and $d_k, \cdots, d_1 < 0$ within the column section.

the equilibrium curve and operating line coincide with each other, resulting in zero dividing force for mass transfer from one stage to another. This phenomenon has been thoroughly discussed by Underwood [19, 146], and Franklin and Forsyth [157] under the scenario of simple column at minimum reflux. They found that each Underwood root is associated with an unique pinch composition. Although some of these pinches may not be physically feasible in an actual distillation column, they play equally important role in constructing the composition profile inside the column section and also the minimum reflux condition of the column. Similarly, for a general column section, each eigenvalue of Equation (5.12) is uniquely associated with a pinch zone as the number of stages becomes infinite. What is more, the eigenvector $\mathbf{z}_i$ actually corresponds to the component liquid flow rate at the pinch zone associated with eigenvalue λ_i. To show this, simply modify Equation (5.1) so that the the liquid

leaving two adjacent stages in the pinch zone have the same composition, denoted as $({l'}_{1,\text{pinch}}, \cdots, {l'}_{c,\text{pinch}})/L$:

$$l'_{k,\text{pinch}} = \frac{V\alpha_k l'_{k,\text{pinch}}}{\sum_{j=1}^{c} \alpha_j l'_{j,\text{pinch}}} - d_k \qquad \forall k = 1, \cdots, c$$

One can then perform the following linear transformation on ${l'}_{k,\text{pinch}}$ on both sides of the equation above followed by substituting Equation (5.13):

$$\sum_{k=1}^{c} \frac{\alpha_k {l'}_{k,\text{pinch}}}{\alpha_k - \gamma_i} = \frac{V\gamma_i}{\sum_{j=1}^{c} \alpha_j {l'}_{j,\text{pinch}}} \sum_{k=1}^{c} \frac{\alpha_k {l'}_{k,\text{pinch}}}{\alpha_k - \gamma_i} \qquad \forall i = 1, \cdots, c$$

which suggests that $V\gamma_i = \lambda_i = \sum_{j=1}^{c} \alpha_j {l'}_{j,\text{pinch}}$. Therefore, the VLE relation at pinch zone associated with λ_i becomes:

$${v'}_{k,\text{pinch}} = V\frac{\alpha_k {l'}_{k,\text{pinch}}}{V\gamma_i} = \frac{\alpha_k {l'}_{k,\text{pinch}}}{\gamma_i} \qquad \forall k = 1, \cdots, c$$

Substituting this result into Equation (5.1) yields:

$${l'}_{k,\text{pinch}} = \frac{\gamma_i d_k}{\alpha_k - \gamma_i} \qquad \forall k = 1, \cdots, c \text{ for pinch associated with } \lambda_i \tag{5.15}$$

which is exactly the kth element of $\mathbf{z}_i$ of Equation (5.14). And the vapor pinch composition associated with λ_i is given by:

$${v'}_{k,\text{pinch}} = \frac{\alpha_k d_k}{\alpha_k - \gamma_i} \qquad \forall k = 1, \cdots, c \text{ for pinch associated with } \lambda_i \tag{5.16}$$

For a c-component system, there are in general c possible liquid pinches, which are essentially all c eigenvectors $\mathbf{z}_1, \cdots, \mathbf{z}_c$. As we can see from Equations (5.15) and (5.16), all possible pinch conditions are completely specified once the net material upward flows for all components and the total vapor or liquid flow in a general column section have been fixed. These pinches are intrinsic characteristics of the considered

general column section and are independent from which part of the column section we are referring to.

One can show that these c pinches are affinely independent. Geometrically, the convex hull of points $\mathbf{z}_1/L, \cdots, \mathbf{z}_c/L$ forms a $(c-1)$-simplex from which one can describe the composition profile in the general column section of a MFMP column. To understand this, let us consider any two adjacent stages n and $(n-1)$ in a column section. Recall that for the lower part of column section, stage n is located one stage above stage $(n-1)$. Using a linear transformation on Equation (5.1) that is similar to the one used for pinch calculations, we get:

$$\sum_{k=1}^{c} \frac{\alpha_k l'_{k,n}}{\alpha_k - x} = \frac{V}{\sum_{j=1}^{c} \alpha_j l'_{j,n-1}} \sum_{k=1}^{c} \frac{\alpha_k^2 l'_{k,n-1}}{\alpha_k - x} - \sum_{k=1}^{c} \frac{\alpha_k d_k}{\alpha_k - x}$$

Now, let $x = \gamma_i$ obtained from Equation (5.13) gives:

$$\sum_{k=1}^{c} \frac{\alpha_k l'_{k,n}}{\alpha_k - \gamma_i} = \frac{V\gamma_i}{\sum_{j=1}^{c} \alpha_j l'_{j,n-1}} \sum_{k=1}^{c} \frac{\alpha_k l'_{k,n-1}}{\alpha_k - \gamma_i}$$

Substituting a different eigenvalue $x = \gamma_j \neq \gamma_i$ gives us a similar equation. Dividing one equation over the other yields the following relationship:

$$\frac{z'_{i,n}}{z'_{j,n}} = \left(\frac{\gamma_i}{\gamma_j}\right) \frac{z'_{i,n-1}}{z'_{j,n-1}}$$

where $z'_{i,n}$ is for now defined as $\sum_{k=1}^{c} \frac{\alpha_k l'_{k,n}}{\alpha_k - \gamma_i}$ and so forth.

As we can see, this is a recursive relationship from which one can relate the liquid composition on any two stages in the lower part of column section in a MFMP column, namely n and m, operated at partial reflux:

$$\frac{z'_{i,n}}{z'_{j,n}} = \left(\frac{\gamma_i}{\gamma_j}\right)^{n-m} \frac{z'_{i,m}}{z'_{j,m}} \tag{5.17}$$

Equation (5.17) is analogous to the Fenske equation [85] which is itself a recursive relationship relating the liquid composition on any two stages in a simple column at total reflux.

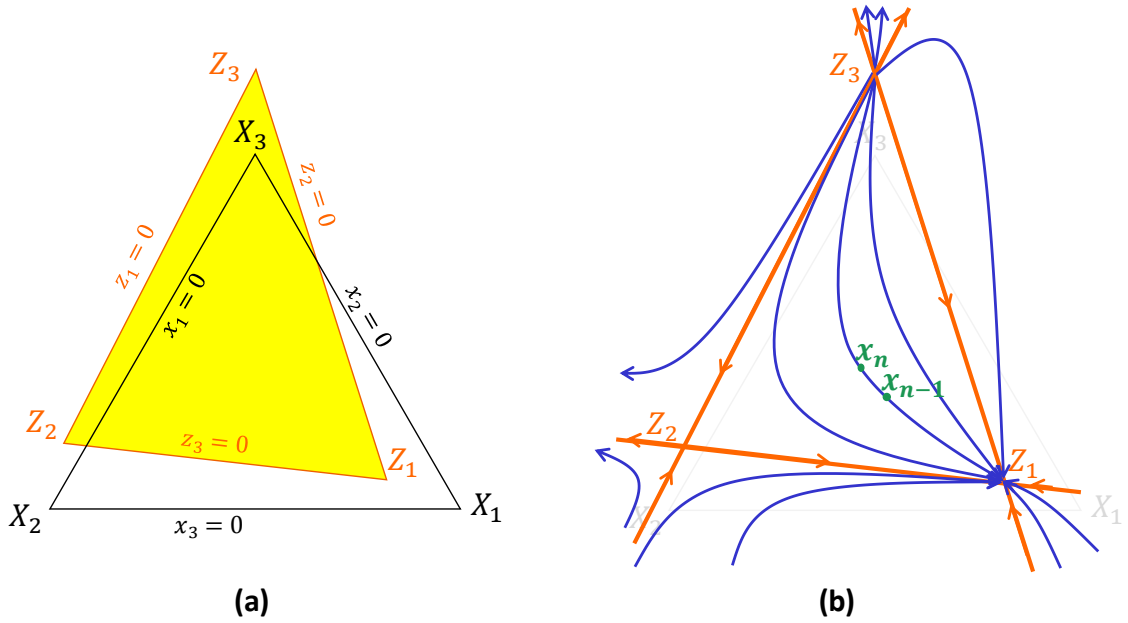

Figure 5.5. (a) For ternary separation, the standard X-simplex $X_3X_2X_1$ gives the feasible region for liquid composition, whereas the Z-simplex $Z_3Z_2Z_1$ will give all possible patterns of liquid composition profile in a general column section of a MFMP column; (b) possible liquid composition profile patterns in a general column section. The arrows represent directions of liquid composition profile as we move downward in the column section. The stage numbers associated with the example liquid compositions follow the labeling convention for the lower part of column section.

One can easily visualize the recursive relation of Equation (5.17) geometrically in Figure 5.5 when $c = 3$. Here, the standard 2-simplex $X_3X_2X_1$ is bounded by the halfspaces $x_i \geq 0$ for $i = 1, 2, 3$ satisfying $\sum_{i=1}^{3} x_i = 1$. It encloses the feasible region of liquid compositions inside a distillation column. Therefore, the X-simplex $X_3X_2X_1$ essentially constructs a coordinate system (x_3, x_2, x_1) for plotting possible liquid compositions for ternary systems. The vertices of $X_3X_2X_1$, namely X_3, X_2,

and X_1, denote the liquid composition of pure component 3, 2, and 1, respectively. Moreover, these vertices also represent pinch compositions at total reflux as the number of plates in the column approaches infinity [85]. For example, vertex X_3, which stands for the lightest pure component, is the pinch composition reached by upward calculations using the Fenske equation starting from a stage whose liquid composition lies either in the interior of $X_3X_2X_1$ (i.e. contains all three components in non-negligible amount), or along the hyperplane $x_1 = 0$ (i.e. free of component 1), or along $x_2 = 0$ (i.e. free of component 2). On the other hand, vertex X_1, which stands for the heaviest pure component, is the liquid pinch composition reached by downward calculations starting from any point lying either in the interior of $X_3X_2X_1$, or along the hyperplane $x_2 = 0$ or $x_3 = 0$. X_2 corresponds to a different type of pinch composition. It can only be reached by either upward calculations from any point along $x_3 = 0$ except X_1 or downward calculations from any point along $x_1 = 0$ except X_3 [157]. As a result, from the perspective of upward calculation using the Fenske equation, X_3, X_1, and X_2 represents a stable node, an unstable node, and a saddle pinch, respectively.

By the same token, a 2-simplex $Z_3Z_2Z_1$ can be constructed to characterize the liquid composition profile in a general column section of a MFMP column operated at partial reflux. And the boundaries, or more precisely, the facets of this Z-simplex are hyperplanes defined for now as $z_i = \sum_{j=1}^{3} \frac{\alpha_j x_j}{\alpha_j - \gamma_i} = 0$ for $i = 1, 2, 3$ as in Equation (5.17). Any vertex Z_i in $Z_3Z_2Z_1$ satisfies $z_j = 0 \ \ \forall j \neq i$. Equation (5.17) suggests that these vertices represent three possible liquid pinches. To see this, we number the starting plate as stage m. Thus, stage n is reached by successive upward (downward) calculations using Equation (5.17) from stage m if $n - m > 0$ ($n - m < 0$). Consider the case when $n - m \to +\infty$ and let $j = c = 3$. Thus, as long as $z'_{3,n}$ and $z'_{3,m}$ are both non-zero quantities, we must have $z'_{1,n} \to 0$ and $z'_{2,n} \to 0$ simultaneously since $\gamma_1, \gamma_2 < \gamma_3$ in Equation (5.13). In this case, Z_3 is the liquid pinch composition reached by upward calculations starting from stage n. Next, consider the case of downward calculation and let $j = 1$. If $z'_{1,n}$ and $z'_{1,m}$ are both non-zero quantities, then $z'_{2,n} \to 0$

and ${z'}_{3,n} \to 0$ simultaneously as $n - m \to -\infty$. In this case, the liquid composition eventually converges to Z_1 as pinch by downward calculations from stage m. Finally, Z_2 can only be reached as liquid pinch by either upward calculations if the liquid composition on the starting plate satisfies ${z'}_{3,m} = 0$ (except at Z_1) or by downward calculations if the liquid composition on the starting plate satisfies ${z'}_{1,m} = 0$ (except at Z_3). As shown in Figure 5.5(b), from the standpoint of upward calculation at partial reflux, Z_3, Z_2, and Z_1 of $Z_3Z_2Z_1$ represents a stable node, an unstable node, and a saddle pinch, respectively.

The discussions above can be easily generalized to any c-component system, in which by solving Equation (5.13) a $(c-1)$-simplex $Z_c \cdots Z_1$ called the "Z-simplex" can be constructed under the coordinate system set up by the standard $(c-1)$-simplex $X_c \cdots X_1$ called the "X-simplex". The vertices of $Z_c \cdots Z_1$ should represent possible liquid pinch compositions. Specifically, Z_c and Z_1 represent the stable node pinch and unstable node pinch based on upward calculation, respectively. And all other vertices, namely Z_{c-1} to Z_2, are saddle pinches, meaning that they can only be reached when the liquid composition on the starting stage satisfies certain conditions. In general, the saddle pinch Z_i when $i \in \{c-1, \cdots, 2\}$ can be reached by either upward calculations if the liquid composition on the starting plate satisfies ${z'}_{k,m} = 0 \quad \forall k \geq i+1$ or by downward calculations if the liquid composition on the starting plate satisfies ${z'}_{k,m} = 0 \ \ \forall k \leq i-1$.

Essentially, our goal is to construct the Z-simplex which accurately captures all possible liquid composition profiles and pinch conditions under the same coordinate system $(x_c, \cdots, x_1)$ which is set up by the standard X-simplex. As a direct consequence of goal and Equation (5.17), each liquid pinch composition determined from Equation (5.15) must match exactly with its corresponding vertex in the Z-simplex. In other words, $\sum_{j=1}^{c} \frac{\alpha_j x_{j,\text{pinch}}}{\alpha_j - \gamma_i} = \sum_{j=1}^{c} \frac{\gamma_i \alpha_j d_j}{L(\alpha_j - \gamma_i)^2} = 1 \quad \forall i = 1, \cdots, c$. However, this condition will not be satisfied under the original transformation of $z_{i,n}$ and hyperplanes $z_i = 0$ defined earlier. This is because Equation (5.13) can be written as $\sum_{j=1}^{c} \frac{\alpha_j (d_j/V)}{\alpha_j - \gamma_i} = 1 \ \forall i = 1, \cdots, c$, which suggests that $(x_1, \cdots, x_c) = (d_1/V, \cdots, d_c/V)$,

rather than $(l'_{1,\text{pinch}}, \cdots, l'_{c,\text{pinch}})/L$, is the solution to the following linear system of order c: $\sum_{j=1}^{c} \frac{\alpha_j x_j}{\alpha_j - \gamma_i} = 1$. Therefore, $\sum_{j=1}^{c} \frac{\alpha_j x_{j,\text{pinch}}}{\alpha_j - \gamma_i} \neq 1 \quad \forall i = 1, \cdots, c$ in general. To fix this issue, we just need to modify the linear transformation $z'_{i,n}$ by simply including a scaling factor k_i:

$$z'_{i,n} = k_i \sum_{j=1}^{c} \frac{\alpha_j l'_{j,n}}{\alpha_j - \gamma_i} \qquad \forall i = 1, \cdots, c;\ n = 1, 2, \cdots \tag{5.18}$$

and in turn the hyperplanes forming the facets of Z-simplex $Z_c \cdots Z_1$ are modified as:

$$z_i = k_i \sum_{j=1}^{c} \frac{\alpha_j x_j}{\alpha_j - \gamma_i} \qquad \forall i = 1, \cdots, c \tag{5.19}$$

where k_i can be explicitly solved by substituting the liquid pinch composition of Equation (5.15) with respect to γ_i into Equation (5.19):

$$k_i \sum_{j=1}^{c} \frac{\alpha_j l'_{j,\text{pinch}}/L}{\alpha_j - \gamma_i} = \frac{k_i \gamma_i}{L} \sum_{j=1}^{c} \frac{\alpha_j d_j}{(\alpha_j - \gamma_i)^2} = 1 \qquad \forall i = 1, \cdots, c \tag{5.20}$$

Suppose in the general column section of concern, $d_c, \cdots, d_{k+1} \geq 0$ whereas $d_k, \cdots, d_1 \leq 0$. For this system, one can show that:

$$\begin{aligned} &\text{sgn}(k_i) = +1 \qquad \forall i \in \{k+1, \cdots, c\} \\ &\text{sgn}(k_i) = -1 \qquad \forall i \in \{1, \cdots, k\} \end{aligned} \tag{5.21}$$

in other words, $\text{sgn}(k_i) = \text{sgn}(d_i)$. In fact, k_i are also intrinsic to the column section and are independent from which part of the column section we are referring to.

Before moving on to deriving the analytical expression for the liquid or vapor composition profile in the column section, we would like to introduce a useful relation by writing Equation (5.13) for two distinct eigenvalues, $\lambda_i \neq \lambda_j$ and then subtracting one expression from the other:

$$\sum_{k=1}^{c} \frac{\alpha_k d_k}{\alpha_k - \gamma_i} - \sum_{k=1}^{c} \frac{\alpha_k d_k}{\alpha_k - \gamma_j} = (\gamma_i - \gamma_j) \sum_{k=1}^{c} \frac{\alpha_k d_k}{(\alpha_k - \gamma_i)(\alpha_k - \gamma_j)} = 0 \tag{5.22}$$

which implies that the quantity $\sum_{k=1}^{c} \frac{\alpha_k d_k}{(\alpha_k-\gamma_i)(\alpha_k-\gamma_j)}$ will always be 0 unless in the case of $\lambda_i = \lambda_j$ when it becomes $L/k_i\gamma_i$ as shown earlier. As we will see later, Equation (5.22) is helpful in deriving several important relations and properties of the model.

Now, let us solve for the liquid or vapor composition on any stage in a general column section. Writing Equation (5.4) recursively followed by rewriting it as a linear combination of all eigenvectors with coefficients of a_i shown in Equation (5.14) will give:

$$\mathcal{L'}_n = \mathbf{A}^{n-1}\mathcal{L'}_1 = \sum_{i=1}^{c} a_i\lambda_i^{n-1}\mathbf{z}_i = V^{n-1}\sum_{i=1}^{c} a_i\gamma_i^{n-1}\Big(\frac{\gamma_i d_1}{\alpha_1-\gamma_i}, \cdots, \frac{\gamma_i d_c}{\alpha_c-\gamma_i}\Big)^T$$

Here, we introduce two independent strategies to determine a_i. In the first strategy, recall that matrix $\mathbf{A}$ is associated with two eigenproblems, one of which is $\mathbf{A}\mathbf{z}_i = \lambda_i\mathbf{z}_i$, while the other is given by:

$$\mathbf{A}^T\mathbf{y}_i = \eta_i\mathbf{y}_i = \lambda_i\mathbf{y}_i \qquad \forall i = 1, \cdots, c$$

since $\mathbf{A}^T$ and $\mathbf{A}$ have the same eigenvalues. Furthermore, both $\{\mathbf{z}_i\}$ and $\{\mathbf{y}_i\}$ are linearly independent sets, and $\mathbf{y}_i^T\mathbf{z}_j = 0$ as long as $i \neq j$. With the aid of Equation (5.22), one can easily verify that the eigenvector $\mathbf{y}_i$ associated with eigenvalue $\eta_i = \lambda_i$ for the eigenproblem of $\mathbf{A}^T$ is:

$$\mathbf{y}_i = \Big(\frac{\alpha_1}{\alpha_1-\gamma_i}, \cdots, \frac{\alpha_c}{\alpha_c-\gamma_i}\Big)^T \qquad \forall i = 1, \cdots, c \tag{5.23}$$

Left multiplying $\mathcal{L}'_1$ by $\mathbf{y}_i^T$ yields:

$$\mathbf{y}_i^T\mathcal{L'}_1 = \sum_{j=1}^{c} a_j\mathbf{y}_i^T\mathbf{z}_j = a_i\mathbf{y}_i^T\mathbf{z}_i = a_i\gamma_i\sum_{j=1}^{c}\frac{\alpha_j d_j}{(\alpha_j-\gamma_i)^2} \qquad \forall i = 1, \cdots, c$$

Therefore, the coefficient a_i is determined as:

$$a_i = \frac{\sum_{j=1}^{c} \frac{\alpha_j l'_{j,1}}{\alpha_j - \gamma_i}}{\gamma_i \sum_{j=1}^{c} \frac{\alpha_j d_j}{(\alpha_j - \gamma_i)^2}} = \frac{k_i \sum_{j=1}^{c} \frac{\alpha_j l'_{j,1}}{\alpha_j - \gamma_i}}{L} \qquad \forall i = 1, \cdots, c \tag{5.24}$$

in which we use $\sum_{j=1}^{c} \frac{\alpha_j d_j}{(\alpha_j - \gamma_i)^2} = \frac{L}{\gamma_i k_i}$ as we have derived before. Also, we can show that $\sum_{i=1}^{c} a_i = 1$ since:

$$\sum_{j=1}^{c} \mathcal{L}'_{j,1} = L = \sum_{j=1}^{c} \sum_{i=1}^{c} a_i \frac{\gamma_i d_j}{\alpha_j - \gamma_i} = \sum_{i=1}^{c} a_i \sum_{j=1}^{c} \frac{\gamma_i d_j}{\alpha_j - \gamma_i} = L \sum_{i=1}^{c} a_i$$

From Equation (5.24), we can see that if the liquid stream leaving the general column section from the bottom satisfies satisfies $\sum_{j=1}^{c} \frac{\alpha_j l'_{j,1}}{\alpha_j - \gamma_i} = 0$ for any γ_i, then $a_i = 0$. This is consistent with the earlier discussion about the geometric interpretation of Equation (5.17).

To find ${v'}_{k,n}$ or ${l'}_{k,n}$, first one can verify by direct substitution that the VLE relation can also be expressed using ${\mathcal{L}'}_{i,n}$ variables defined in Equation (5.3):

$${v'}_{k,n} = V \frac{\alpha_k {\mathcal{L}'}_{k,n}}{\sum_{j=1}^{c} \alpha_j {\mathcal{L}'}_{j,n}} \qquad \forall k = 1, \cdots, c$$

Thus, to derive the final expression for ${v'}_{k,n}$, we would like to first determine $\sum_{k=1}^{c} \alpha_k {\mathcal{L}'}_{k,n}$. We know that the kth element of ${\mathcal{L}'}_n$ is:

$${\mathcal{L}'}_{k,n} = V^{n-1} d_k \sum_{i=1}^{c} \frac{a_i \gamma_i^n}{\alpha_k - \gamma_i} \qquad \forall k = 1, \cdots, c;\ n = 1, 2, \cdots$$

Thus, $\sum_{k=1}^{c} \alpha_k {\mathcal{L}'}_{k,n}$ can be determined as:

$$\sum_{k=1}^{c} \alpha_k {\mathcal{L}'}_{k,n} = V^{n-1} \sum_{k=1}^{c} \alpha_k d_k \sum_{i=1}^{c} \frac{a_i \gamma_i^n}{\alpha_k - \gamma_i} = V^n \sum_{i=1}^{c} a_i \gamma_i^n \qquad n = 1, 2, \cdots$$

which utilizes Equation (5.13). From here, ${v'}_{k,n+1}$ can be derived as:

$$ {v'}_{k,n} = \alpha_k d_k \frac{\sum_{i=1}^{c} \frac{a_i \gamma_i^n}{\alpha_k - \gamma_i}}{\sum_{i=1}^{c} a_i \gamma_i^n} \qquad \forall k = 1, \cdots, c;\ n = 1, 2, \cdots \tag{5.25} $$

and ${l'}_{k,n+1}$ can simply be calculated using Equation (5.1). Overall, the liquid and vapor composition leaving any stage in the lower part of a general column section belonging to a MFMP column can be precisely determined by solving Equations (5.13),(5.20),(5.24),and (5.25) simultaneously.

Now, we introduce another strategy to solve for a_i in Equation (5.24). Recall that the ijth element of $\mathbf{A}$ is $\alpha_j(V\delta_{ij} - d_i)$. We can easily see that multiplying it with α_i/d_i gives $V\alpha_i\alpha_j\delta_{ij}/d_i - \alpha_i\alpha_j$, which is a symmetric product. This allows us to define a functional as:

$$ f(x, y) = \sum_{i=1}^{c} \frac{\alpha_i}{d_i} x_i y_i \tag{5.26} $$

The definition of Equation (5.26) satisfies all the requirements of a bilinear functional. Also, $f(x, y)$ has the following nice property:

$$ f({\mathcal{L}'}_{n+1}, \mathbf{z}_i) = f(\mathbf{A}{\mathcal{L}'}_n, \mathbf{z}_i) = f({\mathcal{L}'}_n, \mathbf{A}\mathbf{z}_i) = \lambda_i f({\mathcal{L}'}_n, \mathbf{z}_i) = \cdots = \lambda_i^n f({\mathcal{L}'}_1, \mathbf{z}_i) $$

As we have discussed, ${\mathcal{L}'}_1$ can be expressed as $\sum_{j=1}^{c} a_j \mathbf{z}_j$. This gives:

$$ f({\mathcal{L}'}_{n+1}, \mathbf{z}_i) = \lambda_i^n f(\sum_{j=1}^{c} a_j \mathbf{z}_j, \mathbf{z}_i) = \lambda_i^n a_i f(\mathbf{z}_i, \mathbf{z}_i) $$

which uses the fact that $f(\mathbf{z}_j, \mathbf{z}_i) = 0 \quad \forall j \neq i$ due to Equation (5.22). Since a_i is independent of stage number n, we can directly solve for a_i by letting $n = 0$ in the expression above:

$$ a_i = \frac{f(\mathcal{L}'_1, \mathbf{z}_i)}{f(\mathbf{z}_i, \mathbf{z}_i)} = \frac{\gamma_i \sum_{j=1}^{c} \frac{\alpha_j l'_{j,1}}{\alpha_j - \gamma_i}}{L\gamma_i/k_i} = \frac{k_i \sum_{j=1}^{c} \frac{\alpha_j l'_{j,1}}{\alpha_j - \gamma_i}}{L} \qquad \forall i = 1, \cdots, c $$

since $f(\mathbf{z}_i, \mathbf{z}_i) = \gamma_i^2 \sum_{k=1}^{c} \frac{\alpha_k d_k}{(\alpha_k - \gamma_i)^2} = \frac{L\gamma_i}{k_i}$. Clearly, both strategies lead to the same answer to a_i. The remaining steps to solve for $v'_{k,n+1}$ and $l'_{k,n+1}$ are identical.

5.3.2 Modeling of Upper Part of Column Section

Once we have successfully built the mathematical model for the lower part of a general column section in a MFMP column at partial reflux, the procedure for constructing the model for the upper part of the column section becomes straightforward. Here, we just list the key results. First, the component mass balance equation can be written based on Figure 5.3 as:

$$l_{i,n} = v_{i,n+1} - d_i \qquad \forall i = 1, \cdots, c;\ n = 0, 1, \cdots \tag{5.27}$$

To linearize this system, we define a new variable $\mathcal{L}_{i,m}$ as:

$$\mathcal{L}_{i,m} = l_{i,m} \prod_{j=m+1}^{n} \sum_{i=1}^{c} \alpha_i l_{i,j} \qquad \forall i = 1, \cdots, c;\ m = 0, 1, \cdots, n-1 \tag{5.28}$$

from which a linear system in terms of $\mathcal{L}$ for the upper part of section can be written as:

$$\mathcal{L}_0 = \begin{pmatrix} \mathcal{L}_{1,0} \\ \vdots \\ \mathcal{L}_{c,0} \end{pmatrix} = \begin{pmatrix} l_{1,0} \\ \vdots \\ l_{c,0} \end{pmatrix} = \mathbf{A}\mathcal{L}_1 \tag{5.29}$$

Here, matrix $\mathbf{A}$ here is identical to the one defined in Equation (5.2). However, in this case, we are interested in computing $\mathbf{A}^{-1}$ in Equation (5.29) so as to express $\mathcal{L}_n$ in terms of $\mathcal{L}_0$. To find out $\mathbf{A}^{-1}$, first notice that its eigenvalues are simply the reciprocals of the eigenvalues of $\mathbf{A}$:

$$\begin{aligned} \lambda_i &= \frac{1}{V\alpha_i} \qquad \forall i \text{ such that } d_i = 0 \\ \lambda_i &= \frac{1}{V\gamma_i} \qquad \forall i \text{ such that } d_i \neq 0 \end{aligned} \tag{5.30}$$

in which γ_i are again the solutions to Equation (5.13).

The inverse of $\mathbf{A}$, $\mathbf{A}^{-1}$, can be found using eigendecomposition. Recall that the eigenvector $\mathbf{z}_i$ associated with eigenvalue λ_i of $\mathbf{A}$ is expressed in Equation (5.14). Thus, matrix $\mathbf{S}$ which contains all eigenvectors is simply:

$$\mathbf{S} = \begin{pmatrix} \mathbf{z}_1 & \cdots & \mathbf{z}_c \end{pmatrix} = \begin{pmatrix} \frac{\gamma_1 d_1}{\alpha_1 - \gamma_1} & \cdots & \frac{\gamma_c d_1}{\alpha_1 - \gamma_c} \\ \vdots & \ddots & \vdots \\ \frac{\gamma_1 d_c}{\alpha_c - \gamma_1} & \cdots & \frac{\gamma_c d_c}{\alpha_c - \gamma_c} \end{pmatrix}$$

One can verify that the inverse of $\mathbf{S}$ is given by:

$$\mathbf{S}^{-1} = \frac{1}{L} \begin{pmatrix} \frac{\alpha_1 k_1}{\alpha_1 - \gamma_1} & \cdots & \frac{\alpha_c k_1}{\alpha_c - \gamma_1} \\ \vdots & \ddots & \vdots \\ \frac{\alpha_1 k_c}{\alpha_1 - \gamma_c} & \cdots & \frac{\alpha_c k_c}{\alpha_c - \gamma_c} \end{pmatrix}$$

in which k_i have already been defined in Equation (5.20). Thus, $\mathbf{A}^{-n}$ can be expressed as $(\mathbf{S}\Lambda\mathbf{S}^{-1})^{-n} = \mathbf{S}\Lambda^{-n}\mathbf{S}^{-1}$. And Λ^{-n} a diagonal matrix in which the ith diagonal element is given by λ_i^n of Equation (5.30).

Similar to the lower part of the column section, we can express $\mathcal{L}_0$ as a linear combination of all eigenvectors with coefficients b_i defined as:

$$b_i = \frac{k_i}{L} \sum_{j=1}^{c} \frac{\alpha_j l_{j,0}}{\alpha_j - \gamma_i} \qquad \forall i = 1, \cdots, c \tag{5.31}$$

from which one can easily show that $\sum_{i=1}^{c} b_i = 1$. With this, the vapor flow for component i leaving stage n can finally be derived as:

$$v_{k,n} = \alpha_k d_k \frac{\sum_{i=1}^{c} \frac{b_i / \gamma_i^{n-1}}{\alpha_k - \gamma_i}}{\sum_{i=1}^{c} b_i / \gamma_i^{n-1}} \tag{5.32}$$

In all, the liquid and vapor composition leaving any stage in the upper part of a general column section can be calculated by simultaneously solving Equations (5.13),(5.20),(5.31),and (5.32).

So far, we have developed the mathematical model based on the concept of countercurrent mass exchange unit that describes the liquid and vapor composition profiles in a general column section within a MFMP column operated at partial reflux. Before exploring some of the useful mathematical properties of the model, we would like to derive two additional interesting relations based on the characteristic polynomial of **A** shown in Equation (5.11), which can be expanded as:

$$\det(\lambda \mathbf{I} - \mathbf{A}) = V^c \prod_{i=1}^{c} (\alpha_i - \lambda/V) - V^{c-1} \sum_{i=1}^{c} \alpha_i d_i \prod_{\substack{j=1 \\ j \neq i}}^{c} (\alpha_j - \lambda/V)$$

This can be viewed as a polynomial of degree c with roots $\lambda_j \; \forall j = 1, \cdots, c$ defined in Equation (5.12). Thus, we have the following equality:

$$V \prod_{i=1}^{c} (\alpha_i - x) - \sum_{i=1}^{c} \left[\alpha_i d_i \prod_{\substack{j=1 \\ j \neq i}}^{c} (\alpha_j - x) \right] = V \prod_{i=1}^{c} (x - \gamma_i) \qquad \forall x \in \mathbb{R}$$

Letting $x = 0$ gives us the following useful relation of the L/V ratio which has been derived by Underwood [19], Franklin [158], and Wachter et al. [149]:

$$\frac{L}{V} = \prod_{i=1}^{c} \gamma_i \Bigg/ \prod_{i=1}^{c} \alpha_i \tag{5.33}$$

Now, if we let $x = \alpha_k$, then $\prod_{i=1}^{c} (\alpha_i - \alpha_k) = 0$ and $\alpha_i d_i \prod_{j \neq i}^{c} (\alpha_j - \alpha_k) = 0 \; \forall i \neq k$. Therefore, we get another relation for the net material upward flow of component k in a general column section:

$$d_k = V \prod_{i=1}^{c} (\alpha_k - \gamma_i) \Bigg/ \alpha_k \prod_{\substack{i=1 \\ i \neq k}}^{c} (\alpha_k - \alpha_i) \qquad \forall k = 1, \cdots, c$$

5.4 Some Properties of the Model

So far, we have taken for granted that in any general column section within a MFMP column, as the number of stages becomes infinite, a pinch zone will form in which there is no change in vapor or liquid composition from tray to tray. Here, we rigorously show that such a pinch zone exists in a general column section of a MFMP column and can be obtained from the model developed earlier. To do this, we need to show that $v'_{i,n}$ for the lower part or $v_{i,n}$ for the upper part of the column section is a convergence sequence with respect to n. We also need to make sure that both quantities converge to the same limit as the number of plates comes to infinity. To do this, we construct two functions, $f'_n(x)$ for the lower part of column section and $f_n(x)$ for the upper part, that will be very useful in proving convergence as well as other important properties:

$$\begin{aligned} f'_n(x) &= \sum_{i=1}^{c} \frac{v'_{i,n}}{\alpha_i - x} \\ f_n(x) &= \sum_{i=1}^{c} \frac{v_{i,n}}{\alpha_i - x} \end{aligned} \tag{5.34}$$

where n stands for the stage number following the convention illustrated in Figure 5.3. Since the direction of component vapor flow leaving any stage is always pointing upward, there must exist, for any given n, one *single real* root denoted as $x'_k(n)$ or $x_k(n) \in (\alpha_k, \alpha_{k+1})$ $\forall k = 1, \cdots, c-1$, such that $f'_n(x'_k(n)) = 0$ or $f_n(x_k(n)) = 0$, respectively. Thus, we have the following proposition for the lower part of the column section:

Proposition 5.4.1 *Within any given* (α_k, α_{k+1}) *where* $k = 1, \cdots, c-1$, *the roots to* $f'_n(x) = 0$ *for* $n = 0, 1, \cdots$ *form a monotonic sequence* $\{x'_k(n)\}$ *with respect to* n.

Proof Since $v'_{i,n} \geq 0$ $\forall i = 1, \cdots, c$; $n = 0, 1, \cdots$, at any given n, $f'_n(x)$ is a monotonically increasing function with respect to $x \in (\alpha_k, \alpha_{k+1})$ for $k = 1, \cdots, c-1$. Now, since $v'_{i,n} - l'_{i,n+1} = v'_{i,n-1} - l'_{i,n}$ for $n = 1, 2, \cdots$ in Equation (5.1), perform-

ing the transformation of Equation (5.34) followed by subtracting both sides by V gives $\sum_{i=1}^{c} \frac{\alpha_i v'_{i,n}}{\alpha_i - x} - V - \sum_{i=1}^{c} \frac{\alpha_i l'_{i,n+1}}{\alpha_i - x} = \sum_{i=1}^{c} \frac{\alpha_i v'_{i,n-1}}{\alpha_i - x} - V - \sum_{i=1}^{c} \frac{\alpha_i l'_{i,n}}{\alpha_i - x}$. Substituting $\sum_{i=1}^{c} \frac{\alpha_i v'_{i,n}}{\alpha_i - x} - V = x \sum_{i=1}^{c} \frac{v'_{i,n}}{\alpha_i - x} = x f'_n(x)$ and the VLE relation $l'_{i,n} = \frac{L v'_{i,n}/\alpha_i}{\sum_{j=1}^{c} v'_{j,n}/\alpha_j}$ gives $x f'_n(x) - \frac{L}{\sum_{j=1}^{c} v'_{j,n+1}/\alpha_j} f'_{n+1}(x) = x f'_{n-1}(x) - \frac{L}{\sum_{j=1}^{c} v'_{j,n}/\alpha_j} f'_n(x)$.

Let $x = x'_k(n)$, then $f'_{n+1}(x'_k(n)) = -\frac{x'_k(n) \sum_{j=1}^{c} v'_{j,n+1}/\alpha_j}{L} f'_{n-1}(x'_k(n))$. Clearly, this implies that $f'_{n+1}(x'_k(n)) f'_{n-1}(x'_k(n)) < 0$ since $x'_k(n) > 0$. Because $f'_n(x)$ is monotonic within (α_k, α_{k+1}), Bolzano's theorem suggests that the bound for $x'_k(n)$ must be given by $(\min\{x'_k(n-1), x'_k(n+1)\}, \max\{x'_k(n-1), x'_k(n+1)\})$. Thus, if $x'_k(n+1) > x'_k(n-1)$, then $\{x'_k(n)\}$ is a monotonically increasing sequence. Otherwise, it is a monotonically decreasing sequence. In either case, $\{x'_k(n)\}$ is monotonic. ■

Since the sequence $\{x'_k(n)\}$ is bounded by (α_k, α_{k+1}) and is monotonic, it must be convergent based on the monotone convergence theorem. To determine the limit of $\{x'_k(n)\}$ as the number of stages approaches to infinity, we substitute Equation (5.25) into Equation (5.34) and get:

$$f'_n(x) = \sum_{i=1}^{c} \frac{\alpha_i d_i \sum_{j=1}^{c} \frac{a_j \gamma_j^n}{\alpha_i - \gamma_j}}{(\alpha_i - x) \sum_{j=1}^{c} a_j \gamma_j^n} = \frac{\sum_{j=1}^{c} a_j \gamma_j^n \left(\sum_{i=1}^{c} \frac{\alpha_i d_i}{(\alpha_i - \gamma_j)(\alpha_i - x)} \right)}{\sum_{j=1}^{c} a_j \gamma_j^n}$$

By letting x to be the root of Equation (5.13) that lies in (α_k, α_{k+1}), which we label as γ_K, we can show that:

$$f'_n(\gamma_K) = \frac{a_K \gamma_K^n \sum_{j=1}^{c} \frac{\alpha_j d_j}{(\alpha_j - \gamma_K)^2}}{\sum_{j=1}^{c} a_j \gamma_j^n} = \frac{L a_K \gamma_K^{n-1}}{k_K \sum_{j=1}^{c} a_j \gamma_j^n}$$

from Equation (5.22). As a result, $\lim_{n \to \infty} f'_n(\gamma_K) = 0$, implying that $\{x'_k(n)\}$ converges to γ_K as the number of stages becomes infinite. In other words, if we define $f'(x)$ as $\lim_{n \to \infty} f'_n(x)$, we can write:

$$f'(\gamma_K) = \lim_{n \to \infty} \sum_{i=1}^{c} \frac{v'_{i,n}}{\alpha_i - \gamma_K} = \sum_{i=1}^{c} \frac{v'_i}{\alpha_i - \gamma_K} = 0 \qquad \gamma_K \in (\alpha_k, \alpha_{k+1}),\ k = 1, \cdots, c-1$$

where we denote $v'_i = \lim_{n\to\infty} v'_{i,n}$. Notice that only $c-1$ out of the c roots to Equation (5.13) are used. These $c-1$ linearly independent equations of v'_i, when combining with $\sum_{i=1}^{c} v'_{i,n} = V$, gives a fully specified linear system for which an unique solution of $(v'_1, \cdots, v'_c)^T$ exists. This shows the existence of pinch based on the model for the lower part of column section when the number of stages becomes infinite.

Likewise, one can demonstrate the existence of pinch for the upper part of column section as the number of stages becomes infinite by proving a similar proposition as Proposition 5.4.1 that within a given interval (α_k, α_{k+1}) where $k = 1, \cdots, c-1$, the roots to $f_n(x) = 0$ for $n = 0, 1, \cdots$ form a monotonic sequence $\{x_k(n)\}$ with respect to n. Also it can be readily seen that these two pinches, namely v'_i and $v_i = \lim_{n\to\infty} v_{i,n}$, actually correspond to the same pinch because corresponding two linear systems are identical. For simplicity, for the remaining discussions, we will use $f(x)$ to denote both $\lim_{n\to\infty} f'_n(x)$ for the lower part of column section and $\lim_{n\to\infty} f_n(x)$ for the upper part at pinch. Also, we will use v_i and l_i to respectively indicate the pinch vapor and liquid flow for component i.

Now that we have demonstrated the existence and uniqueness of pinch zone in a general column section as the number of stages approaches infinity, we would like to examine the pinch composition in more detail. To do this, we consider a new function $g(x)$:

$$g(x) = \sum_{i=1}^{c} \frac{\alpha_i d_i}{\alpha_i - x} - V \tag{5.35}$$

whose zeros are essentially $\gamma_1, \cdots, \gamma_c$. Replacing d_i with pinch zone component vapor and liquid flows $v_i - l_i$ gives:

$$g(x) = \sum_{i=1}^{c} \Big(\frac{\alpha_i (v_i - l_i)}{\alpha_i - x} - v_i \Big) = \Big(x - \frac{L}{\sum_{j=1}^{c} v_j/\alpha_j} \Big) f(x)$$

in which we again utilize the VLE relation $l_i/L = \frac{v_i/\alpha_i}{\sum_{j=1}^{c} v_j/\alpha_j}$.

Since $f(x) = 0$ has $c-1$ distinct real roots whereas $g(x) = 0$ has c roots, $\frac{L}{\sum_{j=1}^{c} v_j/\alpha_j}$ must correspond to one of the roots to $g(x) = 0$. For simplicity, we refer this root

as γ_I, from which $g(x)$ then becomes $(x-\gamma_I)f(x)$. It turns out that this root γ_I is closely related to the pinch zone composition from three major aspects. First, by substituting the definition of γ_I and the VLE relationship into the pinch zone mass balance equation $v_i - l_i = d_i$, we can show that the actual pinch zone component vapor and liquid flows are simply given by:

$$v_i = \frac{\alpha_i d_i}{\alpha_i - \gamma_I} \qquad l_i = \frac{\gamma_I d_i}{\alpha_i - \gamma_I} \qquad \forall i = 1, \cdots, c \tag{5.36}$$

Second, if $g(x) = 0$ or Equation (5.13) ever has complex root, then there must be at least two of them forming complex conjugate pair. However, since all $(c-1)$ roots to $f(x) = 0$ are distinct and real, all c roots to $g(x) = 0$ must be real and only one of them can have a multiplicity of 2. And if so, γ_I must be one of them. This result clears a potential misconception in the literature which argues that complex roots to $g(x) = 0$ are also possible in a general column section or any countercurrent equilibrium-staged separation unit operations [158].

Third, as we have already discussed, the physical meaning of d_i of Equation (5.13) or (5.35) in a general column section stands for the net material upward flow for component i. As a result, one of the three following cases are possible:

1. All $d_i \geq 0 \ \forall i = 1, \cdots, c$. This usually happens to the topmost section in a general MFMP column or the rectifying section in a simple column. In this case, γ_I must simultaneously satisfy the following conditions according to Equation (5.36): $\alpha_1 - \gamma_I > 0, \cdots, \alpha_c - \gamma_I > 0$. Thus, we have: $\gamma_I < \min\{\alpha_1, \cdots, \alpha_c\} = \alpha_1$, or $\gamma_I \in (0, 1)$.

2. All $d_i \leq 0 \ \forall i = 1, \cdots, c$. This usually happens to the bottommost section in a MFMP column or the stripping section in a simple column. In this case, γ_I must satisfy $\gamma_I \in (\alpha_c, \infty)$.

3. There is a sign change of d_i between component k and component $k+1$, i.e. $d_1, \cdots, d_k < 0, \ d_{k+1}, \cdots, d_c > 0$. This case might happen to an intermediate

column section in a MFMP column. In this case, we have $\max\{d_1, \cdots, d_k\} < \gamma_I < \min\{\alpha_{k+1}, \cdots, \alpha_c\}$, or $\gamma_I \in (\alpha_k, \alpha_{k+1})$.

Case 3 suggests us that γ_I must lie in the same interval in which the sign change in d_i occurs. In addition, due to the uniqueness of pinch zone in a general column section, it follows that at most one sign change in d_i is allowed.

To ensure that the pinch zone component vapor flow is indeed given by Equation (5.36), we further explore the conditions that $v'_{i,n}$ in Equation (5.25) and $v_{i,n}$ in Equation (5.32) need to satisfy. Since $\gamma_c > \cdots > \gamma_1$, if $a_c \neq 0$, then the numerator and denominator of Equation (5.25) will approach $\alpha_i d_i \frac{a_c \gamma_c^n}{\alpha_i - \gamma_c}$ and $a_c \gamma_c^n$ respectively as the number of stages tends to infinity. Thus, $v'_i = \lim_{n\to\infty} v'_{i,n} = \frac{\alpha_i d_i}{\alpha_i - \gamma_c}$ instead of $\frac{\alpha_i d_i}{\alpha_i - \gamma_I}$. Repeating this process allows us to conclude that $a_{I+1} = \cdots = a_c = 0$. Note that a_{I+1} is associated with γ_{I+1} which is the smallest root to $g(x) = 0$ of Equation (5.35) that is greater than γ_I. Similarly, for the upper part of the column section, we must have: $b_1 = \cdots = b_{I-1} = 0$. And b_{I-1} is associated with γ_{I-1} which is the largest root to $g(x) = 0$ of Equation (5.35) that is less than γ_I.

Now, let us consider two functions $F_1(x)$ and $F_2(x)$ defined as follows:

$$F_1(x) = \sum_{i=1}^{c} \frac{\alpha_i l_{i,0}}{\alpha_i - x} \tag{5.37}$$

$$F_2(x) = \sum_{i=1}^{c} \frac{\alpha_i v'_{i,0}}{\alpha_i - x} - V \tag{5.38}$$

We will denote the roots to $F_1(x) = 0$ as $\phi_1, \cdots, \phi_{c-1}$ with $\phi_1 < \cdots < \phi_{c-1}$ and the roots to $F_2(x) = 0$ as $\varphi_1, \cdots, \varphi_{c-1}$ with $\varphi_1 < \cdots < \varphi_{c-1}$. And $\phi_k, \varphi_k \in (\alpha_k, \alpha_{k+1}) \quad \forall k = 1, \cdots, c-1$. Therefore, we have the following result:

Proposition 5.4.2 *The roots to g(x)=0, i.e.* $\gamma_1, \cdots, \gamma_c$, *coincide with the roots of* $F_1(x) = 0$ *and* $F_2(x) = 0$ *as follows:*

$$\gamma_i = \phi_i \quad \forall i \text{ such that } \gamma_i < \gamma_I$$
$$\gamma_i = \varphi_{i-1} \quad \forall i \text{ such that } \gamma_i > \gamma_I$$

Proof First, we prove the second part of the proposition. Substituting Equation (5.25) into Equation (5.34) with the fact that $a_{I+1}, \cdots, a_c = 0$, we have: ${f'}_n(x) = \frac{\sum_{j=1}^{I} a_j \gamma_j^n \left(\sum_{i=1}^{c} \frac{\alpha_i d_i}{(\alpha_i - \gamma_j)(\alpha_i - x)} \right)}{\sum_{j=1}^{I} a_j \gamma_j^n} = 0$. Thus, from Equation (5.22), ${f'}_n(\gamma_{I+1}) = \cdots = {f'}_n(\gamma_c) = 0$ for any $n = 0, 1, \cdots$. Now, $F_2(x)$ can be written as $F_2(x) = \sum_{i=1}^{c} \frac{\alpha_i v'_{i,0}}{\alpha_i - x} - V = x{f'}_0(x)$, it must be true that $\gamma_{I+1}, \cdots, \gamma_c$ are also roots to $F_2(x) = 0$. Since $\gamma_k \in (\alpha_{k-1}, \alpha_k)$ for any k such that $\gamma_k > \gamma_I$ based on Figure 5.5, we have $\gamma_i = \varphi_{i-1}$ $\forall i = I+1, \cdots, c$.

Similarly, for the first part of the proposition, substituting Equation (5.32) into Equation (5.34) followed by using the fact that $b_{I-1}, \cdots, b_1 = 0$ gives $f_n(\gamma_1) = \cdots = f_n(\gamma_{I-1}) = 0$ for any $n = 0, 1, \cdots$. One shall keep in mind that component vapor flow $v_{i,0}$ in $f_0(x)$ is not physically present in the column section as seen from Figure 5.3. Instead, it represents the hypothetical vapor composition that's in equilibrium with $l_{i,0}$ that enters the column section from the top. Since $F_1(x) = \sum_{i=1}^{c} \frac{\alpha_i (v_{i,1} - d_i)}{\alpha_i - x} = \sum_{i=1}^{c} \frac{\alpha_i v_{i,1}}{\alpha_i - x} - g(x) - V = xf_1(x) - g(x)$, $\gamma_{I-1}, \cdots, \gamma_1$ are also roots to $F_1(x) = 0$. In other words, $\gamma_i = \phi_i$ $\forall i = 1, \cdots, I-1$. ■

To understand Proposition 5.4.2, recall that when $n = 0$ for the lower part of column section, all the roots to ${f'}_0(x) = 0$ coincide with the roots φ to $F_2(x) = 0$. As n increases, the roots to ${f'}_n(x) = 0$ that are less than γ_I begin to move monotonically towards the roots ϕ of $F_1(x) = 0$, whereas the roots greater than γ_I will remain where they are. Finally, when $n \to \infty$, the roots of $f'(x) = 0$ that are less than γ_I, which are essentially $\gamma_1, \cdots, \gamma_{I-1}$, will coincide with the roots of ϕ to $F_1(x) = 0$. Similarly, when $n = 0$ for the upper part of section, all roots to $f_0(x) = 0$ coincide with roots of ϕ to $F_1(x) = 0$. As n increases, the roots to $f_n(x) = 0$ which are greater than γ_I

begin to move monotonically towards φ to $F_2(x) = 0$, whereas the roots less than γ_I will stay where they are. Finally, when $n \to \infty$, the roots of $f(x) = 0$ that are greater than γ_I, i.e. $\gamma_{I+1}, \cdots, \gamma_c$, will coincide with the corresponding roots of φ to $F_2(x) = 0$. As a result, once $v'_{i,0}$ and $l_{i,0}$ are known, we would have determined all roots to Equation (5.35) except γ_I. To understand the root behavior of γ_I, suppose again that the net material upward flow satisfies $d_c, \cdots, d_{k+1} \geq 0$ and $d_k, \cdots, d_1 \leq 0$ for some $k \in \{1, \cdots, c-1\}$. In this case, the interval (α_k, α_{k+1}) has two roots to Equation (5.35), one of which is γ_I. Therefore, we have the following proposition:

Proposition 5.4.3 *Suppose $\gamma_I \in (\alpha_k, \alpha_{k+1})$. If γ_I is the larger root to $g(x) = 0$ in (α_k, α_{k+1}), then $\gamma_I > \max\{\phi_k, \varphi_k\}$. If γ_I is the smaller root, then $\gamma_I < \min\{\phi_k, \varphi_k\}$.*

Proof In the first case, the other root to $g(x) = 0$, denoted as γ_{I-1}, is less than γ_I. From Proposition 5.4.2, $\phi_k = \gamma_{I-1} < \gamma_I$. We will show that $\gamma_I > \varphi_k$ as well. The statement is obvious when $\phi_k > \varphi_k$. When $\phi_k < \varphi_k$, it is clear that $\{x'_k(n)\}$ for Equation (5.34) forms a monotonically decreasing sequence due to Proposition 5.4.1 since $\phi_k = \lim_{n\to\infty} x'_k(n) < \varphi_k = x'_k(0)$. Therefore, $f'_1(\varphi_k) > f'_1(x'_k(1)) = 0$. Next, since $F_2(x) = \sum_{j=1}^{c} \frac{\alpha_j l'_{j,1}}{\alpha_j - x} + g(x) = \frac{L}{\sum_{j=1}^{c} v'_{j,1}/\alpha_j} f'_1(x) + g(x)$, $g(\varphi_k) = -\frac{L}{\sum_{j=1}^{c} v'_{j,1}/\alpha_j} f'_1(x) < g(\gamma_I) = 0$. This suggests that $\varphi_k < \gamma_I$.

In the second case, the other root to $g(x) = 0$ within $(\alpha_k, \alpha_{k+1}$, denoted as γ_{I+1}, is greater than γ_I. From Proposition 5.4.2, $\gamma_{I+1} = \varphi_k > \gamma_I$. We will show that $\gamma_I < \phi_k$ as well. The statement is obvious when $\phi_k > \varphi_k$. When $\phi_k < \varphi_k$, then $\{x_k(n)\}$ for $f_n(x) = 0$ forms a monotonically increasing sequence as a result of Proposition 5.4.1. Thus, $f_1(x_k(1)) = 0 > f_1(x_k(0)) = f_1(\phi_k)$. Since $F_1(\phi_k) = 0 = \phi_k f_1(\phi_k) - g(\phi_k)$, $g(\phi_k) < 0$. As a result, $\gamma_I < \phi_k$. ■

The results from Proposition 5.4.3 can be summarized in Figure 5.6. As we prove Proposition 5.4.2 and 5.4.3, we have captured the behavior of all roots to Equation (5.35). Up to this point, we have been focusing on understanding the pinch condition associated with a single general column section, which is the smallest unit of a MFMP column. As the next step, we would like to stack one column section on top of another

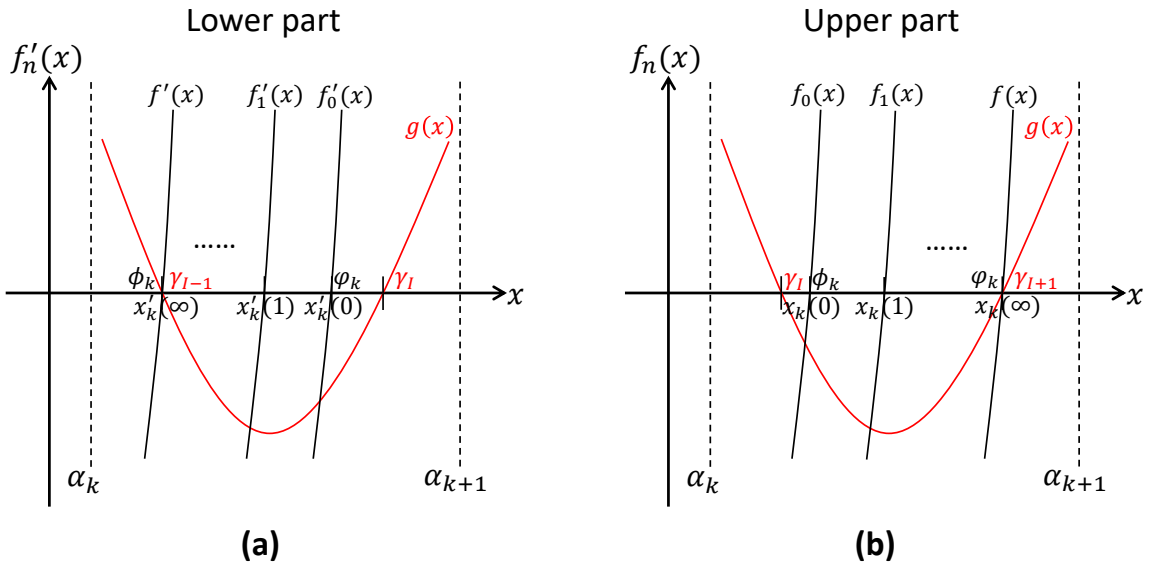

Figure 5.6. Relative location of γ_I with respect to the roots to $F_1(x) = 0$ and $F_2(x) = 0$ in the interval (α_k, α_{k+1}) where $d_k \leq 0$ and $d_{k+1} \geq 0$ for some $k \in \{1, \cdots, c-1\}$. (a) Evolution of $f'_n(x)$ for the lower part of column section when γ_I is the larger root; (b) Evolution of $f_n(x)$ for the upper part of column section when γ_I is the smaller root.

section and connect them via appropriate liquid and vapor balances. Recall that two distinct column sections are separated by a feed or a sidedraw stream, as shown in Figure 5.7. And notice that the labeling of column sections is relative to the specific feed or sidedraw stream that is concerned. For example, the same general column section may be regarded as the bottom section associated with an upper feed stream while at the same time regarded as the top section associated with a lower feed stream.

Now, let us first consider the case of Figure 5.7a, in which the component net material upward flow for the top and bottom section is given by d_{i,TOP_F} and d_{i,BOT_F}, respectively. The lower part of column section TOP_F and the upper part of section

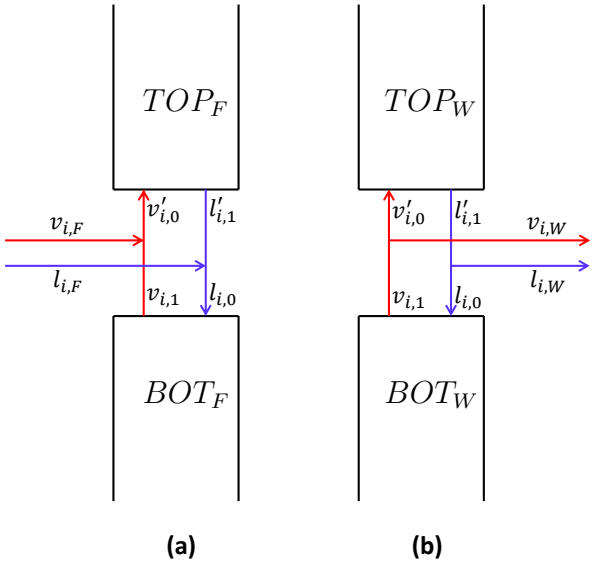

Figure 5.7. Two general column sections stacked and connected by (a) a feed stream; (b) a sidedraw product stream. The column sections are labeled by the location based on their relative locations to the feed or sidedraw stream.

BOT_F are connected by the feed. Similar to Equation (5.37) and (5.38), we define another function $F_3(x)$ for the feed stream as:

$$F_3(x) = \sum_{i=1}^{c} \frac{\alpha_i v_{i,F}}{\alpha_i - x} - V_F \tag{5.39}$$

For sidedraw stream, the term $v_{i,F}$ and V_F in Equation (5.39) are simply replaced by $v_{i,W}$ and V_W, respectively. Note that by convention, the signs of $v_{i,W}$ and V_W are both negative which indicates liquid and/or vapor outflow. Since $F_3(x) = x\sum_{i=1}^{c} \frac{v_{i,F}}{\alpha_i - x} = xf'_0(x)_{TOP_F} - xf_1(x)_{BOT_F}$, we immediately see that the $c-1$ non-trivial solutions to $F_3(x) = 0$, denoted as $\theta_i \in (\alpha_i, \alpha_{i+1})$ for $i = 1, \cdots, c-1$, gives $f'_0(\theta_i)_{TOP_S} - f_1(\theta_i)_{BOT_S} = \sum_{j=1}^{c} \frac{v_{j,F}}{\alpha_j - \theta_i} = 0$ for any $i = 1, \cdots, c-1$.

In fact, we have the following proposition that relates the θ_i roots to $F_3(x) = 0$ with the γ_i roots to $g(x) = 0$ in Equation (5.35) for general column sections TOP_F and BOT_F as the number of stages in both sections approaches infinity. Suppose in

TOP_F, $d_{i,TOP_F} \geq 0\ \forall i \geq k'+1$, whereas in BOT_F, $d_{i,BOT_F} \geq 0\ \forall i \geq k+1$. Due to the presence of feed stream F, we must have $k \geq k'$. As a result, the roots to Equation (5.35) for TOP_F and BOT_F, given respectively by γ_{i,TOP_F} and γ_{i,BOT_F}, are located at:

$$\begin{aligned}
\gamma_{i,TOP_F}, \gamma_{i,BOT_F} &\in (\alpha_{i-1}, \alpha_i) \quad \forall i = k+1, \cdots, c \\
\gamma_{i+1,TOP_F}, \gamma_{i,BOT_F} &\in (\alpha_i, \alpha_{i+1}) \quad \forall i = k', \cdots, k \\
\gamma_{i,TOP_F}, \gamma_{i,BOT_F} &\in (\alpha_i, \alpha_{i+1}) \quad \forall i = 1, \cdots, k'
\end{aligned}$$

Theorem 5.4.1 *The roots to g(x)=0 for sections TOP_F and BOT_F will satisfy $\gamma_{i+1,TOP_F} = \gamma_{i,BOT_F} = \theta_i \in (\alpha_i, \alpha_{i+1})\ \forall i = k', \cdots, k$ if and only if both TOP_F and BOT_F require infinite number of stages.*

Proof We will prove sufficiency here. The necessity of this proposition can be verified by applying Propositions 5.4.1 and 5.4.2. Suppose both TOP_F and BOT_F require infinite number of stages. According to Proposition 5.4.2, it is clear that $F_2(\gamma_{i,TOP_F}) = 0\ \forall i = k'+1, \cdots, c$ for section TOP_F. Meanwhile, $F_1(\gamma_{i,BOT_F}) = 0\ \forall i = 1, \cdots, k$ for section BOT_F. Note that $F_2(x)_{TOP_F} = \sum_{i=1}^{c} \frac{\alpha_i (l'_{i,1} + d_i)}{\alpha_i - x} - V_{TOP_F} = \sum_{i=1}^{c} \frac{\alpha_i l'_{i,1}}{\alpha_i - x} + g(x)_{TOP_F}$. Thus, $\sum_{i=1}^{c} \frac{\alpha_i l'_{i,1}}{\alpha_i - \gamma_{i,TOP_F}} = 0\ \forall i = k'+1, \cdots, c$. Overall, to determine $(l'_{1,1}, \cdots, l'_{c,1})^T$, we have the following system of equations: $\sum_{j=1}^{c} \frac{\alpha_j l'_{j,1}}{\alpha_j - \gamma_{i,TOP_F}} = 0\ \forall i = k'+1, \cdots, c$; $F_1(\gamma_{i,BOT_F}) = \sum_{j=1}^{c} \frac{\alpha_j l'_{j,1}}{\alpha_j - \gamma_{i,BOT_F}} + \sum_{j=1}^{c} \frac{\alpha_j l_{j,F}}{\alpha_j - \gamma_{i,BOT_F}} = 0\ \forall i = 1, \cdots, k$. Together with $\sum_{j=1}^{c} l'_{j,1} = L_{TOP_F}$, we have $k + (c - k') + 1$ linear equations for c unknowns, meaning that a total of $k - k' + 1 \geq 1$ equations are not independent. This will lead to the conclusion that $\gamma_{i+1,TOP_F} = \gamma_{i,BOT_F}\ \forall i = k', \cdots, k$.

Now, we show that these common roots are identical to the roots to $F_3(x) = 0$. It can be shown that $F_3(x) = F_2(x)_{TOP_F} - [F_1(x) + g(x)]_{BOT_F}$. Thus, $F_2(\theta_i)_{TOP_F} = [F_1(\theta_i) + g(\theta_i)]_{BOT_F}$, i.e. $\sum_{j=1}^{c} \frac{\alpha_j l_{j,0}}{\alpha_j - \theta_i} = \sum_{j=1}^{c} \frac{\alpha_j l'_{j,1}}{\alpha_j - \theta_i} = 0$, implying that $\gamma_{i+1,TOP_F} = \gamma_{i,BOT_F} = \theta_i\ \forall i = k', \cdots, k$. ■

It is worth pointing out the wording of Theorem 5.4.1 emphasizes that both sections TOP_F and BOT_F *require* (not "have") infinite stages, which is closely related

to the minimum reflux condition of distillation columns. When a distillation column is operated above minimum reflux, the desired separation can be achieved with finite number of stages, even though one can always feel free to use as many stages in the column as they want. On the other hand, when a distillation column is operated at minimum reflux, the desired separation will no longer be achievable unless certain neighboring column sections have infinite number of stages [159]. These sections thus "control" the separation in the column. Theorem 5.4.1 sheds light on the possible connection between minimum reflux condition of the distillation column and the root behavior of Equation (5.35) for certain adjacent column sections, which We will analyze this connection in detail in the next section.

Theorem 5.4.1 also results in the following relationship:

$$\sum_{j=1}^{c} \frac{\alpha_j l_{j,F}}{\alpha_j - \theta_i} = 0 \qquad \forall i = k', \cdots, k \tag{5.40}$$

which, when combining with Equation (5.39), naturally yields:

$$\begin{aligned} \sum_{j=1}^{c} \frac{\alpha_j f_{j,F}}{\alpha_j - \theta_i} = \sum_{j=1}^{c} \frac{\alpha_j (v_{j,F} + l_{j,F})}{\alpha_j - \theta_i} &= F_3(\theta_i) + V_F + \sum_{j=1}^{c} \frac{\alpha_j l_{j,F}}{\alpha_j - \theta_i} \\ &= V_F = (1 - q_F)F \qquad \forall i = k', \cdots, k \end{aligned} \tag{5.41}$$

where q_F is the thermal quality of the feed stream. Equation (5.41) reduces to the well-known Underwood's feed equation [146] when Theorem 5.4.1 is applied to simple columns. Undoubtedly, the classic Underwood's method [19] used to characterize simple distillation columns is nothing but a special case of Equation (5.41). Although a similar equation as Equation (5.41) has been unintentionally used under various occasions as discussed earlier to determine the minimum reflux conditions for MFMP columns without careful examination, we believe that the derivations and proofs presented above contribute the first rigorous demonstration on the validity of Equation (5.41) for MFMP columns. Also, note that Equation (5.41) does not require $l_{i,F}$ and $v_{i,F}$ to be in thermodynamic equilibrium. Furthermore, it will become clear that

this simple equation, which only involves information about the feed stream that is usually known to practitioners in priori, offers valuable insights about the minimum reflux condition of a MFMP column.

Next, we consider the case of Figure 5.7b in which a product stream is withdrawn between column sections TOP_W and BOT_W as sidedraw. Once again, suppose in TOP_W, $d_{i,TOP_W} \geq 0 \ \forall i \geq k'+1$, whereas in BOT_W, $d_{i,BOT_W} \geq 0 \ \forall i \geq k+1$. Since $d_{i,TOP_W} - d_{i,BOT_W} \leq 0 \ \forall i$, we must have $k' \geq k$. As a result, the roots to Equation (5.35) for TOP_W and BOT_W, given respectively by γ_{i,TOP_W} and γ_{i,BOT_W}, are located at:

$$\begin{aligned}
\gamma_{i,TOP_W}, \gamma_{i,BOT_W} &\in (\alpha_{i-1}, \alpha_i) \quad \forall i = k'+1, \cdots, c \\
\gamma_{i+1,BOT_W}, \gamma_{i,BOT_W} &\in (\alpha_i, \alpha_{i+1}) \quad \forall i = k, \cdots, k' \\
\gamma_{i,TOP_W}, \gamma_{i,BOT_W} &\in (\alpha_i, \alpha_{i+1}) \quad \forall i = 1, \cdots, k
\end{aligned}$$

Similar to Theorem 5.4.1, we have the following proposition for sidedraw product streams:

Theorem 5.4.2 *The roots to g(x)=0 for sections TOP_W and BOT_W will satisfy $\gamma_{i+1,BOT_W} = \gamma_{i,TOP_W} = \theta_i \in (\alpha_i, \alpha_{i+1}) \ \forall i = k, \cdots, k'$ if and only if both TOP_W and BOT_W require infinite number of stages.*

The proof is a straightforward modification of the proof to Theorem 5.4.1. Note that in Theorem 5.4.2, θ_i are the solutions to $F_3(x) = \sum_{j=1}^{c} \frac{\alpha_j v_{j,W}}{\alpha_j - x} - V_W = 0$ for the sidedraw stream. Theorem 5.4.2 also yield the following equality:

$$\sum_{j=1}^{c} \frac{\alpha_j l_{j,W}}{\alpha_j - \theta_i} = 0 \qquad \forall i = k, \cdots, k' \tag{5.42}$$

which eventually leads to a similar expression as Equation (5.41) for the sidedraw stream:

$$\sum_{j=1}^{c} \frac{\alpha_j f_{j,W}}{\alpha_j - \theta_i} = V_W \qquad \forall i = k, \cdots, k' \tag{5.43}$$

keep in mind that since the sidedraw product is withdrawn from the column, quantities such as $f_{j,W}$, $v_{j,W}$, $l_{j,W}$, $V_W < 0$ in Equation (5.43) as depicted in Figure 5.7. To our knowledge, such a defining equation for sidedraw streams has not been previously explored in the literature. For the first time, we have come up with the right mathematical tool to characterize the case in which the minimum reflux condition is associated with infinite column sections connected by a sidedraw stream.

5.5 Minimum Reflux Condition for MFMP Columns

To determine the minimum reflux of a MFMP column, all column sections are stacked back and connected via appropriate liquid and vapor balances. As we have mentioned, when the MFMP column is operated above or at the minimum reflux, the desired separation can be achieve using finite or infinite number of separation stages, respectively. When we say that a given separation is feasible, what we mean is that the liquid or vapor composition profile of the entire distillation column is continuous and desired product specifications (flow rate, composition, and thermal quality) are met for all product streams. However, if the reflux ratio is further reduced, even by an infinitesimal amount, the desired separation can never be achieved, even with an infinite tall column, because the liquid or vapor composition profile in the column no longer forms a continuous path.

Recall that the liquid composition profile in a general column section, which is described using Equation (5.17), can be characterized by constructing the Z-simplex using Equation (5.19), as shown in Figure 5.5 for ternary systems. Such a geometric linkage between the composition profile inside a column section and its corresponding Z-simplex has been found and discussed in the context of simple column by Franklin and Forsyth [157] as well as countercurrent separation cascade by Franklin [158, 160, 161]. However, as far as we know, no attempt has ever made to exploit the similar linkage for MFMP columns. We believe that this is primarily due to the lack of rigorous mathematical model to determine the composition profile inside a MFMP column, which hinders people from observing the existence of such linkage. Now that

we have successfully constructed the model and derived its mathematical and physical properties, we clearly see the connection for the first time.

To understand how to use this connection to derive the minimum reflux condition of a MFMP column, let us first consider the case of a simple column. As we can see from an illustrative example in Figure 5.8, a continuous liquid composition profile which connects the distillate composition (red dot) and bottoms composition (black dot) is required for a feasible separation. This implies that, with the top and bottom product composition respectively being in the interior of the Z-simplex associated with the rectifying and stripping section, the rectifying section Z-simplex must intersect with the stripping section Z-simplex according to Figure 5.5. Of course, for each Z-simplex, only the portion falling inside the standard X-simplex is physically meaningful. As the reflux ratio decreases, both Z-simplices start to shift and eventually barely "touch" each other by sharing a common "edge". This indicates that the minimum reflux is achieved, as shown in Figure 5.8b. If the reflux ratio is further reduced, as illustrated in Figure 5.8c, the two Z-simplices no longer intersect. Hence, there exists no continuous distillation path connecting the top and bottom products when the column is operated at such reflux ratio. As we can conclude from this case, the feasibility of separation at a given reflux ratio is directly related to the connectivity of the Z-simplices associated with adjacent column sections.

Generalizing this finding to multicomponent systems, we establish the minimum reflux condition for MFMP columns as follows. To achieve feasible separation, the intersection of the two Z-simplices for any pair of neighboring column sections in a MFMP column must be non-empty. Recall that the facets of the Z-simplex associated with a general column section is given by $z_i(x_1, \cdots, x_c) = k_i \sum_{j=1}^{c} \frac{\alpha_j x_j}{\alpha_j - \gamma_i} = 0 \ \forall i = 1, \cdots, c$ of Equation (5.19), in which the sign of k_i defined in Equation (5.20) is consistent with the sign of net material upward flow of component i in the column section considered. Let us first consider the case when two adjacent column sections TOP_F and BOT_F are connected by a feed stream F. Then, checking connectivity of

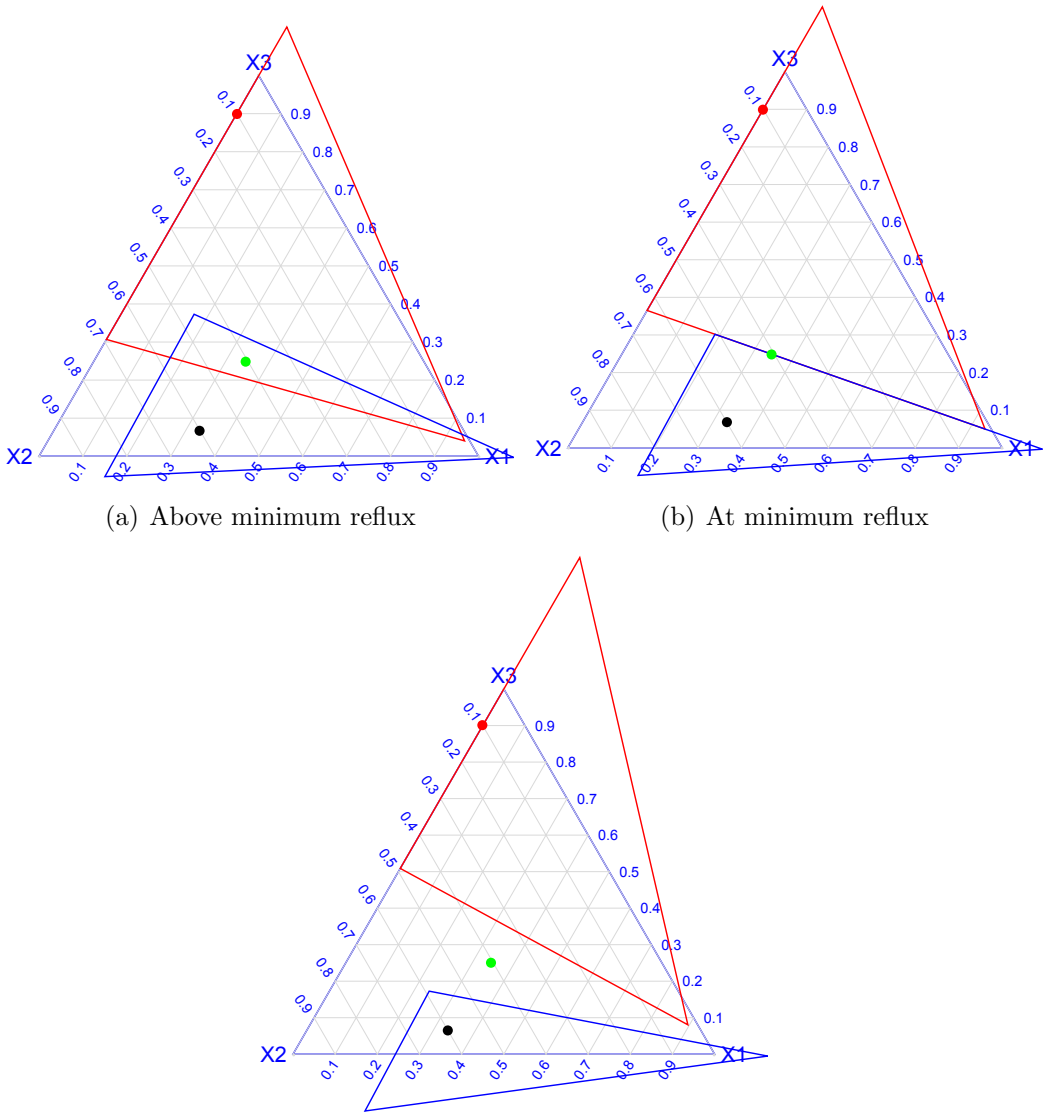

(a) Above minimum reflux

(b) At minimum reflux

(c) Below minimum reflux

Figure 5.8. Illustrative example of the Z-simplex diagram for a simple column operated (a) above minimum reflux; (b) at minimum reflux; (c) below minimum reflux. The red and blue Z-simplex describes the rectifying and stripping section, respectively. And the red, green, and black dot represents the liquid composition of distillate, feed, and bottoms product, respectively. Note that the feed is not saturated liquid, otherwise the feed composition is colinear with top and bottom product compositions.

the Z-simplices associated with these two column sections is equivalent to checking feasibility of $(x_1, \cdots, x_c)$ for the following set of linear inequalities:

$$\sum_{j=1}^{c} \frac{\alpha_j x_j}{\alpha_j - \gamma_{i,TOP_F}} \geq 0 \quad i = k'+1, \cdots, c; \; \sum_{j=1}^{c} \frac{\alpha_j x_j}{\alpha_j - \gamma_{i,TOP_F}} \leq 0 \quad i = 1, \cdots, k'$$
$$\sum_{j=1}^{c} \frac{\alpha_j x_j}{\alpha_j - \gamma_{i,BOT_F}} \geq 0 \quad i = k+1, \cdots, c; \; \sum_{j=1}^{c} \frac{\alpha_j x_j}{\alpha_j - \gamma_{i,BOT_F}} \leq 0 \quad i = 1, \cdots, k$$

in which again we have assumed that $d_{i,TOP_F} \geq 0 \; \forall i = k'+1, \cdots, c$ and $d_{i,BOT_F} \geq 0 \; \forall i = k+1, \cdots, c$. Notice that when constructing the Z-simplices, $(x_1, \cdots, x_c)$ is a set of free variables with $x_i \in \mathbb{R} \; \forall i = 1, \cdots, c$. However, to ensure that the liquid composition on any stage within a general column section is physically meaningful, we ensure that $x_i \geq 0 \; \forall i = 1, \cdots, c$, i.e. we consider the portion of the Z-simplices that fall in the interior of the standard X-simplex. After imposing this condition, it can be easily shown that the linear inequalities above can be directly converted to the following set of inequalities with respect to the roots to Equation (5.35):

$$\begin{aligned} \gamma_{i,TOP_F}, \gamma_{i,BOT_F} &\in (\alpha_{i-1}, \alpha_j) \quad \forall i = k+1, \cdots, c \\ \gamma_{i+1,TOP_F} \geq \gamma_{i,BOT_F} &\in (\alpha_i, \alpha_{i+1}) \quad \forall i = k', \cdots, k \\ \gamma_{i,TOP_F}, \gamma_{i,BOT_F} &\in (\alpha_i, \alpha_{i+1}) \quad \forall i = 1, \cdots, k' \end{aligned} \tag{5.44}$$

One can quickly verify that for a simple column, the constraints in Equation (5.44) automatically reduces to the Underwood root relations for the rectifying as well as the stripping sections [88,146,157]. In the example of Figure 5.8, the heaviest component is removed in the distillate product in the simple column, whereas all three components are present in non-negligible amount in the stripping section. At minimum reflux, one must therefore have $\gamma_{3,TOP_F} = \gamma_{2,BOT_F} = \theta_2 \in (\alpha_2, \alpha_3)$ based on the Underwood's method [146]. This is consistent with Equation (5.44) and the observation of Figure 5.8b in which hyperplanes $z_3 = 0$ of the rectifying section Z-simplex and $z_2 = 0$ of the stripping section Z-simplex coincide with each other at

minimum reflux, i.e. we recover the exact Underwood root relation that we just listed.

Similarly, we now consider the case where two adjacent column sections TOP_W and BOT_W are connected by a sidedraw product stream W. In TOP_W, $d_i \geq 0$ when $i \geq k' + 1$, whereas in BOT_W, $d_i \geq 0$ when $i \geq k + 1$, which means $k \leq k'$. Following the same procedure in deriving Equation (5.44), we obtain the following set of inequalities with respect to the roots to Equation (5.35) for both sections:

$$\begin{aligned} \gamma_{i,TOP_W}, \gamma_{i,BOT_W} &\in (\alpha_{i-1}, \alpha_j) \quad \forall i = k' + 1, \cdots, c \\ \gamma_{i+1,BOT_W} \geq \gamma_{i,TOP_W} &\in (\alpha_i, \alpha_{i+1}) \quad \forall i = k, \cdots, k' \\ \gamma_{i,TOP_W}, \gamma_{i,BOT_W} &\in (\alpha_i, \alpha_{i+1}) \quad \forall i = 1, \cdots, k \end{aligned} \tag{5.45}$$

However, this is not the end of the story for sidedraw streams. One distinct feature about sidedraw stream is that its liquid composition, denoted as $x_W = (l_{1,W}, \cdots, l_{c,W})/L_W$, always lies on the liquid composition profile of the column, i.e. $x_W \in (Z_1 \cdots Z_c)_{TOP_W} \cap (Z_1 \cdots Z_c)_{BOT_W}$. When the sidedraw product is taken as a vapor-only stream, x_W stands for the hypothetical liquid composition which is in equilibrium with the vapor sidedraw. We would like to emphasize that this condition is not required for feed streams whose compositions are unrestricted and are generally different from their feed tray compositions. Thus, for the sidedraw product stream W, in addition to Equation (5.45), we must include:

$$\begin{aligned} &\sum_{j=1}^{c} \frac{\alpha_j x_{j,W}}{\alpha_j - \gamma_{i,TOP_W}} \geq 0 \quad \forall i = k' + 1, \cdots, c; \ \sum_{j=1}^{c} \frac{\alpha_j x_{j,W}}{\alpha_j - \gamma_{i,TOP_W}} \leq 0 \quad \forall i = 1, \cdots, k' \\ &\sum_{j=1}^{c} \frac{\alpha_j x_{j,W}}{\alpha_j - \gamma_{i,BOT_W}} \geq 0 \quad \forall i = k + 1, \cdots, c; \ \sum_{j=1}^{c} \frac{\alpha_j x_{j,W}}{\alpha_j - \gamma_{i,BOT_W}} \leq 0 \quad \forall i = 1, \cdots, k \end{aligned}$$

which, together with Equation (5.42), we get:

$$\begin{aligned}
\gamma_{i,TOP_W} \geq \theta_{i-1,W} \in (\alpha_{i-1}, \alpha_i) \quad & \forall i = k'+1, \cdots, c \\
\gamma_{i,TOP_W} \leq \theta_{i,W} \in (\alpha_i, \alpha_{i+1}) \quad & \forall i = 1, \cdots, k' \\
\gamma_{i,BOT_W} \geq \theta_{i-1,W} \in (\alpha_{i-1}, \alpha_i) \quad & \forall i = k+1, \cdots, c \\
\gamma_{i,BOT_W} \leq \theta_{i,W} \in (\alpha_i, \alpha_{i+1}) \quad & \forall i = 1, \cdots, k
\end{aligned} \tag{5.46}$$

where θ_i are the roots to Equation (5.43).

Suppose the MFMP column of interest has a total of N_{SEC} general column sections (including the topmost and bottommost sections), we need to consider $N_{SEC} - 1$ neighboring column section pairs, each of which is associated with a set of inequality constraints of either Equation (5.44) if it is related with a feed stream or Equations (5.45) and (5.46) if it is related with a sidedraw product. Once completed, these constraints can be easily incorporated into an optimization algorithm that contains mass balance equations and Equation (5.35) written for each general column section. We will discuss the detailed formulation of this global optimization framework as well as a number of case studies in Chapter 6.

5.6 Conclusion

Multi-feed, multi-product distillation columns are very common in many industrial applications. The minimum reflux ratio of a distillation column is related to its energy consumption and capital cost, and thus is a key parameter in distillation design. To solve this lingering problem of determining the minimum reflux condition of a general MFMP column in an accurate and efficient manner, we derive a first-of-its-kind mathematical model for characterizing a general MFMP column based on the assumptions of constant relative volatility, constant molar overflow, and ideal vapor-liquid equilibrium. We then derive the mathematical properties associated with this model which lead to the geometric interpretation of the minimum reflux condition, after which they are translated into a set of algebraic constraints that can be easily

incorporated into an optimization algorithm which guarantees global optimality by using state-of-the-art global solvers such as BARON in GAMS [39]. Compared with existing approaches, our method is simple and efficient to use and does not require guessing of pinch location or controlling split, which may lead to incorrect solutions. As expected, when we consider the extreme case of a simple column, the mathematical model and constraints automatically reduce to the classic Underwood's method [146].

As we have mentioned, this method uses the same underlying assumptions as the Underwood's method. In particular, the constant molar overflow assumption implies that all components have similar latent heat of vaporization. However, it turns out that this assumption can be relaxed to account for variable molar overflow situations. With only slight modification of the Underwood's model, the extended model, which can handle mixtures whose components have very different latent heats, has been independently developed by Nandakumar and Andres [162] and Rev [163] for the case of simple column. The final expression, despite its great similarity compared to the Underwood's equation [146], directly calculates the reboiler heat duty requirement rather than its vapor duty in a simple column, which has significantly more practical relevance. For example, the Underwood distillate equation of Equation (5.41) can be transformed into:

$$\sum_{j=1}^{c} \frac{\alpha_j f_{j,F}}{\alpha_j - \theta_i} = V_F \implies \sum_{j=1}^{c} \frac{\alpha_j \Delta H_j f_{j,F}}{\alpha_j - \tau_i} = Q_F \qquad \forall i = 1, \cdots, c-1$$

where ΔH_j is the latent heat of vaporization of component j and Q_F stands for the difference between the enthalpy of the feed and enthalpy of a saturated liquid feed (which is commonly referred to as the reference point). We find out that the model developed in this chapter can also be extended to determine the total heat duty requirement of a MFMP column by allowing for unequal component latent heats. Using a simple transformation of variables as introduced by [162, 163], all the mathematical treatments used and properties discovered in this chapter still apply to the extended model. We will devote this extension in a separate article in the future.

So far, we have successfully answered the first question proposed at the beginning of the chapter about constructing an accurate model for MFMP columns. In Chapter 6, we will discuss how to incorporate this mathematical model into the global optimization framework. We will then present a number of illustrative case studies which have both intellectual and practical significance. Thorough these case studies, we will provide readers with answers to all the questions raised at the beginning of the chapter.

6. AN ACCURATE MINIMUM REFLUX CALCULATION METHOD FOR MULTI-FEED, MULTI-PRODUCT DISTILLATION COLUMNS DISTILLING IDEAL MULTICOMPONENT MIXTURES: 2. OPTIMIZATION MODEL AND CASE STUDIES

Continuing from the mathematical model developed in Chapter 5, we present the first-of-its-kind global optimization formulation whose objective is to minimize the reboiler vapor duty requirement for a general multi-feed, multi-product (MFMP) distillation column separating ideal multicomponent mixtures. We verify the accuracy of this algorithm through a few case studies using rigorous Aspen Plus simulations. The results obtained from these case studies also provide valuable insights on optimal design of multicomponent distillation systems as well as the minimum reflux behavior for MFMP columns. Many of these insight turn out to be counterintuitive and are against the heuristics that the chemical engineering community has taken for granted. We find out, for example, that placing a colder feed stream above a hotter feed stream may in fact lead to higher energy requirement; decomposing a general MFMP column into individual simple columns to estimate the minimum reflux ratio for the MFMP column may lead to incorrect results, etc. Overall, the shortcut based algorithmic method presented here can be very useful to industrial practitioners in designing attractive, energy efficient, and cost effective multicomponent distillation systems.

6.1 Introduction

The determination of minimum reflux condition for distillation columns with multiple feed and/or one or more sidedraw streams is of great theoretical and practical importance to the distillation community and has remained unsolved for the past 80 years. In Chapter 5, we develop the first shortcut mathematical model to character-

ize a general MFMP column merely based on the assumptions of ideal vapor-liquid equilibrium, constant relative volatility as well as constant molar overflow for every component. No additional restriction concerning the structure of the MFMP column or the type of separation it performs is needed. The physical and mathematical properties associated with the model have also been explored, from which we have derived the necessary and sufficient conditions for any general MFMP column operated at minimum reflux.

In this chapter, we introduce a solution approach which incorporates the model developed in Chapter 5 to determine the minimum reboiler vapor duty requirement for a general MFMP column separating a multicomponent mixture. This algorithmic approach can either be used by itself to find the minimum reflux condition for a standalone MFMP column, or can be embedded into a global optimization framework such as the one recently developed by Nallasivam et al. [34] to simultaneously optimize an entire multicomponent distillation configuration. Later, we present a few illustrative case studies to illustrate the accuracy and effectiveness of our algorithm. Apart of this, these case studies also serve the purpose of answering the conceptual questions raised in Chapter 5 regarding the validity of some of the well-accepted heuristics and rules researchers and industrial practitioners use when designing and operating a MFMP column. As we will see, the answers to these questions are not as obvious as we would expect. The shortcut approach presented in this chapter thus gives practitioners a different perspective on these heuristics and offers them a new, more accurate way to solve for the minimum reflux condition for MFMP columns.

6.2 Formulation of the Global Optimization Algorithm

In this section, we will describe the formulation of the global optimization algorithm. In particular, we will discuss the formulation of constraints to ensure feasibility of separation. To begin, recall that any optimization problem is described by: the decision variables, the objective function, and the constraints. Following the convention used in Chapter 5, we number the components either as 1, 2, $\cdots$, c in the decreasing

order of their relative volatilities ($\alpha_c > \cdots > \alpha_1$), or as capital letters A, B, C, and so on to represent pure components with their volatilities decreasing in alphabetical order. The notations in this chapter, unless explicitly mentioned, follow the same definitions as in Chapter 5.

For a c-component system, the domain of roots γ_j to Equation (5.13) can be split into $c+1$ distinct intervals using the relative volatilities of the c components. These intervals are $(0, \alpha_1)$, (α_1, α_2), $\cdots$, (α_{c-1}, α_c), and finally $(\alpha_c, \alpha_c + \delta)$ where δ is a sufficiently large positive number. Among these $c+1$ distinct intervals, there must exists at least one distinct root to Equation (5.13) in each of the $c-1$ intervals, namely (α_1, α_2), $\cdots$, (α_{c-1}, α_c). And there is only one more root left. We denote it as γ^* whose location depends on where the sign change in d_i occurs. To account for this, we define a set of binary variables $\mu_i \in \{0, 1\}\ \forall i = 0, \cdots, c$ to dictate if γ^* lies in the interval (α_i, α_{i+1}). As a special case, $\mu_0 = 1$ means that $\gamma^* \in (0, 1)$, which occurs only when all $d_i \leq 0$. On the other hand, $\mu_c = 1$ means that $\gamma^* \in (\alpha_c, \alpha_c + \delta)$, which occurs only when all $d_i \geq 0$. As a result, the binary variable set $\{\mu_0, \cdots, \mu_c\}$ and the location of γ^* is related by the following constraint:

$$\sum_{i=0}^{c} \alpha_i \mu_i \leq \gamma^* \leq \sum_{i=0}^{c} \alpha_{i+1} \mu_i \tag{6.1}$$

where again $\alpha_0 = 0$ and $\alpha_{c+1} = \alpha_c + \delta > \alpha_c$. And obviously, $\sum_{i=0}^{c} \mu_i = 1$.

When two adjacent general column sections labeled as TOP_{F_k} (upper section) and BOT_{F_k} (lower section) are connected by a feed stream F_k, $d_{i,TOP_{F_k}} \geq d_{i,BOT_{F_k}}\ \forall i = 1, \cdots, c$. Similarly, when two adjacent column sections labeled as TOP_{W_k} and BOT_{W_k} are connected by a sidedraw product stream W_k, then $d_{i,TOP_{W_k}} \leq d_{i,BOT_{W_k}}\ \forall i = 1, \cdots, c$. This leads to:

$$\begin{aligned} \text{Feed stream } F_k: \sum_{i=0}^{c} i\mu_{i,BOT_{F_k}} &\geq \sum_{i=0}^{c} i\mu_{i,TOP_{F_k}} \quad \forall k = 1, \cdots, N_F \\ \text{Sidedraw stream } W_k: \sum_{i=0}^{c} i\mu_{i,BOT_W} &\leq \sum_{i=0}^{c} i\mu_{i,TOP_W} \quad \forall k = 1, \cdots, N_W \end{aligned} \tag{6.2}$$

where N_F and N_W stands for the total number of feed streams and sidedraw product streams in the MFMP column, respectively. Note that the quantity $\sum_{i=0}^{c} i\mu_i$ essentially gives the index of the lightest component with non-positive net upward flow. If $d_1, \cdots, d_c \geq 0$, then $\sum_{i=0}^{c} i\mu_i = 0$. If $d_1, \cdots, d_c \leq 0$, then $\sum_{i=0}^{c} i\mu_i = c$. Next, we define a set of binary variables $K_i \in \{0, 1\}\ \forall i = -1, 0, \cdots, c$ as:

$$\begin{aligned} &K_{-1} = 0; \\ &K_i = K_{i-1} + \mu_i \quad \forall i = 0, ..., c \end{aligned} \tag{6.3}$$

As we can see, $K_i = 0$ if and only if $\mu_0, ..., \mu_{i-1} = 0$. In the case of feed stream F_k, we see that $K_{i,TOP_{F_k}} - K_{i-1,BOT_{F_k}}$ can take either 0 or 1, since $K_{i,TOP_{F_k}} \geq K_{i-1,BOT_{F_k}}$. It turns out that the set $\{i | K_{i,TOP_{F_k}} - K_{i-1,BOT_{F_k}} = 1,\ i = 0, \cdots, c\}$ is equivalent to $\{\sum_{i=0}^{c} i\mu_{i,TOP_{F_k}}, \sum_{i=0}^{c} i\mu_{i,TOP_{F_k}} + 1, \cdots, \sum_{i=0}^{c} i\mu_{i,BOT_{F_k}}\}$. Similarly, for a sidedraw product stream W_k, the set $\{i | K_{i,BOT_{W_k}} - K_{i-1,TOP_{W_k}} = 1,\ i = 0, \cdots, c\}$ is equivalent to $\{\sum_{i=0}^{c} i\mu_{i,BOT_{W_k}}, \sum_{i=0}^{c} i\mu_{i,BOT_{W_k}} + 1, \cdots, \sum_{i=0}^{c} i\mu_{i,TOP_{W_k}}\}$. Using this relation, we can easily rewrite the necessary and sufficient conditions for a feasible separation discussed in Chapter 5 in terms of the connectivity of adjacent Z-simplicies as follows:

$$\begin{aligned} \text{Feed } F_k &: (K_{i,TOP_{F_k}} - K_{i-1,BOT_{F_k}})(\gamma_{i+1,TOP_{F_k}} - \gamma_{i,BOT_{F_k}}) \geq 0 \\ \text{Sidedraw } W_k &: (K_{i,BOT_{W_k}} - K_{i-1,TOP_{W_k}})(\gamma_{i+1,BOT_{W_k}} - \gamma_{i,TOP_{W_k}}) \geq 0 \end{aligned} \tag{6.4}$$

where $i = 1, \cdots, c-1$. Thus, we have completely transformed the connectivity constraints of adjacent Z-simplicies into a set of mixed-integer constraints.

Recall that for each sidedraw product stream W_k when $k = 1, \cdots, N_W$, in addition to Equation (6.4), we also need ensure that its liquid product composition (or the hypothetical liquid composition that is in equilibrium with the vapor product) always

lies on the liquid composition profile. Correspondingly, we have an additional set of mixed-integer constraints based on Chapter 5:

$$\begin{aligned} K_{i,TOP_{W_k}}(\gamma_{i+1,TOP_{W_k}} - \theta_{i,W_k}) &\geq 0 \\ K_{i,BOT_{W_k}}(\gamma_{i+1,BOT_{W_k}} - \theta_{i,W_k}) &\geq 0 \\ (1 - K_{i-1,TOP_{W_k}})(\gamma_{i,TOP_{W_k}} - \theta_{i,W_k}) &\leq 0 \\ (1 - K_{i-1,BOT_{W_k}})(\gamma_{i,BOT_{W_k}} - \theta_{i,W_k}) &\leq 0 \end{aligned} \tag{6.5}$$

where $i = 1, \cdots, c-1$ and $k = 1, \cdots, N_W$. The root $\theta_{i,W_k} \in (\alpha_i, \alpha_{i+1})$ is the solution to the following defining equation for sidedraw stream W_K as discussed in Chapter 5:

$$\sum_{j=1}^{c} \frac{\alpha_j f_{j,W_k}}{\alpha_j - \theta_{i,W_k}} = V_{W_k} \qquad \forall i = 1, \cdots, c-1 \tag{6.6}$$

In the limiting case when $d_1, \cdots, d_c \geq 0$ in a general column section, $K_1, \cdots, K_c = 1$. Equation (6.5) essentially yields $\gamma_{i+1} \geq \theta_{i,W_k}$ for all $i = 1, \cdots, c-1$. On the other hand, when all $d_1, \cdots, d_c \leq 0$ in a column section, $1-K_0, \cdots, 1-K_{c-1} = 1$, suggesting that $\gamma_i \leq \theta_{i,W_k}$ for all $i = 1, \cdots, c-1$.

To illustrate how these constraints can be implemented, we consider a MFMP column of Figure 6.1a for quaternary mixture separation. This MFMP column contains four column sections, an upper feed stream F_1 containing stream ABC, a lower feed stream F_2 that contains BCD, as well as a sidedraw product stream W_1 that contains BC. It undergoes two different separations, $ABC \rightarrow AB/BC$ and $BCD \rightarrow BC/CD$. The most volatile component A must be completely recovered in the distillate, whereas the least volatile component D must be completely recovered in the bottoms product. The distribution of intermediate components B and C, on the other hand, are subject to be determined by the optimization program. In column section 2, the net material upward flow for component B could be either positive or negative. Similar behavior applies to the net material upward flow for component C in column section 3. Therefore, the γ^* root for column section 2, which corresponds

to $\gamma_{3,2}$, lies in the interval (α_2, α_4). And the γ^* root for column section 3, which corresponds to $\gamma_{2,3}$, belongs to the interval (α_1, α_3). This requires us to introduce two binary variables $\mu_{2,2}$, $\mu_{3,2}$ to determine the location of $\gamma_{3,2}$ as well as two other binary variables $\mu_{1,3}$, $\mu_{2,3}$ for $\gamma_{2,3}$. In Appendix A, we provide all the equations and constraints needed to determine the minimum reboiler vapor duty requirement for this MFMP column. The resulting formulation, which is a mixed-integer nonlinear program (MINLP), can be solved to global optimality using standard global solvers such as BARON [39]. As we can clearly see from Appendix A, the simplicity of the formulation shows that our model can be easily incorporated in a global optimization framework.

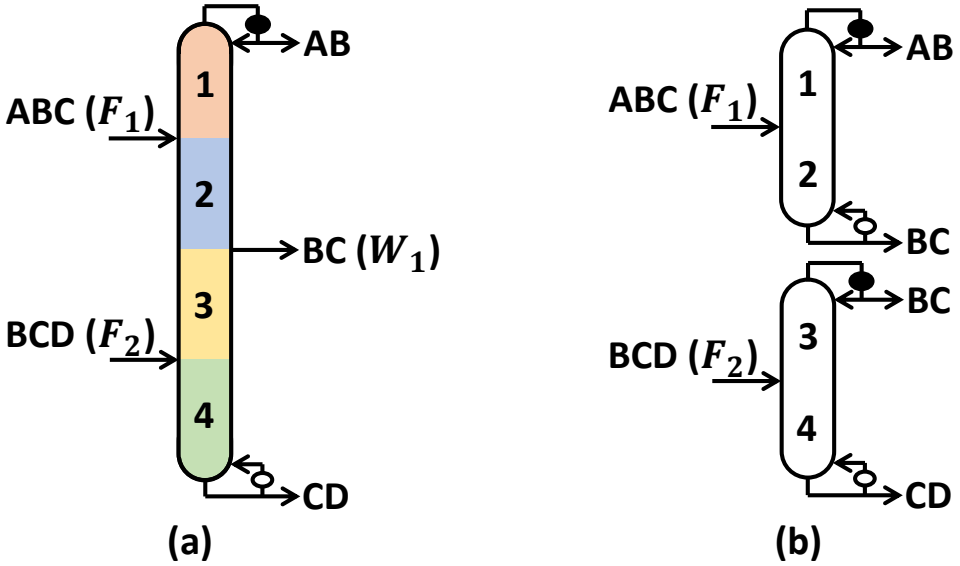

Figure 6.1. (a) A MFMP column for quaternary separation; (b) the decomposed version of (a).

However, in many practical situations, the product specifications of the MFMP column have already been fully specified. Under these circumstances, the search for minimum reflux ratio of the MFMP column reduces to a much simpler problem. Since the net material upward flow for all components in all column sections can be directly calculated by mass balances, Equations (6.4) and (6.5) can be easily modified so that the binary variables are no longer needed. As a result, formulating an optimization

problem and solving it using global solvers is not required anymore. Instead, we can use a simple verification algorithm as shown in Algorithm 1 to achieve the same goal. In Chapter 5, we show that the MFMP column operated at minimum reflux always has a controlling split, which can be associated with either a feed stream or a sidedraw product stream. We assume that each and every feed or sidedraw stream is a candidate that controls the separation at minimum reflux. Correspondingly, the vapor flows in each column section $i = 1, \cdots, N_F + N_W + 1$ and thus its respective $\gamma_{j,i}$ where $j = 1, \cdots, c$ can be determined using Equation (5.13). Next, by simply performing a satisfiability check for all $\gamma_{j,i}$ for all $i = 1, \cdots, N_F + N_W + 1$ and $j = 1, \cdots, c$ on the simplified root relations of Equations (6.4) and (6.5), we immediately know if this separation, based on the assumption that this feed or sidedraw stream of interest is associated with the controlling split, is feasible. If the separation is feasible, then the topmost column section vapor flow V_1 is stored, and the entire process is repeated by assuming that a different feed or sidedraw stream controls. Eventually, the actual minimum top column section vapor flow (i.e. the minimum reflux ratio) is given by the smallest value corresponding to a feasible separation obtained from this process.

So far, we have introduced two approaches, depending on the problem specifications, to implement the mathematical model described in Chapter 5 to determine the minimum vapor duty requirement of a MFMP column. In the next section, we consider a few examples to illustrate the accuracy and effectiveness of these methods, while at the same time provide industrial practitioners an accurate and clear understanding of the minimum reflux behavior of a MFMP column for the first time.

6.3 Case Studies

Example 1: Two-Feed Distillation Column

In the first example, we examine a two-feed distillation column shown in Figure 6.2a undergoing ternary mixture separations. Two-feed columns are commonly used in extractive distillation for separations that are hard to perform using a simple

input : c, N_F, N_W, V_{F_i}, V_{W_k}, $f_{j,i}$, $w_{j,k}$, $d_{j,1}$ $\forall i = 1, \cdots, N_F$; $k = 1, \cdots, N_W$; $j = 1, \cdots, c$

output: $R_{\min}$

begin

Calculate the net material upflow for component j in each section i : $d_{j,i}$ $\forall j = 1, \cdots, c$; $i = 1, \cdots, N_F + N_W + 1$;

Determine $K_{j,i}$ in Equations (6.4) and (6.5) for all $j = -1, 0, \cdots, c$ and $i = 1, \cdots, N_F + N_W + 1$;

Solve Equation (6.6) for $\theta_{s,W_i} \in (\alpha_s, \alpha_{s+1})$ $\forall s = 1, \cdots, c-1$, $i = 1, \cdots, N_W$;

for $i \leftarrow 1$ **to** N_W **do**

  for $s \leftarrow 1$ **to** $c - 1$ **do**

    Calculate the top column section vapor flow $V_{TOP,s}$ associated with θ_{s,W_i} from vapor balances;

    for $j \leftarrow 1$ **to** $N_F + N_W + 1$ **do**

      Calculate V_j for $j = 1, \cdots, N_F + N_W + 1$;

      Solve Equation (5.13) for all $\gamma_{k,j}$ where $k = 1, \cdots, c$;

    end

    if *the simplified constraints of Equations* (6.4) *and* (6.5) *are satisfied for all adjacent column section pairs* **then** store $V_{TOP,s}$;

    else $V_{TOP,s}$ = a large value; Continue;

  end

end

for $i \leftarrow 1$ **to** N_F **do**

  Solve $\sum_{j=1}^{c} \frac{\alpha_j f_{j,i}}{\alpha_j - \theta_{s,F_i}} = V_{F_i}$ for θ_{s,F_i} $\forall s = 1, \cdots, c-1$;

  for $s \leftarrow 1$ **to** $c - 1$ **do**

    Calculate $V_{TOP,s}$ associated with θ_{s,F_i};

    for $j \leftarrow 1$ **to** $N_F + N_W + 1$ **do**

      Calculate V_j for $j = 1, \cdots, N_F + N_W + 1$;

      Solve Equation (5.13) for all $\gamma_{k,j}$ where $k = 1, \cdots, c$;

    end

    if *the simplified constraints of Equations* (6.4) *and* (6.5) *are satisfied for all adjacent column section pairs* **then** store $V_{TOP,s}$;

    else $V_{TOP,s}$ = a large value; Continue;

  end

end

$R_{\min} = \min_i\{V_{TOP,i}\} / \sum_{j=1}^{c} d_{j,1} - 1$

end

Algorithm 1: Finding the minimum reflux ratio $R_{\min}$ of a MFMP column

column. Another powerful feature recently discovered by Madenoor Ramapriya [164] for two-feed columns is the opportunity for large energy savings when the two feed streams having the same components but different compositions are kept separate and introduced at two different locations instead of pre-mixing them to form a single feed before introducing it to the next column. For illustration, we consider a ternary hydrocarbon mixture involving hexane (component 3), heptane (component 2), and octane (component 1).

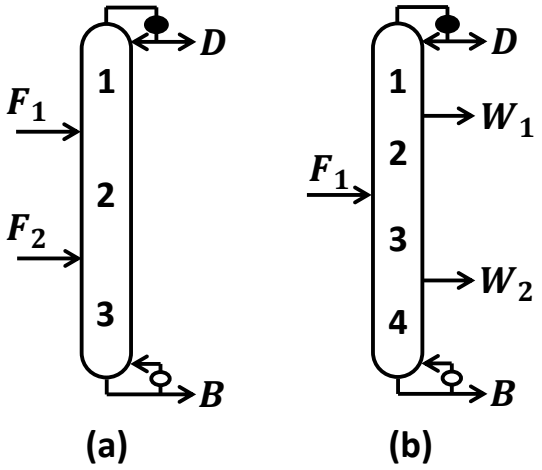

Figure 6.2. (a) A two-feed distillation column with no sidedraw product; (b) a one-feed, two-(side)product distillation column. Both columns have four general column sections.

First, the users need to provide the relative volatility information for all components. We use Aspen Plus to fetch the relative volatility information at 1 atm pressure. To ensure constant relative volatility and constant molar overflow assumptions for establishing a common basis for comparison, we appropriately modify the property parameters in Aspen Plus listed under PLXANT and DHVLDP. The IDEAL thermodynamic package is used. The relative volatilities of these components are determined to be $(\alpha_3, \alpha_2, \alpha_1) = (5.291, 2.300, 1)$. In the first case, the upper feed F_1 in the MFMP column is a saturated liquid stream containing 30 mol/s of hexane, 60 mol/s of heptane, and 10 mol/s of octane. The lower feed F_2 is also a saturated liquid stream with 20 mol/s of hexane, 10 mol/s of heptane, and 70 mol/s of octane.

The distillate product has a flow rate of 52.63 mol/s and its composition is given by $(x_{3,D}, x_{2,D}, x_{1,D}) = (0.95, 0.05, \text{trace})$. Octane is completely removed in the top product. The bottoms product flow rate and composition can be directly determine to be 147.37 mol/s and $(x_{3,B}, x_{2,B}, x_{1,B}) = (0.001, 0.457, 0.542)$, respectively.

Using Algorithm 1, we identify that $R_{\min} = 2.116$ which occurs when the controlling split is associated with F_1. We construct the corresponding Z-simplex diagram shown in Figure 6.3 to visualize the minimum reflux condition. As we can see, the Z-simplices associated with column sections 1 and 2 of Figure 6.2a share a common edge, i.e. $\gamma_{3,TOP_{F_1}} = \gamma_{2,BOT_{F_1}} = \theta_{2,F_1} \in (\alpha_2, \alpha_3)$ at minimum reflux. If the reflux ratio is further reduced, these two Z-simplices will no longer intersect, indicating that the minimum reflux has been achieved and the controlling split is given by F_1.

We verify the minimum reflux condition for this MFMP column using rigorous tray-by-tray calculations on Aspen Plus. Each column section is given 50 stages, much greater than needed for the separation, to ensure that the true minimum reflux is achieved. Aspen Plus gives its minimum reflux ratio prediction of 2.145, which is only 1.4% different compared to our shortcut calculation result. The liquid composition profile determined by Aspen Plus at minimum reflux is plotted along with the Z-simplex diagram in Figure 6.3 and is explicitly shown in Figure 6.4. From these figures, we can quickly identify the pinch locations in each column section. Since $x_{1,D} = 0$, it can be shown that the distillate composition $(x_{3,D}, x_{2,D}, x_{1,D})$ lies on the hyperplane $z_1 = 0$ of section 1 Z-simplex. This hyperplane also coincides with $x_1 = 0$ of the X-simplex [157]. Based on the analysis in Chapter 5, it is clear that tray-by-tray downward calculations will finally bring the liquid composition to the saddle pinch $(x_3, x_2, x_1)_{\text{pinch}} = (0.325, 0.675, 0)$ in the middle of column section 1. The pinch composition can also be verified in Figure 6.4. Below this pinch, the liquid composition profile continues following along the hyperplane $z_3 = 0$ of section 1 Z-simplex until it reaches the feed stage of F_1 at which its liquid composition actually corresponds to the unstable node (in terms of downward calculations) of section 2 Z-simplex. This implies that the pinch in column section 2 is located at the top of

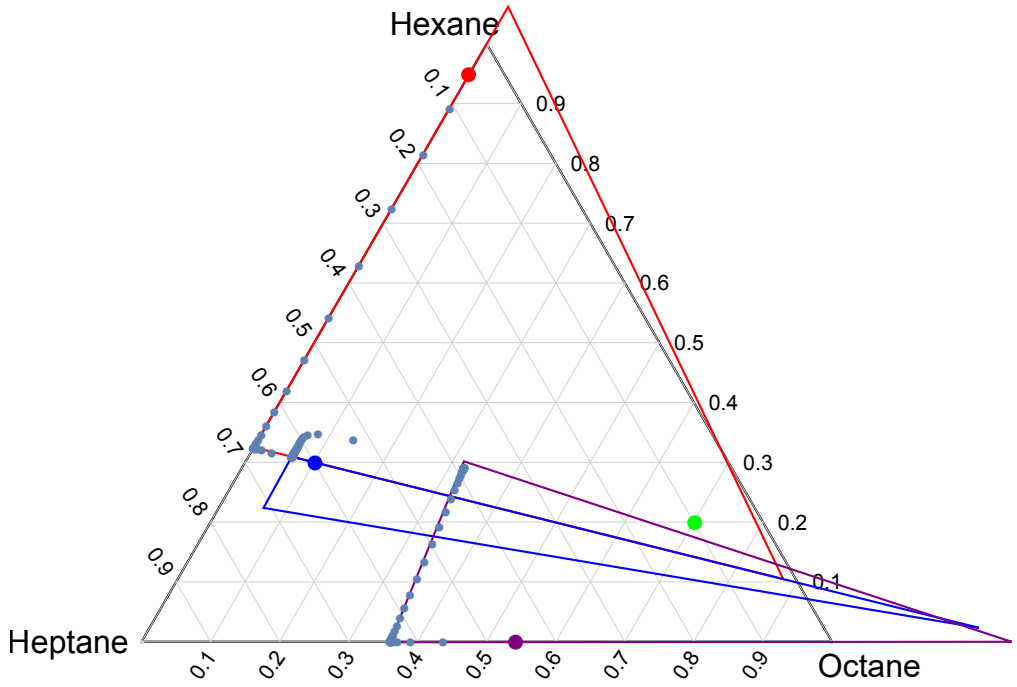

Figure 6.3. The Z-simplex diagram at the minimum reflux of $R_{\min} = 2.116$ calculated using Algorithm 1 and the tray-by-tray liquid composition profile at the minimum reflux of $R_{\min} = 2.145$ determined by Aspen Plus. The red, blue, green, and purple dot respectively corresponds to the liquid composition of distillate, upper feed stream, lower feed stream, and the bottoms product. The red, blue, and purple Z-simplex is associated with column sections 1, 2, and 3 of Figure 6.2a, respectively.

the section. Beyond this unstable node pinch, the liquid composition profile diverges and reaches another pinch associated with column section 3 Z-simplex. This pinch is located at the lower feed stage, from which the liquid composition profile follows the trajectory inside section 3 Z-simplex and heads towards the stable node until it reaches the bottoms product composition $(x_{3,B}, x_{2,B}, x_{1,B})$. Keep in mind that even though $x_{3,B}$ is small, it is more than trace amount. Thus, the liquid composition profile inside section 3 may appear to be approaching close to the saddle point pinch but in fact will never actually reach the saddle pinch, as we can see from Figure 6.3 and 6.4.

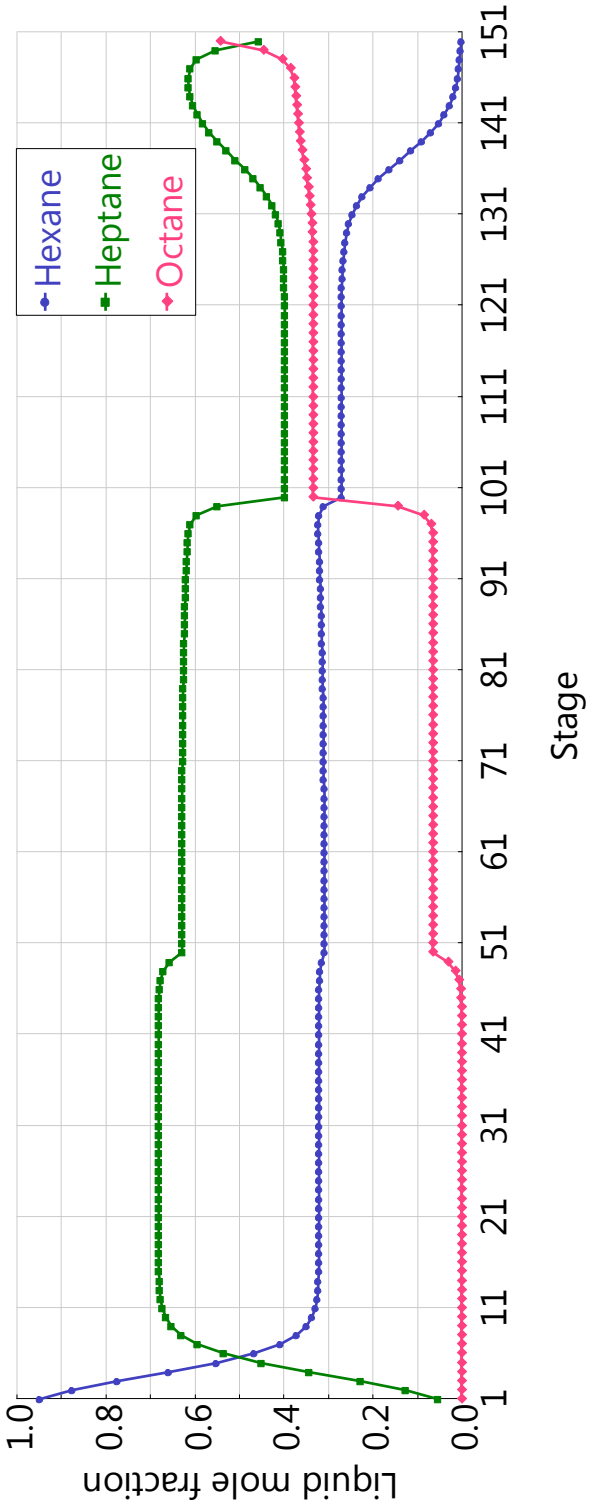

Figure 6.4. The liquid composition profile retrieved from Aspen Plus at its predicted minimum reflux ratio of $R_{\min} = 2.145$.

Before moving on to the next case, we would like to use this example to examine the validity of the assumption [152] that a MFMP column can be decomposed into a series of simple columns, and that the actual minimum reflux ratio of the original MFMP column is given by the largest minimum reflux ratio determined for all decomposed simple columns using the classic Underwood's method [146]. In this case, the two-feed column of Figure 6.2a is decomposed into two simple columns. One contains F_1 as the feed stream and column sections 1 and 2, while the other contains F_2 as the feed stream and sections 2 and 3 as the rectifying and stripping section, respectively. It turns out that, under the same product specifications, the largest minimum reflux ratio for the two simple columns is 2.590 associated with F_2 being the "controlling split". Clearly, such a decomposition method overestimates the true minimum reflux ratio in this case. Apparently, the minimum reflux condition for a general MFMP column is not as simple as what we may think. And using these simplifying assumptions without verification can lead to incorrect results.

From Figure 6.3, we observe that the feed stream liquid composition does not necessarily have to lie on the liquid composition profile or within the Z-simplices associated with adjacent column sections. This is because the feed stream liquid composition is generally different from the feed stage liquid composition, which must always lie on the liquid composition profile. However, we need to emphasize that when the feed or sidedraw stream is associated with the controlling split at minimum reflux, its liquid composition must lie on the common facets of the Z-simplices associated with adjacent column sections. This is a direct consequence of Proposition 4 and 5 demonstrated in Chapter 5. In this particular case, since F_1 is associated with the controlling split, the blue dot in Figure 6.3, which is the liquid composition of F_1, lies on $z_3 = 0$ of section 1 Z-simplex as well as $z_2 = 0$ of section 2 Z-simplex.

Next, we consider a different scenario of the same MFMP column of Figure 6.2a by simply switching location of the two feed stream locations as in the first case. In other words, the upper feed F_1 now contains 20 mol/s of hexane, 10 mol/s of heptane, and 70 mol/s of octane, while the lower feed F_2 now has 30 mol/s of hexane,

60 mol/s of heptane, and 10 mol/s of octane. Using Algorithm 1, we calculate that the minimum reflux ratio for this arrangement is $R_{\min} = 1.634$ which corresponds to the circumstance when the lower split controls, as we can see from the Z-simplex diagram of Figure 6.5.

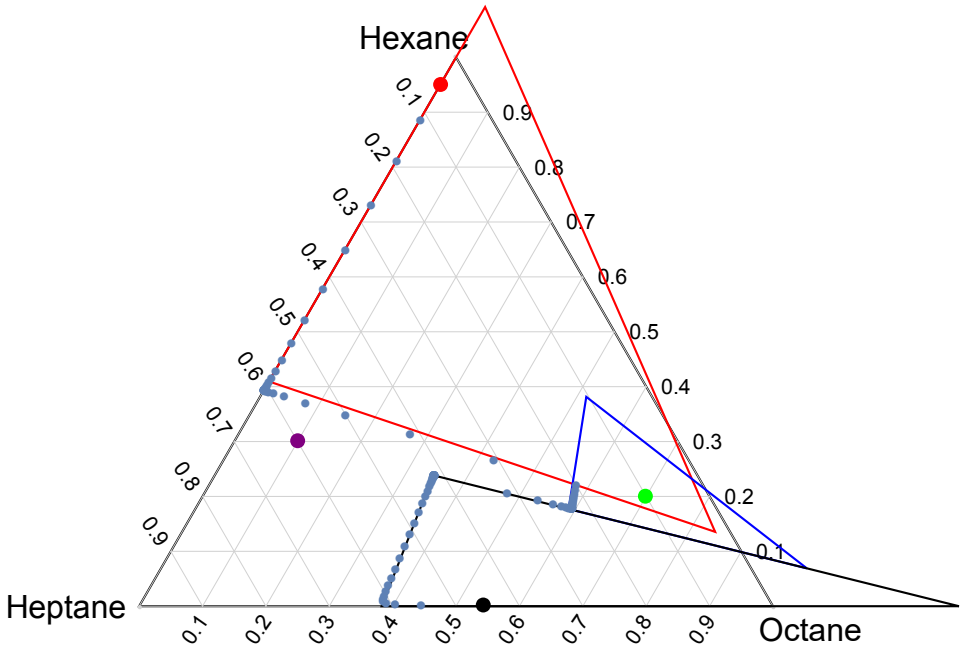

Figure 6.5. The Z-simplex diagram at the minimum reflux of $R_{\min} = 1.634$ calculated using Algorithm 1 and the tray-by-tray liquid composition profile at the minimum reflux of $R_{\min} = 1.738$ determined by Aspen Plus. Again, the red, blue, green, and purple dot respectively corresponds to the liquid composition of distillate, upper feed stream, lower feed stream, and the bottoms product. The red, blue, and purple Z-simplex is associated with column sections 1, 2, and 3 of Figure 6.2a, respectively.

Rigorous Aspen Plus simulation shows that the minimum reflux ratio is 1.738. Thus, the result obtained using Algorithm 1 gives a 6.0% relative difference compared to Aspen Plus prediction. To our surprise, if we simply use the decomposition method suggested by Nikolaides and Malone [152], we would end up with a "minimum reflux ratio" that is as high as 19.336, which is almost 12 times larger than the true minimum

reflux! Obviously, designing or operating a distillation column based on this mistaken assumption may lead to huge waste in capital and operating costs.

An equally striking observation we get from these two cases is that the optimal feed arrangement in a MFMP column is not as intuitive as one would normally think. One would naturally expect that the higher temperature feed should be introduced at a lower location of the column than the lower temperature feed to lower the energy consumption. The first case follows this heuristic, in which the the feed stream enriched with octane is introduced right above stage 100 and has a temperature that is 15 °C hotter than the upper feed stream introduced above stage 50. Surprisingly, despite having the same product specifications, the minimum reflux ratio in this case ($R_{\min} = 2.116$) is much higher than the second case ($R_{\min} = 1.634$) in which the feed stream locations are reversed! This finding is consistent with the observation from Levy and Doherty [135]. Thus, we have given a counterexample which contradicts the rule of introducing a higher boiling feed to a lower location of the column. Industrial practitioners should not simply rely on this heuristic and believe that it would always guarantee minimum energy requirement. Our shortcut method thus offers an instant and reliable screening tool to identify the best feed arrangement for a multi-feed distillation column.

Example 2: A One-Feed, Two-(Side)Product Column

In this example, we consider a distillation column with one feed stream and two sidedraw product streams, as shown in Figure 6.2b. When both sidedraw products are withdrawn as saturated liquids, Sugie and Lu [150] and many others such as Glinos and Malone [151] made the assumption that the controlling split can only be associated with the feed stream. This assumption comes directly from the observation of McCabe-Thiele diagram for binary separations. To verify if it is still true for multicomponent systems, we present this example in which the saturated liquid feed stream F_1 contains 30 mol/s of hexane, 40 mol/s of heptane, and 30 mol/s of octane. The distillate has 24 mol/s of hexane, 6 mol/s of heptane and no octane, whereas the

bottoms product is 20 mol/s of pure octane. The upper sidedraw W_1, which is located above the feed stream, is a saturated liquid stream containing 6 mol/s of hexane and 24 mol/s of heptane. The lower saturated liquid sidedraw W_2 is located below the feed stream and contains 10 mol/s of heptane and 10 mol/s of octane.

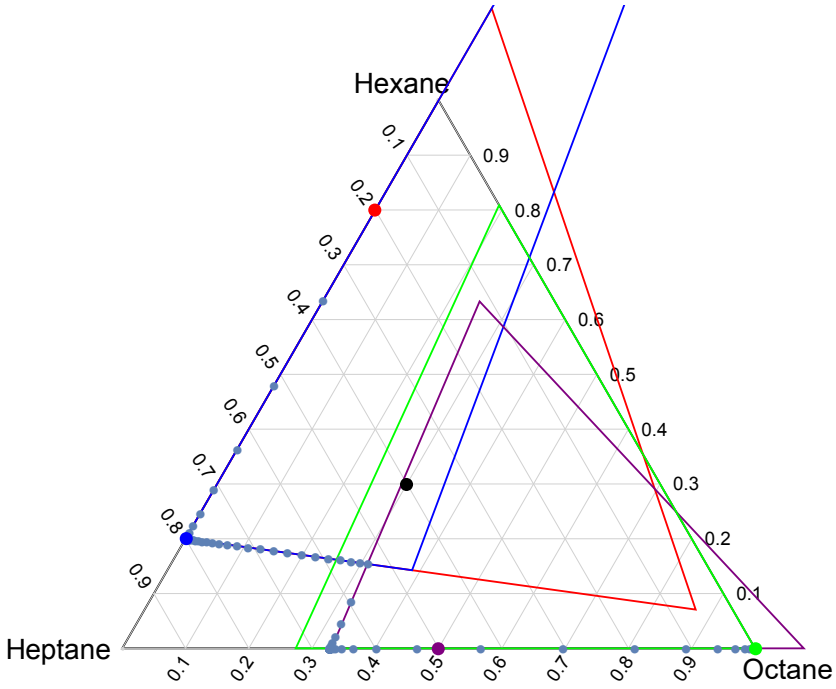

Figure 6.6. The Z-simplex diagram at the minimum reflux of $R_{\min} = 2.634$ calculated using our algorithm and the tray-by-tray liquid composition profile at the minimum reflux of $R_{\min} = 2.668$ determined by Aspen Plus. The red, blue, black, purple, and green dot in the figure respectively corresponds to the liquid composition of distillate, upper sidedraw, liquid feed stream, lower sidedraw, and the bottoms product. The red, blue, purple, and green Z-simplex is associated with column sections 1, 2, 3, and 4 of Figure 6.2b, respectively.

Using Algorithm 1, we find out that the minimum reflux ratio is given by $R_{\min} = 2.634$, 1.3% different compared to rigorous Aspen Plus simulation result of 2.668. From the minimum reflux Z-simplex diagram of Figure 6.6, it is clear that the controlling split is actually associated with W_1 as shown in Figure 6.2b. From the Z-simplices associated with column sections 1 and 2 as shown in 6.6, we see that the

composition of W_1 corresponds to saddle point pinch. Starting from the distillate composition (red dot in Figure 6.6) which has negligible amount of octane, the liquid composition profile follows along the hyperplane associated with section 1 Z-simplex $z_1 = 0$ which coincide with $x_1 = 0$ where the composition of W_1 also lies. As the liquid composition profile reaches x_{W_1}, it enters hyperplane $z_3 = 0$ of the section 2 Z-simplex and continues traveling along the hyperplane until it intersects with the hyperplane $z_1 = 0$ of section 3 Z-simplex. This intersection point corresponds to the liquid composition on the feed stage which can be easily determined. Clearly, it is different from the feed stream liquid composition (black dot in Figure 6.6). After that, the liquid composition profile evolves along the hyperplane $z_1 = 0$ of section 3 Z-simplex until it arrives at the saddle point pinch located at an intermediate location of section 3, after which it follows along the hyperplane $z_3 = 0$ and reaches the lower sidedraw composition x_{W_2}. Finally, the liquid composition profile arrives at the bottoms composition denoted as the green dot which is pure octane shown in Figure 6.6.

If the reflux ratio is further lowered, the desired composition for W_1, represented by the blue dot in Figure 6.6, cannot be achieved anymore since it no longer lies within the Z-simplices associated with section 1 or 2. This violates the constraint of Equation (6.5). Suppose that the controlling split occurs at the feed plate location. This would result in a "minimum reflux" ratio of 2.472, which is lower than the true minimum reflux. Therefore, we conclude that when determining the minimum reflux condition for a general MFMP column, it is not correct to simply ignore the presence of sidedraw streams or the role sidedraw streams play, which unfortunately, has been the case in the literature. As far as we know, our work is the first of its kind to point out the unique feature of sidedraw streams explicitly which is essential in deriving the first accurate shortcut based approach to determine the minimum reflux condition for a distillation column with sidedraws. The method proposed in this chapter can fully capture the possible circumstances when the controlling split of a MFMP column is associated with the one of the sidedraw streams.

Example 3: A Two-Feed, One-(Side)Product Column

As the final example, we consider the MFMP column shown in Figure 6.2a in which a sidedraw stream producing BC is located between two feed streams. Such a column scheme is very common in a multicomponent distillation configuration [7]. As we can see in Figure 6.2b, this MFMP column can be synthesized by consolidating two simple columns, one performing $ABC \rightarrow AB/BC$ split while the other performing $BCD \rightarrow BC/CD$ split. The stream containing BC, which is commonly produced as product from both simple columns, is now withdrawn from the MFMP column as sidedraw after column consolidation. However, if we only consider the decomposed case of Figure 6.2b rather than the entire MFMP column as a whole, we lose the possibility that the sidedraw stream BC is associated with the controlling split. We verify that this scenario is indeed possible by considering the following quaternary mixture system: hexane (component 4 or A), heptane (component 3 or B), octane (component 2 or C), and nonane (component 1 or D). The relative volatility of hexane, heptane, and octane with respect to nonane is determined from Aspen Plus to be 12.332, 5.361, and 2.300, respectively. The feed and product stream specifications are listed in Table 6.1.

Table 6.1.
Stream and product specifications of a two-feed, one-(side)product column of Figure 6.2a. For the upper feed stream ABC which is saturated vapor, we need to use the vapor-liquid equilibrium relation to obtain the liquid composition that is in equilibrium with the vapor composition listed in the table for minimum reflux calculation.

Streams	**Flow rate (mol/s)**	**Net composition** (z_4, z_3, z_2, z_1)	**Thermal quality**
AB	70	(3/7, 4/7, trace, trace)	1
ABC	100	(0.3, 0.3, 0.4, 0)	0
BC	70	(trace, 3/7, 4/7, trace)	1
BCD	100	(0, 0.4, 0.3, 0.3)	1
CD	60	(trace, trace, 0.5, 0.5)	1

It turns out that, in this case, the minimum reflux condition is achieved when sections 2 and 3 are pinched. Thus, the controlling split occurs at the sidedraw stream. The minimum reflux ratio calculated using Algorithm 1 is $R_{\min} = 2.002$, which is only 0.1% different from the minimum reflux ratio of 2.000 predicted by Aspen Plus simulation. On the other hand, the decomposition method which considers the case of Figure 6.2b gives a "minimum reflux ratio" of 1.806, which is significantly lower than the true minimum reflux ratio. This suggests that if we were to consider only the feed streams for minimum reflux calculations, we may end up with designing a distillation column that cannot achieve the desired product specification that we want.

Of course, we can further extend this case study by solving the MINLP problem formulated in Appendix A whose objective is to obtain the lowest possible minimum reboiler vapor duty that is needed by varying the distribution of intermediate components heptane and octane in the product streams in order to recover all hexane from the distillate and all nonane from the bottoms. We use the same feed specifications as in Table 6.1. The sidedraw is again in saturated liquid state. For a simple column, it is known that the optimal objective function value can always be calculated analytically from the preferred split solution using the Underwood's method [88]. For MFMP columns, however, we have to rely on global optimization. But before solving the optimization problem as it is in Appendix A, we need to modify the equations for section vapor flow calculation for V_2 and V_3 using Equation (5.13) to account for possible singularity issue. As we have mentioned, $\gamma_{2,3}$ can either be in (α_3, α_4) or (α_2, α_3), whereas $\gamma_{3,2}$ can either be in (α_1, α_2) or (α_2, α_3). As a result, singularity issue might arise in V_2 or V_3 expression using Equation (5.13) when $\gamma_{3,2}$ crosses over α_3 or as $\gamma_{2,3}$ crosses over α_2. To avoid such an issue, we reformulate Equation (5.13) by multiplying both sides with the bound factor $(\alpha_k - \gamma_j)$, where α_k is the relative

volatility over which γ_j might cross. For example, for V_2, we multiply both sides of Equation (5.13) with $(\alpha_3 - \gamma_{2,3})$ followed by partial fraction decomposition and get:

$$\begin{aligned} V_2(\alpha_3 - \gamma_{3,2}) &= (\alpha_3 - \gamma_{3,2})\frac{\alpha_2 d_{2,2}}{\alpha_2 - \gamma_{3,2}} + \alpha_3 d_{3,2} \\ &= \alpha_2 d_{2,2} - (\alpha_2 - \alpha_3)\frac{\alpha_2 d_{2,2}}{\alpha_2 - \gamma_{3,2}} + \alpha_3 d_{3,2} \end{aligned}$$

Similarly, we can reformulate Equation (5.13) for V_3. Multiplying these equations with the appropriate bound factors followed by partial fraction decomposition allows us to get rid of the singularity issue that can arise when $\gamma_{3,2} = \alpha_3$ in V_2 or when $\gamma_{2,3} = \alpha_2$ in V_3. Now, the MINLP can be solved using solvers such as BARON in GAMS [39]. The lowest possible minimum reboiler vapor duty is determined to be 171.9 mol/s with the corresponding optimal product distribution summarized in Table 6.2.

Table 6.2.
Optimal product corresponding to the lowest possible minimum reboiler vapor duty requirement of 171.9 mol/s.

Streams	**Component flow rate** (mol/s)
AB	(30, 13.4, 0, 0)
BC	(0, 56.6, 48.9, 0)
CD	(0, 0, 21.1, 30)

We verify this result by performing exhaustive sensitivity analysis using Aspen Plus. The lowest possible minimum vapor duty requirement subject to the product specifications is 177.9 mol/s, which is within 5% relative difference compared to the MINLP results. The corresponding product distribution for intermediate components heptane and octane also match very well with Table 6.2. Therefore, it is easy to imagine how much time and effort industrial practitioners can save by simply using our shortcut based approach to obtain a relative accurate solution in a matter of

seconds, instead of spending hours or even days to perform tedious sensitivity analysis or local optimization using Aspen Plus.

Furthermore, we would like point out that global optimization algorithm proposed in this chapter can do much more than finding the minimum energy requirement of a MFMP column and its corresponding product distribution. For example, there has been a debate of whether all heptane can be recovered from the distillate product in this MFMP column. We can easily answer questions like this one by modifying the relevant variable bounds or by adding/removing relevant constraints in the MINLP formulation. In this case, when fixing the heptane distillate flowrate $d_{3,1}$ to be the same as $f_{3,1} + f_{3,2}$, the corresponding MINLP problem turns out to be infeasible. Consequently, it is impossible to recover all heptane from the distillate. Detailed Aspen Plus simulation later confirms that some heptane is always present in the sidedraw product stream regardless of how much vapor is generated at the reboiler. Our algorithm thus allows practicing engineers to get a quick, reliable first-hand answer to these type of "feasibility" questions when they design or operate a MFMP column.

6.4 Additional Applications

In the light of process intensification opportunities discussed in Chapter 2, a series of new distillation configurations have been synthesized. These novel configuration schemes include heat and mass integrated configurations, thermally coupled configurations, thermodynamically equivalent configurations synthesized by converting thermal couplings into liquid-only transfer streams, distillation columns having intermediate reboilers and intermediate condensers, and so on. Despite their unique characteristics, these new configurations all belong to the category of MFMP columns. As a result, our proposed method and algorithm are found useful to derive the minimum reflux condition of these new configurations. In this section, we will consider the determination of the minimum reflux ratio for some of these configurations and

establish some solid theoretical understandings regarding these configurations under minimum reflux operations.

6.4.1 Heat and Mass Integrated Configuration – Using the Brugma Configuration as An Example

Here, we would like to consider one of the earliest and most well-known examples of heat and mass integrated configurations [8]; that is, the well-known Brugma configuration [71]. The Brugma configuration, as shown in Figure 6.7a, is a classic example of PI applied in multicomponent distillation. It is derived from the regular-column basic configuration of Figure 6.7b by simultaneous heat and mass integration of distillation columns that produce final pure component products B and C. As discussed in Chapter 2, such heat and mass integration is possible because the bottoms product of column 2 of Figure 6.7b (i.e. component B) is more volatile than the distillate product of column 3 (i.e. component C). Given sufficient separation stages in the HMA-section, the original composition profile in columns 2 and 3 of Figure 6.7b remains undisturbed even after heat and mass integration takes place. The task of the additional HMA-section is to simply perform mass exchange between the ascending C-rich vapor from the bottom section of column 2-3 and the descending B-rich liquid from the top section of the column [8].

It is believed [8] that through heat and mass integration of this sort, the sum of vapor duty requirements of the unconsolidated columns, i.e. columns 2 and 3 of Figure 6.7b, will be replaced by the greater of the two duties in the consolidated column 2-3 of Figure 6.7a. In this example, we would like use Algorithm 1 to verify if this claim is true, and if so, how we can generalize this fact to other HMP configurations [102].

Compared to Aspen Plus's predicted minimum reflux ratio of 3.6889, our method predicts that the minimum reflux occurs when the lower feed is controlling, at which the reflux ratio is determined to be 3.5385. Since the sidedraws only produce pure components, Equation (5.43) is not applicable for these streams. In fact, we only need to consider the reflux ratios obtained by solving Equation (5.41) for the two

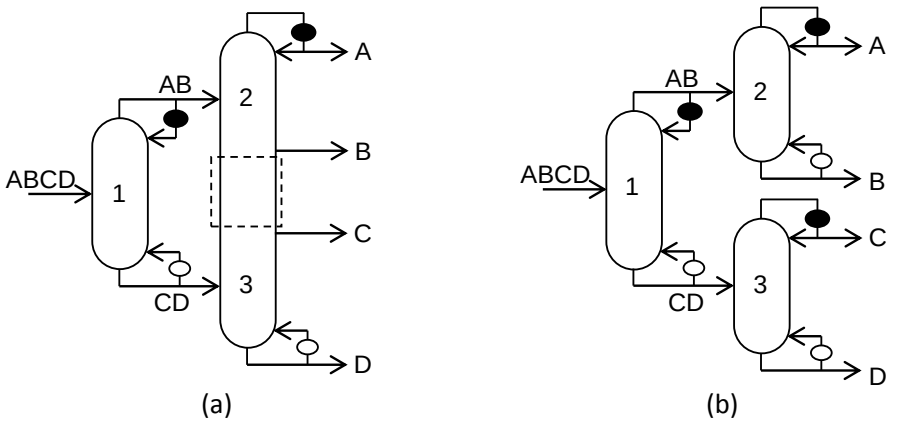

Figure 6.7. (a) The Brugma configuration; (b) Regular-column basic configuration before heat and mass integration.

Table 6.3.
Feed and product specifications to column 2-3 of the Brugma configuration of Figure 6.7a

Streams	**Normalized flow rate**	**Net composition** (z_A z_B z_C z_D)	**Thermal quality**
A	0.5	(1 trace trace trace)	1
AB	1	(0.5 0.5 0 0)	0
B	0.5	(trace 1 trace trace)	1
C	0.5	(trace trace 1 trace)	1
CD	1	(0 0 0.5 0.5)	1
D	0.5	(trace trace trace 1)	1

feed streams. This is because the HMA-section highlighted in Figure 6.7a has zero net mass flow. Therefore, given sufficient stages, column 2-3 actually retains the ability of the basic regular-column configuration from which it is derived, in the sense that components B and C can be obtained with arbitrarily high purity [8]. In other words, column 2-3 can be decomposed as two separate simple columns. As a result, the surrogate model can be used in this case to determine the true minimum reflux ratio of the consolidated column, which is given by the largest minimum reflux

obtained for all splits. We believe that the surrogate model works only when the HMA-section has zero net mass flow and acts only as a place for mass exchange.

The overall solution strategy is as follows. Given any general MFMP column, we first compute the net material flow for each column section. If a column section has zero net material flow, we shall separate the MFMP column apart based on this zero-flow section and decompose the column into two standalone columns. Then, for each separated column, we apply Algorithm 1 to determine the minimum reflux ratio. Finally, the true minimum reflux ratio of the original complex column is given by the largest minimum reflux ratio value of all decomposed columns:

$$R_{\min} = \max_{i \in C} \{R_{min,i}\} \qquad C = \{\text{all decomposed columns}\} \tag{6.7}$$

6.4.2 Thermodynamic Equivalence between Thermal Couplings and Liquid-Only Transfer Streams

In Chapter 2, we discuss a process intensification strategy of eliminating the operational hurdle of thermally coupled configurations by converting thermal couplings into LOT streams. This conversion is thermodynamically equivalent, i.e. both configurations would have the same heat duty requirement. Madenoor Ramapriya et al. [58] mathematically showed that the L/V ratios of all column sections involved in such conversion remain unchanged before and after this conversion occurs. Here, we would like to use the method developed in this chapter to verify the thermodynamical equivalence of converting thermal couplings to liquid-only transfers.

We consider the three-component fully thermally coupled Petlyuk configuration shown in Figure 6.8a. A thermodynamically equivalent version, which is drawn by converting the thermal couplings at AB and BC into liquid-only transfers, is drawn in Figure 6.8b. The saturated vapor feed contains 20 mol% of hexane, 30 mol% of heptane, and 50 mol% of octane. We can use the Underwood's method to calculate the product distribution at preferred split [165]. We briefly outline the calculation steps in the following paragraph.

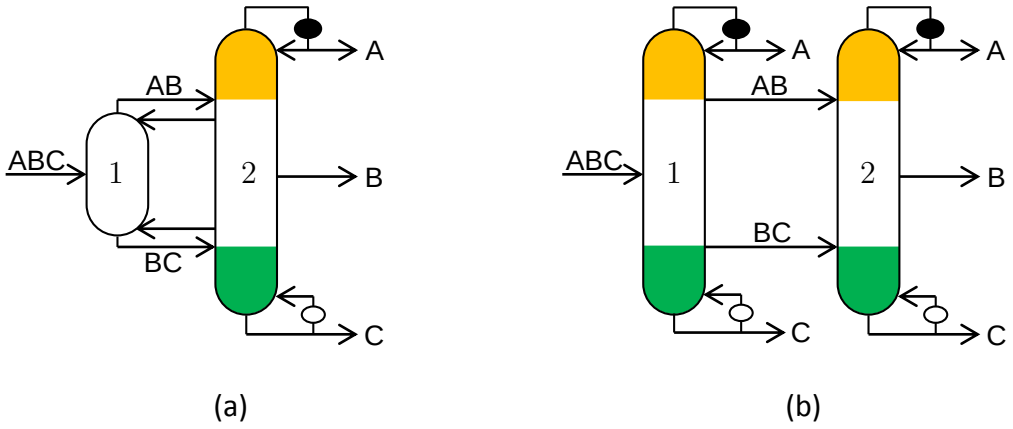

Figure 6.8. (a) The Petlyuk column [26]; (b) A thermodynamic equivalent version by converting thermal couplings of AB and BC into LOT streams. The colored sections have the same number of trays and L/V ratio.

Solving Equation (5.41) gives the common Underwood roots for the main feed as $\theta_1 = 1.78378, \theta_2 = 4.55914$. Therefore, at preferred split, the prefractionator column satisfies $V_{TOP} = \frac{\alpha_3 f_3}{\alpha_3 - \theta_1} + \frac{\alpha_2 d_2}{\alpha_2 - \theta_1}$ and also $V_{TOP} = \frac{\alpha_3 f_3}{\alpha_3 - \theta_2} + \frac{\alpha_2 d_2}{\alpha_2 - \theta_2}$. Solving this linear system gives $V_{TOP} = 1.23305, d_2 = 0.20910$.

In the next step, we can determine the common Underwood root for submixture AB by solving $V_{TOP} = \frac{\alpha_3 f_3}{\alpha_3 - \theta_{AB}} + \frac{\alpha_2 d_2}{\alpha_2 - \theta_{AB}}$. This gives $\theta_{AB} = 4.55914$, which is identical to θ_2 determined from the main feed. This is consistent with the "flow of Underwood root" behavior first explained by Glinos and Malone [166]. The bottom vapor flow for $AB \rightarrow A/B$ split is given by $-\frac{\alpha_2 d_2}{\alpha_2 - \theta_{AB}} = 0.21292$. Similarly, for submixture BC, the common Underwood root is given by $\theta_{BC} = 1.78378 = \theta_1$. And the corresponding top vapor flow for $BC \rightarrow B/C$ split is given by $\frac{\alpha_2 (f_2 - d_2)}{\alpha_2 - \theta_{BC}} = 0.40489$. As a result, for the second column, $BC \rightarrow B/C$ is the controlling split. Thus, the reboiler vapor duty of the FTC configuration is $V_{reb} = -\frac{f_1}{1 - \theta_1} = 0.63794$. The condenser vapor duty is related to V_{reb} by the overall vapor balance around the configuration: $V_{cond} = V_{reb} + (1 - q_F)F = 1.63794$.

Now, we would like to check if, we could get the same minimum reboiler duty requirement using Algorithm 1. Alternatively, we are checking if the separation is feasible under the same product distribution and vapor duty requirement. In Figure 6.8b, both AB and BC streams are now withdrawn as saturated liquid. We have calculated before that, for the first column, the preferred split top vapor duty is $V_{TOP} = 1.23305$. Thus, the corresponding bottom vapor duty is $V_{BOT} = 0.23305$. To make sure that the additional sections in the first column of Figure 6.8b which are highlighted in color are equivalent to the corresponding sections in the second column with the same color, the number of trays as well as the L/V ratios must be the same for both sections [58]. This argument fixes the net material flow of the additional sections in the first column as:

$$d_3 = \frac{V_{TOP}}{V_{cond}} f_3 = 0.15056$$
$$b_1 = \frac{V_{BOT}}{V_{reb}} f_1 = 0.18266$$

where d_3 and b_1 stands for the distillate flow rate of hexane and the bottoms flow rate of octane from the first column condenser, respectively. In face, we can generalize this result to a thermal coupling in any configuration. When the thermal coupling is replaced by liquid-only transfer, the distribution of net material produced by the reboiler or condenser is determined by the distribution of vapor flow:

$$\frac{d_{i,bef}}{d_{i,aft}} = \frac{V_{top,bef}}{V_{top,aft}}, \ \frac{b_{i,bef}}{b_{i,aft}} = \frac{V_{bot,bef}}{V_{bot,aft}} \tag{6.8}$$

Based on the analysis above, we construct a one-feed, two-sidedraw column that's identical to the first column of Figure 6.8b. The specifications of this complex column is stated in Table 6.4.

Using Algorithm 1, we quickly identify that the minimum reboiler vapor duty requirement for this complex column is $V_{\min} = 0.23304800$, which is exactly the same as V_{BOT} determined by the Underwood's method. For the second column of Figure 6.8b, the minimum vapor duty requirement is given by Equation (6.7) as 0.40488782,

Table 6.4.
Calculation results for column 1 of Figure 6.8b.

Streams	**Normalized flow rate**	**Net composition** (z_A, z_B, z_C)	**Thermal quality**
A	0.15056	(1 trace trace)	1
AB	0.25854	(0.19123 0.80877 trace)	1
ABC	1	(0.2 0.3 0.5)	0
BC	0.40824	(trace 0.22267 0.77733)	1
C	0.18266	(trace trace 1)	1

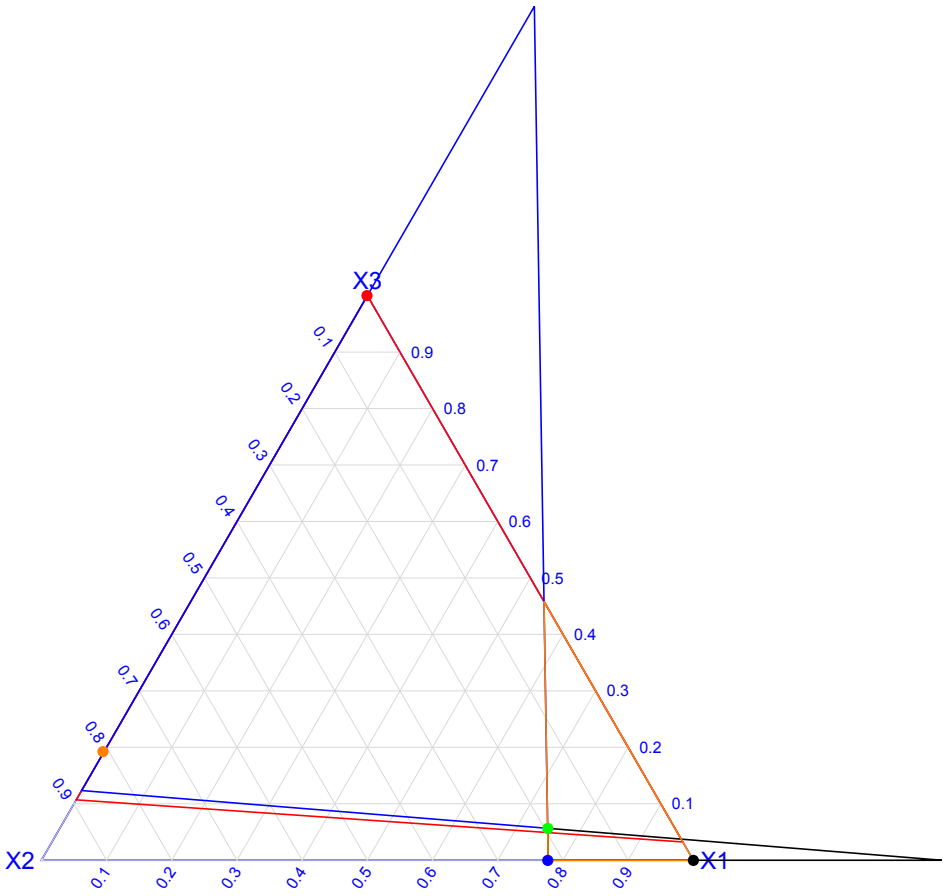

Figure 6.9. Z-simplex diagram for the first column of Figure 6.8b at minimum reflux. The column is clearly pinched at the feed stage (green dot) and preferred split is achieved.

which is exactly the difference between the total vapor duty requirement V_{reb} of the original FTC configuration and $V_{\min}$ calculated before. In other words, the overall minimum reboiler vapor duty requirement of the new configuration is exactly the same as the original FTC configuration. This shows that converting thermal couplings into liquid-only transfers indeed preserve thermodynamic equivalence. We believe that this statement is true not only for this particular FTC configuration, but for any thermally coupled configuration. The reason is because, through conversion, the newly added column section has the same L/V ratio as the original column section from which the new section is derived. Based on Equation (5.33), we see that the Underwood roots of these newly added sections due to conversion will be identical to their "parent" sections. That is, the Z-simplices for these new sections completely superimpose with those of the "parent" sections. Consequently, the minimum reflux condition remains unchanged before and after conversion, regardless of whether where the controlling split of the configuration is located at.

6.4.3 "Flow of Underwood Roots" for Thermally Coupled Columns

A distinct feature of thermally coupled configuration is that the section Underwood roots corresponding to column sections connected by thermal coupling can be "carried over" at minimum reflux. This reduces the number of variables needed for modeling thermally coupled configurations. The "flow of Underwood roots" phenomenon for thermally coupled columns is first discovered by Glinos and Malone [166] and then observed by Carlberg and Westerberg [32, 167]. Later, Halvorsen and Skogestad [46] developed mathematical reasoning for such behavior. Without loss of generality, assume that two columns are connected by a thermal coupling at the condenser node (See Figure 6.10a). The product leaving the top of column section 2 of Figure 6.10a is either withdrawn by a reboiler or by another thermal coupling, i.e. not as sidedraw. We recognize that the Underwood's distillate equation of Equation

(5.13) of section 1 of Figure 6.10a is at the same time the Underwood's feed equation of Equation (5.41) for the next column. This gives:

$$\theta_i = \gamma_{1,i+1} \in (\alpha_i, \alpha_{i+1}) \qquad \forall i = 1, ..., c-1 \tag{6.9}$$

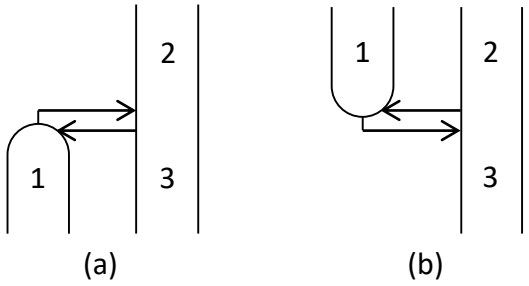

Figure 6.10. (a) A theraml coupling that replaces a condenser; (b) a thermal coupling that replaces a reboiler

Equation (6.9) serves as the bridge connecting the Underwood roots between one column and the other, and can be used to arrive at the "flow of Underwood roots" relation. To derive this relation, note that the liquid transfer of the thermal coupling must be a real composition and thus satisfies $k_{2,i} \sum_{j=1}^{c} \frac{\alpha_j x_{j,TC}}{\alpha_j - \gamma_{2,i}} \geq 0 \quad \forall i = 1, ..., c$ (notice that here we shall use $x_{j,TC}$ instead of $l_{j,TC}$ due to the direction of $l_{j,TC}$). Therefore, $\sum_{j=1}^{c} \frac{\alpha_j x_{j,TC}}{\alpha_j - \gamma_{2,i}} \geq 0$. Substituting this result into Equation (5.46) relates the Underwood roots for section 2 with the feed Underwood roots as:

$$\gamma_{2,i+1} \geq \theta_i \in (\alpha_i, \alpha_{i+1}) \qquad \forall i = 1, ..., c-1$$

and, along with Equation (6.9), we arrive at the "flow of Underwood roots" relations:

$$\gamma_{2,i+1} \geq \theta_i = \gamma_{1,i+1} \geq \theta'_i \qquad \forall i = 1, ..., c-1 \tag{6.10}$$

where θ_i and θ'_i represent the feed Underwood root for the second and first column in Figure 6.10a, respectively. Similarly, when a reboiler is replaced by a thermal

coupling (See Figure 6.10b), the Underwood roots column sections 1 and the feed Underwood roots are related by:

$$\gamma_{1,i} = \theta_i \in (\alpha_i, \alpha_{i+1}) \qquad \forall i = 1, ..., c-1$$

Relating the common Underwood root θ with the Underwood roots for section 3 is a little bit trickier for a thermal coupling associated with a bottom submixture stream. For the thermal coupling of Figure 6.10b, the liquid transfer composition does not necessarily lie within the Z-simplex. However, the liquid composition that's in equilibrium with that of the vapor transfer must lie on the actual composition profile. This means that $k_i \sum_{j=1}^{c} \frac{y_{j,TC}}{\alpha_j - \gamma_{3,i}} \geq 0$ in order for $y_{i,TC}$ (and of course, the liquid composition that is in equilibrium with it) to reside within the Z-simplex of column section 3 of Figure 6.10b. Again, due to Equation (5.43) and the fact that all k_i are non-positive whereas all $y_{i,TC}$ are nonnegative, we have:

$$\gamma_{3,i} \leq \theta_i \in (\alpha_i, \alpha_{i+1})$$

from which we finally have:

$$\gamma_{3,i} \leq \theta_i = \gamma_{1,i} \leq \theta'_i \qquad \forall i = 1, ..., c-1 \tag{6.11}$$

where θ'_i stands for the common Underwood root for the first column of Figure 6.10b. The discussion above shows that the "flow of Underwood roots" behavior is not only applicable to two simple columns connected by thermal coupling, but is also the case for a general thermally coupled MFMP configuration.

6.5 Conclusion

We present the mathematical formulation that incorporates the model developed in Chapter 5 in a global optimization framework to determine the minimum reflux condition of a general MFMP column. When the full product specifications are not

known to users a priori, a set of binary variables is to be introduced to convert the necessary and sufficient conditions for a feasible separation into a set of inequality constraints. The resulting optimization problem is a MINLP in general. By solving this MINLP, users will be able to not only obtain the minimum vapor duty requirement of the MFMP column of interest, but also determine the product specifications to achieve this minimum vapor duty. The applicability of this proposed algorithm is not limited to single MFMP column, but can also be easily implemented in a large optimization framework such as the one recently developed by Nallasivam et al. [34] to determine the minimum energy requirement of an entire multicomponent distillation configuration or a family of configurations. If the objective is simply to determine the minimum reflux ratio of a MFMP column while the full product specifications are already known, a simple verification algorithm that does not involve any optimization, i.e. Algorithm 1, is proposed. Using Algorithm 1, we examine several examples of different MFMP columns, in which the minimum reflux condition calculated using our approach matches very well with rigorous Aspen Plus simulation results.

The second outcome achieved by considering these case studies, besides validating the accuracy and effectiveness of our approach, is to challenge some of the well-accepted heuristics people have used regarding how a MFMP column should be designed and operated. In Example 1, we show a counterexample where placing a cooler feed stream above a hotter feed stream in a distillation column actually leads to a higher minimum vapor duty requirement than if the feed stream locations are reversed. Thus, one needs to analyze all possible permutations of relative feed locations to determine the optimal feed stream arrangement. Our shortcut based approach is particularly suitable for this kind of analyses compared to rigorous simulations which can be quite time consuming to perform, especially as the number of feed streams and/or sidedraw streams increases.

Another crucial finding that we would like to highlight is that decomposing a MFMP column into individual simple columns and analyzing each column individually using the classic Underwood's method is not the correct approach to determine

the minimum reflux of the MFMP column. In fact, this approach can lead to results that are significantly off from the true minimum reflux ratio. In order to determine the minimum reflux condition accurately, such a decomposition should not be performed. Our shortcut based approach, which is based on an accurate shortcut model for each general column section, is thus the correct method to handle MFMP columns.

Finally, when a MFMP column has one or more sidedraw streams, it is possible that one of the sidedraw streams controls the separation at minimum reflux, even when they are all withdrawn as saturated liquid streams. Sidedraw streams have often been neglected in the past due to lack of understanding of their role played on minimum reflux condition of a MFMP column. We believe that the mathematical model developed in Chapter 5 fills this gap, which allows us to fully capture the sidedraw contribution in a MFMP column for the first time. In all, we hope that researchers as well as industrial practitioners can find these results and discussions helpful when designing and operating an efficient and cost-effective MFMP column.

7. UNDERSTANDING REVERSIBLE DISTILLATION

The initial motivation to investigate the concept of reversible distillation is originated from the encounter of a peculiar three-feed distillation column case when testing our algorithm developed in Chapters 5 and 6. Although our algorithm correctly predicted the true minimum reflux ratio, the liquid composition profile within one of the intermediate column sections did not match well with Aspen Plus results. Within a period of six months from early-February, 2017 to mid-October, 2017, we were essentially stuck in this single case without moving anywhere further. After delving in the literature for months, we finally found the actual cause of the composition mismatch based on the theory of reversible separation, from which one can further reach various interesting observations and results.

7.1 Problem Statement and Thermodynamic Analysis

The peculiar case that caught my attention is a three-feed distillation column separating hexane (component A or 3), heptane (component B or 2), and octane (component C or 1). From Table 7.1 which lists the feed and product specifications for this three-feed column, it can be seen that all components are presents in non-negligible amount in the bottom product. Therefore, there will be one and only one pinch in the bottom section; and this pinch must correspond to Z_3 which is located at the lower feed stage [19].

As shown in Figure 7.1, the orange simplex $Z_1Z_2Z_3$ stands for the Z-simplex for the bottom column section, whereas the black simplex $Z_1'Z_2'Z_3'$ is the Z-simplex for the intermediate column section lying in between the middle and lower feed streams. Since Z_3 is the only pinch within the bottom section and it lies right below the lower feed, the composition profile within the bottom section must start from Z_3. On

Table 7.1.
Feed and product specifications of the peculiar case.

Streams	**Flow rate (mol/s)**	**Net composition** (z_A z_B z_C)	**Thermal quality**
Distillate	0.8	(0.99 0.01 trace)	1
Upper feed	1	(0.1 0.8 0.1)	1
Middle feed	1	(0.3 0.4 0.3)	0
Lower feed	1	(0.4 0.4 0.2)	0.5
Bottoms	2.2	(0.00$\dot{3}\dot{6}$ 0.72$\dot{3}\dot{6}$ 0.$\dot{2}\dot{7}$)	1

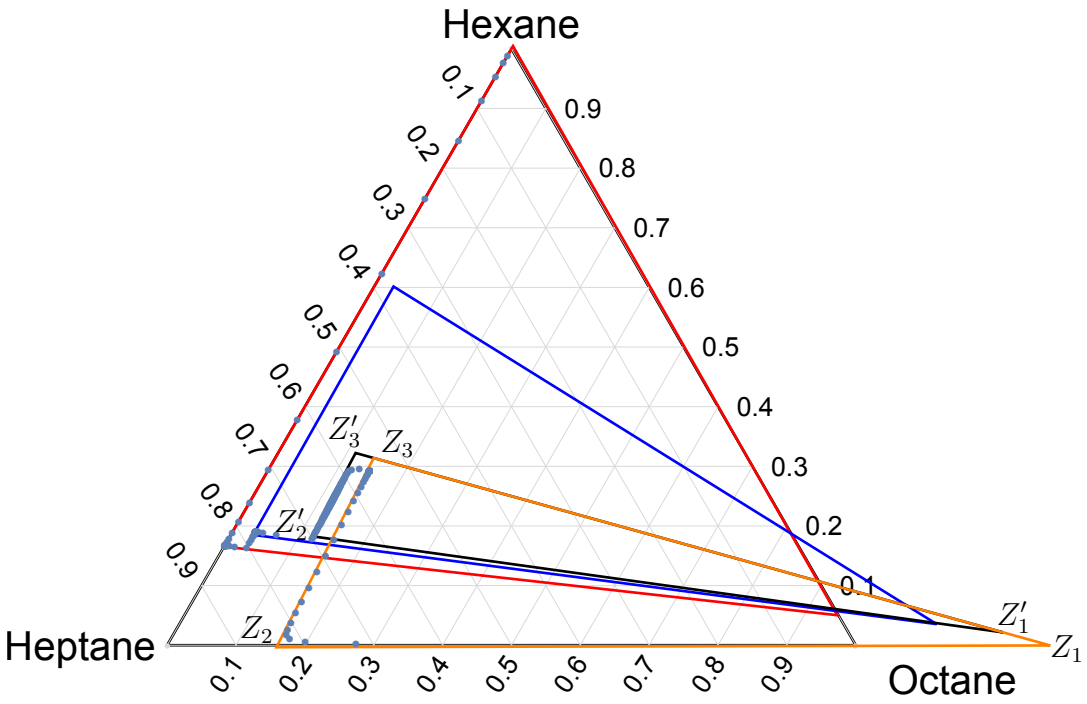

Figure 7.1. The Z-simplex diagram of the three-feed column at minimum reflux of $R = 4.582917$.

the other hand, when $R = 4.582917$, starting from the distillate product, tray-by-tray downward calculations that strictly follow the constant molar overflow (CMO) assumption will reach Z_2'. This imposes two requirements for the composition profile in the intermediate column section:

1. It must form a continuous path from Z_2' to Z_3.

2. It must end at Z_3. Otherwise, there must exist a segment of composition profile in the bottom section that leads to pinch Z_3, which is not possible.

However, Figure 7.1 suggests that under CMO assumption, as the composition profile reaches Z_2', the composition profile generated by further downward calculations must reside on the hyperplane $Z_2'Z_1'$. In this case, it is impossible to satisfy the two criteria listed above. This implies that the CMO assumption has to be relaxed for the intermediate section.

This argument, though too bold to be true from the first glance, can be supported by performing rigorous thermodynamic analysis on the intermediate section. In other words, we want to show that under strict CMO assumption, it is against thermodynamics to have a higher temperature pinch on top of a lower temperature pinch point within a column section. Therefore, the CMO assumption is not valid under this case.

Recall that the steady-state entropy balance for a separation process is a summation of the physical contribution due to energy exchange and the chemical contribution related to material inflows and outflows. The entropy balance for a simple distillation column at steady state is then given by [26, 168]:

$$\sum_{j=1}^{c} \frac{Q_j}{T_j} + \Delta S_{irr} + (S_F - S_D - S_B) = 0 \tag{7.1}$$

where $\Delta S_{irr} \geq 0$. The first term describes the entropy change of the system to the surroundings, ΔS_{irr} stands for overall entropy production due to irreversibilities, and $S_F - S_D - S_B$ is basically the entropy difference between entering and leaving material streams.

For the intermediate section, assuming that two pinches Z_2' and Z_3' exist in the intermediate column section and Z_2' lies above Z_3' in the section, we can draw a control volume denoted as p between the pinches. Equation 7.1 then becomes:

$$\Delta S_{irr} = S_{p,top} + S_{p,bot} - \sum_{j=1}^{c} \frac{Q_j}{T_j}$$

where $S_{p,top}$ and $S_{p,bot}$ represent the entropy of the net material stream of top pinch Z_2' and bottom pinch Z_3', respectively. $S_{p,top} + S_{p,bot}$ stands for the entropy generation due to material in- and out-flows, which is given by:

$$S_{p,top} + S_{p,bot} = -(S_{p,in} - S_{p,out}) = V(\underline{S}_{p,top}^{vap} - \underline{S}_{p,bot}^{vap}) - L(\underline{S}_{p,top}^{liq} - \underline{S}_{p,bot}^{liq})$$

The net work consumption within the control volume p can be determined following the Clausius-Clapeyron relationship. By assuming an adiabatic column section with negligible pressure, and suppose that the multicomponent mixture strictly satisfies CRV and CMO assumptions, we have [121]:

$$-\sum_j \frac{Q_j}{T_j} = \Delta S_{sur} = \Delta H V \Big(\frac{1}{T_{p,top}} - \frac{1}{T_{p,bot}}\Big) = RV \ln\Big(\frac{\sum_i \alpha_i x_{i,p,top}}{\sum_{i=1}^{c} \alpha_i x_{i,p,bot}}\Big)$$

Note that we must have $\sum_i \alpha_i x_{i,p,top} > \sum_i \alpha_i x_{i,p,bot}$, which implies that $T_{p,top} > T_{p,bot}$. This result is consistent with Zhang and Linninger [169]. Next, using Equations (5.15) and (5.16), the liquid and vapor compositions at both pinches Z_2' and Z_3' can be easily calculated. And by appropriately defining these streams in Aspen Plus, we can also obtain the molar entropy value for each stream using Aspen's IDEAL thermodynamic model at 1 atm, as shown in Table 7.2.

Table 7.2.
Liquid and vapor compositions at pinches Z_2' and Z_3'.

Streams	**Stream composition** $(z_A\ z_B\ z_C)$	**Molar entropy** $\underline{S}$ **(cal/mol K)**
$Z'_{2,vap}$	(0.35918 0.59686 0.04396)	-139.5
$Z'_{2,liq}$	(0.18281 0.69882 0.11837)	-165.6
$Z'_{3,vap}$	(0.54700 0.41690 0.03609)	-135.8
$Z'_{3,liq}$	(0.32233 0.56514 0.11253)	-162.8

Now at $R = 4.582917$ obtained by directly applying Algorithm 1, the liquid and vapor flows in control volume p are respectively given by $L_p = 4.66633$ mol/s and $V_p = 3.46633$ mol/s. Thus, $S_{p,top} + S_{p,bot} = 0.2403$ cal/Ks > 0. On the other hand,

since $T_{p,top} > T_{p,bot}$, we have $\sum_i \alpha_i x_{i,p,top} < \sum_i \alpha_i x_{i,p,bot}$. And $\Delta S_{sur} = -\sum_j \frac{Q_j}{T_j} = 1.98720 \text{ cal/molK} \times 3.466333 \text{ mol/s} \times \ln \frac{2.6929}{3.1178} = -1.0092 \text{ cal/Ks}$. Clearly, $\Delta S_{irr} < 0$, which is against the 2nd law of thermodynamics.

In fact, we have the following fact:

Fact 7.1.1 *Within an infinite, adiabatic column section that satisfies the CMO assumption, it is thermodynamically infeasible to have a higher temperature pinch above a lower temperature pinch.*

Now the remaining questions are: How do we interpret the composition profile predicted by Aspen Plus so that neither Fact 7.1.1 nor the two requirements for the intermediate section would be violated? Also, can such interpretation be successfully characterized by our method? To answer these questions, we would like to first introduce the methodology of Koehler et al. [170], which discusses how to calculate the minimum vapor duty of a simple column when the CRV and/or CMO assumption are relaxed. The key is to describe the composition profile inside this particular column section using the concept of reversible distillation.

7.2 Reversible Distillation Model

Consider a simple adiabatic column with infinite stages. The composition profile within the rectifying and stripping sections can be easily determined by performing tray-by-tray calculations using the Underwood's method [19]. The profile will always terminate at a pinch point, at which liquid and vapor streams reach equilibrium. For a series of L/V ratios, a series of composition profiles can be obtained. For example, Figure 7.2 below, which is extracted from Koehler et al. [170], depicts liquid composition profiles in the stripping section of an adiabatic column for ternary alcohol separations under five different reboil ratios. The pinch points are numbered in the order of increasing reboil ratio.

The variation of adiabatic composition profile with respect to reboil ratio can be easily captured using the Underwood's method [19]. If we vary the reboil ra-

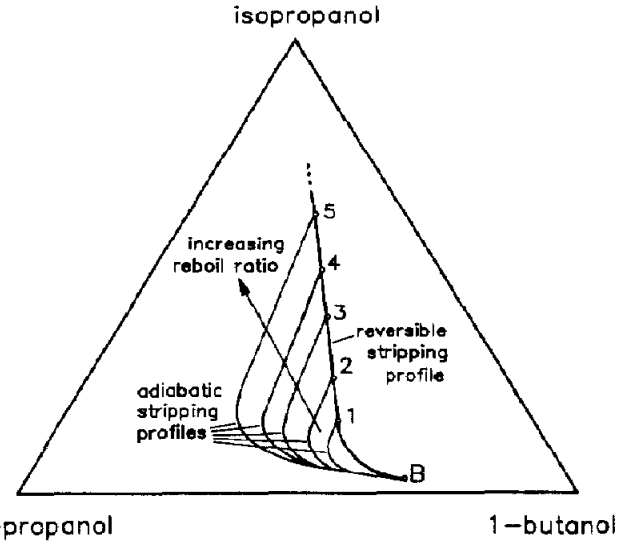

Fig. 5. Adiabatic and reversible concentration profiles for a stripping section. ($p = 101.3$ kPa, $B = 0.587$ mol/s, $x_B(i\text{-prop.}) = 0.02$, $x_B(1\text{-propanol}) = 0.2989$, $x_B(1\text{-butanol}) = 0.6811$, $Q_B = 21.68/28.52/38.79/49.06/69.59$ kW/mol.)

Figure 7.2. Illustration of adiabatic and reversible liquid composition profile for the stripping section in a simple distillation column. This figure is extracted from Koehler et al. [170].

tio infinitesimally and connect the pinch points associated with these reboil ratios, we will obtain a smooth path which corresponds to reversible stripping composition profile. The reversible path, generated by adding infinitesimal heat onto each stage continuously, consists of all pinch points in scenario of adiabatic distillation. And the following fact holds:

Fact 7.2.1 *The composition profile in a reversible column section under continuously energy addition or withdrawal exactly corresponds to the pinch point profile obtained in an adiabatic section, where the same amount of energy is introduced or withdrawn only at the bottom end.*

Clearly, the difference between the reversible column model and the adiabatic column model lies only in their exergy losses (i.e. distribution of heat addition/removal).

Therefore, Fact 7.2.1 gives the correct analysis tool to understand the peculiarity associated with the composition profile in the intermediate column section.

Franklin [161] discusses the use of the Underwood's method [19] for reversible multicomponent separation processes. Suppose that heat can be progressively added to or removed from stages within the separation cascade in such a way that the effective operating lines continuously follow the equilibrium curve and are only infinitesimally below it. By doing this, the "no mixing" condition is met on all the plates where heat addition or removal occurs. Thus, instead of having only one local pinch in the cascade, each and every stage where heat addition or removal occurs is pinched. For reversible operation of a simple column, given the feed and distillate specifications, we start from one of the pinches so that "no mixing" condition becomes valid across the section of interest.

Let us imagine a scenario under which the distillate product x_D contains all components present in non-negligible amount. This implies that there exists one and only one pinch, denoted as $(Z_1)_{R_{\min}}$, in the adiabatic rectifying section with infinite number of stages. If we are interested in the reversible operation of the rectifying section, we shall start from $(Z_1)_{R_{\min}}$ and gradually lower the local V, i.e. lower the local reflux ratio while fixing d_i. Each new reflux ratio R corresponds to a new local pinch $(Z_1)_R$. The reversible composition profile in the rectifying section can be obtained by repeating the process above at continuously decreasing values of local R, followed by connecting the local pinch points: $(Z_1)_{R_{\min}} \rightarrow (Z_1)_R \rightarrow ...$

Going back to the intermediate section of interest between middle and lower feed streams. At $R = 4.582917$, the Z-simplex for the column section following the Underwood's CMO assumption is shown as $Z_1'Z_2'Z_3'$ in Figure 7.1. As discussed above, the only part of the section which is not thermodynamically infeasible is the one between Z_2' and Z_3'. One may then naturally raise the following question: "Is it possible to construct a continuous composition profile if Z_2' and Z_3' actually correspond to the same pinch point?"

It turns out that, as we relax the CMO assumption and use the reversible distillation model for the section, we will eventually be able to form a continuous composition profile in which Z_2' and Z_3' coincide to form only one pinch point within the section. Also, based on Fact 7.2.1, the minimum vapor duty requirement is unchanged.

To do this, we simply solve Equation (5.13) for the intermediate section. The component net upward flows are fixed: $(d_3, d_2, d_1) = (0.392, -1.192, -0.4)$. The resulting roots to Equation (5.13), as shown in Figure 7.3, are given by $(\gamma_3, \gamma_2, \gamma_1) = (4.19714, 3.62514, 1.0767)$. Now, as we relax the CMO assumption, intermediate reboilers (IRs) will be placed and heat will be continuously added to section starting from the original Z_2'. As we further traverse downward along the section, the local boilup ratio gradually decreases because the cumulative vapor duty generated at the IRs increases. In terms of Figure 7.3, the reduction of local boilup ratio implies that the horizontal line decreases. Thus, γ_1 and γ_2 increases, whereas γ_3 decreases. Correspondingly, hyperplanes $z_2 = 0$ and $z_3 = 0$ of the Z-simplex for the intermediate section will start approaching each other. It will continue as local boilup ratio keeps decreasing until $\gamma_2 = \gamma_3$, which means $z_2 = 0$ and $z_3 = 0$ coincide with each other. Beyond this point, no further reduction in local reboil ratio is possible, so the non-adiabatic operation section terminates. The bottom reboiler will produce the rest of the vapor duty required to carry out the separation at $R = 4.582917$.

In Figure 7.4, we illustrate how the Z-simplex corresponding to the intermediate section changes as the local boilup ratio gradually decreases. The reversible operation within the section is achieved using a series of IRs. As we can see, pinch Z_2' gradually moves towards X_3. And its trajectory follows almost like along the straight line of $z_1 = 0$ since γ_1 changes only a small amount as local V decreases. Therefore, the composition profile also moves along with the pinch point Z_2' until it reaches the horizontal line which is the limiting case when $z_2 = 0$ and $z_3 = 0$ collapse into a single hyperplane. This marks the end of the non-adiabatic zone. In the adiabatic zones, namely Zone 1 and Zone 2 shown in Figure 7.5, the CMO assumption strictly holds.

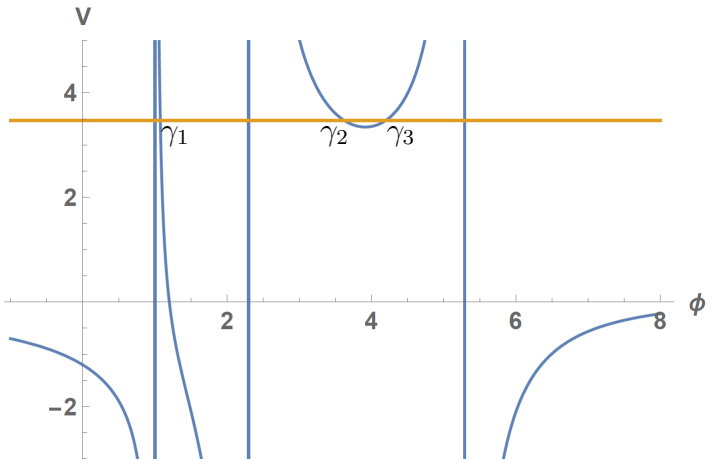

Figure 7.3. The plot of γ root behavior of Equation (5.13) associated with the intermediate column section at $R = 4.582917$.

Figure 7.6 shows the complete composition profile of the entire column at minimum reflux. The blue dots are Aspen Plus simulation results, whereas the brown dots are the results by performing tray-by-tray upward calculation starting from Z_3 of the bottom section using the Underwood's method, i.e. adiabatic Zone 2 shown in Figure 7.5. It can be readily seen that in Zone 2, Aspen Plus results match with tray-by-tray calculations results precisely. The termination point of Zone 2 lies on the degenerate hyperplane $z_2 = 0$ or $z_3 = 0$ when γ_2 and γ_3 coincide. Beyond this point, the CMO assumption has to be relaxed in order to carry out the separation.

Finally, it should be emphasized that $R_{\min}$ value remains unchanged even if we relax the CMO assumption when needed for some part(s) of the distillation column. Therefore, Algorithm 1 still remains as a valid approach to determine the minimum reflux condition for a multi-feed column. Only under the scenario when we need the precise composition profile should we be worried about potentially relaxing the CMO assumption for certain column sections.

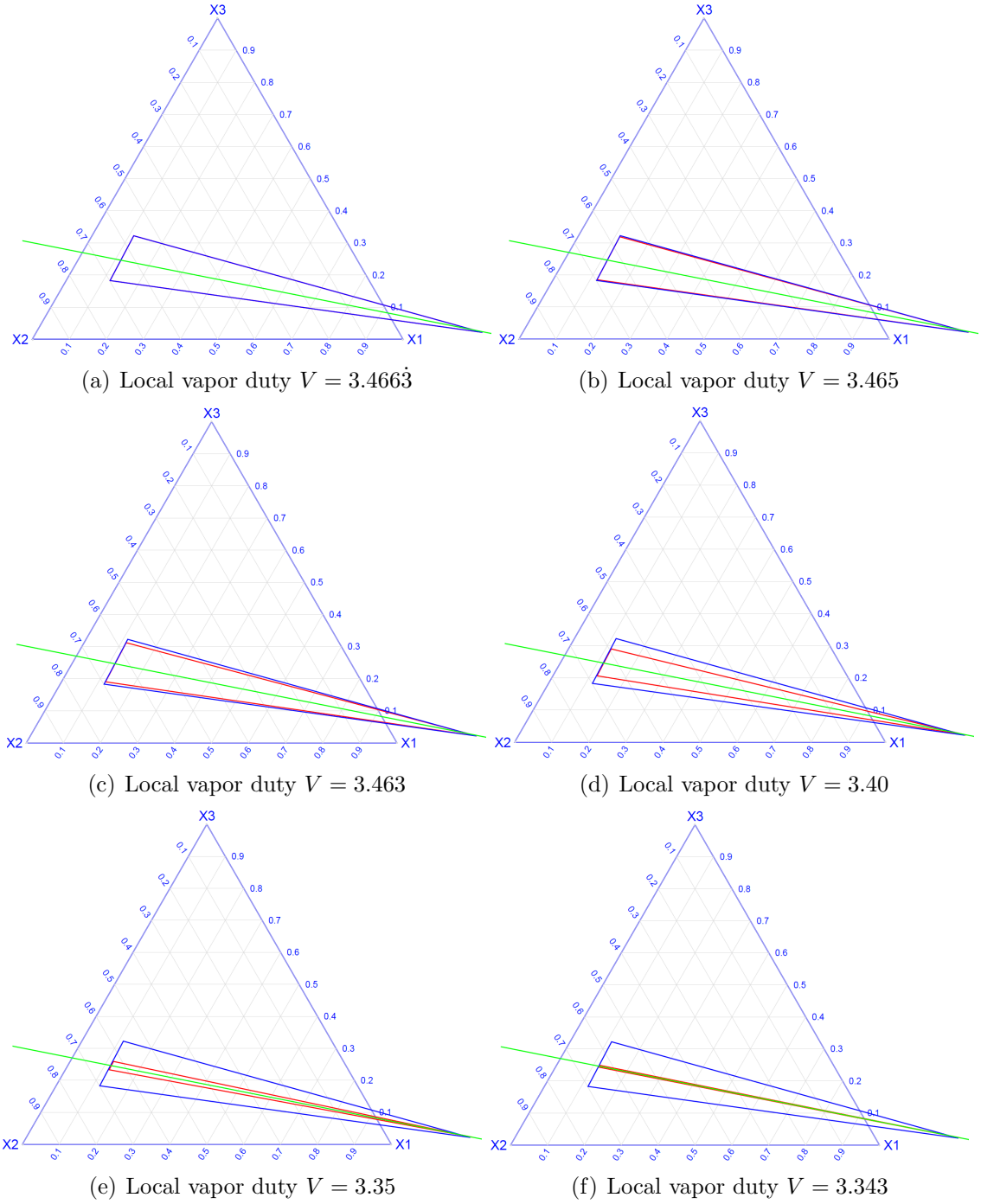

(a) Local vapor duty $V = 3.466\dot{3}$

(b) Local vapor duty $V = 3.465$

(c) Local vapor duty $V = 3.463$

(d) Local vapor duty $V = 3.40$

(e) Local vapor duty $V = 3.35$

(f) Local vapor duty $V = 3.343$

Figure 7.4. The variations of Z-simplex for the intermediate section. Notice how pinch points Z_2' and Z_3' move as local vapor flow decreases. The green line stands for $z_2 = z_3 = 0$ when the section vapor flow $V = 3.342125$.

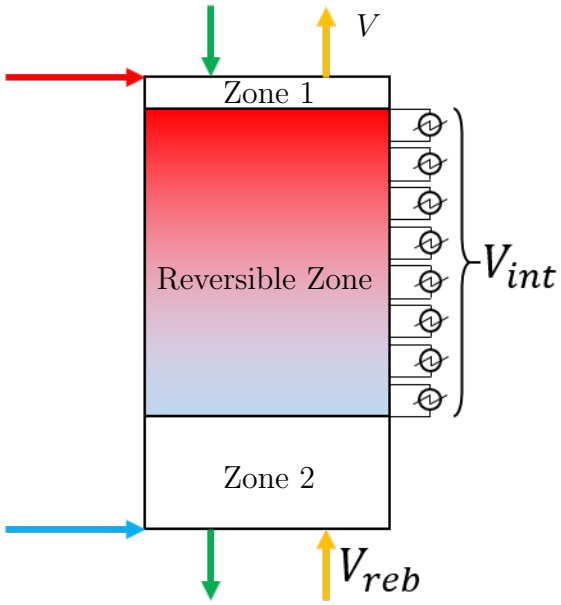

Figure 7.5. A schematic diagram for the third column section. Notice that the non-adiabatic section is only part of the entire column section.

7.3 Another Example – A Two-Feed, Two-(Side)Product Column

To conluce the discussion, we would like to consider another example involving a two-feed, two-(side)product distillation column in which the reversible distillation model is used to predict its composition profile under minimum reflux operation. Once again, the feed stream into the distillation column contains hexane, heptane, and octane, as listed in Table 7.3.

Our method predicts the correct minimum reflux ratio of 2.32464, as compared to $R_{\min} = 2.39291438$ obtained from Aspen Plus (2.85% relative difference). For any $R < R_{\min}$, the liquid composition of the upper sidedraw stream will no longer satisfy $k_{3,1}\sum_{j=1}^{c}\frac{\alpha_j x_{j,W_1}}{\alpha_j-\gamma_{3,1}}$ and $k_{3,2}\sum_{j=1}^{c}\frac{\alpha_j x_{j,W_1}}{\alpha_j-\gamma_{3,2}} > 0$, indicating that this is the indeed the minimum reflux ratio. However, if we examine the Z-simplex diagram shown in Figure 7.8, we realize that the liquid composition profile fail to match well with the Z-simplex for the intermediate section in between the upper and lower feed streams.

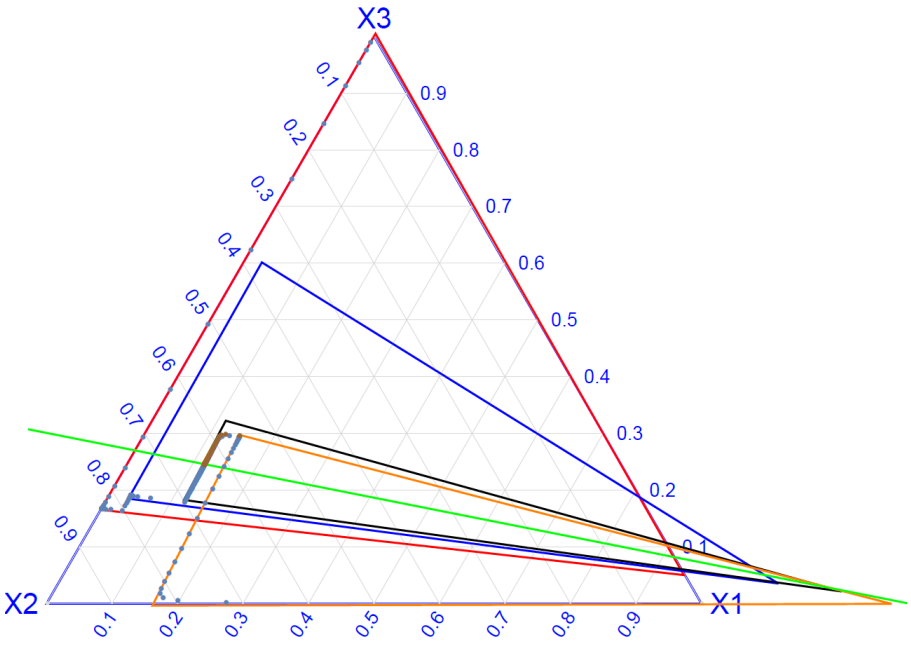

Figure 7.6. A schematic diagram for the third column section. Notice that the non-adiabatic section is only part of the entire column section.

Table 7.3.
Feed and product specifications for the two-feed, two-(side)product column example.

Streams	**Flow rate (mol/s)**	**Net composition** (z_A z_B z_C)	**Thermal quality**
Distillate	70	(0.8499956 0.1500044 trace)	1
Upper sidedraw	40	(0.1922978 0.5248507 0.2828515)	1
Upper feed	100	(0.2 0.3 0.5)	0
Lower feed	100	(0.5 0.4 0.1)	1
Lower sidedraw	50	(0.0561548 0.7701282 0.173717)	0
Bottoms	40	(trace trace 1)	1

To understand this discrepancy, we need to study the composition and temperature profile of the column, which are shown in Figure 7.7 below.

It can be seen from the temperature profile that there is a temperature inversion in the section between the upper and lower feed streams. In fact, from the composition profile as well as the Z-simplex diagram, we can clearly see that this column section

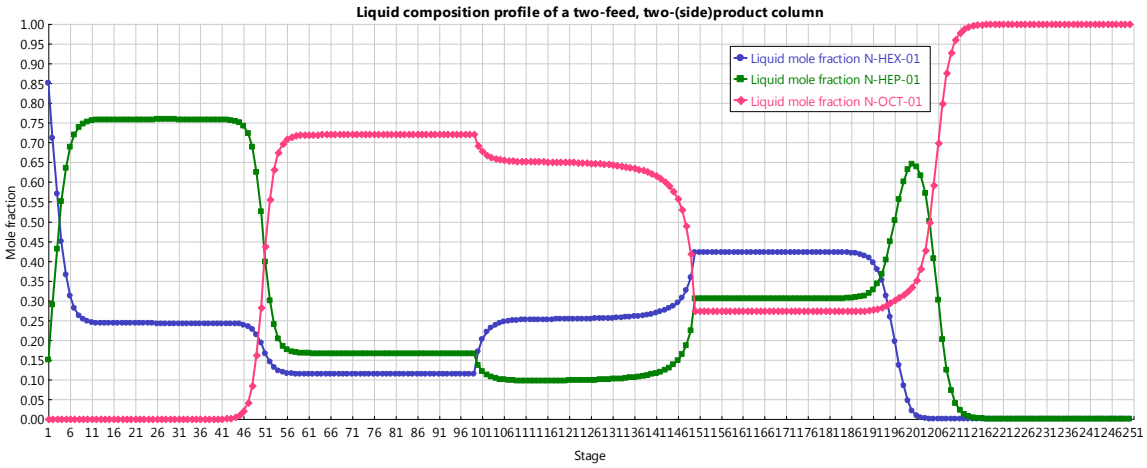

(a) Liquid composition profile at minimum reflux

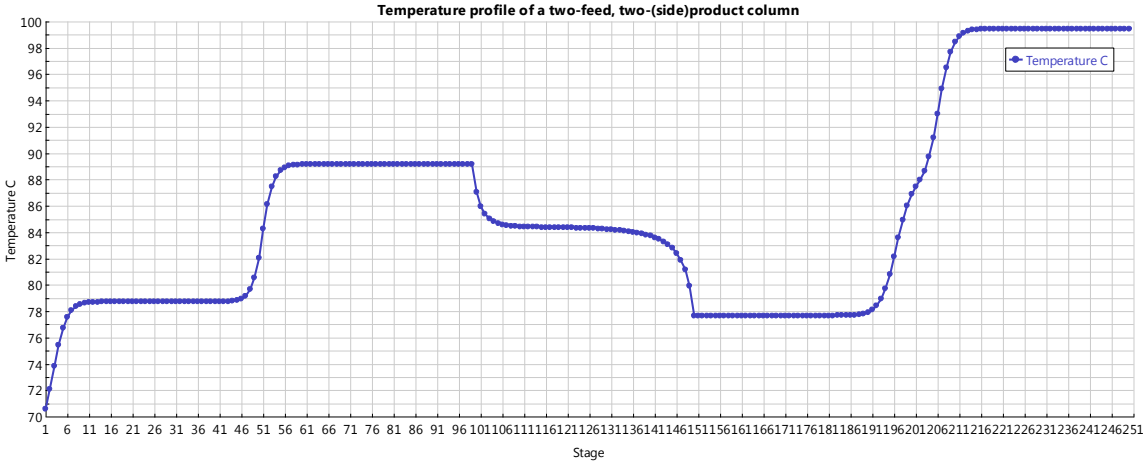

(b) Temperature profile at minimum reflux

Figure 7.7. Composition and temperature profile of the 2-feed, 2-(side)product column of interest under minimum reflux operation.

is sandwiched in between two pinch zones, with the top one corresponding to Z_1 of the second column section and the bottom one corresponding to Z_3 of the fourth section. Thus, according to Fact 7.1.1, it is thermodynamically infeasible to construct a continuous composition profile that connects these two pinches by strictly following the CMO assumption. Similar to the discussion above, we relax the CMO assumption using reversible distillation model by successively reducing the local reflux ratio.

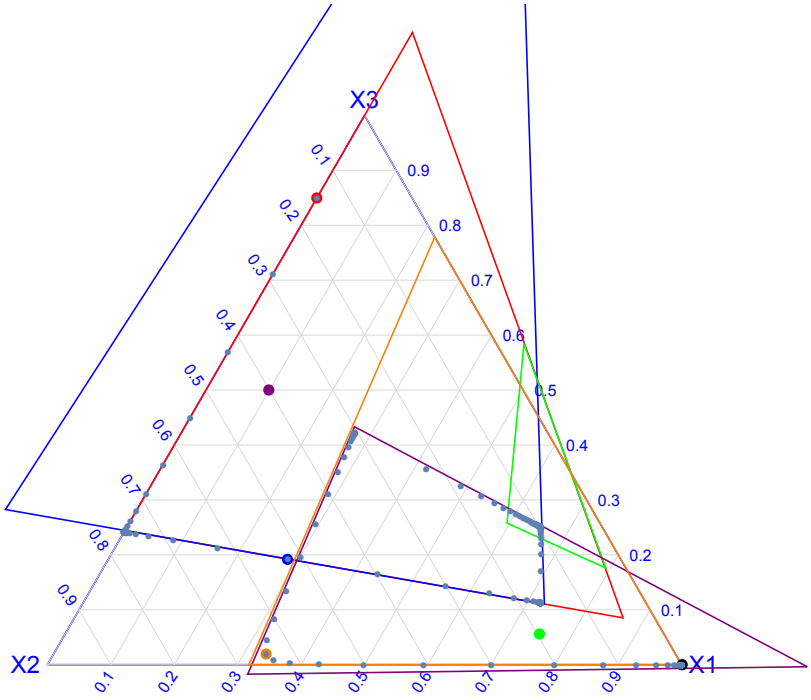

Figure 7.8. Z-simplex diagram of a two-feed, two-(side)product example for reversible distillation analysis. The red, blue, green, purple, orange, and black dots represent the liquid composition (or equilibrium liquid composition if the stream is in vapor state) of distillate, upper sidedraw, upper feed, lower feed, lower sidedraw, and bottoms streams, respectively.

Specifically, as the liquid composition reaches Z_1 of the second column section (and we know from earlier discussions that Z_1 must lie at the bottom of the section), the local reflux ratio starts to reduce at infinitesimal rate. This process is illustrated in Figure 7.9. As the local reflux ratio gets reduced, the Z-simplex for the third column section "shrinks", whereas that for the second column section remains more or less the same. This evolution continues till the point when $\gamma_{2,2} = \gamma_{3,1}$, at which the local vapor flow is reduced by 0.05517426. At this point, Figure 5.5 suggests that normal downward calculation will carry the liquid composition from the bottom of the second column section to Z_2 of the third column section, followed by continuing from Z_2 to pinch Z_3 of the fourth column section, which is located at its top.

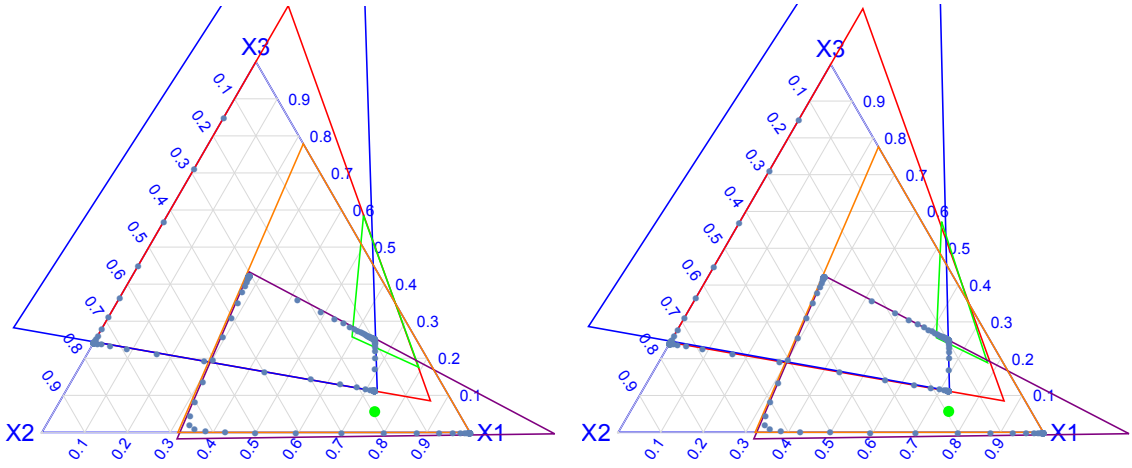

(a) Local vapor duty $V = 2.32725$

(b) Local vapor duty reduced by 0.03

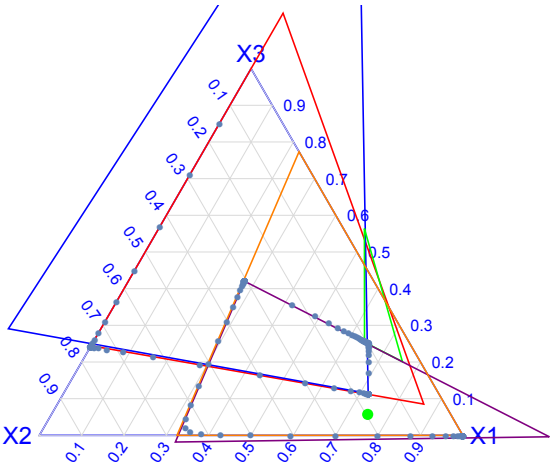

(c) Local vapor duty reduced by 0.05

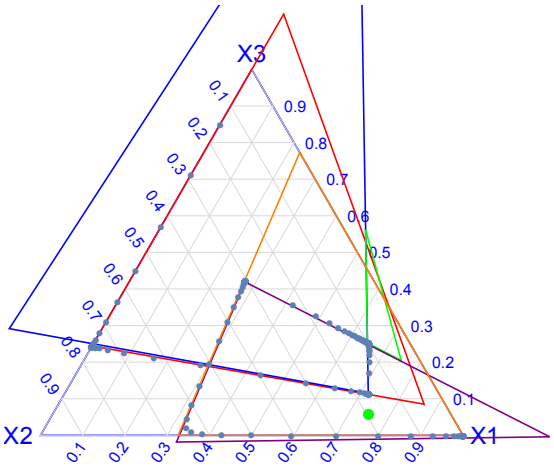

(d) Local vapor duty reduced by 0.05517426

Figure 7.9. The evolution of Z-simplex as local vapor duty is reduced starting from Z_1 of the second column section (blue triangle). The local vapor duty is reduced at most by 0.05517426, at which $\gamma_{2,2} = \gamma_{3,1} = 1.78378$.

7.4 Conclusion

In this chapter, we discuss a peculiar three-feed distillation column case in which, at minimum reflux operation, the liquid composition profile within an intermediate column section obtained from Aspen Plus simulation does not exactly follow the trajectory predicted by the Z-simplices using the method discussed in Chapters 5 and 6. We realize that this discrepancy is originated from the CMO assumption that is made

when constructing the Z-simplex diagram. Under the CMO assumption, the liquid and vapor flows across different stages remain unchanged within a general column section. The CMO assumption implicitly implies three inferences: 1) the distillation column, expect at the reboiler and condenser, is operated adiabatically; 2) the enthalpic contributions due to temperature changes are negligible relative to those to phase change; and 3) all components involved have the same latent heat of vaporization, and this value does not vary from stage to stage. Nevertheless, in this particular three-feed column case, we identify that the CMO assumption does not necessarily hold true anymore in one of the column sections in which there simultaneously exists a higher temperature pinch zone that is located above a lower temperature pinch zone. Therefore, the CMO assumption must be relaxed in this column section. And part of the column section is not operated adiabatically. In this case, the theory of reversible distillation is used to model this column section. In reversible distillation, differential heat exchange between the distillation column and the environment is allowed in order to ensure that the operation of this section is completely thermodynamically reversible. We theoretically demonstrate that using reversible distillation model, the two pinch zones finally collapse into a single pinch zone, thus making the overall composition profile continuous. We also show that the final minimum reflux ratio value remains unaltered even if we relax the CMO assumption in one of the column sections and utilize the reversible distillation model. This fact has been pointed out by Koehler et al. [170] and Agrawal and Fidkowski [171]. As a result, the validity of our algorithm developed in Chapters 5 and 6 still hold. In fact, it turns out that we can use our proposed algorithm to identify exactly where the CMO assumption needs to be relaxed and how the composition profile behaves when part of the column is operated reversibly.

7.5 Future Work – Efficient Use of An Intermediate Reboiler or Condenser for Multicomponent Distillation

Apart from this direct research finding of how the relaxation of the CMO assumption impacts the composition profile, the analysis approach employed in this chapter also sheds light on the efficient use of intermediate reboiler (IR) and intermediate condenser (IC) in multicomponent distillation. It is known that the thermodynamic efficiency of a distillation column can be improved by using IR and IC. Agrawal and Herron [116, 117] analyzed the impact of an IR or IC on the efficiency of binary distillation by performing exergy analysis. The composition of the vapor/liquid stream that enters the IC/IR can be quickly read off from the McCabe-Thiele diagram, making the exergy loss calculation straightforward. However, this luxury no longer exists once we begin to consider multicomponent systems. As a result, so far we have not seen any successful attempt in the literature to analytically determine the optimal IR and IC placement for multicomponent distillation column that maximizes its thermodynamic efficiency. Now that we have understood the how the pinch zone evolves respect to the L/V ratio of the column section, we can model the distillation column with IR and IC effectively.

Here, we consider a ternary distillation column performing $ABC \rightarrow AB/BC$ split. The Z-simplex diagram for this column at minimum reflux without an IR is shown in Figure 7.10. Suppose we are interested in placing an IR somewhere in the stripping section of the column. Then, it is possible to place the IR either above or below the stripping section pinch zone Z_2, which is located inside the section as shown in Figure 7.10. If we place the IR below Z_2, i.e. the composition of the liquid entering the IR lies somewhere along the $z_3 = 0$ hyperplane which coincides with $x_3 = 0$ line in Figure 7.10 since component A is absent in the bottoms product [157], then the problem automatically reduces to the binary case discussed in Agrawal and Herron [116, 117].

On the other hand, if we place the IR above Z_2 (See Figure 7.11), i.e. the composition of the liquid stream entering the IR x_I lies on $z_1 = 0$ hyperplane of the stripping section Z-simplex, it can be easily shown that the liquid composition of

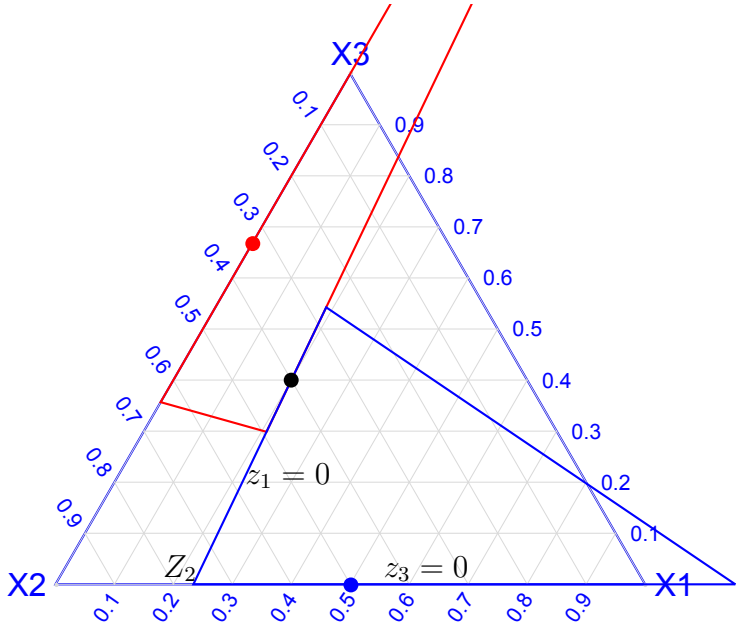

Figure 7.10. Z-simplex diagram for a distillation column performing $ABC \rightarrow AB/BC$ split at minimum reflux. The red, black, and blue dots represent distillate, feed, and bottoms compositions, respectively. The stripping section pinch Z'_2 is highlighted.

the two-phase stream leaving the IR, x_{IR}, must still lie on $z_1 = 0$ hyperplane of the original stripping section Z-simplex. For each x_I, there exists an unique x_{IR} which can be determined by the mass balance around the IR:

$$x_{i,I} = q_{IR} x_{i,IR} + (1 - q_{IR}) \frac{\alpha_i x_{i,IR}}{\sum_j \alpha_j x_{j,IR}} \qquad j = 1, 2, 3$$

in which q_{IR} stands for the liquid fraction of the stream eventually leaving the IR (See Figure 7.11). Note that y_{IR} is in equilibrium with x_{IR}.

Meanwhile, we need to construct a third Z-simplex for the column section below the intermediate condenser, as the liquid and vapor flows have been changed. Analogous to the binary case discussed in Agrawal and Herron [116], x_{IR} must be one of the pinch compositions in the third Z-simplex to maximize the thermodynamic efficiency of the column. Therefore, the vapor flow composition right below the IR must also

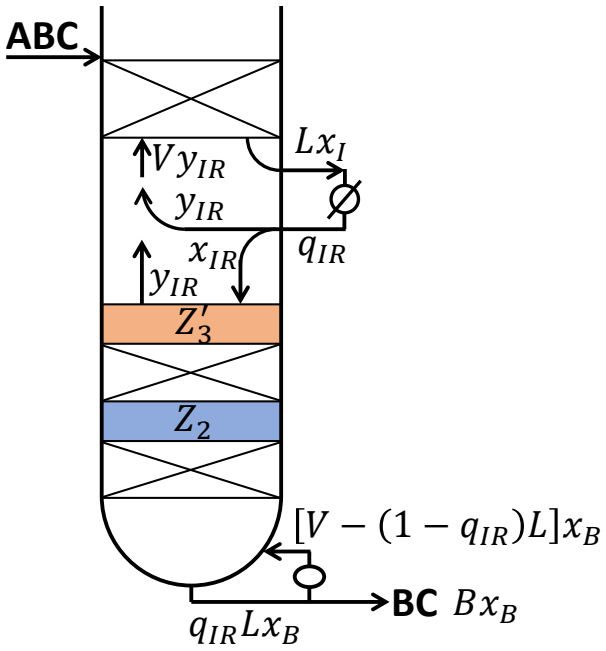

Figure 7.11. Stripping section of a column in which an IR is placed above the saddle pinch Z_2 higlighted in Figure 7.10. There exists a new pinch, Z'_3, due to the presence of the IR.

be y_{IR}. In fact, it can be shown that this pinch, denoted as Z'_3, corresponds to the unstable node pinch by downward calculation as discussed in Chapter 5 as shown in Figure 7.12. Thus, x_{IR} satisfies:

$$z'_1(x_{IR}) = \sum_{i=1}^{3} \frac{\alpha_i x_{i,IR}}{\alpha_i - \gamma'_1} = 0$$

$$z'_2(x_{IR}) = \sum_{i=1}^{3} \frac{\alpha_i x_{i,IR}}{\alpha_i - \gamma'_2} = 0$$

from which $\gamma'_1 \in (\alpha_1, \alpha_2)$ and $\gamma'_2 \in (\alpha_2, \alpha_3)$ can be solved simultaneously. In fact, root γ'_1 associated with the stripping section bpart elow the IR is equal to that associated with the stripping section part above the IR. Basically, two our of three hyperplanes forming the Z-simplices of these two parts of the stripping section coincide. Given this, we can use Equation (5.33) to relate the L/V ratios for these two parts of

stripping section, from which the vapor duty generated by the IR, $(1-q_{IR})L$, can be determined by solving the following equation:

$$\frac{q_{IR}L}{V-(1-q_{IR})L} = \frac{\gamma'_2}{\gamma_2}\frac{L}{V}$$

where γ_2 is obtained by solving Equation (5.13) for stripping section part above the IR, which is identical to the corresponding root by solving the Underwood's stripping section equation [19] assuming that no IR is present, implying that the sum of reboiler vapor duty remains unchanged by adding the IR.

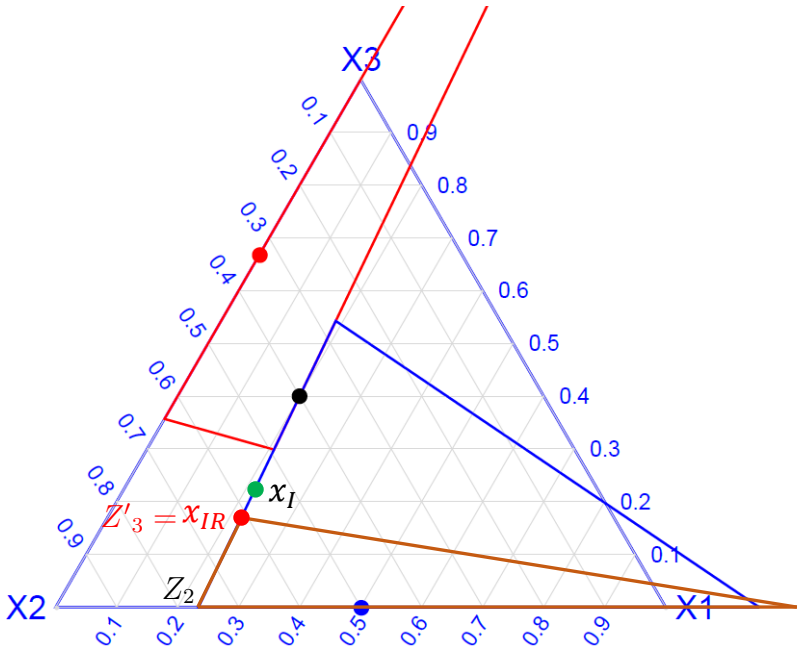

Figure 7.12. Z-simplex diagram when an IR is placed above the saddle pinch Z_2.

The analysis approach presented above can be easily incorporated as an optimization problem to identify the optimal placement of IR to maximize the thermodynamic efficiency of the column. We believe that the extension of this approach to different splits and other multicomponent systems with four or more components is relatively straightforward.

8. MULTICOMPONENT BATCH DISTILLATION MODELING

The first (unconscious) use of distillation dates back to around 3500 BC as the Sumerians first applied evaporation and condensation of a liquid to extract essential oils from herbs [172]. Since then, batch distillation remained as the primary chemical separation unit operation until 1800 when the first continuously working distillation column was invented and patented [1]. Since then, there has been a shift from batch to continuous distillation operation, starting from the petrochemical industry and slowly diffused to all areas of large-scale industries. However, small-scale, specialty chemical, and pharmaceutical industries still use batch distillation process even to this day. The goal of this section is to present a simple, easy-to-implement mathematical model for describing batch distillation processes separating ideal or near-ideal multicomponent mixtures.

8.1 Why Batch Distillation?

Batch distillation is superior compared to continuous distillation when it comes to the separation of small-scale, high-value-added chemicals [1]. Batch distillation is also frequently used due to its flexibility when small quantities of chemicals need to handled in seasonally scheduled periods or when the feed specifications change from time to time. Such flexibility makes batch distillation easier in dealing with uncertainties in feed stock and/or product specifications. Furthermore, unlike continuous distillation, one can easily handle several different mixtures just by switching the column's operating conditions when batch distillation system is used. Also, batch distillation requires far less capital cost for separating chemicals with relatively high purities. For multicomponent mixture separation, continuous distillation generally requires a series of columns to achieve the desired high purities of components, whereas batch distil-

lation only needs one single column or far less than $c-1$ columns for c-component separation, as a result of its transient nature as well as high flexibility.

The transient nature of batch distillation also allows us to configure the column in a number of ways. The most commonly used batch distillation column has a reboiler at the bottom and a condenser at the top, which essentially performs rectification. Also, instead of collecting the distillation product in a single pot, several different cuts can be obtained individually by placing several collecting pots. Some cuts may be desired and others might be intermediate cuts, which can then be recycled to minimize waste. On the other hand, the possibility of having multiple multi-fraction operation and recycle schemes also contributes to the complexity of batch distillation configurations. For example, one can use the so called batch stripping column where the liquid feed is initially charged into the top. And the combination of rectifying column and stripping column gives the yet another batch distillation configuration called the middle vessel column [173]. Later, Skogestad et al. [174] adapted the concept of multi-effect batch distillation and developed a new configuration called a multi-vessel column. Accounting for these multiplicities, one can intuitively realize that the number of possible column configurations grows rapidly. Next, we will describe the basic operating modes of conventional batch distillation column.

8.1.1 Operating Modes of Batch Distillation

During a normal batch distillation practice, after a period of total reflux operation, the distillate is continuously withdrawn, making it a non-steady-state process [175]. A conventional batch column can be operated under the following operating modes:

1. Constant reflux and variable product composition
2. Variable reflux and constant product composition of the key component
3. Optimal reflux and optimal product composition

Under Constant Reflux (CR) mode, the instantaneous composition of the distillate keeps changing. On the other hand, under Variable Reflux (VR) mode, the

composition of the key component in the distillate can be kept constant by increasing the reflux ratio. The third type of operation, known as Optimal Reflux (OR), lies somewhere between the first two operating modes and is usually based on certain objectives (e.g. shortest processing time, maximum profit, minimum waste generation). The calculation for this operating policy is rather difficult and relies on optimal control theory. Figure 8.1 below shows the comparison of these three operating modes for a batch rectification column separating a binary mixture. One can clearly see that the OR mode is essentially a trade-off between CR mode and VR mode. In this section, we will focus on developing mathematical models for CR and VR modes.

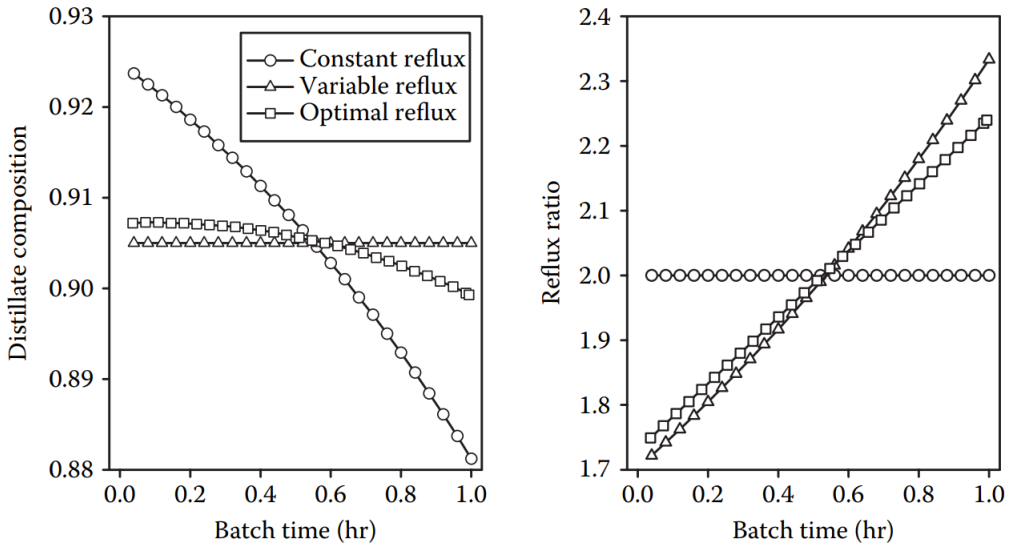

Figure 8.1. Three operating modes of batch rectification column. This figure is extracted from Korovessi and Linninger [175].

8.2 Shortcut Model for Batch Distillation Columns

As we know, rigorous modeling of batch distillation operation involves simultaneously solving a system of differential equations for each and every tray. The computational time and memory requirement for solving the problem increases drastically

with increasing number of stages and components. This poses theoretical as well as practical urge to develop a robust shortcut model for batch distillation operation.

Most of the existing shortcut based methods employ the same underlying assumptions of the Underwood's method [87, 176, 177]. These authors simplified the batch distillation column model by treating it as a continuous distillation column with varying feed. In their proposed algorithms, the minimum number of stages and the minimum reflux ratio are first determined using Fenske's equation [85] and Underwood's method [19], respectively. Then, these results are substituted into Gilliland's correlation [92] to obtain the actual number of stages and the actual reflux ratio. In other words, these methods rely on the so called Fenske-Underwood-Gilliland (FUG) relationship to arrive at a converged solution. However, as pointed out by Salomone et al. [177], the FUG relationship for continuous distillation can be very different from that for batch distillation. Also, the FUG relationship is highly nonlinear and iterative in nature, which poses unnecessary computational burden onto the solver. Directly applying the FUG relationship onto modeling batch columns may lead to significant error and inferior design. In this section, we attempt to propose a shortcut based method to model batch distillation columns that directly calculates the actual number of stages without needing the FUG relationship. This method is based on direct determination of liquid composition leaving any stage using the Underwood's method [19]. Thus, it is expected that this approach would give more robust and accurate results than most of the existing algorithms.

8.2.1 Constant Reflux Mode

Assuming negligible liquid and vapor holdup, the overall and component material balance for a batch distillation column can be written as:

$$\frac{dB}{dt} = -D$$
$$\frac{d(Bx_{i,B})}{dt} = -Dx_{i,D}$$

from which we can easily get:

$$Bdx_{i,B} + x_{i,B}dB = x_{i,D}dB$$

or in other words,

$$dx_{i,B} = (x_{i,D} - x_{i,B})\frac{dB}{B} \qquad \forall i = 1, \cdots, c \tag{8.1}$$

from which one can integrate and get:

$$\int_{x_{i,B_0}}^{x_{i,B}} \frac{dx_{i,B}}{x_{i,D} - x_{i,B}} = \ln(B/B_0) \qquad \forall i = 1, \cdots, c \tag{8.2}$$

where $B = B(t)$ is the amount of material remaining in the still, and B_0 is the amount of material in the feed at $t = 0$. Equation (8.2) was originally derived for binary simple distillation by Rayleigh [178]. To solve Equation (8.1), Sundaram and Evans [87] considered a time step of δt and approximated $dx_{i,B}$ and dB with $x_{i,B}^{\text{new}} - x_{i,B}^{\text{old}}$ and $B^{\text{new}} - B^{\text{old}} = -D\delta t$, respectively:

$$x_{i,B}^{\text{new}} = x_{i,B}^{\text{old}} - (x_{i,D}^{\text{old}} - x_{i,B}^{\text{old}})\frac{D}{B^{\text{old}}}\delta t \tag{8.3}$$

At the beginning of the distillation ($t = 0$), $x_{i,B}^{\text{old}} = x_{i,B_0}$ and $B^{\text{old}} = B_0$. To calculate $x_{i,D}^{\text{old}}$, recall that most batch distillation process starts with total reflux operation mode. If we again assume for now that each stage has negligible holdup, we can directly use the Fenske equation to solve for $x_{i,D}^{\text{old}}$ at $t = 0$ given x_{i,B_0}:

$$\frac{x_{i,D}^{\text{old}}}{x_{c,D}^{\text{old}}} = \left(\frac{\alpha_i}{\alpha_c}\right)^N \frac{x_{i,B_0}}{x_{c,B_0}} \qquad \forall i = 1, \cdots, c-1$$
$$\sum_{i=1}^{c} x_{i,D}^{\text{old}} = 1$$

where N is the number of stages in the distillation column. As we can see, the assumption of negligible liquid and vapor holdup leads to great simplification of the

mathematical model that describes the batch column in operation. However, using finite difference method to predict the distillate composition at any time in operation, it is important for us to accurately determine the initial condition of $x_{i,D}^{\text{old}}$ at $t = 0$, as the accuracy of subsequent calculations highly depends on the accuracy of the starting point. As a result, it is actually not a good idea to use the negligible holdup assumption for initial condition determination. Instead, we may assume that each stage has a constant liquid holdup H. Therefore, at $t = 0$, we have:

$$B_0 x_{i,B_0} = H(x_{i,1}^{\text{old}} + \cdots + x_{i,N}^{\text{old}}) + (B_0 - NH)x_{i,B}^{\text{old}} \qquad i = 1, \cdots, c \tag{8.4}$$

in which the stage is numbered from top to bottom. Now, writing down the Fenske equation for every component i and every stage j, we have:

$$\begin{aligned} x_{c,j}^{\text{old}} &= x_{1,j}^{\text{old}} \alpha_c^{N-j+1} \frac{x_{c,B}^{\text{old}}}{x_{1,B}^{\text{old}}} \\ x_{c-1,j}^{\text{old}} &= x_{1,j}^{\text{old}} \alpha_{c-1}^{N-j+1} \frac{x_{c-1,B}^{\text{old}}}{x_{1,B}^{\text{old}}} \qquad j = 1, \cdots, N \\ &\vdots \\ x_{1,j}^{\text{old}} &= x_{1,j}^{\text{old}} \end{aligned} \tag{8.5}$$

Adding all equalities in Equation (8.5), one can express $x_{i,j}^{\text{old}}$ all in terms of still compositions $x_{i,B}^{\text{old}}$:

$$\begin{aligned} x_{1,j}^{\text{old}} &= \frac{1}{1 + \alpha_2^{N-j+1} \frac{x_{2,B}^{\text{old}}}{x_{1,B}^{\text{old}}} + \cdots + \alpha_c^{N-j+1} \frac{x_{c,B}^{\text{old}}}{x_{1,B}^{\text{old}}}} \\ x_{1,j}^{\text{old}} &= \frac{\alpha_2^{N-j+1} \frac{x_{2,B}^{\text{old}}}{x_{1,B}^{\text{old}}}}{1 + \alpha_2^{N-j+1} \frac{x_{2,B}^{\text{old}}}{x_{1,B}^{\text{old}}} + \cdots + \alpha_c^{N-j+1} \frac{x_{c,B}^{\text{old}}}{x_{1,B}^{\text{old}}}} \qquad j = 1, \cdots, N \\ &\vdots \\ x_{c,j}^{\text{old}} &= \frac{\alpha_c^{N-j+1} \frac{x_{c,B}^{\text{old}}}{x_{1,B}^{\text{old}}}}{1 + \alpha_2^{N-j+1} \frac{x_{2,B}^{\text{old}}}{x_{1,B}^{\text{old}}} + \cdots + \alpha_c^{N-j+1} \frac{x_{c,B}^{\text{old}}}{x_{1,B}^{\text{old}}}} \end{aligned} \tag{8.6}$$

Substituting the results of Equation (8.6), for all $j = 1, \cdots, N$, into the mass balance of Equation (8.4) at $t = 0$ leads to c nonlinear equations with c unknowns, $x_{i,B}^{\text{old}} \quad \forall i = 1, \cdots, c$, from which one can solve for the liquid composition remaining in the still numerically. Although these equations are highly nonlinear, they do not contribute to the complexity of the global optimization algorithm if the starting point is not a decision variable to the optimization framework.

Next, to relate $x_{i,B}$ and $x_{i,D}$ at any time instance $t > 0$, one could develop a model to describe the dynamic behavior within the batch column using shock wave theory. In fact, Nandakumar and Andres [162] and Wachter et al. [149] have come up with such a model for continuous distillation column capturing its transient behavior when a step change in operating condition (e.g. feed composition, liquid and vapor flow). Although such a model can yield very accurate predictions, it can be quite computationally challenging to be implemented in a global optimization algorithm. Moreover, it seems like such a model over-complicates the problem without offering much extra benefit. The reason is because in a typical batch distillation column, the still composition changes continuously at a relative slow rate. It's rare to observe a step change in operating conditions. Also, in batch distillation column, the stage dynamics are generally significantly faster than the reboiler dynamics due to relatively small stage holdups [175]. As a result, we believe that a batch distillation process can be modeled as a countinuous countercurrent mass exchanger with feed changing at any instant. In other words, there are two levels in the modeling hierarchy: (a) the reboiler, where the dynamics are slower, can be represented by differential equations, and (b) the rest of the column can be approximated to be at *quasi-steady state*. This is known as the "semi-rigorous model" for batch distillation [179].

Under the quasi-steady state approximation, we can relate $x_{i,D}$ with $x_{i,B}$ at any instance using Equation (5.17). To do so, let N be the number of stages in the

column. And suppose, for the sake of this analysis, that all components are present in the distillate product. Then, we have:

$$\frac{z_{i,0}}{z_{1,0}} = \left(\frac{\gamma_i}{\gamma_1}\right)^N \frac{z_{i,N}}{z_{1,N}} = 1 \quad \forall i = 2, \cdots, c$$

As a result, it must be true that the still composition satisfies:

$$\gamma_i^N \sum_{j=1}^{c} \frac{\alpha_j x_{j,B}}{\alpha_j - \gamma_i} = \gamma_1^N \sum_{j=1}^{c} \frac{\alpha_j x_{j,B}}{\alpha_j - \gamma_1} \qquad \forall i = 2, \cdots, c \tag{8.7}$$

where in both forms the Underwood roots satisfy Equation (5.13). After substituting $x_{i,B}^{\text{new}}$ into the relationships above, we end up with a total of $c-1$ independent unknowns, namely $d_2, \cdots, d_c$. As far as we know, despite its simplicity, this relationship has not yet been developed for characterizing batch distillation columns. We can simultaneously solve these equations numerically.

Here, we provide a good initial guess for d_i. From the overall mass balance, we can write:

$$B^{\text{old}} x_{i,B}^{\text{old}} - B^{\text{new}} x_{i,B}^{\text{new}} = D \int_{t_{\text{old}}}^{t_{\text{new}}} x_{i,D} dt = D x_{i,D}^{\text{ave}} \delta t$$

and assuming that $x_{i,D}^{\text{ave}}$ is the arithmetic average of $x_{i,D}^{\text{old}}$ and $x_{i,D}^{\text{new}}$, i.e. the integral is approximated using trapezoid rule. Therefore, we would have:

$$(x_{i,D}^{\text{new}})_{\text{init}} = 2x_{i,D}^{\text{ave}} - x_{i,D}^{\text{old}} = 2(B^{\text{old}} x_{i,B}^{\text{old}} - B^{\text{new}} x_{i,B}^{\text{new}})/D\delta t - x_{i,D}^{\text{old}}$$

For minimum reflux calculations, since all c components will be present in the distillate during normal operation of batch distillation, there would exist a pinch corresponding to Z_1 at the bottom of the column when the number of stages in the column approaches to infinity. Recall from the proof of Proposition 5.4.2 stated in Chapter 5 that $\gamma_i \in (\alpha_i, \alpha_{i+1})$ of Equation (5.13) satisfy $f_n(x) = 0$ for $i = 2, \cdots, c$.

Moreover, these roots must also satisfy $F_2(x) = \sum_{i=1}^{c} \frac{\alpha_i v'_{i,0}}{\alpha_i - x} - V = x f_0(x) = 0$. As a result, we have, at any time instance:

$$\sum_{i=1}^{c} \frac{\alpha_i x_{i,B}}{\alpha_i - \gamma_j} = 0 \qquad \forall j = 2, \cdots, c \tag{8.8}$$

A similar expression has also been pointed out by Diwekar [179], Diwekar and Madhavan [176], Barolo and Guarise [180], Salomone et al. [177] and many others in which an analogy was drawn between batch distillation column and the rectifying section of a continuous distillation column. These authors then proposed a modified version of Equation (5.41) by substituting $q = 1$. However, the logic behind this analogy is not accurate as Underwood's feed equation is a natural consequence of vapor balance around the feed stage when the two column sections sandwiching the feed all have infinite number of stages. Therefore, we should not draw such an analogy even though a similar expression as Equation (8.8) can be obtained. Instead, we believe that our analysis approach offers the correct reasoning behind the derivation of Equation (8.8).

Solving for these $c - 1$ roots of γ allows us to establish the linear system from which one can obtain distillate composition:

$$\begin{pmatrix} \frac{\alpha_1}{\alpha_1-\gamma_2} & \cdots & \frac{\alpha_c}{\alpha_c-\gamma_2} \\ \vdots & \ddots & \vdots \\ \frac{\alpha_1}{\alpha_1-\gamma_c} & \cdots & \frac{\alpha_c}{\alpha_c-\gamma_c} \\ 1 & \cdots & 1 \end{pmatrix} \begin{pmatrix} d_1 \\ \vdots \\ d_c \end{pmatrix} = \begin{pmatrix} V \\ \vdots \\ V \\ D \end{pmatrix} \tag{8.9}$$

If the distillate composition is known, then Equation (8.9) can be used to solve for the vapor flow V which in turn gives the minimum reflux ratio. On the other hand, if the vapor flow is known, then solving this linear system gives the distillate component distribution corresponding to minimum reflux condition.

8.2.2 Variable Reflux Mode

Next, let us examine the case when the column operates at VR mode. Diwekar and Madhavan [176] considered two sub-cases for this situation: (1) Constant distillate composition for all components; (2) Constant distillate composition for the key component as reference. By examining two examples, they found that the first case was not strictly valid, i.e. it is impossible to fix the distillate composition for more than one component by varying reflux. This can also been seen by performing a degree of freedom analysis. Therefore, we will focus on the second sub-case for the remaining discussion on VR mode.

Although the choice of reference component is arbitrary, it is always more convenient to consider the lightest component that's present in infinitesimal amount in the distillate product as the key component. If all components are present in non-negligible amount in the distillate, then we generally fix the distillate composition for the heaviest component to be of constant value. Thus, we need to examine two cases.

If all components are present in the distillate, and suppose $x_{1,D}$ and the total distillate flow are fixed, then Equation (8.3) can be used to approximate $x_{1,B}^{\text{new}}$ at any time instance:

$$x_{1,B}^{\text{new}} = x_{1,B}^{\text{old}} + \frac{D\delta t x_{1,B}^{\text{old}} - d_1}{B^{\text{old}}}$$

Now, the variation of other components with respect to component 1 is given by simply:

$$x_{i,B}^{\text{new}} = x_{i,D}^{\text{new}} - \frac{x_{1,D} - x_{1,B}^{\text{new}}}{x_{1,D} - x_{1,B_0}}(x_{i,D}^{\text{new}} - x_{i,B_0}) \qquad \forall i = 2, \cdots, c$$

Substituting $x_{1,B}^{\text{new}}$ into the relationship above allows us to relate $x_{i,B}^{\text{new}}$ with $x_{i,D}^{\text{new}}$. On the other hand, Equation (8.7) gives another set of relationships between $x_{i,B}^{\text{new}}$ with $x_{i,D}^{\text{new}}$. Together with Equation (5.13), one can solve for the distillate composition as well as the vapor flow at that particular time instance.

In the second case, suppose $x_{1,D}, \cdots, x_{k,D} = 0$. Thus, component k is selected as the key component. Previous analysis based on Z-simplex demonstrates that

this implies that the distillate composition x_D must always satisfy the hyperplanes $z_1, \cdots, z_k = 0$. Thus, Equation (8.7) needs to be rewritten as:

$$\frac{z_{i,0}}{z_{k+1,0}} = \left(\frac{\gamma_i}{\gamma_{k+1}}\right)^N \frac{z_{i,n}}{z_{k+1,n}} = 1 \quad \forall i = k+2, \cdots, c$$

which further leads to:

$$\gamma_i^N \sum_{j=1}^{c} \frac{\alpha_j x_{j,B}}{\alpha_j - \gamma_i} = \gamma_{k+1}^N \sum_{j=1}^{c} \frac{\alpha_j x_{j,B}}{\alpha_j - \gamma_{k+1}} \qquad \forall i = k+2, \cdots, c$$

Along with Equation (5.13) for $\gamma_j \in (\alpha_{j-1}, \alpha_j)$ when $j = k+1, \cdots, c$, we have enough independent equations to solve for the distillate composition and the vapor flow at any time instance.

8.3 Conclusion and Future Work

In this chapter, we study the mathematical modeling of multicomponent batch distillation with the aid of the tools developed in Chapter 5. We considered two major operating modes, namely the CR mode and VR mode, and attempted to construct the model for both modes. It turns out that the model developed in Chapter 5 can be applied to yield more accurate predictions to the composition profile compared to existing models available in the literature even for batch distillation columns.

In the next phase, we will continue this ongoing work by focusing on two aspects. First, we need to understand the impact of liquid holdup and incorporate it into our model in a more accurate manner. This is necessary because under certain circumstances, liquid holdup plays an important role in the design and operation of batch columns [181] and dynamic behavior of batch columns can no longer be neglected. Diwekar [179] categorized the holdup effect into two forms, namely the dynamic "flywheel effect" and the steady state "capacitance effect". The flywheel effect can be characterized by the time constant τ = column holdup$/(R_D \times D)$. Diwekar and Madhavan [176] showed that the shortcut method results agreed well with the results

obtained for small τ. However, for large τ (large holdup and small reflux ratio), the initial part of the composition profile for the more volatile component showed a gradual change for rigorous simulations, whereas the shortcut method predicted a sharp drop in the composition. As a result, the shortcut method needs to be modified to account for the flywheel effect for the state variables that exhibit dominant dynamic characteristics.

In a batch distillation column, the input variable that changes significantly is the reflux ratio. Thus, Diwekar and Madhavan [176] suggested a lumped dynamic to be incorporated at the top of the column. A quasi-steady-state approximation was then assumed for the remaining part of the column, as the composition changes were slower in this part of the column. The shortcut based method can be used for that section of the column. In other words, the modified shortcut based method uses dynamic model for condenser and the first stage (the sensitive stage), but conventional shortcut method for the rest of the column. At each time instance, the shortcut based method uses the composition predicted by the dynamic model at the top. As shown by Diwekar and Madhavan [176], incorporating the dynamic effect in the modified shortcut based model offers much closer prediction compared to rigorous simulation results.

The capacitance effect is observed at the end of initial total reflux operation when the given charge distributes itself throughout the column. It accounts for the steady state difference of liquid composition on a tray when the holdup of liquid on the tray changes. As suggested by Diwekar [179], it is associated with the equilibration time which is defined as the time required to reach equilibrium at total reflux. The shortcut based method presented earlier assumes instance equilibrium during total reflux operation, which may or may not be an accurate assumption for real cases.

Once a more accurate shortcut model is developed, we will work on the second aspect by incorporating this model into a global optimization algorithm to identify the optimal batch distillation configuration and its corresponding optimal design parameters. This requires us to first formulate a superstructure to include all possible

multicomponent batch distillation schemes. As far as we know, this is still an open problem. Once the complete superstructure of batch configurations is formulated, we will develop an enumeration based global optimization algorithm to efficiently and robustly evaluate all possible schemes. We will implement tight relaxations and bounds for the constraints and variables in the optimization model, as well as adding redundant constraints that are helpful to the relaxation of the problem. We intend to adopt the enumeration based approach rather than proposing an MINLP framework mainly because the search space of batch distillation configurations might be much smaller compared to that of continuous distillation configurations when certain restrictions on the search space are employed. Therefore, solving a single but more complex MINLP problem might not offer much computational time benefit than solving a system of less complex optimization problems. Of course, the choice of optimization problem type is subject to many other factors, all of which need to be carefully addressed in our future work.

9. SUMMARY

Distillation is the primary separation process that is ubiquitous in the chemical industry. This predominant position for distillation is unlikely to alter in the near future. Therefore, even small improvements to the current industrial practices of conducting distillation can generate huge economical and environmental impact. Despite being misunderstood as a "mature" technology or simply a "dead field", we find out that, using novel mathematical modeling and global optimization approaches as well as systematic process intensification strategies, a number of compact, easy-to-operate multicomponent distillation configurations that can save up to 50% of capital and operating costs compared to conventional distillation schemes can be identified within a short amount of time. Such significant room for improvement has proven that distillation is still a young research field and is full of breakthrough opportunities.

In this thesis, we explore several aspects of multicomponent distillation by following a three-level research approach as shown in Figure 9.1. In the bottom level, we are interested in developing a shortcut based mathematical model to characterize a general multi-feed, multi-product distillation column and calculate its minimum reflux ratio for a given separation task. This is important as MFMP columns have been widely used in various industrial applications and are common in many multicomponent distillation configurations. At the same time, the minimum reflux ratio is a key parameter in the design and operation of distillation columns. For nearly 80 years, a number of methods have been proposed to calculate the minimum reflux ratio of an MFMP column accurately and efficiently. However, these methods either rely on several simplifying assumptions, some of which turn out to be incorrect, or require rigorous tray-by-tray calculations, which are computationally expansive and often infeasible to be implemented for large scale problems. In Chapter 6, for the

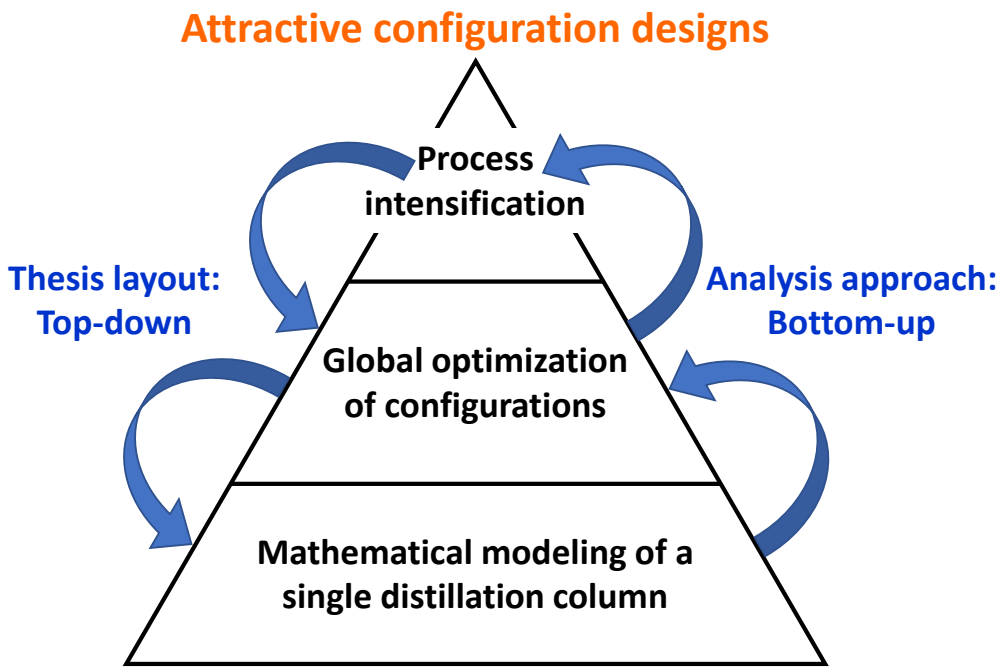

Figure 9.1. Hierarchy of the three-level research approach.

first time we develop a simple, easy-to-use shortcut based approach to solve this longstanding challenge in chemical engineering. This approach starts from realizing the fact that the smallest unit in a MFMP column is a general column section. Thus, in the first step, we devote ourselves in developing the accurate mathematical model to characterize a general column section in a MFMP column. Then, we explore the mathematical and physical properties of this model when the general column section is pinched by taking the number of stages to infinity. Finally, we stack these infinite column sections back to form the original MFMP column, and derive simple mathematical constraints corresponding to minimum reflux operation of the MFMP column. In Chapter 6, we demonstrate the use of this method under two scenarios. If the feed and product specifications are known to us, then our proposed algorithm becomes completely algebraic and can be directly solved by hand. In this case, this method is as easy-to-use as the McCabe-Thiele method for binary distillation or the classic Underwood's method [19] for solving simple columns. However, this method

can be applied to any MFMP column, whereas the Underwood's method can only be applied for simple columns. In the second scenario in which the product distribution is unknown to us, our method can be formulated as a mixed-integer nonlinear program (MINLP). The MINLP is used to determine the minimum reflux ratio and its corresponding optimal product distribution while satisfying all user specifications. This MINLP can also be easily incorporated into a global optimization framework to solve an entire configuration or even the entire search space of configurations.

In Chapters 6, 7 and 8, we show that our modeling approach for distillation columns is not just limited to calculating their minimum reflux conditions. Instead, it can also be Incorporated into the global optimization framework to optimize an entire distillation configuration. Moreover, it can be utilized to model and understand many important applications in distillation, such as intermediate reboiler/condenser in multicomponent distillation, reversible distillation, and batch distillation, as well as separation processes other than distillation, including liquid-liquid extraction and absorption processes.

Once we fully understand the physics and mathematics behind a single distillation column, we move up to the intermediate level by focusing on the global optimization of distillation configuration search space synthesized by the SA method [7]. Due to the humongous size of distillation configuration search space, one must rely on formulating an optimization problem to consider and solve all configurations in the search space in a timely manner in order to identify the global optimal configuration for a separation task. However, current optimization algorithms in the literature possess several drawbacks and often cannot guarantee global optimality. In the earlier work of Nallasivam et al. [34], we developed the first enumeration based global optimization algorithm named the GMA for minimizing the total reboiler vapor duty requirement of any basic or TC configuration. The GMA formulates a nonlinear program (NLP) for each and every configuration in the search space and solves it to global optimality within a matter of seconds. In this thesis, we continue this work by developing the first global optimization algorithm for minimizing the total cost (GMAC, in Chapter 3)

and total exergy loss (GMAE, in Chapter 4) of a distillation configuration. We explain why these two objectives are of importance to process engineers and how to formulate the corresponding optimization problems. For the first time in the literature, both the GMAC and the GMAE frameworks guarantee global optimality. In particular, the GMAE is the first available global optimization algorithm devoted to maximize the thermodynamic efficiency of a multicomponent distillation configuration. This powerful tool not only allows industrial practitioners to identify thermodynamically efficient configurations, but also opens up many exiting opportunities that people may consider, such as heat pump assisted distillation, double-effect distillation, etc. Finally, through case studies, we generate insightful heuristics and guidelines for designing new attractive configurations as well as retrofitting existing ones to enhance their efficiency and cost-effectiveness.

Finally, all methods and algorithms developed at the bottom and the intermediate levels converge to the highest level in the conceptual design of multicomponent distillation systems using process intensification. PI is an emerging concept in chemical engineering which describes the design innovations that lead to significant shrink in size and dramatic boost in efficiency in a process plant. In the context of multicomponent distillation, we define PI as the innovative process synthesis strategies leading to minimizing the number of pieces of equipment as well as total cost while maintaining high efficiency. In Chapter 2, we introduce the first systematic, multi-layer approach for performing PI in multicomponent distillation. For the first time, industrial practitioners have an easy-to-follow yet powerful recipe to conduct PI in multicomponent distillation. We point out that the central element in this PI methodology lies in the strategic introduction of thermal couplings to selectively eliminate reboilers and/or condensers associated with certain submixture locations in a distillation configuration. To some extent, it serves as the "catalyst" in the overall process of PI, without which other PI strategies will not be possible. To identify useful thermal couplings that offer the maximum energy and cost savings while minimizing the incurred exergy loss, we need to rely on global optimization algorithms developed at the intermediate

level as the guiding star. This shows that this three-level research approach as shown in Figure 9.1 are closely interconnected.

Overall, through a three-level approach consisting of mathematical modeling, global optimization, and process intensification, we have redefined the field of multicomponent distillation in this thesis. We show that distillation is far from being a "mature" technology, even from a conceptual design perspective. For any non-azeotropic multicomponent separation, configurations that can show significant energy and cost savings compared to current industrially implemented configurations are highly likely to exist and can be systematically identified using our systematic approach. In summary, the future of multicomponent distillation research is still bright.

REFERENCES

[1] A. Gorak and Z. Olujic. *Distillation: Fundamentals and Principles*. Elsevier Inc., July 2014.

[2] Norbert Kockmann. 200 years in innovation of continuous distillation. *ChemBioEng Reviews*, 1(1):40–49, 2014.

[3] Jimmy L. Humphrey. Separation technologies: an opportunity for energy savings. *Chemical Engineering Progress*, 88:32–42, March 1992.

[4] British Petroleum. Bp statistical review of world energy 2018, June 2018.

[5] Miguel Bagajewicz and Shuncheng Ji. Rigorous procedure for the design of conventional atmospheric crude fractionation units. part i: targeting. *Industrial & Engineering Chemistry Research*, 40(2):617–626, 2001.

[6] U.S. Energy Information Administration. U.s. energy facts, May 2018.

[7] Vishesh H. Shah and Rakesh Agrawal. A matrix method for multicomponent distillation sequences. *AIChE Journal*, 56(7):1759–1775, 2010.

[8] Anirudh A. Shenvi, Vishesh H. Shah, and Rakesh Agrawal. New multicomponent distillation configurations with simultaneous heat and mass integration. *AIChE Journal*, 59(1):272–282, 2013.

[9] Arun Giridhar and Rakesh Agrawal. Synthesis of distillation configurations: I. characteristics of a good search space. *Computers & Chemical Engineering*, 34(1):73 – 83, 2010.

[10] Rakesh Agrawal. Synthesis of multicomponent distillation column configurations. *AIChE Journal*, 49(2):379–401, 2003.

[11] F.J. Lockhart. Multi-column distillation of natural gasoline. *Petroleum Refiner*, 26(8):104–108, 1947.

[12] Christodoulos A Floudas. *Nonlinear and mixed-integer optimization: fundamentals and applications*. Topics in Chemical Engineering. Oxford University Press, New York, 1995.

[13] Roger W. Thompson and C. Judson King. Systematic synthesis of separation schemes. *AIChE Journal*, 18(5):941–948, 1972.

[14] R.W.H. Sargent and K. Gaminibandara. Optimal design of plate distillation columns. In L.C.W. Dixon, editor, *Optimization in Action*, New York, 1976. Conference on Optimization in Action (1975 : University of Bristol), Academic Press.

[15] Rakesh Agrawal. Synthesis of distillation column configurations for a multicomponent separation. *Industrial & Engineering Chemistry Research*, 35(4):1059–1071, 1996.

[16] Jos A. Caballero and Ignacio E. Grossmann. Design of distillation sequences: from conventional to fully thermally coupled distillation systems. *Computers & Chemical Engineering*, 28(11):2307 – 2329, 2004.

[17] Javad Ivakpour and Norollah Kasiri. Synthesis of distillation column sequences for nonsharp separations. *Industrial & Engineering Chemistry Research*, 48(18):8635–8649, 2009.

[18] Arun Giridhar and Rakesh Agrawal. Synthesis of distillation configurations. ii: A search formulation for basic configurations. *Computers & Chemical Engineering*, 34(1):84 – 95, 2010.

[19] A. J. V. Underwood. Fractional distillation of multicomponent mixtures. *Industrial & Engineering Chemistry*, 41(12):2844–2847, 1949.

[20] Juan Gabriel Segovia-Hernndez and Adrin Bonilla-Petriciolet. *Process Intensification in Chemical Engineering Design Optimization and Control*. Springer, 2016.

[21] David G Reay. *Process Intensification engineering for efficiency, sustainability and flexibility*. Isotopes in Organic Chemistry. Elsevier/BH, Amsterdam ; Boston, 2nd ed. edition, 2013.

[22] C Ramshaw. The incentive for process intensification. In *1st Intl. Conf. Proc. Intensif. for Chem. Ind.*, volume 18, London, 1995.

[23] Andrezej Stankiewicz and Jacob Moulijn. Process intensification: Transforming chemical engineering. *Chemical Engineering Progress*, 96(1), 2000.

[24] Jos Mara Ponce-Ortega, Musaed M. Al-Thubaiti, and Mahmoud M. El-Halwagi. Process intensification: New understanding and systematic approach. *Chemical Engineering and Processing: Process Intensification*, 53:63 – 75, 2012.

[25] Rakesh Agrawal and Terrence F. Yee. Heat pumps for thermally linked distillation columns: An exercise for argon production from air. *Industrial & Engineering Chemistry Research*, 33(11):2717–2730, 1994.

[26] FB Petlyuk, VM Platonov, and DM Slavinskii. Thermodynamically optimal method for separating multicomponent mixtures. *Int. Chem. Eng.*, 5(3):555–561, 1965.

[27] Richard O. Wright. Fractionation apparatus, us patent 2471134a, 1949.

[28] Zbigniew Fidkowski and Lechoslaw Krolikowski. Thermally coupled system of distillation columns: Optimization procedure. *AIChE Journal*, 32(4):537–546, 1986.

[29] Zbigniew Fidkowski and LechosW Krlikowski. Minimum energy requirements of thermally coupled distillation systems. *AIChE Journal*, 33(4):643–653, 1987.

[30] Rakesh Agrawal and Zbigniew T. Fidkowski. New thermally coupled schemes for ternary distillation. *AIChE Journal*, 45(3):485–496, 1999.

[31] Zbigniew T. Fidkowski and Rakesh Agrawal. Multicomponent thermally coupled systems of distillation columns at minimum reflux. *AIChE Journal*, 47(12):2713–2724, 2001.

[32] Neil A. Carlberg and Arthur W. Westerberg. Temperature-heat diagrams for complex columns. 2. underwood's method for side strippers and enrichers. *Industrial & Engineering Chemistry Research*, 28(9):1379–1386, 1989.

[33] Ulaganathan Nallasivam, Vishesh H. Shah, Anirudh A. Shenvi, Mohit Tawarmalani, and Rakesh Agrawal. Global optimization of multicomponent distillation configurations: 1. need for a reliable global optimization algorithm. *AIChE Journal*, 59(3):971–981, 2013.

[34] Ulaganathan Nallasivam, Vishesh H. Shah, Anirudh A. Shenvi, Joshua Huff, Mohit Tawarmalani, and Rakesh Agrawal. Global optimization of multicomponent distillation configurations: 2. enumeration based global minimization algorithm. *AIChE Journal*, 62(6):2071–2086, 2016.

[35] Jos A. Caballero and Ignacio E. Grossmann. Generalized disjunctive programming model for the optimal synthesis of thermally linked distillation columns. *Industrial & Engineering Chemistry Research*, 40(10):2260–2274, 2001.

[36] Jos A. Caballero and Ignacio E. Grossmann. Structural considerations and modeling in the synthesis of heat-integrated-thermally coupled distillation sequences. *Industrial & Engineering Chemistry Research*, 45(25):8454–8474, 2006.

[37] Jos A. Caballero and Ignacio E. Grossmann. Thermodynamically equivalent configurations for thermally coupled distillation. *AIChE Journal*, 49(11):2864–2884, 2003.

[38] Jos A. Caballero and Ignacio E. Grossmann. Synthesis of complex thermally coupled distillation systems including divided wall columns. *AIChE Journal*, 59(4):1139–1159, 2013.

[39] M. Tawarmalani and N. V. Sahinidis. A polyhedral branch-and-cut approach to global optimization. *Mathematical Programming*, 103:225–249, 2005.

[40] Gautham Madenoor Ramapriya, Ajiththaa Selvarajah, Luis Eduardo Jimenez Cucaita, Joshua Huff, Mohit Tawarmalani, and Rakesh Agrawal. Shortcut methods versus rigorous methods for performance-evaluation of distillation configurations. *Industrial & Engineering Chemistry Research*, 57(22):7726–7731, 2018.

[41] Vishesh H. Shah and Rakesh Agrawal. Are all thermal coupling links between multicomponent distillation columns useful from an energy perspective? *Industrial & Engineering Chemistry Research*, 50(3):1770–1777, 2011.

[42] Zbigniew T. Fidkowski. Distillation configurations and their energy requirements. *AIChE Journal*, 52(6):2098–2106, 2006.

[43] Konstantinos N. Glinos, Ioannis P. Nikolaides, and Michael F. Malone. New complex column arrangements for ideal distillation. *Industrial & Engineering Chemistry Process Design and Development*, 25(3):694–699, 1986.

[44] C. Triantafyllou and R Smith. Design and optimisation of fully thermally coupled distillation columns. *Chemical Engineering Research and Design*, 70(42):118 – 132, 1992.

[45] Omar Annakou and Peter Mizsey. Rigorous comparative study of energy-integrated distillation schemes. *Industrial & Engineering Chemistry Research*, 35(6):1877–1885, 1996.

[46] Ivar J. Halvorsen and Sigurd Skogestad. Minimum energy consumption in multicomponent distillation. 3. more than three products and generalized petlyuk arrangements. *Industrial & Engineering Chemistry Research*, 42(3):616–629, 2003.

[47] Rakesh Agrawal and Zbigniew T. Fidkowski. Are thermally coupled distillation columns always thermodynamically more efficient for ternary distillations? *Industrial & Engineering Chemistry Research*, 37(8):3444–3454, 1998.

[48] M.I. Abdul Mutalib and R. Smith. Operation and control of dividing wall distillation columns: Part 1: Degrees of freedom and dynamic simulation. *Chemical Engineering Research and Design*, 76(3):308 – 318, 1998. Techno-Economic Analysis.

[49] Erik A. Wolff and Sigurd Skogestad. Operation of integrated three-product (petlyuk) distillation columns. *Industrial & Engineering Chemistry Research*, 34(6):2094–2103, 1995.

[50] Olga A. Flores, J. Carlos Crdenas, Salvador Hernndez, and Vicente Rico-Ramrez. Thermodynamic analysis of thermally coupled distillation sequences. *Industrial & Engineering Chemistry Research*, 42(23):5940–5945, 2003.

[51] Rakesh Agrawal and Zbigniew T. Fidkowski. More operable arrangements of fully thermally coupled distillation columns. *AIChE Journal*, 44(11):2565–2568, 1998.

[52] R. Agrawal. More operable fully thermally coupled distillation column configurations for multicomponent distillation. *Chemical Engineering Research and Design*, 77(6):543 – 553, 1999.

[53] Gerd Kaibel. Distillation columns with vertical partitions. *Chemical Engineering & Technology*, 10(1):92–98, 1987.

[54] Robin Smith and B. Linnhoff. The design of separators in the context of overall processes. *Chemical Engineering Research and Design*, 66(3):195–228, 1988.

[55] Konstantinos Glinos and Michael F. Malone. Minimum vapor flows in a distillation column with a sidestream stripper. *Industrial & Engineering Chemistry Process Design and Development*, 24(4):1087–1090, 1985.

[56] K. Liebmann and V.R. Dhole. Integrated crude distillation design. *Computers & Chemical Engineering*, 19:119 – 124, 1995. European Symposium on Computer Aided Process Engineering.

[57] Rakesh Agrawal. Thermally coupled distillation with reduced number of intercolumn vapor transfers. *AIChE Journal*, 46(11):2198–2210, 2000.

[58] Gautham Madenoor Ramapriya, Mohit Tawarmalani, and Rakesh Agrawal. Thermal coupling links to liquid-only transfer streams: A path for new dividing wall columns. *AIChE Journal*, 60(8):2949–2961, 2014.

[59] Gautham Madenoor Ramapriya and Rakesh Agrawal. Multicomponent dividing wall columns, us patent 9504934b2, 2016.

[60] K.A. Amminudin, R. Smith, D.Y.-C. Thong, and G.P. Towler. Design and optimization of fully thermally coupled distillation columns: Part 1: Preliminary design and optimization methodology. *Chemical Engineering Research and Design*, 79(7):701 – 715, 2001.

[61] Salvador Hernndez, Salvador Pereira-Pech, Arturo Jimnez, and Vicente Rico-Ramrez. Energy efficiency of an indirect thermally coupled distillation sequence. *The Canadian Journal of Chemical Engineering*, 81(5):1087–1091, 2003.

[62] Phillip C. Wankat. Multieffect distillation processes. *Industrial & Engineering Chemistry Research*, 32(5):894–905, 1993.

[63] Hao Chieh Cheng and William L. Luyben. Heat-integrated distillation columns for ternary separations. *Industrial & Engineering Chemistry Process Design and Development*, 24(3):707–713, 1985.

[64] Rakesh Agrawal. Multieffect distillation for thermally coupled configurations. *AIChE Journal*, 46(11):2211–2224, 2000.

[65] Hilde K. Engelien and Sigurd Skogestad. Minimum energy diagrams for multi-effect distillation arrangements. *AIChE Journal*, 51(6):1714–1725, 2005.

[66] Samuel S. Ding and William L. Luyben. Control of a heat-integrated complex distillation configuration. *Industrial & Engineering Chemistry Research*, 29(7):1240–1249, 1990.

[67] P. Mizsey, N.T. Hau, N. Benko, I. Kalmar, and Z. Fonyo. Process control for energy integrated distillation schemes. *Computers & Chemical Engineering*, 22:S427 – S434, 1998. European Symposium on Computer Aided Process Engineering-8.

[68] Mansour Emtir, Endre Rv, and Zsolt Fony. Rigorous simulation of energy integrated and thermally coupled distillation schemes for ternary mixture. *Applied Thermal Engineering*, 21(13):1299 – 1317, 2001.

[69] E. Rv, M. Emtir, Z. Szitkai, P. Mizsey, and Z. Fony. Energy savings of integrated and coupled distillation systems. *Computers & Chemical Engineering*, 25(1):119 – 140, 2001.

[70] Ben-Guang Rong, Andrzej Kraslawski, and Ilkka Turunen. Synthesis of heat-integrated thermally coupled distillation systems for multicomponent separations. *Industrial & Engineering Chemistry Research*, 42(19):4329–4339, 2003.

[71] Antoine Johan Brugma. Process and device for fractional distillation of liquid mixtures, more particularly petroleum, us patent 2295256a, 1942.

[72] Gautham Madenoor Ramapriya, Anirudh A. Shenvi, Mohit Tawarmalani, and Rakesh Agrawal. A new framework for combining a condenser and reboiler in a configuration to consolidate distillation columns. *Industrial & Engineering Chemistry Research*, 54(42):10449–10464, 2015.

[73] Robert P. Cahn, Alphonso G Di Miceli, and Elizabeth Di Miceli. Separation of multicomponent mixture in single tower, us patent 3058893a, 1962.

[74] Zheyu Jiang, Gautham Madenoor Ramapriya, Mohit Tawarmalani, and Rakesh Agrawal. Minimum energy of multicomponent distillation systems using minimum additional heat and mass integration sections. *AIChE Journal*, 64(9):3410–3418, 2018.

[75] Rakesh Agrawal. Multicomponent distillation columns with partitions and multiple reboilers and condensers. *Industrial & Engineering Chemistry Research*, 40(20):4258–4266, 2001.

[76] Gautham Madenoor Ramapriya, Mohit Tawarmalani, and Rakesh Agrawal. A systematic method to synthesize all dividing wall columns for n-component separation: Part i. *AIChE Journal*, 64(2):649–659, 2018.

[77] Gautham Madenoor Ramapriya, Mohit Tawarmalani, and Rakesh Agrawal. A systematic method to synthesize all dividing wall columns for n-component separation: Part ii. *AIChE Journal*, 64(2):660–672, 2018.

[78] F. Lestak and C. Collins. Advanced distillation saves energy and capital. *Chemical Engineering*, 104(7), 7 1997.

[79] MA Schultz, DG Stewart, JM Harris, SP Rosenblum, MS Shakur, and DE OBrien. Reduce costs with dividing-wall columns. *Chemical Engineering Progress*, 98(5):64–71, 2002.

[80] Brbel Kolbe and Sascha Wenzel. Novel distillation concepts using one-shell columns. *Chemical Engineering and Processing: Process Intensification*, 43(3):339 – 346, 2004. Special Issue on Distillation and Absorption.

[81] I. Dejanovi, Lj. Matijaevi, and . Oluji. Dividing wall column – a breakthrough towards sustainable distilling. *Chemical Engineering and Processing: Process Intensification*, 49(6):559 – 580, 2010.

[82] Ivar J. Halvorsen and Sigurd Skogestad. Energy efficient distillation. *Journal of Natural Gas Science and Engineering*, 3(4):571 – 580, 2011.

[83] Z. Olujic, M. Jodecke, A. Shilkin, G. Schuch, and B. Kaibel. Equipment improvement trends in distillation. *Chemical Engineering and Processing: Process Intensification*, 48(6):1089 – 1104, 2009.

[84] Rosanna Franco and Ignacio E. Grossmann. Optimal separation sequences based on thermally coupled distillation, 2014.

[85] M. R. Fenske. Fractionation of straight-run pennsylvania gasoline. *Industrial & Engineering Chemistry*, 24(5):482–485, May 1932.

[86] Richard Turton, Richard C. Bailie, Wallace B. Whiting, Joseph A. Shaeiwitz, and Debangsu Bhattacharyya. *Analysis, synthesis, and design of chemical processes*. Prentice-Hall international series in the physical and chemical engineering sciences. Prentice Hall, Upper Saddle River, NJ, 4th ed. edition, 2012.

[87] Suresh Sundaram and Lawrence B. Evans. Shortcut procedure for simulating batch distillation operations. *Industrial & Engineering Chemistry Research*, 32(3):511–518, 1993.

[88] Ivar J. Halvorsen and Sigurd Skogestad. Minimum energy consumption in multicomponent distillation. 1. vmin diagram for a two-product column. *Industrial & Engineering Chemistry Research*, 42(3):596–604, 2003.

[89] R. Tumbalam Gooty, M. Tawarmalani, and R. Agrawal. An MINLP formulation for the optimization of multicomponent distillation configurations. *In preparation*, 2018.

[90] H. J. Lang. Engineering approach to preliminary cost estimates. *Chemical Engineering*, 54:117–122, October 1947.

[91] H.E. Eduljee. Equations replace gilliland plot. *Hydrocarbon Processing*, 54(9):120–122, 1975.

[92] E. R. Gilliland. Multicomponent rectification estimation of the number of theoretical plates as a function of the reflux ratio. *Industrial & Engineering Chemistry*, 32(9):1220–1223, 1940.

[93] Michael F Doherty. *Conceptual design of distillation systems*. McGraw-Hill chemical engineering series. McGraw-Hill, Boston, 2001.

[94] J.R. Fair. *Handbook of separation process technology*. John Wiley Sons,New York, NY, 1987.

[95] James Merrill Douglas. *Conceptual design of chemical processes*. McGraw-Hill chemical engineering series. McGraw-Hill, New York, 1988.

[96] John Anderson. Determining manufacturing costs. *Chemical Engineering Progress*, 105(12):27–32, January 2009.

[97] Bruce E Poling, J.M. Prausnitz, and J.P. O'Connell. *The properties of gases and liquids*. McGraw-Hill, New York, 5th ed.. edition, 2001.

[98] Michael C. Ferris, Steven Dirkse, and Jagdish Ramakrishnan. Matlab and gams: Interfacing optimization and visualization software (the gdxmrw utilities), 2011.

[99] Zheyu Jiang and Rakesh Agrawal. Process intensification in multicomponent distillation. unpublished, 2018.

[100] Rakesh Agrawal. Thermally coupled distillation with reduced number of intercolumn vapor transfers. *AIChE Journal*, 46(11):2198–2210, 2000.

[101] Rakesh Agrawal and Zbigniew T. Fidkowski. More operable arrangements of fully thermally coupled distillation columns. *AIChE Journal*, 44(11):2565–2568, 1998.

[102] Zheyu Jiang, Gautham Madenoor Ramapriya, Mohit Tawarmalani, and Rakesh Agrawal. Minimum energy of multicomponent distillation systems using minimum additional heat and mass integration sections. *AIChE Journal*, 64(9):3410–3418, 2018.

[103] Rakesh Agrawal and Zbigniew T. Fidkowski. Thermodynamically efficient systems for ternary distillation. *Industrial & Engineering Chemistry Research*, 38(5):2065–2074, 1999.

[104] Yaar Demirel. Thermodynamic analysis of separation systems. *Separation Science and Technology*, 39(16):3897–3942, 2004.

[105] R. Agrawal and D.W. Woodward. Efficient cryogenic nitrogen generators: An exergy analysis. *Gas Separation & Purification*, 5(3):139 – 150, 1991.

[106] M Seidel. Verfahren zur gleichzeitigen zerlegung von verflussigten gasgemischen und anderen flussigkeitsgemischen mit mehr als zwei bestandteilen durch rektifikation, german patent 610503, 1935.

[107] Rakesh Agrawal and D.W. Woodward. Inter-column heat integration for multicolumn distillation system, us patent 5230217, 7 1993.

[108] F.G. Ho and G.E. Keller. *Process Integration*. Wiley, New York, NY, 1987.

[109] Rakesh Agrawal and Zbigniew T. Fidkowski. Improved direct and indirect systems of columns for ternary distillation. *AIChE Journal*, 44(4):823–830, 1998.

[110] E. L. Cussler and Binay K. Dutta. On separation efficiency. *AIChE Journal*, 58(12):3825–3831, 2012.

[111] V Kaiser and L.P. Gourlia. The ideal column concept: Applying exergy to distillation. *Chemical Engineering*, 92(17):45–53, 1985.

[112] Ruchira Taprap and Masaru Ishida. Graphic exergy analysis of processes in distillation column by energy-utilization diagrams. *AIChE Journal*, 42(6):1633–1641, 1996.

[113] R. E. Fitzmorris and R. S. H. Mah. Improving distillation column design using thermodynamic availability analysis. *AIChE Journal*, 26(2):265–273, 1980.

[114] T.J. Kotas. *The exergy method of thermal plant analysis*. Butterworth Publishers, Stoneham, MA, 1985.

[115] Rakesh Agrawal and D. Michael Herron. Optimal thermodynamic feed conditions for distillation of ideal binary mixtures. *AIChE Journal*, 43(11):2984–2996, 1997.

[116] Rakesh Agrawal and D. Michael Herron. Intermediate reboiler and condenser arrangement for binary distillation columns. *AIChE Journal*, 44(6):1316–1324, 1998.

[117] Rakesh Agrawal and D. Michael Herron. Efficient use of an intermediate reboiler or condenser in a binary distillation. *AIChE Journal*, 44(6):1303–1315, 1998.

[118] Phillip C. Wankat and David P. Kessler. Two-feed distillation. same-composition feeds with different enthalpies. *Industrial & Engineering Chemistry Research*, 32(12):3061–3067, 1993.

[119] Zheyu Jiang, Tony Mathew, Joshua Huff, Haibo Zhang, Ulaganathan Nallasivam, Mohit Tawarmalani, and Rakesh Agrawal. Global optimization of multicomponent distillation configurations: 3. global minimization of total cost for multicomponent mixture separations. unpublished manuscript, 2018.

[120] K. Glinos, M. F. Malone, and J. M. Douglas. Shortcut evaluation of δt and qδt for the synthesis of heat integrated distillation sequences. *AIChE Journal*, 31(6):1039–1040, 1985.

[121] K. Glinos and M.F. Malone. Net work consumption in distillation short-cut evaluation and applications to synthesis. *Computers & Chemical Engineering*, 13(3):295 – 305, 1989.

[122] Steven C Chapra. *Numerical methods for engineers*. McGraw-Hill Higher Education, New York, NY, seventh edition.. edition, 2015.

[123] Keith A. Bullin and Peter E. Krouskop. Compositional variety complicates processing plans for us shale gas. *Oil & Gas Journal*, 101(10):50–55, 2009.

[124] Chang He and Fengqi You. Shale gas processing integrated with ethylene production: Novel process designs, exergy analysis, and techno-economic analysis. *Industrial & Engineering Chemistry Research*, 53(28):11442–11459, 2014.

[125] Mohit Tawarmalani and Nikolaos V Sahinidis. *Convexification and global optimization in continuous and mixed-integer nonlinear programming : theory, algorithms, software, and applications*. Nonconvex optimization and its applications ; v. 65. Kluwer Academic Publishers, Dordrecht ; Boston, 2002.

[126] FB Petlyuk, VM Platonov, and DM Slavinskii. Thermodynamically optimal method for separating multicomponent mixtures. *Int. Chem. Eng.*, 5(3):555–561, 1965.

[127] E. R. Gilliland. Multicomponent rectification. *Industrial & Engineering Chemistry*, 32(8):1101–1106, August 1940.

[128] Zbigniew Fidkowski and LechosW Krlikowski. Minimum energy requirements of thermally coupled distillation systems. *AIChE Journal*, 33(4):643–653, 1987.

[129] Zbigniew T. Fidkowski and Rakesh Agrawal. Multicomponent thermally coupled systems of distillation columns at minimum reflux. *AIChE Journal*, 47(12):2713–2724, 2001.

[130] Ruth C. Erbar and R. N. Maddox. Minimum reflux rate for multicomponent distillation systems by rigorous plate calculations. *The Canadian Journal of Chemical Engineering*, 40(1):25–30, 1962.

[131] Henry H. Y. Chien. A rigorous method for calculating minimum reflux rates in distillation. *AIChE Journal*, 24(4):606–613, 1978.

[132] Mehdi Tavana and Donald N. Hanson. The exact calculation of minimum flows in distillation columns. *Industrial & Engineering Chemistry Process Design and Development*, 18(1):154–156, 1979.

[133] Charles Donald Holland. *Fundamentals of multicomponent distillation*. McGraw-Hill chemical engineering series. McGraw-Hill, New York, 1981.

[134] Angelo Lucia, Amit Amale, and Ross Taylor. Distillation pinch points and more. *Computers & Chemical Engineering*, 32(6):1342 – 1364, 2008.

[135] Sanford G. Levy and Michael F. Doherty. Design and synthesis of homogeneous azeotropic distillations. 4. minimum reflux calculations for multiple-feed columns. *Industrial & Engineering Chemistry Fundamentals*, 25(2):269–279, 1986.

[136] Juergen Koehler, Thomas Kuen, and Eckhart Blass. Minimum energy demand for distillations with distributed components and side-product withdrawals. *Chemical Engineering Science*, 49(19):3325–3330, 1994.

[137] Vivek Julka and Michael F. Doherty. Geometric behavior and minimum flows for nonideal multicomponent distillation. *Chemical Engineering Science*, 45(7):1801 – 1822, 1990.

[138] Angelo Lucia and Ross Taylor. The geometry of separation boundaries: I. basic theory and numerical support. *AIChE Journal*, 52(2):582–594, 2005.

[139] Rafiqul Gani and Erik Bek-Pedersen. Simple new algorithm for distillation column design. *AIChE Journal*, 46(6):1271–1274, 2000.

[140] Z. T. Fidkowski, M. F. Malone, and M. F. Doherty. Nonideal multicomponent distillation: Use of bifurcation theory for design. *AIChE Journal*, 37(12):1761–1779, 1991.

[141] J. Bausa, R. V. Watzdorf, and W. Marquardt. Shortcut methods for nonideal multicomponent distillation: I. simple columns. *AIChE Journal*, 44(10):2181–2198, October 1998.

[142] R. Yu. Danilov, F. B. Petlyuk, and L. A. Serafimov. Minimum-reflux regime of simple distillation columns. *Theoretical Foundations of Chemical Engineering*, 41(4):371–383, Aug 2007.

[143] Raymond E. Rooks, Michael F. Malone, and Michael F. Doherty. A geometric design method for side-stream distillation columns. *Industrial & Engineering Chemistry Research*, 35(10):3653–3664, 1996.

[144] Rdiger Von Watzdorf, Jrgen Bausa, and Wolfgang Marquardt. Shortcut methods for nonideal multicomponent distillation: 2. complex columns. *AIChE Journal*, 45(8):1615–1628, August 1999.

[145] Mirko Skiborowski, Sebastian Recker, and Wolfgang Marquardt. Shortcut-based optimization of distillation-based processes by a novel reformulation of the feed angle method. *Chemical Engineering Research and Design*, 132:135 – 148, 2018.

[146] A. J. V. Underwood. Fractional distillation of multicomponent mixtures. *Chemical Engineering Progress*, 44:603–614, January 1948.

[147] Gautham Madenoor Ramapriya, Ajiththaa Selvarajah, Luis Eduardo Jimenez Cucaita, Joshua Huff, Mohit Tawarmalani, and Rakesh Agrawal. Shortcut methods versus rigorous methods for performance-evaluation of distillation configurations. *Industrial & Engineering Chemistry Research*, 57(22):7726–7731, 2018.

[148] F. J. Barnes, D. N. Hanson, and C. J. King. Calculation of minimum reflux for distillation columns with multiple feeds. *Industrial & Engineering Chemistry Process Design and Development*, 11(1):136–140, January 1972.

[149] John A. Wachter, Terry K. T. Ko, and Ronald P. Andres. Minimum reflux behavior of complex distillation columns. *AIChE Journal*, 34(7):1164–1184, July 1988.

[150] H. Sugie and Benjamin Lu. On the determination of minimum reflux ratio for a multicomponent distillation column with any number of side-cut streams. *Chemical Engineering Science*, 25(12):1837–1846, 1970.

[151] Konstantinos N. Glinos and Michael F. Malone. Design of sidestream distillation columns. *Industrial & Engineering Chemistry Process Design and Development*, 24(3):822–828, July 1985.

[152] I.P. Nikolaides and M.F. Malone. Approximate design of multiple-feed/side-stream distillation systems. *IND. ENG. CHEM. RES.*, 26(9), 1987.

[153] Lorena E. Ruiz-Marn, Nelly Ramrez-Corona, Angel Castro-Agero, and Arturo Jimnez-Gutirrez. Shortcut design of fully thermally coupled distillation systems with postfractionator. *Industrial & Engineering Chemistry Research*, 50(10):6287–6296, 2011.

[154] Chafika Adiche and Alfons Vogelpohl. Short-cut methods for the optimal design of simple and complex distillation columns. *Chemical Engineering Research and Design*, 89(8):1321 – 1332, 2011. Special Issue on Distillation & Absorption.

[155] Fernando Israel Gmez-Castro, Vicente Rico-Ramrez, Juan Gabriel Segovia-Hernndez, Salvador Hernndez-Castro, Guillermo Gonzlez-Alatorre, and Mahmoud M. El-Halwagi. Simplified methodology for the design and optimization of thermally coupled reactive distillation systems. *Industrial & Engineering Chemistry Research*, 51(36):11717–11730, 2012.

[156] Chafika Adiche and Belaid Ait Aissa. A generalized approach for the conceptual design of distillation columns with complex configurations. *Chemical Engineering Research and Design*, 109:150 – 170, 2016.

[157] N.L. Franklin and J.S. Forsyth. The interpretation of minimum reflux conditions in multi-component distillation. *Trans. Instn. Chem. Engrs.*, 31:S56 – S81, 1953.

[158] N. L. Franklin. Counterflow cascades: Part i. *Chemical Engineering Research and Design*, 64a:56–66, January 1986.

[159] Sanford G. Levy, David B. Van Dongen, and Michael F. Doherty. Design and synthesis of homogeneous azeotropic distillations. 2. minimum reflux calculations for nonideal and azeotropic columns. *Industrial & Engineering Chemistry Fundamentals*, 24(4):463–474, 1985.

[160] N Franklin. Theory of multicomponent countercurrent cascades. *Chemical Engineering Research and Design*, 66:65–74, January 1988.

[161] N.L. Franklin. Counterflow cascades: Part ii. *Chemical Engineering Research and Design*, 66(1):47–64, January 1988.

[162] K. Nandakumar and R. P. Andres. Minimum reflux conditions, part i: Theory. *AIChE Journal*, 27(3):450–460, 1981.

[163] Endre Rev. The constant heat transport model and design of distillation columns with one single distributing component. *Industrial & Engineering Chemistry Research*, 29(9):1935–1943, 1990.

[164] Ramapriya Gautham Madenoor, Tawarmalani Mohit, and Agrawal Rakesh. Modified basic distillation configurations with intermediate sections for energy savings. *AIChE Journal*, 60(3):1091–1097, 2014.

[165] Ivar J. Halvorsen and Sigurd Skogestad. Minimum energy consumption in multicomponent distillation. 2. three-product petlyuk arrangements. *Industrial & Engineering Chemistry Research*, 42(3):605–615, 2003.

[166] Konstantinos Glinos and Michael F. Malone. Minimum vapor flows in a distillation column with a sidestream stripper. *Industrial & Engineering Chemistry Process Design and Development*, 24(4):1087–1090, 1985.

[167] Neil A. Carlberg and Arthur W. Westerberg. Temperature-heat diagrams for complex columns. 3. underwood's method for the petlyuk configuration. *Industrial & Engineering Chemistry Research*, 28(9):1386–1397, 1989.

[168] Hassiba Benyounes, Weifeng Shen, and Vincent Gerbaud. Entropy flow and energy efficiency analysis of extractive distillation with a heavy entrainer. *Industrial & Engineering Chemistry Research*, 53(12):4778–4791, 2014.

[169] Libin Zhang and Andreas A. Linninger. Temperature collocation algorithm for fast and robust distillation design. *Industrial & Engineering Chemistry Research*, 43(12):3163–3182, June 2004.

[170] J. Koehler, P. Aguirre, and E. Blass. Minimum reflux calculations for nonideal mixtures using the reversible distillation model. *Chemical Engineering Science*, 46(12):3007 – 3021, 1991.

[171] Rakesh Agrawal and Zbigniew T. Fidkowski. On the use of intermediate reboilers in the rectifying section and condensers in the stripping section of a distillation column. *Industrial & Engineering Chemistry Research*, 35(8):2801–2807, 1996.

[172] Eckhart Blass, Thomas Liebl, and Michael Hberl. Extraktion ein historischer rckblick. *Chemie Ingenieur Technik*, 69(4):431–437, 1997.

[173] Arthur G. Davidyan, Valerii N. Kiva, George A. Meski, and Manfred Morari. Batch distillation in a column with a middle vessel. *Chemical Engineering Science*, 49(18):3033 – 3051, 1994.

[174] Sigurd Skogestad, Bernd Wittgens, Rajab Litto, and Eva Srensen. Multivessel batch distillation. *AIChE Journal*, 43(4):971–978, 1997.

[175] Ekaterini Korovessi and Andreas Linninger. *Batch processes*. Chemical Industries. CRC/Taylor & Francis, Boca Raton, FL, 2006.

[176] Urmila M. Diwekar and K. P. Madhavan. Multicomponent batch distillation column design. *Industrial & Engineering Chemistry Research*, 30(4):713–721, April 1991.

[177] H. E. Salomone, O. J. Chiotti, and O. A. Iribarren. Short-cut design procedure for batch distillations. *Industrial & Engineering Chemistry Research*, 36(1):130–136, 1997.

[178] Lord Rayleigh. Lix. on the distillation of binary mixtures. *The London, Edinburgh, and Dublin Philosophical Magazine and Journal of Science*, 4(23):521–537, November 1902.

[179] Urmila M Diwekar. *Batch distillation : simulation, optimal design, and control*. CRC Press, Boca Raton, FL, 2nd ed.. edition, 2012.

[180] M. Barolo and G.B. Guarise. Batch distillation of multicomponent systems with constant relative volatilities. *Chemical Engineering Research and Design*, 74(8):863 – 871, 1996. Heat and Mass Transfer.

[181] R. R. Stewart, Elliot Weisman, B. M. Goodwin, and C. E. Speight. Effect of design parameters in multicomponent batch distillation. *Industrial & Engineering Chemistry Process Design and Development*, 12(2):130–136, 1973.

A. EXAMPLE MINLP FORMULATION FOR MINIMUM REBOILER DUTY CALCULATION

We provide the objective function equation and all the constraint equations for the configuration shown in Figure 6.2a.

Objective function

$$\text{minimize } V_4$$

Constraints

1. Mass balance equations:

$$f_{i,1} + f_{i,2} = w_{i,1} + d_{i,1} - d_{i,4} \quad \forall i = 1, \cdots, 4$$

$$d_{i,2} = d_{i,1} - f_{i,1};\ d_{i,3} = d_{i,2} + w_{i,1}; d_{i,4} = d_{i,3} - f_{i,2} \quad \forall i = 1, \cdots, 4$$

$$f_{4,1} = d_{4,1};\ f_{1,2} = -d_{1,4}$$

$$F_1 = \sum_{i=1}^{4} f_{i,1};\ F_2 = \sum_{i=1}^{4} f_{i,2};\ W_1 = \sum_{i=1}^{4} w_{i,1}$$

2. Vapor and liquid balances in each column section:

$$V_j - L_j = \sum_{i=1}^{4} d_{i,j} \quad \forall j = 1, \cdots, 4$$

$$F_1 = V_{F_1} + L_{F_1};\ F_2 = V_{F_2} + L_{F_2};\ W_1 = V_{W_1} + L_{W_1}$$

$$V_1 = V_2 + V_{F_1};\ V_2 = V_3 + V_{W_1};\ V_3 = V_4 + V_{F_2}$$

2. Vapor duty calculation for each column section using Equation (5.13):

$$V_1 = \sum_{i=1}^{4} \frac{\alpha_i d_{i,k}}{\alpha_i - \gamma_{4,1}}$$

$$V_1 = \sum_{i=1}^{4} \frac{\alpha_i d_{i,k}}{\alpha_i - \gamma_{3,1}}$$

$$V_2(\alpha_3 - \gamma_{3,2}) = \alpha_2 d_{2,2} - (\alpha_2 - \alpha_3)\frac{\alpha_2 d_{2,2}}{\alpha_2 - \gamma_{3,2}} + \alpha_3 d_{3,2}$$

$$V_2 = \sum_{i=1}^{4} \frac{\alpha_i d_{i,k}}{\alpha_i - \gamma_{2,2}}$$

$$V_3(\alpha_2 - \gamma_{2,3}) = \alpha_2 d_{2,3} - (\alpha_3 - \alpha_2)\frac{\alpha_3 d_{3,3}}{\alpha_3 - \gamma_{2,3}} + \alpha_3 d_{3,3}$$

$$V_3 = \sum_{i=1}^{4} \frac{\alpha_i d_{i,k}}{\alpha_i - \gamma_{3,3}}$$

$$V_4 = \sum_{i=1}^{4} \frac{\alpha_i d_{i,k}}{\alpha_i - \gamma_{1,4}}$$

$$V_4 = \sum_{i=1}^{4} \frac{\alpha_i d_{i,k}}{\alpha_i - \gamma_{2,4}}$$

3. Defining equation for the sidedraw stream W_1, i.e. Equation (5.43):

$$V_{W_1} = \sum_{i=1}^{4} \frac{\alpha_i w_{i,1}}{\alpha_i - \theta_{j,W_1}} \quad \forall j = 1, \cdots, 4$$

4. Bounds on $\gamma_{i,j}$ and θ_{i,W_1} variables:

$$\gamma_{1,1} = \alpha_1;\ \gamma_{2,1} = \alpha_2;\ \gamma_{3,1} \in (\alpha_2, \alpha_3);\ \gamma_{4,1} \in (\alpha_3, \alpha_4)$$

$$\gamma_{1,2} = \alpha_1;\ \gamma_{2,2} \in (\alpha_2, \alpha_3);\ \gamma_{3,2} \in (\alpha_2, \alpha_4);\ \gamma_{4,2} = \alpha_4$$

$$\gamma_{1,3} = \alpha_1;\ \gamma_{2,3} \in (\alpha_1, \alpha_3);\ \gamma_{3,3} \in (\alpha_2, \alpha_3);\ \gamma_{4,3} = \alpha_4$$

$$\gamma_{1,4} \in (\alpha_1, \alpha_2);\ \gamma_{2,4} \in (\alpha_2, \alpha_3);\ \gamma_{3,4} = \alpha_3;\ \gamma_{4,4} = \alpha_4$$

$$\theta_{i,W_1} \in (\alpha_i, \alpha_{i+1}) \quad \forall i = 1, \cdots, 3$$

5. Definition of binary variable μ:

$$\mu_{2,2}, \mu_{3,2}, \mu_{1,3}, \mu_{2,3} \in \{0, 1\}$$
$$\mu_{2,2} + \mu_{3,2} = 1;\ \mu_{1,3} + \mu_{2,3} = 1$$

6. Necessary and sufficient constraints on $\gamma_{i,j}$ to ensure feasible separation, which correspond to Equations (6.4) and (6.5):

$$\alpha_2\mu_{2,2} + \alpha_3\mu_{3,2} \leq \gamma_{3,2} \leq \alpha_3\mu_{2,2} + \alpha_4\mu_{3,2}$$
$$\alpha_1\mu_{1,3} + \alpha_2\mu_{2,3} \leq \gamma_{2,3} \leq \alpha_2\mu_{1,3} + \alpha_3\mu_{2,3}$$
$$\gamma_{2,1} \geq \gamma_{1,2};\ \gamma_{3,1} \geq \gamma_{2,2};\ (1 - \mu_{2,2})(\gamma_{4,1} - \gamma_{3,2}) \geq 0$$
$$\mu_{1,3}(\gamma_{2,3} - \gamma_{1,2}) \geq 0;\ \gamma_{3,3} \geq \gamma_{2,2};\ (1 - \mu_{2,2})(\gamma_{4,3} - \gamma_{3,2}) \geq 0$$
$$\mu_{1,3}(\gamma_{2,3} - \gamma_{1,4}) \geq 0;\ \gamma_{3,3} \geq \gamma_{2,4};\ \gamma_{4,3} \geq \gamma_{3,4}$$
$$\theta_{2,W_1} \in (\alpha_2, \alpha_3);\ \mu_{2,2}(\gamma_{3,2} - \theta_{2,W_1}) \geq 0;\ \gamma_{2,2} \leq \theta_{2,W_1}$$
$$\gamma_{3,3} \geq \theta_{2,W_1};\ (1 - \mu_{1,3})(\gamma_{2,3} - \theta_{2,W_1}) \leq 0$$

VITA

Zheyu Jiang was born to Liliang Jiang and Jufang Shen in Nanjing, China on August 9, 1991. He moved to Guangzhou, China in 1993 and grew up there. He received his education from Guangzhou Shihua Primary School (1998 to 2004), Guangzhou No.86 Middle School (2004 to 2007), and Guangdong Experimental High School (2007 to 2010) before leaving for his undergraduate studies in the United States. He received his B.ChE. degree (with distinction and Honors) from the University of Minneosta in May 2014. He subsequently joined Purdue University in August 2014, working with Professor Rakesh Agrawal towards this thesis. Zheyu will graduate with a Ph.D. in chemical engineering from Purdue University in October 2018. Upon graduation, Zheyu is joining Corteva Agriscience, the agriculture division of DowDuPont, starting as a senior chemical engineer.